UNIVERSITY OF CALIFORNIA

Santa Barbara

Bottom-up Drivers of Bacterial Community Composition and

Metabolism of Dissolved Organic Carbon in the Santa Barbara Channel, CA

A dissertation submitted in partial satisfaction of the

requirements for the degree Doctor of Philosophy

in Marine Science

by

Emma Kate Wear

Committee in charge:

Professor Craig Carlson, Chair

Professor Mark Brzezinski

Professor David Siegel

March 2017

The dissertation of Emma Kate Wear is approved.

_____

Mark Brzezinski

_____

David Siegel

_____

Craig Carlson, Committee Chair

March 2017

Bottom-up Drivers of Bacterial Community Composition and

Metabolism of Dissolved Organic Carbon in the Santa Barbara Channel, CA

Copyright © 2017

by

Emma Kate Wear

ACKNOWLEDGEMENTS

VITA OF EMMA KATE WEAR

March 2017

EDUCATION

Bachelor of Science in Biology, Illinois Wesleyan University, May 2007 (magna cum laude)
Master of Science in Coastal Marine and Wetland Studies, Coastal Carolina University, September 2009
Doctor of Philosophy in Marine Science, University of California, Santa Barbara, March 2017 (expected)

PROFESSIONAL EMPLOYMENT

Summer 2005: Laboratory Intern, City of Bloomington, IL, Water Treatment Plant
Summer 2006: Interdisciplinary Watershed Studies REU Fellow, The College of William & Mary
2007: Teaching Assistant, Department of Biology, Illinois Wesleyan University
2007-2008: Research Assistant, Coastal Carolina University
Summer 2009: Laboratory Student Worker, Environmental Quality Lab, Coastal Carolina University
2010-2012: Teaching Assistant, Department of Ecology, Evolution, and Marine Biology, University of California, Santa Barbara
2015: Teaching Assistant: Department of Molecular, Cellular, and Developmental Biology, University of California, Santa Barbara

PUBLICATIONS

EK Wear, CA Carlson, LA Windecker, and MA Brzezinski. 2015. Roles of diatom nutrient stress and species identity in determining the short- and long-term bioavailability of diatom exudates to bacterioplankton. Marine Chemistry 177: 335-348. doi:10.1016/j.marchem.2015.09.001

EK Wear, CA Carlson, AK James, MA Brzezinski, LA Windecker, and CE Nelson. 2015. Synchronous shifts in dissolved organic carbon bioavailability and bacterial community responses over the course of an upwelling-driven phytoplankton bloom. Limnology and Oceanography 60: 657-677. doi:10.1002/lno.10042

CE Nelson and **EK Wear**. 2014. Microbial diversity and the lability of dissolved organic carbon. PNAS 111: 7166-7167. doi:10.1073/pnas.1405751111

BP Durham, J Grote, KA Whittaker, SJ Bender, H Luo, SL Grim, JM Brown, JR Casey, A Dron, L Florez-Leiva, A Krupke, CM Luria, AH Mine, OD Nigro, S Pather, A Talarmin, **EK Wear**, TS Weber, JM Wilson, MJ Church, EF DeLong, DM Karl, GF Steward, JM Eppley, NC Kyrpides, S Schuster, and MS Rappé. 2014. Draft genome sequence of marine alphaproteobacterial strain HIMB11, the first cultivated representative of a unique lineage

within the Roseobacter clade possessing a remarkably small genome. Standards in Genomic Sciences 9: 632-645. doi: 10.4056/sigs.4998989

EK Wear, ET Koepfler, and EM Smith. 2014. Spatiotemporal variability in dissolved organic matter composition is more strongly related to bacterioplankton community composition than to metabolic function in a blackwater estuarine system. Estuaries and Coasts 37: 119-133. doi: 10.1007/s12237-013-9651-y

EK Wear. 2009. Effects of inter-tributary dissolved organic carbon variability on heterotrophic microbial communities in upper Winyah Bay, SC. Master's thesis, Coastal Carolina University.

AWARDS

NASA Earth and Space Science Fellowship; 2012-2015

National Estuarine Research Reserve System Graduate Research Fellowship, North Inlet-Winyah Bay NERR; 2008

ABSTRACT

Bottom-up Drivers of Bacterial Community Composition and

Metabolism of Dissolved Organic Carbon in the Santa Barbara Channel, CA

by

Emma Kate Wear

Approximately 50 percent of marine primary production passes through the dissolved

organic matter (DOM) pool (Myklestad 2000; Nagata 2000). The major consumers of DOM

are marine bacterioplankton, which can direct DOM down three pathways: respiration to

inorganic constituents, incorporation into biomass, or modification or lack of consumption

leading to persistence as DOM. The aspects of DOM source and composition that determine

its bioavailability, and its interactions with the clades comprising the bacterial community,

are broadly understood, but many of the finer details remain to be studied. This dissertation

investigates bottom-up controls on bacterial community composition (BCC) and activity

through a time-series study in the Santa Barbara Channel (SBC), CA, and examines the

effects of phytoplankton DOM on bacterial metabolism, in field and laboratory experiments.

Chapter II describes the results of a four-year time-series study of BCC and metabolic

activity in the SBC. BCC showed the greatest variability over depth; at the surface, the

seasonal cycle was significantly more influential on BCC than spatial variability within

cruises. Community types showed repeating patterns following the annual upwelling and

phytoplankton bloom season; however, new community types appeared in the second half of

the time-series, possibly in association with the Pacific warm anomaly observed in 2014.

Individual operational taxonomic units (OTUs) were strongly correlated with environmental parameters, reflecting a successional pattern in OTUs following the spring upwelling. Seasonality was moderately repeatable in both the community as a whole and in individual OTUs, with long-term changes in BCC possibly linked to broader climatological phenomena.

In Chapter III, interactions between dissolved organic carbon (DOC) and bacterioplankton were examined during a diatom and *Phaeocystis* bloom in the SBC over 5 days following an upwelling event, encompassing phytoplankton physiological states from a healthy bloom through the onset of silicon (Si) stress. DOC bioavailability, bacterial growth, and BCC responses were assessed with dilution batch-culture bioassays. In these experiments, as the bloom state progressed: bacterioplankton DOC usage increased; bacterial growth efficiencies increased; and measureable DOC that accumulated during the bloom remained unutilized in the bioassays. Thus, DOC released by the plankton community during a bloom simultaneously contributes to several DOM pools of variable longevity.

In Chapter IV, the ecological role of carbon-rich DOM exuded by nutrient-stressed phytoplankton was assessed using DOM from four coastal diatoms following depletion of nitrogen (N), Si, or both N+Si. In bioassay experiments, short-term responses were affected both by diatom source species and by the nutrient stress under which the DOM was produced. Si-stress DOM was generally the most bioavailable over several days and led to higher bacterial growth efficiencies. However, the amount of diatom-derived DOC that persisted over months differed among source diatom species, with no evidence of a nutrient stress effect. The identity of the nutrient that terminates a phytoplankton bloom can therefore impact heterotrophic activity in the short term, while source phytoplankton species is more likely to influence DOC persistence in surface waters and its potential export.

TABLE OF CONTENTS

I. Introduction

Interactions between heterotrophic bacterioplankton and dissolved organic matter (DOM) comprise a critical juncture in the global carbon cycle. The carbon contained in oceanic DOM (~662 Pg; Hansell et al. 2009) is similar in magnitude to that present in atmospheric CO_2, suggesting that the ongoing anthropogenic perturbations to the latter reservoir have the potential to impact the former (Carlson and Hansell 2015). Around 50% of marine primary production is thought to pass through the dissolved phase, with phytoplankton instantaneous release spanning a potential range of 5-80% of total primary production, depending on the physiological state of the phytoplankton (Myklestad 2000; Nagata 2000). Correspondingly, bacteria are estimated to consume 50% or more of marine primary production (though mass balance is often problematic; Williams 2000). Furthermore, DOC can constitute a significant portion of carbon exported from the surface ocean into the mesopelagic: often under 20%, but up to 30-50% at particular sites (Carlson et al. 2001).

By virtue of their small size and high surface-area-to-volume ratio (Azam et al. 1983) heterotrophic bacteria and archaea are the primary consumers of marine DOM (Pomeroy 1974) [photochemical oxidation by short-wave sunlight chemically degrades an additional portion directly to CO_2 and CO (Mopper and Kieber 2002), and a poorly constrained pool of polysaccharides may form transparent exopolymer particles (TEP), with highly altered metabolic and biogeochemical implications (Passow 2002; Windecker 2016)], and thus the nature of their use of that DOM can have large-scale consequences. If bacteria use the DOM to build biomass, they act as a link in the marine food chain, returning what would otherwise be lost energy to the biological pool (Azam et al. 1983). In contrast, if they remineralize the DOM to its inorganic constituents while extracting energy for maintenance and movement,

1

they act as a sink, removing the energy held in the DOM from the system; however, this process simultaneously makes inorganic nutrients such as nitrogen and phosphorus available to primary producers (Ducklow et al. 1986). Bacterial "link" and "sink" functions thus both fulfill an important role in marine carbon biogeochemistry, and an understanding of the factors determining whether one or the other will predominate is critical to developing accurate models of the global carbon cycle.

A. Dissolved organic matter

DOM is conventionally defined as those organic compounds that pass through a glass fiber filter (Whatman GF/F; nominal pore size 0.7 μm), though for certain analyses specialized cutoffs such as a 0.2 μm membrane filter or a molecular weight in tangential flow filtration may be used (Hedges 2002). This definition encompasses a broad range of compounds, from truly dissolved small monomers to macromolecules and polymers to colloids (Hedges 2002), which are both dilute and difficult to isolate from seawater. Investigators have therefore historically focused on characterizing either bulk properties or specific pools of molecular types. Bulk characterization includes quantification of specific dissolved organic elements, particularly carbon (DOC), nitrogen (DON), and phosphorus (DOP) (Sharp 2002) and ratios thereof (e.g., Benner et al. 1997), as well as qualitative descriptors such as bioavailability measured through dilution batch-culture remineralization bioassays (e.g. Carlson et al. 2004) and source or age discerned from stable isotopic ratios (Benner et al. 1997; Bauer 2002; Guo et al. 2003) and radiocarbon dating (Bauer 2002; e.g., Santschi et al. 1995; Repeta and Aluwihare 2006). Individual pools frequently described include: amino acids (Keil and Kirchman 1993) and dissolved combined neutral sugars

(DCNS) (Borch and Kirchman 1997; Skoog and Benner 1997; Goldberg et al. 2009; Goldberg et al. 2010; Goldberg et al. 2011), characterized by high pressure liquid chromatography (HPLC); chromophoric dissolved organic matter (CDOM) measured by ultraviolet-visible light spectroscopy (Blough and Del Vecchio 2002; Nelson and Siegel 2002) and characterized by excitation-emission matrix spectroscopy (Coble 1996); and specific classes of biogeochemically or ecologically relevant compounds such as siderophores (Vraspir and Butler 2009) and phosphonates (Clark et al. 1998; Kolowith et al. 2001; Dyhrman et al. 2009).

More recently, advanced analytical techniques have begun to allow characterization of the molecular structure of the DOM pool as a whole. For example, mass spectrometry and nuclear magnetic resonance spectroscopy can be used to identify and quantify known constituents and small compounds such as metabolites or to provide a "fingerprint" analysis of the composition of the DOM pool (Mopper et al. 2007; Kujawinski 2011; Repeta 2015). One of the most striking results of these studies is the emphasis that thousands of compounds constitute marine DOM, regardless of whether the sample is dominated by fresh production or is deep ocean water composed of primarily refractory compounds (Repeta 2015). Although it is currently difficult or impossible to identify many of the compounds extracted from bulk seawater beyond the level of elemental composition and compound class (i.e., carbohydrates, proteins, etc.), these techniques can be used to track changes in DOM composition over space and time, or to characterize the results of microbial or abiotic processing (e.g., Kujawinski et al. 2009; Flerus et al. 2012) and to identify specific compounds for further study (e.g., Kujawinski et al. 2009; Fiore et al. 2015; Longnecker et al. 2015).

Not surprisingly, given its varied composition, marine DOM originates from a broad range of sources. The DOM source most relevant to this work is phytoplankton, which release DOM: through leakage, i.e., passive diffusion across permeable lipid membranes (Bjornsen 1988); as toxins or an allelopathic mechanism (Granéli and Turner 2006); and as a (hypothesized) carbon-rich photon shunt under high-light, low-nutrient conditions (Carlson 2002; see Chapter IV). Sources that are important DOM contributors but that will not be discussed further here include: zooplankton, through sloppy feeding, excretion, and dissolution of fecal pellets; viral lysis of algal and bacterial cells and bacterial lysis of algal cells; and bacterial solubilization of sinking particles (Carlson 2002: Carlson and Hansell 2015). In coastal regions, terrestrial runoff and subsidies from macroalgae, marshes, and estuaries can be locally important sources (Cauwet 2002; e.g., Moran et al. 1991); terrestrial-derived DOM is present but quite dilute in the open ocean (Meyers-Schulte and Hedges 1986; Opsahl and Benner 1997). In addition to consuming DOM, bacteria also produce an at times substantial amount, both through normal growth processes and death and dissolution (McCarthy et al. 1998; Kaiser and Benner 2008) and through active release of functional compounds such as siderophores (Vraspir and Butler 2009) and ectohydrolytic enzymes (Martinez et al. 1996) (though these released compounds may not be quantitatively significant).

DOC concentrations generally range between 50-80 μM in the surface ocean (with seasonal oscillations above the baseline concentration spatially variable and spanning undetectable levels to a range of 30 μM; Williams 2000) and 35-45 μM in the deep ocean (Benner 2002; Hansell et al. 2009). Coastal regions and estuaries, however, can easily reach millimolar DOC concentrations from inputs of allochthonous DOC (Hopkinson et al. 1998).

DON concentrations are generally 3.5-7.5 and 1.5-3.0 µM in the surface and deep oceans, respectively, while DOP concentrations are 0.1-0.4 and 0.02-0.15 µM (Benner 2002); marine DOM is therefore quite carbon-rich relative to the canonical Redfield ratio (C:N:P of 106:16:1) of its most common source, marine phytoplankton (Hedges et al. 2002). While components of freshly produced DOM may turn over on timescales of hours to days, more refractory compounds persist for years to millennia (Bauer 2002; Carlson 2002). For example, the mean age of DOM in the interior of the North Pacific has been radiocarbon dated at 6000 years (Williams and Druffel 1987), several times the measured duration of global ocean circulation. DOM resistance to degradation has been observed through short-term accumulation in field studies (Hansell 2002; e.g., Carlson et al 1994; Williams 1995; Halewood et al. 2012) as well as empirically demonstrated by experiments in which bacterial communities consumed a limited portion of DOM, even that from the euphotic zone (e.g., Carlson et al. 2004; Halewood et al. 2012) or appeared to be experiencing energy limitation *in situ* (e.g., Kirchman 1990). Though in reality its degree of reactivity is a continuum (Flerus et al. 2012), DOM can be conceptually divided into labile (turned over on scales of minutes to days), semi-labile (months to years), and refractory (centuries to millennia) subcategories (Carlson 2002; Hansell 2013); experimental approaches therefore assess processing of the longer-lived labile and shorter-lived semi-labile components. Various approaches indicate that the composition of the DOM pool changes with age, due to the effects of bacterial and photochemical degradation (Amon and Benner 1996; Mopper and Kieber 2002; Carlson et al. 2004; Goldberg et al. 2011).

The cause of what makes recalcitrant, deep-ocean DOM "recalcitrant" is still a matter of debate, in large part due to the relatively short time-scales of measured "recalcitrance"

5

tractable to laboratory analysis compared with those detected via DOM persistence in the field. Further, as noted by Hansell (2013), overall "recalcitrance" and the various pools on the labile to refractory continuum are at present only definable by DOM removal. The initial stages of DOM processing are relatively intuitive, as bacteria assimilate the least aged, most reactive DOM and leave behind more processed, less bioavailable compounds (Amon and Benner 1996). However, there remains a debate over what proportion of the DOM left behind, and which accumulates over time in the deep oceans, consists of the various posited source pools (Dittmar 2015; Moran et al. 2016): byproducts of microbial metabolism modified in a way that induces recalcitrance; compounds that are fundamentally bioavailable but too dilute for the bacterioplankton to access at an energetically favorable rate (Arrieta et al. 2015; Traving et al. 2015); molecules that are only recalcitrant in the context of the environment at the time of observation (Jiao et al. 2014); or compounds that simply never constituted a viable food source. For example, some phytoplankton are known to produce compounds inherently resistant to microbial degradation over scales of months, such as acyl heteropolysaccharides (Aluwihare and Repeta 1999). Over longer time-scales, the "microbial carbon pump" framework posits that repeated bacterial processing of DOM, as well as inputs of DOM sourced from bacterial cellular components via the viral shunt, gradually form a carbon-rich pool of recalcitrant DOM (Jiao et al. 2010). Microcosm experiments where simple sugars were transformed by a bacterial inoculum into complex "exometabolite" molecules resembling natural DOM indicate that this is mechanistically plausible (Lechtenfeld et al. 2015). Field surveys demonstrating the accumulation of fluorescent DOM, and the humic-like fractions in particular, in the ocean's interior in conjunction with increasing apparent oxygen utilization support the hypothesis of microbial generation of at

6

least a portion of the presumably moderately recalcitrant deep DOM pool (Yamashita and Tanoue 2008; Jørgensen et al. 2011).

A major loss mechanism for this recalcitrant DOM is the photobleaching that can occur when deep waters are brought to the surface through upwelling or ventilation. One of the effects of photobleaching is direct oxidation of DOM to CO and CO_2, which is estimated to occur in the oceans at a quantitatively significant rate, slightly exceeding that of the input of DOM from the world's rivers (Mopper et al. 2015). More importantly here, photobleaching can alter the bioavailability of DOM to bacteria by changing the structure of its molecular bonds and producing low molecular weight compounds, although the circumstances under which photobleaching increases or decreases availability and microbial processing are at present not fully constrained (Mopper et al. 2015). Photobleaching can thereby have additional downstream effects on the bacterial community through alterations of bacterial growth efficiency (e.g., Smith and Benner 2005) and community composition (e.g, Lønborg et al. 2016).

As knowledge of DOM concentrations and reactivity throughout the oceans continues to increase, many of the outstanding questions in marine DOM research aim to expand our understanding of how reactivity relates to source, age, and composition of specific, measureable pools, and how those multiple pools interact with microbial communities of in turn varying composition (Repeta 2015; Moran et al. 2016).

B. Bacterioplankton community activity

Historically, bacterioplankton communities have been considered as bulk aggregates, with much attention focused upon community-level bacterial production and cell abundance.

As techniques have been developed to open up the microbial "black box," however, the field has progressed towards traditional community ecology questions, such as: what controls distributions of individual phylotypes, and how do resource gradients impact and interact with community structure as well as function? Both approaches provide valuable insights into bacterial dynamics, and indeed, research that links the bulk processes and rates impacting biogeochemistry with community ecology and genomic analyses of distinct phylotypes will be key to refining our understanding of DOM processing and microbial carbon cycling.

At their most fundamental, bulk analyses of bacterioplankton communities begin with measures of the standing stock and production of biomass. Bacterial abundance (BA), or the concentration of individual cells, is generally constrained between 10^5 and 10^7 bacteria ml^{-1} in marine systems (Cole et al. 1988) by a combination of bottom-up and top-down factors. While BA increases in conjunction with chlorophyll *a* biomass, demonstrating the influence of bottom-up resources, BA only increases by two orders of magnitude in natural systems, while chlorophyll *a* spans three (Cole et al. 1988). This upper limitation or carrying capacity has been ascribed to top-down control by micrograzers such as flagellates and ciliates (Strom 2000) and by viruses (Fuhrman 2000).

Net bacterial production (BP) measures how much biomass a community (or, if normalized to BA, an average cell in the community) is synthesizing over time, extrapolated from incorporation of an amino acid, leucine (Kirchman et al. 1985), or a nucleotide, thymidine (Fuhrman and Azam 1982), which can be converted to carbon units through empirical conversion factors. In marine systems, BP values have been reported between roughly 0.05 and 8.5 μmol C L^{-1} day^{-1}, though the higher end of those values are most likely

from estuarine or bloom-influenced samples rather than from oligotrophic regions (converted from Cole et al. 1988). BP is positively correlated with primary production, chlorophyll *a* biomass, and bacterial abundance (Cole et al. 1988), and generally falls in the range of 10-20% of primary production in oceans (Ducklow 2000). The specific growth rate, or μ, is distinct from measures of BP, as it addresses increases in discrete cell numbers while BP deals in carbon units, though the parameters are mathematically and conceptually related. Growth rates are difficult to measure in natural environments without manipulations such as dilution and size fractionation to minimize grazing and are therefore less commonly reported than BP (Ducklow 2000); studies across a range of marine environments have found *in situ* community growth rates spanning an order of magnitude from 0.05 to 1 day^{-1} (Ducklow 2000), with cross-study mean values slightly below 0.1 day^{-1} (although measurement technique induces variability in the mean value; Kirchman 2016).

Bacterial growth efficiency (BGE) is the proportion of DOC taken up by bacteria that is used to build biomass rather than expended on maintenance and motility, or in traditional ecological terms, the assimilation efficiency. In natural bacterioplankton populations, BGE may span a range from as little as 1% up to 60% or higher, though values towards the lower end of this range are most common in marine settings (del Giorgio and Cole 1998), with one review reporting an open ocean mean of 15% and a coastal mean of 27% (del Giorgio and Cole 2000). Because BGE is the quantitative measure of the degree to which a bacterial community is functioning as a link or sink, much attention has been paid to exploring those factors that may influence it. In the definitive review on the subject, del Giorgio and Cole (1998) argue that the main determinant of BGE is the trophic status of the ecosystem in which it is measured, though teasing apart the relative importance of the concentration and

9

composition of organic substrates, the availability of nutrients, and the particular metabolic implications of different environments, communities, and mixtures of single-cell activity states has proved challenging. Other factors, such as temperature (Rivkin and Legendre 2001), abiotic stressors, and bacterial community richness, are supported by some studies but remain more controversial (Carlson et al. 2007). The assessment of bottom-up controls on BGE is further complicated by an apparent bacterial ability to partition DOC compounds of different quality between growth and respiration in a differential manner; in some circumstances, more labile DOC may not necessarily be used to directly increase production of bacterial biomass, as would be expected from the traditional understanding of controls on BGE, but rather may act primarily as an energy source to facilitate synthesis of biomass from poorer quality DOC (Guillemette et al. 2016).

C. Bacterioplankton community composition

Bacterial community composition is controlled by a broad range of physical, chemical, and biological factors. [While archaea are important contributors to the heterotrophic microbial community at depth and in certain regions of the surface ocean, in these studies they constitute a minority of the community, and the general term "bacterial" community composition is used herein for simplicity.] Standard ecological controls include bottom-up factors (i.e., nutrient and carbon substrate availability and composition), top-down influences of viruses (Fuhrman 2008; Breitbart 2012) and grazers (Jürgens and Massana 2008), and potentially competition with other bacterial phylotypes, though the latter is less well studied in the pelagic environment (Fuhrman and Hagström 2008). While individual bacterial cells may be responding to environmental cues at spatial and temporal resolutions

10

smaller than our ability to resolve using standard community analysis techniques (Stocker 2012), nonetheless evidence exists for the importance of a number of bottom-up drivers that act over larger scales amenable to sampling. Certain phylotypes, particularly the roseobacters, flavobacteria, and select *Gammaproteobacteria*, are positively associated with phytoplankton blooms, and these groups have been observed to demonstrate succession following phytoplankton bloom progression in a manner suggestive of niche partitioning (Amin et al. 2012; Teeling et al. 2012; Buchan et al. 2014). Potential physicochemical controls include salinity (e.g., Bouvier and del Giorgio 2002; Crump et al. 2004; Kirchman et al. 2005), pH (Yannarell and Triplett 2005), metal chemistry (Methé and Zehr 1999), light (as a stressor, e.g., Arrieta et al. 2000; Winter et al. 2001; or as an energy source, e.g., Béjà et al. 2000; Straza and Kirchman 2011), and climate- and weather-driven factors such as water-column structure (Nelson 2009; Nelson et al. 2014; Bryant et al. 2016). BCC has been shown to follow repeating annual cycles in diverse systems, presumably following seasonal transitions in some combination of these drivers (see further discussion in Chapter II). As is often the case in microbial ecology, investigating the importance of a given bottom-up factor independently is challenging, as many of the common marine bacterioplankton phylotypes remain unculturable (and even within groups with cultured representatives, some, such as SAR11, display a notable resistance to manipulation; Giovannoni and Stingl 2007), restricting the field to correlation analyses in field settings or experiments that manipulate the community as a whole.

The difficulty of assessing bottom-up controls in general, combined with the complexity of natural DOM pools, complicates quantifying the role of DOM in shaping BCC; however, there is growing evidence to support the concept that specific DOM

compounds support distinct heterotrophic communities. Some of the most clear-cut evidence

for interactions between DOM and BCC comes from manipulative experiments, where a

known or characterized DOM source is exposed to a known or characterized bacterial

community, leading either to changes in overall BCC or bacterial activity within the

experiments or to selective uptake of labeled DOM by particular phylotypes. Numerous

studies utilizing fluorescent *in situ* hybridization combined with microautoradiography have

shown that different clades preferentially take up different DOM compounds, even on broad

phylogenetic scales of class or sub-class (Cottrell and Kirchman 2000; Sarmento and Gasol

2012; see also those reviewed in Kujawinski 2011). [Recent work suggests that such

metabolic specialization may be reduced when high concentrations of labile DOC, in this

case phytoplankton exudate, are available; however, the concentrations of freshly produced

DOC observed to reduce specialization would rarely if ever be expected in oligotrophic

marine systems (Sarmento et al. 2016).] Other studies that have generated isotopically

labeled DNA or proteins or used –omics approaches have shown that this metabolic

selectivity extends to lower phylogenetic levels as well (McCarren et al. 2010; Nelson and

Carlson 2012; Bryson et al. 2016). Evidence also exists for specific taxa that act as

generalists and can utilize diverse compounds (Mou et al. 2008; Gómez-Consarnau et al.

2012; Pedler et al. 2014), possibly related to the practice of a copiotrophic (or patch-

associated, in alternative terminology), rather than oligotrophic (or free-living), lifestyle

(Lauro et al. 2009; Yooseph et al. 2010; Luo and Moran 2015; Kirchman 2016). Increasingly,

sequenced genomes, including those from single isolated cells, and –omics techniques are

strengthening these observations by providing evidence for the presence or expression of

distinct metabolic genes (that is, transporters and genes associated with degradation

pathways, such as dehydrogenases and hydrolases) in distinct bacterial taxa (Newton et al. 2010; Gifford et al. 2013; Swan et al. 2013). A relatively new approach addresses the question from the opposite direction, demonstrating variability in the composition of the DOM remaining after incubation with different bacterial communities, with low molecular weight DOM generally universally available but utilization of high molecular weight DOM more related to BCC (Logue et al. 2016).

Recent improvements in sequencing technologies have greatly and rapidly increased our ability to sample larger numbers of bacterial communities, and to sample those communities to a greater sequencing depth, in the context of both –omics techniques and the more traditional 16S ribosomal RNA (rRNA) gene amplicon sequencing. One of the results of the increased accessibility of sequencing has been a series of projects conducting ambitious sampling transects across the surface ocean, expanding from the first exploratory metagenomes in the Sargasso Sea (Venter et al. 2004) to the Global Ocean Sampling Expedition (Rusch et al. 2007) and the *Tara* Oceans Expedition (Sunagawa et al. 2015). These projects have provided insight into microbial biogeography and potential controls on community structure on basin scales (Rusch et al. 2007; Sunagawa et al. 2015; Villar et al. 2015) and have begun to be used to address biogeochemical questions (Guidi et al. 2016), as well as establishing extensive reference databases of microbial genes and their distributions. Other studies have leveraged abundant sequences to investigate associations between planktonic taxa at unprecedented resolutions, suggesting that suites of co-occurring phylotypes respond to similar, or at least synchronous, environmental drivers (Gilbert et al. 2012; Lima-Mendez et al. 2015; Needham and Fuhrman 2016).

While much progress has been made towards understanding the driving forces behind bacterial community structure and activity in the past several decades, in many ways the same improvements in analytical techniques that have allowed for these broad understandings have also raised more detailed questions about BCC and the scale at which we study it. One example of this is the improved ability of new sequencing approaches to detect the relatively abundant members of the rare biosphere (sometimes defined as those taxa comprising less than 0.1% of the total community, though this is arbitrary: Fuhrman 2009; Lynch and Neufeld 2015), accompanied by an increased appreciation for the role of "conditionally rare" microbes as a diverse seed bank capable of responding to changing environmental conditions (Shade et al. 2014; Lynch and Neufeld 2015). [It is worth noting that, from a broader ecological perspective, a relatively shallow sequencing depth is effectively sufficient to resolve changes in community structure in response to bottom-up drivers or across large ecological gradients (that is, there are diminishing returns to obtaining increasing numbers of sequences for strictly large-scale ecological questions: Kuczynski et al. 2010; Caporaso et al. 2011), which here is related to the high richness but low evenness characteristic of marine bacterial communities (Sogin et al. 2006; Kirchman 2016).] However, this increased sequencing depth raises the question of when those rare taxa are relevant to addressing ecological questions; for investigations into bottom-up controls on BCC, such relevancy largely rests on determination of whether a rare taxon is active at a given point in time, rather than dormant or in endospore stage, which simple DNA surveying cannot determine. Comparisons of rRNA and the corresponding DNA have shown that some members of the rare biosphere are active while present at low abundance, but the level of activity vs. dormancy can vary widely between taxonomic groups (Jones and Lennon 2010;

Campbell et al. 2011). Another outstanding question is the taxonomic resolution necessary for sampling – specifically, to what degree sub-species variation, for example that seen between ecotypes, matters for community structure or function. The drivers behind single phylotype or ecotype dynamics have been extensively explored in a few specific cases (e.g., SAR11: Carlson et al. 2009; Salter et al. 2015; and *Prochlorococcus*: Johnson et al. 2006; Chandler et al. 2016; and linked to genomic variations: Brown et al. 2012; Kashtan et al. 2014) but the vast majority of these finer-scale taxa remain ecologically uncharacterized, with studies frequently pooling operational taxonomic units (OTUs; traditionally defined as 97% similarity in 16S rRNA gene composition) when discussing community composition at the genus level or higher. Some argue that this overlooks too much, potentially functionally significant diversity [e.g., Kleindienst et al. (2016) found that sub-OTU level differences in 16S rRNA sequences correlated with environmental parameters] but the correct taxonomic resolution to target remains an open question and may well continue to vary, depending on the study question, for the foreseeable future.

Ultimately, from an ecosystem function perspective, the hope is that improved accessibility afforded by the rapid decrease in costs of next-generation sequencing technologies, and the resulting feasibility of –omics approaches, may allow us to address the relationship between phylogeny and function in a more decisive manner: that is, to better discern generalists from specialists, and to identify what those specialists specialize in (Jansson et al. 2012). In particular, advances in molecular techniques that better link biogeochemical processes to traditional ecological inquiries such as community composition and to the roles of individual populations will address some of the currently most intriguing questions in microbial ecology (Giovannoni and Rappé 2000; Fuhrman 2009), as well as

point towards unexpected areas of inquiry. Molecular approaches have, for example, shown the existence of a "cryptic" sulfur cycle in oxygen minimum zones that produces sulfur species too transient to detect by traditional biogeochemical measurements (Canfield et al. 2010). Likewise, metagenomic surveys have revealed unexpectedly widespread and diverse proteorhodopsin genes in bacteria and archaea, greatly expanding potential energy flows in the euphotic ocean (reviewed in Fuhrman and Steele 2008). Finally, beyond improving our basic ecological understanding of the processes underpinning marine microbial ecosystems, developing a more predictive relationship between community structure, metabolic function, and ecosystem characteristics will also improve models of carbon fluxes through the microbial pool (Yokokawa and Nagata 2010), which will become increasingly critical in the coming decades as the effects of climate change impact bacterial-DOM interactions (Moran et al. 2016).

D. Santa Barbara Channel

The studies discussed herein were conducted in, or utilized seawater and bacterial communities obtained from, the Santa Barbara Channel (SBC), California, USA (see Figure 3.1 in Chapter 3). This system is particularly amenable to these investigations due to both marine and general climatological phenomena. Although the SBC is a coastal system, it experiences minimal terrestrial influence as a result of low precipitation the majority of the year, with the exception of localized freshwater and sediment plumes from winter storm events (Otero and Siegel 2004), and, while highly productive (Kostadinov et al. 2007), features gyre-level concentrations of DOM (Halewood et al. 2012; Carlson and Hansell 2015) rather than the elevated allochthonous load typical of nearshore waters. In addition, the

SBC experiences reliable spring upwelling leading to a pronounced phytoplankton bloom

(Otero and Siegel 2004; Antoine et al. 2011; Brzezinski and Washburn 2011), as well as

seasonally variable circulation reflected in alternating equatorward and poleward flow and an

episodic cyclonic eddy (Winant et al. 2003), all of which contribute to observed variability in

DOM composition (Halewood et al. 2012). These phenomena have been characterized for

two decades by the Plumes and Blooms program

[http://www.oceancolor.ucsb.edu/plumes_and_blooms] and for fifteen years by the Santa

Barbara Coastal Long Term Ecological Research project [http://sbc.lternet.edu] cruises, and

several decades of primarily physicochemical data with lower spatial resolution are available

from the California Cooperative Oceanic Fisheries Investigations (CalCOFI;

http;//calcofi.org). This combination of a dynamic yet well-understood system facilitates both

studies that contrast a wide range of bacterial-DOM states and studies that depend upon

locating particular *in situ* conditions.

Chapter II: Annual upwelling and stratification underlie temporal variability in free-living prokaryotic communities in a productive California coastal system

Abstract

Prokaryotic community composition (here, BCC for historical consistency) and metabolic activity were measured over four years in the Santa Barbara Channel (California, USA), a heterogeneous coastal upwelling system. BCC showed the greatest variability over depth, driven by a ten-fold increase in the relative abundance of archaea between the surface and 75 m. At the surface, the seasonal cycle resulted in significantly greater UniFrac distances than spatial variability within cruises. When clustered by UniFrac distance, community types showed repeating patterns following the annual upwelling and phytoplankton bloom season; however, the system experienced a shift in the second half of the time-series, with new community types appearing, possibly in association with the Pacific warm anomaly observed in 2014. Individual operational taxonomic units (OTUs) were strongly correlated with parameters such as temperature, chlorophyll a, and bacterial production, both when sampled simultaneously and when examined over time lags, reflecting a successional pattern in OTUs following the spring upwelling. Shannon diversity and abundance-weighted phylogenetic diversity at the surface were highest during periods of recent upwelling and phytoplankton blooms, and were associated with higher bacterial production; Chao1 estimated richness was more noisy than diversity measures and was generally greater during the fall and winter stratified period. Overall, seasonality as set by upwelling was clear and moderately repeatable in both the community as a whole and in the

18

relative abundance of individual OTUs, with long-term changes in BCC potentially linked to broader climatological phenomena.

Introduction

The importance of physical controls, and their subsequent effects on bottom-up factors like inorganic resource delivery and subsequent organic matter production by phytoplankton, in driving succession in microbial OTUs and thereby prompting repeatable annual patterns in BCC, have been demonstrated in numerous oceanic time-series studies (Bunse and Pinhassi 2017). The seasonally oligotrophic Bermuda Atlantic Time-series Study site, BCC dynamics are ultimately driven by annual patterns of deep winter mixing, with BCC following the resource dynamics of the subsequent phytoplankton bloom and stratification (Morris et al. 2005; Carlson et al. 2009; Treusch et al. 2009). Temperate coastal systems, at least those removed from estuaries and other terrestrial influence, show similarly recurring annual patterns (Fuhrman et al. 2006; Gilbert et al. 2012). In contrast, at sites that have more subtle seasonal cycles, such as that observed at the Hawai'i Oceanic Time-series (Eiler et al. 2011), the influence of short-term physical factors such as wind-driven mixing on BCC are more prominent (Bryant et al. 2016). BCC can also respond to discrete events affecting resource availability on timeframes shorter than seasonal scales. For example, Teeling et al. (2012) observed changes in BCC over days during a strong phytoplankton bloom in the North Sea, and Wear et al. (2015) saw similar shifts in BCC and bacterial production over the build-up of a diatom bloom in the coastal Santa Barbara Channel.

Studies of pelagic marine systems have found basin-scale spatial patterns in BCC that primarily follow broad physicochemical gradients (e.g., Morris et al. 2012). Those explicitly

looking at spatial distance as a driving factor of BCC tend to do so over scales that are so large as to span multiple biogeochemical provinces (Sunagawa et al. 2015; Milici et al. 2016). However, open ocean bacterioplankton may vary spatially over 10s of kms, potentially reflecting the mixing effects of mesoscale features (Hewson et al. 2006; Nelson et al. 2014). On a global scale, coastal regions show greater overall heterogeneity in BCC than open-ocean systems (Zinger et al. 2011), raising the possibility of an interactive effect between more dynamic bottom-up resources and greater effects of spatial heterogeneity on BCC in the near-shore environment.

To examine both the role of bottom-up controls on BCC and the relative importance of, and interactions between, spatial and temporal variability, we sampled a seven-station transect spanning the western Santa Barbara Channel (SBC), California, USA, on the Plumes and Blooms (PnB) cruise line (Fig. 2.1; Henderikx Freitas et al. in prep), for greater than four years. The SBC experiences strong shifts in physical states over the annual cycle, including seasonal and episodic, wind-driven upwelling events; a seasonal internal eddy; and incoming currents from the north and south that trade off over the course of the year and can be opposing across the north-south axis of the SBC (Harms and Winant 1998). These phenomena set up a strong cycle of physicochemical and biological properties featuring upwelling-driven phytoplankton blooms in the spring and stratified, more oligotrophic conditions in the late summer and fall (Otero and Siegel 2004). Previous work over the shallow continental shelf in this system has shown that bacterial production and abundance closely follow these physical drivers over an annual cycle, mediated by organic matter dynamics (Halewood et al. 2012). Because the PnB cruise line spans the spatially distinct physical features of the SBC in addition to capturing its seasonality, it potentially samples

greater heterogeneity than its time-series neighbor to the south, the San Pedro Ocean Time-Series, which features highly predictable BCC over an annual cycle (Fuhrman et al. 2006).

In this study, we compared the extent of variability in BCC over scales of time, transect distance, and depth, and further investigated the role of seasonality in BCC. We examined how bottom-up drivers correlate with the community as a whole and with particular OTUs. Finally, we asked whether diversity metrics and secondary productivity follow similar patterns in spatiotemporal variability and bottom-up correlates as BCC.

Methods

Sample collection

Samples were collected approximately monthly on 43 cruises between July 2010 and September 2014 on the Plumes and Blooms (PnB) cruise program (Antoine et al. 2011; Henderikx Freitas et al. in prep; http://www.oceancolor.ucsb.edu/plumes_and_blooms) in the Santa Barbara Channel (SBC), CA, USA (Fig. 2.1). The PnB transect encompasses 7 stations between the northernmost Channel Islands and the mainland to the north, with the two end stations over the shallow continental shelf and the remainder at sites between ~260 and 540 m bottom depth. Samples were collected for BCC (see Table 2.1 for sampling depths at each station) and bacterial production from Niskin bottles mounted on a sampling rosette. On some cruises, only partial transects were collected due to poor weather or mechanical issues.

Bacterial community composition (BCC)

BCC samples were collected from the Niskin bottles in acid-washed and sample-rinsed 2 L high-density polyethylene bottles with drainage ports on the bottom (Nalgene) stopped with a one-way valve. The seawater was stored in the dark in a cooler at ambient

temperature until return to shore, where it was processed within 10 hours of collection (with the longest storage time for the outermost station, Stn. 7). Samples were pre-filtered through a 1.2 µm filter in a polycarbonate filter holder (to remove particle-attached bacteria and microphytoplankton) then collected on a 0.2 µm polyethersulfone filter cartridge (Sterivex-GP; EMD Millipore, Darmstadt, Germany) under gentle peristaltic pressure (~1L pumped per 20 minutes) and stored frozen at -40°C. For samples collected from 75 m and above, 1 L was filtered; from 150 m and below, 2 L were filtered.

Samples were lysed in sucrose lysis buffer (40 mM EDTA, 50 mM Tris-HCl, 750 mM sucrose, 400 mM NaCl, pH adjusted to 8.0) with 1% w/v sodium dodecyl sulfate and 0.2 mg mL^{-1} proteinase-K at 55° C. Genomic DNA was extracted with a commercial silica centrifugation kit (DNEasy, Qiagen, Valencia, CA) and used to conduct dual-index multiplex amplicon sequencing following a modified protocol of Kozich et al. (2013). PCR reactions (25 µL) were conducted with 3 µL genomic DNA using 0.4 µM each of primers targeting the V4 hypervariable region (515F-Y, Parada et al 2016, and 806RB, Apprill et al. 2015, with adapter and index construction following Kozich et al. 2013), 12.5 µL Kapa Robust 2G HotStart MasterMix (Kapa Biosystems; Wilmington, MA), and PCR water (5 Prime; Hilden, Germany). Reactions were cycled for 3 minutes at 95°C; 30 cycles of 30 seconds at 95°C, 30 seconds at 65°C, and 1 minute at 72°C; and 10 minutes at 72°C. PCR product was cleaned and normalized using SequalPrep plates (Invitrogen, Carlsbad, CA), pooled by equal volumes, and concentrated using Amicon Ultra 30K tubes (EMD Millipore). Amplicons were sequenced on an Illumina MiSeq using PE250 v2 chemistry at the University of California, Davis DNA Technologies Core.

Sequence analysis was conducted in mothur (v1.38.0; Schloss et al. 2009). Quality-controlled sequences were aligned to a non-redundant subset of the SILVA SSU Ref16S alignment database (v115; Quast et al. 2013) curated as in Nelson et al. (2014). Chloroplast sequences were removed, and samples were sub-sampled to 1000 sequences, with those containing fewer than 1000 sequences removed from analysis. Sequences were assigned to operational taxonomic units by abundance-based greedy clustering in VSEARCH (Rognes et al. 2016) at the 97% similarity level, and OTUs were classified at the 70% confidence level. The most abundant OTUs at the surface and 75 m were defined as those comprising on average 1% or more of total BCC at their respective depth. Weighted UniFrac (Lozupone and Knight 2005) was used to calculate phylogenetic distances between samples. UniFrac distance explicitly incorporates phylogenetic relatedness by defining community distance as the proportion of unshared to total branches in a taxonomic tree of the OTUs in two samples, such that less closely related OTUs are more influential in the distance measure; weighted UniFrac incorporates the relative abundance of those OTUs (Lozupone and Knight 2005).

We used a variety of diversity and richness parameters to characterize different aspects of bacterial community biodiversity. Shannon diversity and bias-corrected Chao1 estimated richness (Chao 1984) were calculated in mothur. Phylogenetic diversity measures, including unweighted Faith's phylogenetic diversity (PD; Faith 1992) and abundance-weighted phylogenetic diversity (or balance-weighted PD, BWPD; McCoy and Matsen 2013), were calculated in guppy (McCoy and Matsen 2013) using output from an independent bioinformatics pipeline executed through pplacer (Matsen et al. 2010) as described in Goldberg et al. (in review). Phylogenetic diversity measures were thus based on

a different OTU calling approach than the rest of the data and should be interpreted cautiously.

Bacterial production

Bacterial production (BP) was measured on whole-water samples that were aliquoted from the DNA collection bottles where applicable. Additional samples were collected in 30 mL, acid-washed and sample-rinsed, polycarbonate centrifuge tubes at all depths at Station 4 (Table 2.1); when this resulted in duplicate BP with aliquots from DNA bottles, the median is reported. BP was measured via tritiated leucine incorporation (^{3}H-Leu; specific activity 54.1-58.5 Ci/mmol; Perkin Elmer, Boston, MA) using a modified microcentrifuge method as in Halewood et al. (2012). Samples were spiked to a mean final concentration of 16.5 nmol L^{-1} ^{3}H-Leu (preliminary experiments showed that SBC bacteria saturate above 10 nmol L^{-1}) and incubated in the dark for 1-3 hours in laboratory seawater. ^{3}H-Leu incorporation was converted to bacterial carbon production (BP) using a conversion factor of 1.5 kg C (mol leucine)$^{-1}$ (Simon and Azam 1989). As the laboratory seawater differed in temperature from the sampling location (generally warmer, particularly relative to samples collected below the euphotic zone), the directly measured BP is more correctly seen as potential BP, and therefore we adjusted measured rates of BP (BP$_{meas}$) using *in situ* temperature and a Q10 conversion of 1.5 (Rivkin et al. 1996) to estimate *in situ* BP (BP$_{Q10}$):

Equation 1: $BP_{Q10} = 10\char`^[\log(BP_{meas}) - (\log(1.5) * (temp_{incubation} - temp_{in\ situ})/10))]$

Environmental data

Ancillary data obtained from the Plumes and Blooms program included physical data; inorganic nutrients; phytoplankton variables including chlorophyll *a*, accessory pigments

measured by high performance liquid chromatography, and particulate organic carbon and nitrogen (POC and PON); and chromophoric dissolved organic carbon (CDOM) (Henderikx Freitas in prep; CDOM as in Barrón et al. 2014). The CDOM spectral slope coefficient (S) over 320-420 nm was calculated following Stedmon et al. (2000). Because PnB is primarily an ocean color program, the environmental data are richest at the surface and therefore much of our investigation into bottom-up drivers is likewise focused there.

Statistical analyses

Statistical analyses were conducted in SPSS Statistics v24 (IBM), Primer v6 (Clarke and Gorley 2006), and JMP Pro 12.0.1 (SAS Institute Inc.). Spatial figures were prepared in Ocean Data View v4 (R. Schlitzer; http://odv.awi.de); additional figures were prepared in Prism 7 (GraphPad Software Inc.). All correlations included here are nonparametric Spearman's *rho* unless indicated otherwise.

Data availability

PnB environmental data were curated as in Henderikx Freitas (in prep) and will be available through the Santa Barbara Coastal LTER data archive (http://sbc.lternet.edu//data/), as will be BP and analyzed sequencing results from this study. Raw sequencing output is available in the NCBI Sequence Read Archive, Accession Number PRJNA379850.

Results

After quality control, 581 samples that sequenced successfully contained 1067 - 18764 sequences per sample (mean = 7300, median = 7270) prior to sub-sampling to 1000 sequences. Three samples were subsequently identified as outliers and removed from analysis. The subsampled sequences clustered into 8098 OTUs at 97% similarity, of which

2212 were present in 2 or more samples; there were 50-192 OTUs per sample, with a median of 118.5.

The 18 most abundant surface OTUs (that is, those constituting an average of 1% or more of overall BCC) included representatives of the oligotrophs *Alphaproteobacteria* SAR11 Surface 1, SAR11 Surface 2, and AEGEAN-169 group, as well as traditionally r-selected, copiotrophic groups such as the *Roseobacter* NAC11-7, *Gammaproteobacteria* including SAR86 and SAR92, and assorted *Flavobacteria* (Table 2.2; where they are defined as OTUs S1-S18). The 15 most abundant OTUs at 75 m included representatives of the *Thaumarchaeota* Candidatus *Nitrosopumilus* and an unclassified Marine Group I OTU; the *Alphaproteobacteria* SAR11 Surface 1; and the *Gammaproteobacteria Oceanospirillales* ZD0405 (Table 2.2; D1-D15). Four OTUs met the mean 1% relative abundance cutoff at both the surface and at 75 m: SAR11 Surface 1, *Roseobacter* NAC11-7, SAR11 Surface 2, and *Oceanospirillales* ZD0405. These abundant OTUs were present in the majority of samples (75% or more of discrete samples at their respective depths; Table 2.2), although their relative abundance within samples fluctuated greatly.

The time-series encompassed four full annual cycles in the SBC, with a progression from spring upwelling (indicated by low surface temperature and high surface nitrate concentrations, Fig. 2.2A and B; Fig. 2.3A and B), through subsequent phytoplankton blooms, dominated by diatoms as indicated by chlorophyll *a* and fucoxanthin (Fig. 2.2C and D), and stratification in the late summer through fall (in the sense that high surface temperatures coincide with a larger thermal gradient between surface organisms and nutrient-rich deeper waters, though the mixed layer depth not necessarily shallower, Fig. 2.2A; Fig. 2.3A and B). CDOM spectral slope (CDOM *S*), which was used here as an approximation of

26

dissolved organic matter quality as a substrate for the free-living prokaryotic community, was generally lowest (indicating the freshest, likely most bioavailable DOM; Blough and Del Vecchio 2002) during the spring phytoplankton bloom periods (Fig. 2.2E). This is consistent with the decrease in CDOM *S* seen in conjunction with an increase in DOC bioavailability over a diatom bloom in the SBC (Wear et al. 2015) and is also consistent with the low terrestrial influence on CDOM in the SBC (Barrón 2014).

Scales of variability in BCC

The primary factor explaining overall BCC variability within the total sample pool was depth (Fig. 2.4A; Fig. 2.5A), with UniFrac distances between surface samples and corresponding samples at 75 m or below significantly larger than those of any spatial or temporal comparisons (Tables 2.3 and 2.4). The large community shifts over depth were associated with a strong increase in the relative abundance of archaea (Fig. 2.6), which would be expected to increase the UniFrac distance substantially through incorporating community members from two Domains. Archaea increased over depth from a mean relative abundance of 2.9% of surface prokaryotic communities to 38.5% at 75 m and 45.7% at 300 m (Fig. 2.6).

Temporal variability at the surface was the next largest scale of community variability (Fig 2.4B; Fig. 2.5B). Temporal patterns were examined by taking the mean of the three center stations (Stations 3-5), as the center of the SBC was expected to be the most similar within cruises, based on prior studies of biological parameters across the PnB transect (e.g., Krause et al. 2013). Strong seasonality in BCC was demonstrated by the significantly higher UniFrac distances at three month and six month lags (effectively comparing between seasons) than at one month and one year lags (Tables 2.3 and 2.4). This scale of variability in UniFrac distance is consistent with the timescales of the strong temporal variability in the

physics and subsequent bottom-up factors in the SBC (Fig. 2.2A-F). When all pairwise

comparisons in UniFrac distance were plotted against their respective time-lags, the resulting

curve was a sine wave with a period of approximately one year up through roughly a two-

year lag (Fig. 2.7A), after which the pattern became much noisier.

The temporal variability at 75m was dampened relative to that seen at the surface

(Fig. 2.4C; Fig. 2.5C). There were still significantly greater mean UniFrac distances at 3

month and 6 month lags than at a 1 month lag (Tables 2.3 and 2.4), and the annual cycle

across all pairwise comparisons was still apparent up through roughly a 1.5 year time-lag,

although the amplitude of the overall pattern was muted relative to that at the surface (Fig.

2.7B).

Within-cruise spatial variability was the least important dimension examined. (Station

1 was omitted from analyses of spatial variability, as its frequent relatively large UniFrac

distance from neighboring Station 2 could be plausibly influenced by proximity to a kelp bed

and a natural oil seep, rather than reflecting the more pelagic processes considered in this

dataset.) When defined strictly as the UniFrac distance between points on opposite sides of

the SBC, spatial variability was less than that of temporal variability at both the surface and

the 75 m depth horizon (Fig. 2.5D). However, this approach obscures the true scale of spatial

heterogeneity, as we only saw a traditional, linear distance decay relationship at the surface

in 13 out of 42 cruises where there was sufficient data to evaluate it and in 18 of 39 cruises at

75 m (Fig. 2.8); rather, the pattern of UniFrac distance moving south from Station 2 was

often nonlinear, showing a sawtooth or concave pattern, consistent with the known eddy

dynamics and variable current patterns in the SBC. The greatest UniFrac distance observed

between any two samples at the surface (again omitting Station 1) within cruises was

significantly larger than the UniFrac distance between endpoints the surface, but still

significantly smaller than inter-seasonal variability (Tables 2.3 and 2.4); at 75 m, the greatest

observed spatial variability was not significantly different than temporal variability.

Therefore, while there is a measureable level of spatial variability within cruises in the SBC,

it is less important to understanding BCC dynamics at the surface than the temporal

progression and will not be examined in detail here.

Seasonal succession and bottom-up correlates of community as a whole

To examine bottom-up correlates of the community as a whole, surface samples were

restricted to those with a comprehensive suite of ancillary measurements (205 out of 287

total surface samples; those with measurements of temperature, salinity, inorganic nutrients,

chlorophyll *a*, POC and PON, phytoplankton pigments, BP_{Q10}, and CDOM slope). A BIO-

ENV test identified BP_{Q10} and temperature as the best-fit variables to the UniFrac distance

matrix, albeit with a weak overall correlation (Spearman's R = 0.339). Because far fewer

parameters are measured at 75 m, only temperature, salinity, and BP_{Q10} were examined

(available for 163 out of 199 total 75 m samples); BIO-ENV identified BP_{Q10} alone as the

best correlate with BCC (R = 0.484).

To examine community seasonality on a more refined scale, surface BCC samples

were clustered based on UniFrac distance (Fig. 2.9A) and groups for further examination

were selected at a UniFrac distance of 0.35, yielding 7 groups containing between 2 and 105

samples. There were clear temporal patterns to the presence of the groups in the SBC (Fig.

2.9B), corresponding to the magnitude of environmental parameters associated with each

group (Fig. 2.9C). This is an intentionally qualitative analysis designed to identify the major

parameters that co-vary with the bacterial communities. Mean environmental and OTU

values are presented in Tables 2.5 and 2.6, but we are focusing here on the relative differences in those values between UniFrac groups. Group B was associated with recently upwelled water and was only present during temperature minima; it had high levels of OTU S1 (SAR11 Surface 1, as in Table 2.2) and notably low levels of any of the more copiotrophic OTUs. Groups E and F were associated with phytoplankton blooms; Group F was present annually shortly after upwelling, while Group E was an outlier that was only observed during one cruise. Copiotrophic OTUs were particularly abundant in Group F, including OTU S3 (*Roseobacter* NAC11-7), S7 (a member of the *Alteromonadaceae*), S8 (SAR92), and S13 (*Polaribacter*), associated with moderate Shannon diversity but low Chao1 richness and very low PD. Group G represented a medium level of resources (moderate levels of BP_{Q10}, POC and CDOM *S*), with moderate levels of the same copiotrophs seen in Group F but also increased relative abundance of OTUs such as S6 and S9 (both SAR86). Group G had high levels of Shannon diversity and PD but only moderate BWPD and Chao1 richness; however, Group G contained the most disparate assortment of communities, as grouping at a lower UniFrac distance level would subdivide Group G first (Fig. 2.9A).

Groups C and D both represented communities associated with the warm, stratified summer and fall periods; of these two, only Group C was present during the first half of the time-series, while starting in mid-2012 Groups C and D traded off over time and sometimes co-occurred within a cruise (Fig. 2.9B). Group C had lower relative abundances of OTUs S1 (SAR11 Surface 1) and S2 (SAR11 Surface 2) and higher relative abundances of S4 (AEGEAN-169), S5 (SAR11 Surface 4), and S9 (SAR86) than did Group D, which had a much lower mean Shannon diversity index, BWPD, and PD than Group C.

Group A was an outlier, containing only 7 samples, all of which came from August 2014 (the same samples which are visible outliers in the surface NMS plot, Fig. 2.4B). The main OTU differentiating this group was S16, *Synechococcus*. S16 was present at other dates in the time-series (Fig. 2.10E), albeit at much lower relative abundances. Group A also had higher relative abundances of two *Flavobacteria*, S12 and S14 (NS5 group).

Individual patterns of abundant OTUs

Patterns of relative abundance of individual OTUs at the center three stations were examined over time (Fig. 2.10). Several OTUs showed clear seasonality in relation to temperature (indicative of the transition from upwelling to stratified conditions). For example, OTU S3, the *Roseobacter* NAC11-7, always reached a maximum in relative abundance during or slightly after upwelling, while S2, SAR11 Surface 2, generally was most abundant when the temperature was highest and stratification greatest.

This seasonality was also apparent in a cross-correlation analysis between the most abundant surface OTUs at the center three stations and a subset of environmental parameters sampled simultaneously and 1, 3, and 6 months prior to the BCC sample (Fig. 2.11A). As expected, many OTUs were strongly correlated with environmental parameters from the same month. A smaller number showed strong time-lag patterns related to upwelling, with consistent positive or negative correlations at 1 and sometimes 3 month lags, and the opposite sign correlation at 6 months. For example, OTU S2, SAR11 Surface 2, which was most abundant during the warm stratified period (Fig. 2.10A), was positively correlated with simultaneous temperature and temperature at 1 and 3 month lags but negatively correlated with temperature at a 6 month lag (Fig. 2.11A).

We also observed temporal succession amongst the most abundant OTUs (Fig. 2.10). For example, peak abundances of S6, SAR86, often followed peak abundance of S3, the *Roseobacter* NAC11-7, by about a month, while peak abundance of S4, AEGEAN-169, in turn generally lagged that of S6. However, these apparent successional patterns were generally not significant when examined as cross-correlations of a subset of the surface OTUs (Fig. 2.11B), with simultaneous correlations stronger than those seen over time lags. This is likely due to the strongly episodic nature of the peaks in abundance of these OTUs, in particular the copiotrophic OTUs such as *Roseobacter* and SAR86. For most of the annual cycle, the OTUs are present at low relative abundance, as seen in Fig. 2.10, thereby diluting out the statistical significance of successional patterns over two to three months when succession is examined by correlations incorporating the full time-series.

Community diversity and richness metrics

We used several diversity and richness parameters that describe different aspects of BCC. None of these metrics are necessarily more correct than the others, but rather they address fundamentally different questions. Shannon diversity is the classic diversity measurement that incorporates richness and evenness of OTUs within a sample. The two phylogenetic diversity parameters, BWPD and PD, are calculated in a way that explicitly accounts for the relatedness of the OTUs in a sample, by placing OTUs on a phylogenetic tree and using branch lengths to assess diversity. BWPD is a phylogenetically aware alternative to Shannon diversity, which weights a summation of tree branch length over subdivisions by the evenness of OTU distribution within that tree (McCoy and Matsen 2013). Traditional PD (Faith 1992) is unweighted by abundance and therefore does not incorporate evenness. PD is included for comparison with earlier time-series work (e.g., Gilbert et al

32

2012). Despite its name, without weighting by relative abundance, PD is more accurately a descriptor of phylogenetic richness, in the traditional ecological sense of the word. Chao1 estimated richness uses the ratio of singlet sequences (only present once in the sample) to doublet sequences (present twice) to assess thoroughness of sequencing depth, and from there corrects the observed OTU richness to that expected if the sample were sequenced to the depth where all OTUs were captured (Chao 1984; Hughes et al. 2001).

Shannon diversity was between 1.84 and 3.74 at the surface, with a mean of 2.93 (Fig. 2.12A); diversity increased with depth, to means of 3.27 at 30 m and 3.54 at 75 m, before leveling off at 3.63 at 150 m and 3.58 at 300 m (Fig. 2.12B). The lowest Shannon diversity values at the surface were generally in the late summer and fall and the greatest were in spring and early summer, although there was substantial variability around that trend, particularly in 2014. Shannon diversity was weakly but significantly correlated with environmental parameters indicating higher diversity during recent upwelling and phytoplankton blooms (Table 2.7).

BWPD was between 0.31 and 1.64 at the surface, with a mean of 1.04 (Fig. 2.12C); it increased over depth, primarily within the euphotic zone, to means of 1.27 at 30 m, 1.50 at 75 m, 1.51 at 150 m, and 1.55 at 300 m (Fig. 2.12D). As with Shannon diversity, BWPD correlates indicated higher phylogenetic diversity during upwelling and phytoplankton blooms, with higher correlation coefficients than those seen with Shannon diversity (Table 2.7); this was reflected in higher BWPD values during the spring and early summer, with the exception of 2014 when BWPD showed no clear seasonality. BWPD and Shannon diversity were significantly positively correlated at the surface (R = 0.664; Table 2.7) but were negatively correlated at 75 m (R = -0.449; N = 190; p <0.0001).

Chao1 estimated richness was between 59.2 and 294.6 OTUs at the surface, with a

mean of 158.7 OTUs (Fig. 2.12E); it followed a similar pattern over depth as Shannon

diversity, increasing to means of 203.8 OTUs at 30 m, 275.6 OTUs at 75 m, 325.1 OTUs at

150 m, and 305.8 OTUs at 300 m (Fig. 2.12F). The temporal pattern of Chao1 richness was

different than that of Shannon diversity (although the two metrics were positively correlated;

Table 2.7), with estimated richness minima generally occurring in the spring and late summer

and maxima in the fall and winter, again with substantial noise. Chao1 richness at the surface

was negatively correlated with BP_{Q10}, POC, and fucoxanthin (Table 2.7).

Faith's phylogenetic diversity (PD, which is not weighted by abundance) was

between 5.5 and 16.4 at the surface, with a mean of 10.2 (Fig. 2.12G). PD initially increased

over the euphotic zone to means of 11.5 at 30 m and 11.6 at 75 m, before declining to 11.0 at

150 m and 10.6 at 300 m (Fig. 2.12H). PD at the surface was weakly negatively correlated

with BP_{Q10} and POC, and positively correlated with NO_3 (Table 2.7), but had overall

minimal seasonality (Fig. 2.12G).

While the percent of BCC consisting of archaea is not a measure of diversity per se, it

is a contributing factor to the phylogenetic diversity measures above. Relative abundance of

archaea in the SBC increased with depth, as discussed above (Fig. 2.6B). Percent archaea at

the surface was highest in the winter and early spring, strongly correlated with upwelling

parameters (temperature and NO_3) and less strongly but significantly correlated with

phytoplankton bloom indicators (Table 2.7).

Bacterial production

BP_{Q10} was examined in more detail to see if a measure of bulk prokaryotic

community activity followed similar temporal patterns, and correlated with similar

environmental parameters, as properties of BCC. BP_{Q10} ranged between 0.06 and 2.33 µmol C L^{-1} day^{-1}, with a mean of 0.66 µmol C L^{-1} day^{-1}, at the surface (Fig. 2.2F). Surface BP_{Q10} was strongly associated with phytoplankton blooms and more weakly associated with recent upwelling, based on correlations with environmental parameters (Table 2.8). Correspondingly, BP_{Q10} showed a general seasonality, with lowest rates in the late fall and winter and highest rates during spring and summer. Surface BP_{Q10} was significantly positively correlated with Shannon diversity and BWPD, and negatively correlated with Chao1 estimated richness and PD (Table 2.7).

BP_{Q10} increased slightly over shallow depths, to a mean of 0.83 µmol C L^{-1} day^{-1} at 10 m, and then declined over subsequent depths as would be expected, to a mean of 0.30 µmol C L^{-1} day^{-1} at 30 m, 0.05 at 75 m, 0.02 at 150 m, and 0.01 at 300 m (Fig. 2.3D). BP_{Q10} at 75 m is particularly interesting, with a small number of samples across eight cruises showing increases in BP_{Q10} three- to seven-fold over the mean at that depth (Fig. 2.3F). This is suggestive of an input of organic resources at depth, perhaps by export events; however, we cannot address this definitively with our dataset. These putative export events were associated with slightly higher mean copiotroph relative abundances than in the 75 m samples overall (S4, NAC11-7, had a mean relative abundance of 4.8% in high BP_{Q10} samples, versus 1.2% at 75 m overall; S12, SAR92, 1.4% versus 0.5%; S7, SAR86, 2.9% versus 0.9%; and S14, SAR86, 1.5% versus 0.8%). Overall BP_{Q10} at 75m was significantly negatively correlated with percent archaea (R = -0.387, $p < 0.0001$, N = 163), BWPD (-0.278; N = 163; $p < 0.0001$), and Chao1 estimated richness (R = -0.155, $p = 0.049$, N = 163), and positively correlated with PD (R = 0.232; N = 163; $p = 0.003$).

35

Discussion

Overall BCC patterns: seasonality

Suites of OTUs that show synchronous changes in abundance in response to seasonal patterns, as we saw with our UniFrac groups, are a common feature of BCC time-series studies (Eiler et al. 2011; Lindh et al. 2015). Eiler et al. (2011) argued that this is evidence that bacterial communities are responding to deterministic forcing, rather than reflecting random community assembly. Many time-series studies have also documented succession in BCC during and following the spring phytoplankton bloom (Lamy et al. 2009; Teeling et al. 2012; Treusch et al. 2009; Needham and Fuhrman 2016), which for the free-living community is consistent with the progression in quality and quantity of dissolved organic matter available as the phytoplankton community composition and physiological state change (Buchan et al. 2014; Wear et al. 2015). We observed evidence of succession in some of the individual OTUs, such as the apparent time-lag between the maximum relative abundance in OTU S3, the Roseobacter NAC11-7, and S6, a SAR86 OTU that often reaches a maximum relative abundance a month after the Roseobacter (Fig. 2.10). However, these time-lags between OTUs were mostly not significant in the cross-correlation analysis (Fig. 2.11), likely due to the boom-and-bust nature of these populations. Our sampling frequency is not high enough to capture the full details of shifts in BCC over the upwelling to bloom progression. For example, Needham and Fuhrman (2016) observed shifts in dominant OTUs over timescales of days. Instead, we would have sampled individual phytoplankton blooms and their degradation process at random points in the BCC progression, which could explain why UniFrac Group G, the group associated with moderate resource levels, contained the most diverse suite of communities (Fig. 2.9).

The most geographically relevant time-series with which to compare our study is the San Pedro Ocean Time-series (SPOT), a monthly sampling located approximately 160 km to the southeast in the San Pedro Basin of the Southern California Bight. The SPOT site is relatively oligotrophic compared with the SBC, with chlorophyll *a* concentrations < 1 µg L^{-1} at the surface (Chow et al. 2013) versus annual highs between 8 and 28 µg L^{-1} in the SBC (Fig. 2.2C), lower surface nitrate levels, and a slightly greater prevalence of cyanobacteria (Cram et al. 2015). However, prokaryotic communities in the SBC have a broad compositional similarity to those at SPOT. At the surface, both sites share dominant OTUs from the SAR11, SAR86, OCS155, and AEGEAN-169 clades (Table 2.2; Cram et al. 2015); the most noticeable differences between the sites is the lack of *Roseobacter* clades amongst the most abundant OTUs at SPOT, whereas the *Roseobacter* NAC11-7, OTU S3, repeatedly constitutes about 10-15 percent of BCC in the SBC during the spring phytoplankton bloom (Fig. 2.10). Most time-series community characterization at SPOT has been conducted with a method that does not detect archaea (Cram et al. 2015) and therefore quantitative comparisons with samples at depth are not meaningful. Communities at both sites show similar: seasonality over the course of a year, with BCC largely driven by the progression from upwelling to stratified conditions; and recurring patterns between years; and more apparent seasonality at the surface than at the base of the euphotic zone. However, the exact timing of environmental parameters underlying the seasonality differs between sites (Chow et al. 2013; Cram et al. 2015).

Chao1 richness reached a maximum during the late fall and winter in the SBC, lagging the height of the warm, stratified period but generally preceding strong spring upwelling. Winter maxima in richness have also been observed in the English Channel

(Gilbert et al. 2012), the Sargasso Sea (Vergin et al. 2013), and at SPOT (Cram et al. 2015), although in those systems richness is associated with the winter mixing period, which can increase richness by bringing deep-water clades to the surface and reducing the SAR11 dominance common in stratified summer waters (Bunse and Pinhassi 2017). Richness and diversity were temporally decoupled in the SBC [whereas in Gilbert et al. (2012) OTU richness and PD are tightly linked], with both Shannon diversity and BWPD positively associated with phytoplankton blooms during the spring (Table 2.7; Fig. 2.12). This difference may be partly due to the poor sampling coverage of physical mixing on PnB on account of vessel limitations; one sample encompassing recently upwelled water (11.6 μM NO_3 and temperature of 11.6°C) but with low chlorophyll a (0.9 μg L^{-1}), April 2011 Station 5, had one of the greatest BWPD values of the entire time-series. Thus, it is possible we would see observe similar patterns on a seasonal scale if we had greater sampling coverage of winter mixing and recently upwelling water. Nonetheless, the increased diversity associated with phytoplankton blooms relative to the more stratified summer and fall is real and may represent metabolic niche partitioning (discussed below).

Overall BCC patterns: depth stratification

The largest scale of community variability measured was depth, which is consistent with previous depth profile studies of marine BCC. The SBC is a Case II water system (Otero and Siegel 2004), and thus the samples from 75 m and below in this system are below the euphotic zone. Vertical stratification in BCC is a well-documented phenomenon (Morris et al. 2005; DeLong et al. 2006; Carlson et al. 2009; Treusch et al. 2009; Eiler et al. 2011; Cram et al. 2015; Sunagawa et al. 2015; Walsh et al. 2016), with OTUs often restricted to specific portions of the water column (Brown et al. 2009). Community functional potential

likewise changes with sample depth, whether assessed by genomic (DeLong et al. 2006) or experimental approaches (Carlson et al. 2004).

One of the major drivers of depth stratification as measured by UniFrac distance was the increase in relative abundance of archaea with depth, a trend consistent with previous findings of enhanced archaeal abundance below the euphotic zone (Karner et al. 2001). A previous time-series study of prokaryotic community composition in the SBC measured the percent contribution of archaea (Murray et al. 1999). We observed slightly lower archaeal relative abundance at the surface (a mean of 2.9% in our study vs. a mean of 8.0% in Murray et al.) and slightly greater abundance at depth (38.5% vs. 31.0% at 75 m and 45.7% vs. 39.2% at 300 m). However, considering that our study used 16S rRNA gene sequencing and Murray et al. (1999) used hybridization of group-specific 16S rRNA oligonucleotide probes, these values agree surprisingly well, suggesting long-term stability in the prokaryotic community in the SBC at its broadest sense. The most common surface archaea, Euryarchaeota Marine Group II (MGII) OTU S18 showed moderate seasonality in one- and three-month time lags relative to upwelling and bloom parameters (Fig. 2.11), which in our study could indicate either a physical shoaling of archaeal-enriched deep waters with upwelling or a positive selection by bloom conditions. There is some recent support for the latter scenario: Needham and Fuhrman (2016) observed a high relative abundance of an MGII OTU following a strong phytoplankton and copiotrophic bacteria bloom period at SPOT. Further, Orsi et al. (2015) showed that some MGII populations from the California Current System increase their growth rate in the presence of phytoplankton and are associated with higher chlorophyll *a* levels in field surveys. The Thaumarchaeota Nitrosipumilus OTU D1, the most common and abundant OTU at 75 m in the SBC, was

largely restricted to samples from depth, whereas the similarly dominant OTUs from the

surface were regularly also present at depth (Table 2.2). Mesopelagic Thaumarchaeota have

been shown to lack light stress response genes present in epipelagic Thaumarchaeota clades

(Luo et al. 2014), which may contribute to this vertical partitioning.

Individual OTUs

The seasonality of the individual OTUs is more muted than that of the community as

a whole. While a number of OTUs have distinct maxima over time (Fig. 2.10), this pattern

does not always carry through to statistically significant seasonality in cross-correlations with

environmental parameters (Fig. 2.11). This is likely an effect of the boom-and-bust nature of

the bloom-forming OTUs such as the copiotrophs, which are at effectively a baseline

concentration for much of the year but then increase rapidly to high relative abundances for

one or two months. However, many of the individual OTUs do have clear bottom-up

correlates (Fig. 2.11), which are generally stronger than the correlations between

environmental parameters and the community as a whole.

We measured a high overall relative abundance of SAR11, presumably as a result of

our use of primers modified specifically to improve affinity for SAR11 (Apprill et al. 2015,

which demonstrated that increased degeneracy in the 806R-B primer increased measured

SAR11 relative abundance by an order of magnitude or more over the older version of

806R). The mean relative abundances of the three most abundant SAR11 OTUs at the

surface of (SAR11 surface 1, 32%; Surface 2, 6%; and Surface 4, 1%; Table 2.2) were

consistent with the global SAR11 average of 20-40% (Giovannoni 2017), although the SBC

also showed large oscillations around those means. As SAR11 isolates have been shown to

be incapable of increasing their growth rates in response to substrate additions (Giovannoni

40

2017), their seasonal patterns were most likely driven by changes in the relative abundance of those copiotrophic OTUs that are known to lead boom-and-bust, blooming lifestyles, rather than by growth patterns of the SAR11 OTUs themselves.

One of the most abundant OTUs was a member of the Roseobacter NAC11-7 clade (OTU S3, Table 2.2), which was positively correlated with phytoplankton blooms and showed a seasonal progression in relative abundance subsequent to upwelling (Fig. 2.11). This is consistent with many studies showing a strong association between members of the *Roseobacter* clade and diatoms in particular (reviewed in Amin et al. 2012; Buchan et al. 2014), and NAC11-7 is often notably prominent during diatom blooms (Buchan et al. 2005). The *Flavobacteria* are also commonly associated with diatoms (Amin et al. 2012; Buchan et al. 2014); four members of this class were amongst the most abundant surface OTUs (S11 – S14; Table 2.2), although several of them were poorly correlated with environmental parameters indicative of the upwelling and bloom states (chlorophyll *a* and POC; Fig. 2.11). This could be because *Flavobacteria* are thought to reach maximum abundance during the decay phase of phytoplankton blooms (Buchan et al. 2014), when the pigment signatures would be less pronounced and therefore would not be identified as a bloom period in our analysis.

Gammaproteobacteria are often generalized as copiotrophs (that is, r-selected organisms capable of a rapid and numerically dominant response to resource inputs; Fuhrman et al. 2015). This characterization fits the known lifestyles of such groups as the *Vibrionaceae* and the *Altermonadaceae* (e.g., Mou et al. 2008), including OTU S8, a member of the SAR92 clade that was correlated with phytoplankton blooms in this study (Fig. 2.11). SAR86, a common Gammaproteobacterium in the SBC, is more ambiguous, with some

studies finding it shows low growth rates and reduced DOM uptake compared with other

groups in the subphylum (Nikrad et al. 2014) and weak responses to phytoplankton blooms

(Alderkamp et al. 2006), but others indicating high uptake of model compounds (Mou et al.

2007). This discrepancy is likely due to the large phylogenetic diversity within the SAR86

clade (Treusch et al. 2009). Previous studies either did not specify which subclades they

examined, or, as is the case here, did not have sufficient resolution in their chosen taxonomic

reference to do so. In the SBC, the main SAR86 OTU (S6; Table 2.2) had similar temporal

patterns (albeit often at a month lag) and maximal abundances as the main copiotroph, the

Roseobacter NAC11-7, and was similarly positively correlated with proxies of phytoplankton

blooms (Fig. 2.10 and Fig. 2.11). Although extrapolating activity from abundance is

inherently risky, this suggests that the most abundant SAR86 OTU in this system was likely

practicing a copiotrophic lifestyle. In contrast, a less abundant SAR86 OTU in this study,

OTU S9, was most abundant during stratified periods (Fig. 2.10) and was positively

correlated with chlorophyll *a* at a time-lag of six months (Fig. 2.11A), suggesting different

metabolic preferences than the closely related OTU S6.

Long-term trends

There was a noticeable decrease in the long-term repeatability of the surface

community in the last year of sampling, seen in the increased scatter around the seasonal

pattern of all paired UniFrac samples beyond an approximately 3.5 year time lag (Fig. 2.7).

This plot of aggregate surface pairwise UniFrac comparisons versus time lags (Fig. 2.7)

shows a slight positive slope (0.0075 units year^{-1}), consistent with the gradual shift of an

approximately 1% decrease per year in Bray-Curtis similarity over four years in a similar

analysis by Chow et al. (2013). The progressive UniFrac distance of the surface center

stations in the SBC relative to the start of the time-series in July 2010 (July vs. August, July vs. September, and so forth) has a greater positive slope of 0.028 units year^{-1} (Fig. 2.13), which might be driven by the larger shifts in stratified communities (such as the appearance of UniFrac Group D; Fig. 2.9). The relatively repeatable bloom and moderate resource communities (Groups F and G), in contrast, would be expected to reduce the inter-annual variability seen in the aggregate pairwise comparison of Fig. 2.7. [The 75 m communities were much more consistent, with a slope of UniFrac distances relative to July 2010 of 0.0013 units year^{-1} and an aggregate slope of 0.0019 units year^{-1}.] Individual OTUs reflect this shift at the surface, with new peaks in abundance appearing in 2014 (Fig. 2.10; in particular, OTU S13 *Polaribacter* and OTU S16 *Synechococcus*), as well as the appearance of a new stratification-associated UniFrac group (Group D; Fig. 2.9B) in the second half of the time-series. Perhaps the most obvious example of this is the BCC measured in August 2014, which was a substantial outlier (Fig. 2.4B), differentiated from the rest of the time-series by a strong *Synechococcus* bloom (Fig. 2.9C and 2.10E).

We speculate that at least some of these shifts were related to the Pacific warm anomaly, which led to elevated temperatures and reduced surface nitrate delivery in the near-shore SBC beginning in December 2013 (Reed et al. 2016) and which strengthened in the offshore SBC beginning in June 2014 (Gentemann et al. 2017). For example, *Synechococcus* clades have distinct thermal and macronutrient preferences that correspond with their distribution in the global ocean (Pittera et al. 2014; Sohm et al. 2016). The *Synechococcus* bloom we observed was not a total ecosystem shift, as that OTU was present in 75% of surface samples (Table 2.2), with maxima prior to 2014 mostly occurring in the stratified late summer and fall. However, 16S rRNA genes are notoriously incapable of distinguishing

43

Synechococcus from *Prochlorococcus* at OTU-level similarity (Rocap et al. 2002; Fuhrman et al. 2015), and thus we are potentially combining ecologically distinct cyanobacteria within our 97% OTU definition. Nonetheless, conditions in 2014 must have shifted in some way that favored a cyanobacterial bloom. Assuming this OTU truly represents *Synechococcus*, then this summer maximum was in contrast with cyanobacterial patterns at SPOT, where *Prochlorococcus* OTUs increase in abundance in the summer and fall while *Synechococcus* OTUs bloom following upwelling (Chow et al. 2013). As our time-series sampling ended in the middle of the warm anomaly, we are unable to definitively rule out an association with longer-term, climatic shifts. Our study started towards the end of a strong La Niña period and continued through a more neutral El Niño Southern Oscillation state, though we did not sample any of the very strong El Niño events that are most influential in this system (NOAA Multivariate ENSO Index, https://www.esrl.noaa.gov/psd/enso/mei/). Likewise, our study began during a negative phase in the Pacific Decadal Oscillation, which began increasing towards a positive, warm phase in 2014 (NOAA NCEI PDO index, https://www.ncdc.noaa.gov/teleconnections/pdo/). A number of other studies in the Southern California Bight have seen shifts in the planktonic community over the 3-5 year range, so this may also simply be a sufficiently long time period to capture stochastic change or drift in BCC. For example, Chow et al. (2013) saw decreases in Bray-Curtis similarity over four years, and Martiny et al. 2016) measured increasing POM C:P and C:N ratios over three years in the California Current, although this latter study encompassed the 2014 start of the warm anomaly.

Community function

BP$_{Q10}$ was strongly correlated with phytoplankton blooms at the surface (Table 2.8), which follows the general paradigm of phytoplankton blooms as sources of energy and carbon to the free-living, heterotrophic prokaryotic community. This was also consistent with the prokaryotic activity patterns observed by Murray et al. (1999), who measured strong positive correlations between leucine incorporation and chlorophyll *a* and POM concentrations. Halewood et al. (2012) likewise measured greatest BP during the spring upwelling period and positive correlations between BP and POM in the nearshore SBC. We interpret the strong associations between overall BCC and BP$_{Q10}$, as well as between select copiotrophic OTUs and BP$_{Q10}$, as indications of bacterial responses to increased resources associated with phytoplankton blooms (or, conversely, the seasonal lack thereof during the stratified periods).

We hypothesize that the episodic high bacterial production at 75 m is indicative of export events from the surface ocean. While we cannot address this directly with our environmental data, the greater than average relative abundances of copiotrophic OTUs in those samples supports this hypothesis. It is also possible there is a slight decoupling between the BP$_{Q10}$, which was measured on whole water and therefore might contain some small particles by chance, and the BCC, which was measured on 1.2-µm prefiltered water. However, a strong export event would likely still be visible in the free-living fraction of the BCC, as copiotrophs would respond to the dissolved resource plumes diffusing away as particles are solubilized (Cho and Azam 1988; Stocker et al. 2008).

It is somewhat ambiguous whether the SBC demonstrates a positive relationship between BCC diversity and function as measured by BP$_{Q10}$. Shannon diversity and BWPD were both significantly correlated with BP$_{Q10}$, while Chao1 richness and PD were negatively

45

correlated (Table 2.8). The latter initially appears contrary to the idea that a greater number

of OTUs in the prokaryotic community would be able to fill a greater number of metabolic

niches (e.g., Cottrell and Kirchman 2000), thereby increasing overall growth; however,

Chao1 richness in particular peaks during the stratified fall and winter periods (see Fig. 2.9C,

Groups C and D and Fig. 2.12D) when at times more than half of the community was

comprised of the oligotrophic, slow-growing SAR11 Surface 1 (Giovannoni 2017). In

contrast, diversity reached a maximum during and shortly following phytoplankton blooms

(Fig. 2.9C). Although the BCC during phytoplankton blooms generally reflected

corresponding blooms of copiotrophic bacteria, these bacterial blooms usually consisted of

multiple OTUs at moderate abundances and therefore were more diverse than the stratified

communities. UniFrac Group F had the greatest mean BP_{Q10} with moderately high Shannon

diversity and BWPD, while Group G had particularly high Shannon diversity but lower

BWPD with moderate BP_{Q10}; this is suggestive of a proliferation of niches as resources are

processed post-bloom. The diversity-BP_{Q10} correlations were not especially strong, but

bacterial metabolism can also be driven by one or a few particularly active OTUs (Pedler et

al. 2014), and in this case we cannot distinguish between the effects of diversity itself

enhancing community secondary production and the co-occurrence of copiotroph blooms and

peak diversity.

Conclusions

      Temporal variability was greater than that of within-cruise spatial variability at both

the surface and the base of the euphotic zone in the SBC, although changes over depth were

significantly greater than any variability within depth horizons. Surface communities as a

whole and individual OTUs showed distinct seasonality, although this was relative to upwelling rather than strictly time-based. Bottom-up factors correlated with the community as whole, OTUs, and diversity metrics to varying degrees, with BP_{Q10} and temperature the most frequently significant correlates. Long-term shifts were apparent, with new community states appearing mid-way through the four-year time-series, possibly in association with larger climatological changes in the Southern California Bight.

Table 2.1: Sampling by location and depth

Station	Depth (m)	DNA (volume filtered)	BP	Full PnB data	PnB nutrients and CTD	PnB CTD
7	Surface*	X (1 L)	X	X		
6	Surface	X (1 L)	X	X		
6	75	X (1 L)	X			X
5	Surface	X (1 L)	X	X		
5	75	X (1 L)	X			X
4	Surface	X (1 L)	X	X		
4	5		X	X		
4	10		X	X		
4	20		X	X		
4	30	X (1 L)	X	X		
4	50		X	X		
4	75	X (1 L)	X	X		
4	100		X		X	
4	150	X (2 L)	X		X	
4	200		X		X	
4	300	X (2 L)	X		X	
4	400		X		X	
3	Surface	X (1 L)	X	X		
3	75	X (1 L)	X			X
2	Surface	X (1 L)	X	X		
2	75	X (1 L)	X			X
1	Surface	X (1 L)	X	X		

* Surface samples are collected at approximately 1 m, or with the rosette just below the surface.

Table 2.2: Most abundant OTUs at surface and 75 m

Ref #	Group	Phylogeny	Mean relative abundance (%)	Minimum relative abundance (%)	Maximum relative abundance (%)	% samples present
Surface						
S1	Bacteria: Alphaproteobacteria	SAR11 clade; Surface 1; Surface 1 unclassified*	32.1	1.0	63.4	100
S2		SAR11 clade; Surface 2; uncultured bacterium*	5.8	0	26.5	99.3
S3		Rhodobacterales; Rhodobacteraceae; Roseobacter clade NAC11-7 lineage; uncultured marine bacterium ZD0207*	5.7	0	35.0	98.2
S4		Rhodospirillales; Rhodospirillaceae; AEGEAN-169 marine group; uncultured bacterium	3.3	0	10.7	96.3
S5		SAR11 clade; Surface 4; uncultured alphaproteobacterium	1.1	0	7.9	93.0
S6	Bacteria: Gammaproteobacteria	Oceanospirillales; SAR86 clade; uncultured gammaproteobacterium	5.7	0.1	18.9	100
S7		Alteromonadales; Alteromonadaceae; Alteromonadaceae unclassified	2.0	0	10.5	96.0
S8		Alteromonadales; Alteromonadaceae; SAR92 clade	1.8	0	20.9	94.1
S9		Oceanospirillales; SAR86 clade; uncultured proteobacterium OCS5	1.5	0	5.4	96.0
S10		Oceanospirillales; ZD0405; ZD0405 unclassified*	1.3	0	7.7	94.5
S11	Bacteria: Bacteroidetes; Flavobacteria	Flavobacteriales; Flavobacteriaceae; Tenacibaculum; Tenacibaculum	1.4	0	14.2	82.8

		mesophilum				
S12		Flavobacteriales; Flavobacteriaceae; Flavobacteriaceae unclassified	1.4	0	6.3	98.2
S13		Flavobacteriales; Flavobacteriaceae; Polaribacter	1.3	0	37.9	53.8
S14		Flavobacteriales; Flavobacteriaceae; NS5 marine group; uncultured bacterium	1.1	0	5.2	93.4
S15	Bacteria: Actinobacteria	Acidimicrobiia; Acidimicrobiales; OCS155 marine group; uncultured actinobacterium OCS155	1.4	0	14.2	82.8
S16	Bacteria: Cyanobacteria	Cyanobacteria; Subsection I; Family I; Synechococcus	1.6	0	50.0	75.5
S17	Bacteria: unclassified	Unclassified	1.3	0	11.1	79.9
S18	Archaea: Euryarchaeota	Thermoplasmata; Thermoplasmatales; Marine Group II; Marine Group II unclassified	1.1	0	22.3	81.0
75 m						
D1	Archaea: Thaumarchaeota; Marine Group I	Order Incertae Sedis; Family Incertae Sedis; Candidatus Nitrosopumilus	19.0	1.7	41.2	100
D2		Marine Group I unclassified	8.0	1.2	20.0	100
D3		Marine Group I unclassified	2.0	0	9.4	95.8
D4		Order Incertae Sedis; Family Incertae Sedis; Candidatus Nitrosopumilus	1.3	0.2	3.6	100
D5	Archaea: Euryarchaeota	Thermoplasmata; Thermoplasmatales; Marine Group II; Marine Group II unclassified	1.6	0	6.0	96.3
D6	Bacteria: Alphaproteobacteria	SAR11 clade; Surface 1; Surface 1 unclassified*	11.7	1.7	41.2	100

	Class	Taxonomy				
D7		SAR11 clade; Surface 2; uncultured bacterium*	1.4	0	8.6	99.5
D8		SAR11 clade; SAR11 clade unclassified	1.4	0	4.0	97.4
D9		Rhodobacterales; Rhodobacteraceae; Roseobacter clade NAC11-7 lineage; uncultured marine bacterium ZD0207*	1.2	0	13.1	90.5
D10	Bacteria: Gammaproteobacteria	Oceanospirillales; ZD0405; ZD0405 unclassified*	5.8	0.5	17.5	100
D11	Bacteria: Deltaproteobacteria	Desulfobacterales; Nitrospinaceae; Nitrospina; uncultured deltaproteobacterium	4.2	0.2	10.2	100
D12		Desulfobacterales; Nitrospinaceae; Nitrospina; uncultured deltaproteobacterium	2.6	0	7.6	97.4
D13		SAR324 clade (Marine group B); uncultured bacterium; uncultured bacterium unclassified	1.7	0	5.7	98.9
D14		Desulfobacterales; Nitrospinaceae; Nitrospina	1.6	0.1	5.9	100
D15		Desulfobacterales; Nitrospinaceae;Nitrospina; uncultured deltaproteobacterium	1.4	0	5.3	99.5

Taxonomic name structure follows SILVA format, with editing for legibility and to remove repeated "unclassified" labels. "Ref #" is the internal reference used in associated figures for brevity. *OTUs in common between most abundant at surface and most abundant at depth.

Table 3: Summary of scales of temporal and spatial variability, as UniFrac distance.

	N	Median	Mean	Minimum	Maximum
Depth					
0 vs. 30 m	34	0.280	0.311	0.108	0.636
0 vs. 75m	180	0.598	0.590	0.197	0.782
0 vs. 150m	33	0.656	0.654	0.505	0.796
0 vs. 300m	35	0.670	0.666	0.542	0.825
Temporal – surface					
1 month* lag	36	0.296	0.303	0.161	0.499
3 months lag	34	0.341	0.364	0.221	0.589
6 months lag	33	0.406	0.440	0.273	0.685
1 year	30	0.282	0.306	0.214	0.549
Temporal – 75m					
1 month lag	34	0.153	0.169	0.092	0.327
3 months lag	30	0.199	0.197	0.125	0.300
6 months lag	29	0.219	0.219	0.126	0.354
1 year	28	0.196	0.202	0.091	0.361
Spatial					
Surface, 2 vs. 6	38	0.189	0.204	0.086	0.372
Surface, 2 vs. 7	30	0.199	0.212	0.108	0.428
Surface, max	43	0.276	0.289	0.166	0.481
75m, 2 vs. 6	30	0.134	0.180	0.075	0.543
75m, max	41	0.166	0.208	0.094	0.543

N = number of observations, out of 43 total cruises. *Time lags are nominal, such that one month is defined as any time lag between 0.5 and 1.5 months, and so forth, due to the inconsistent spacing of cruises.

Table 2.4: Mann-Whitney U-tests between UniFrac distances over depth, temporal, and cross-SBC distance scales.

	Depth			Temporal: surface				Temporal: 75 m			
	0-75	0-150	0-300	1 mo	3 mo	6 mo	1 yr	1 mo	3 mo	6 mo	1 yr
0-30	**U = 490** **p < 0.0001**	**31 < 0.0001**	**24 < 0.0001**	572 0.638	**387 0.019**	**238 < 0.0001**	466 0.554	**175 < 0.0001**	**228 < 0.0001**	**280 0.003**	**239 0.001**
0-75		**1704 < 0.0001**	**1518 < 0.0001**	**141 < 0.0001**	**384 < 0.0001**	**885 < 0.0001**	**126 < 0.0001**	**10 < 0.0001**	**16 < 0.0001**	**25 < 0.0001**	**26 < 0.0001**
0-150			531 0.568	**0 < 0.0001**	**14 < 0.0001**	**68 < 0.0001**	**1 < 0.0001**	**0 < 0.0001**	**0 < 0.0001**	**0 < 0.0001**	**0 < 0.0001**
0-300				**0 < 0.0001**	**5 < 0.0001**	**59 < 0.0001**	**1 < 0.0001**	**0 < 0.0001**	**0 < 0.0001**	**0 < 0.0001**	**0 < 0.0001**
S: 1mo					**402 0.014**	**182 < 0.0001**	538 0.979	**119 < 0.0001**	**145 < 0.0001**	**215 < 0.0001**	**188 < 0.0001**
S: 3 mo						**336 0.005**	**325 0.013**	**39 < 0.0001**	**39 < 0.0001**	**86 < 0.0001**	**80 < 0.0001**
S: 6 mo							**135 < 0.0001**	**6 < 0.0001**	**2 < 0.0001**	**20 < 0.0001**	**26 < 0.0001**
S: 1 yr								**71 < 0.0001**	**73 < 0.0001**	**150 < 0.0001**	**124 < 0.0001**
75: 1 mo									**340 0.022**	**251 0.001**	343 0.060
75: 3 mo										341 0.154	403 0.791
75: 6 mo											314 0.142

Statistically significant results are in bold.

Table continues on next page

Table 2.4, continued

	Distance: surface			Distance: 75 m	
	2 vs 6	2 vs 7	max	2 vs 6	max
0-30	**315** **< 0.0001**	**273** **0.001**	730 0.992	**201** **< 0.0001**	**361** **< 0.0001**
0-75	**25** **< 0.0001**	**36** **< 0.0001**	**130** **< 0.0001**	**55** **< 0.0001**	**80** **< 0.0001**
0-150	**0** **< 0.0001**	**0** **< 0.0001**	**0** **< 0.0001**	**1** **< 0.0001**	**1** **< 0.0001**
0-300	**0** **< 0.0001**	**0** **< 0.0001**	**0** **< 0.0001**	**1** **< 0.0001**	**1** **< 0.0001**
S: 1mo	**239** **< 0.0001**	**220** **< 0.0001**	707 0.510	**177** **<0.0001**	**308** **< 0.0001**
S: 3 mo	**90** **< 0.0001**	**106** **< 0.0001**	**409** **0.001**	**110** **< 0.0001**	**186** **< 0.0001**
S: 6 mo	**14** **< 0.0001**	**42** **< 0.0001**	**176** **< 0.0001**	**55** **< 0.0001**	**86** **< 0.0001**
S: 1 yr	**148** **< 0.0001**	**144** **< 0.0001**	560 0.341	**146** **< 0.0001**	**244** **< 0.0001**
75: 1 mo	**422** **0.012**	**322** **0.011**	**151** **< 0.0001**	451 0.427	573 0.187
75: 3 mo	551 0.814	439 0.871	**215** **< 0.0001**	**295** **0.022**	554 0.478
75: 6 mo	489 0.433	380 0.404	**300** **< 0.0001**	**232** **0.002**	454 0.094
75: 1 yr	515 0.825	402 0.779	**251** **< 0.0001**	**284** **0.034**	533 0.616
S: 2v6		567 0.970	**323.5** **< 0.0001**	**384** **0.022**	704 0.462
S: 2v7			**288.5** **< 0.0001**	**292** **0.019**	534 0.346
S: max				**229** **< 0.0001**	**405** **< 0.0001**
75: 2v6					451 0.057

Table 2.5: Mean environmental parameters and diversity metrics in samples falling in UniFrac groups, as defined in Fig. 2.9.

	Definition	Co-occurs with groups	Environmental BP$_{Q10}$ (µM C day^{-1})	Temp. (°C)	NO$_3$ (µM)	Chl. a (µg L^{-1})	POC (µM)	Fuco. (µg L^{-1})	CDOM S (x10^3)	Diversity Shannon	BWPD	Chao1	PD
Group A	August 2014	None	0.42	17.8	0.06	1.21	18.8	0.36	19.96	3.06	1.15	132.7	9.78
Group B	Upwelling	G	0.29	12.9	7.9	0.51	11.2	0.43	18.48	2.41	0.97	124.4	8.47
Group C	Stratified	D, G	0.37	15.5	2.2	1.69	18.65	0.39	18.28	2.92	1.00	173.6	10.67
Group D	Stratified	C, G	0.35	16.6	0.41	1.64	17.9	0.64	17.14	2.34	0.81	165.1	9.41
Group E	Phyto. bloom	F, G	N/A*	13.8	2.3	9.66	37.9	4.90	15.40	3.17	1.38	85.5	9.81
Group F	Phyto. bloom	E, G	1.41	13.8	1.0	5.55	42.2	2.74	14.76	3.05	1.18	113.0	8.48
Group G	Moderate resources	B, C, D, E, F	0.97	14.4	2.66	4.04	32.9	1.45	16.36	3.15	1.14	154.6	10.63

*N/A: data not available for this group.

Table 2.6: Mean relative abundance of top OTUs in UniFrac groups, as in Fig. 2.9. OTU IDs as in Table 2.2.

Group	Alphaproteobacteria S1	S2	S3	S4	S5	Gammaproteobacteria S6	S7	S8	S9	S10	Flavobacteria S11	S12	S13	S14	Actin. S15	Cyano. S16	Unkn. S17	Eury. S18
A	0.041	0.009	0.030	0.032	0.002	0.005	0.004	0.011	0.001	0.001	0.025	0.022	0.006	0.028	0.003	0.257	0.002	0
B	0.511	0.053	0.029	0.010	0.003	0.009	0.004	0.014	0.010	0.003	0.010	0.002	0.003	0.0003	0.011	0	0.025	0.017
C	0.379	0.079	0.018	0.043	0.015	0.054	0.014	0.009	0.021	0.014	0.003	0.014	0.001	0.012	0.019	0.013	0.019	0.004
D	0.513	0.117	0.006	0.039	0.010	0.018	0.006	0.003	0.011	0.004	0.005	0.007	0.001	0.009	0.014	0.017	0.008	0.001
E	0.077	0.030	0.101	0.005	0.005	0.100	0.015	0.038	0.018	0.006	0.009	0.007	0.016	0.001	0.001	0.002	0.006	0.171
F	0.039	0.009	0.170	0.002	0.001	0.058	0.041	0.065	0.003	0.006	0.049	0.008	0.118	0.001	0.004	0.001	0.004	0.044
G	0.258	0.026	0.100	0.028	0.011	0.079	0.029	0.023	0.013	0.019	0.021	0.018	0.010	0.011	0.013	0.005	0.009	0.013

Table 2.7: Spearman's correlations between diversity metrics and a subset of environmental parameters, across all surface samples.

	BP$_{Q10}$	Temp	NO$_3$	Chl a	POC	Fuco.	CDOM S	Shannon	BWPD	Chao1	PD
Shannon diversity	**R = 0.238** **N = 227** ***p* < 0.0001**	**-0.124** **264** **0.045**	**0.138** **271** **0.023**	**0.182** **273** **0.003**	**0.156** **266** **0.011**	**0.183** **245** **0.004**	**-0.185** **269** **0.002**				
BWPD	**0.363** **227** **<0.0001**	**-0.257** **264** **<0.0001**	**0.215** **271** **<0.0001**	**0.285** **273** **<0.0001**	**0.281** **266** **<0.0001**	**0.311** **245** **<0.0001**	**-0.224** **269** **<0.0001**	**0.664** **273** **<0.0001**			
Chao1 estimated richness	**-0.360** **227** **<0.0001**	0.084 264 0.176	0.119 271 0.051	-0.111 273 0.067	**-0.299** **266** **<0.0001**	**-0.176** **245** **0.006**	0.040 269 0.516	**0.279** **273** **<0.0001**	-0.011 273 0.861		
PD	**-0.199** **227** **0.003**	0.051 264 0.412	**0.145** **271** **0.017**	0.000 273 0.994	**-0.155** **266** **0.012**	-0.070 245 0.274	-0.053 269 0.387	**0.525** **273** **<0.0001**	**0.300** **273** **<0.0001**	**0.536** **273** **<0.0001**	
Percent archaea	-0.106 227 0.111	**-0.574** **264** **<0.0001**	**0.585** **271** **<0.0001**	**0.335** **273** **<0.0001**	**0.227** **265** **<0.0001**	**0.240** **245** **<0.0001**	**-0.339** **269** **<0.0001**	**0.479** **273** **<0.0001**	**0.459** **273** **<0.0001**	**0.286** **273** **<0.0001**	**0.405** **273** **<0.0001**

Correlations in bold font are significant. Fuco = fucoxanthin.

Table 2.8: Surface BP_{Q10} correlations with environmental parameters (Spearman's *rho*.) Significant correlations are marked with an *.

Parameter	Correlation with BP_{Q10}
*Temperature	R = -0.169; N = 235; *p* = 0.009
*Salinity	0.298; 234; <0.0001
NO$_3$	-0.060; 233; 0.365
NO$_2$	-0.075; 234; 0.254
*SiO$_2$	-0.269; 235; <0.0001
*PO$_4$	-0.155; 235; 0.017
*Chlorophyll *a*	0.569; 235; <0.0001
*POC	0.789; 228; <0.0001
*PON	0.680; 227; <0.0001
*bSi	0.751; 221; <0.0001
*Fucoxanthin	0.682; 222; <0.0001
*Peridinium	0.135; 222; 0.044
*Zeaxanthin	-0.189; 222; 0.005
*CDOM *S*	-0.314; 232; <0.0001
*Shannon diversity	0.238; 227; <0.0001
*BWPD	0.363; 227; <0.0001
*Chao1 estimated richness	-0.360; 227; <0.0001
*PD	-0.199; 227; 0.003
Percent archaea	-0.106; 227; 0.111
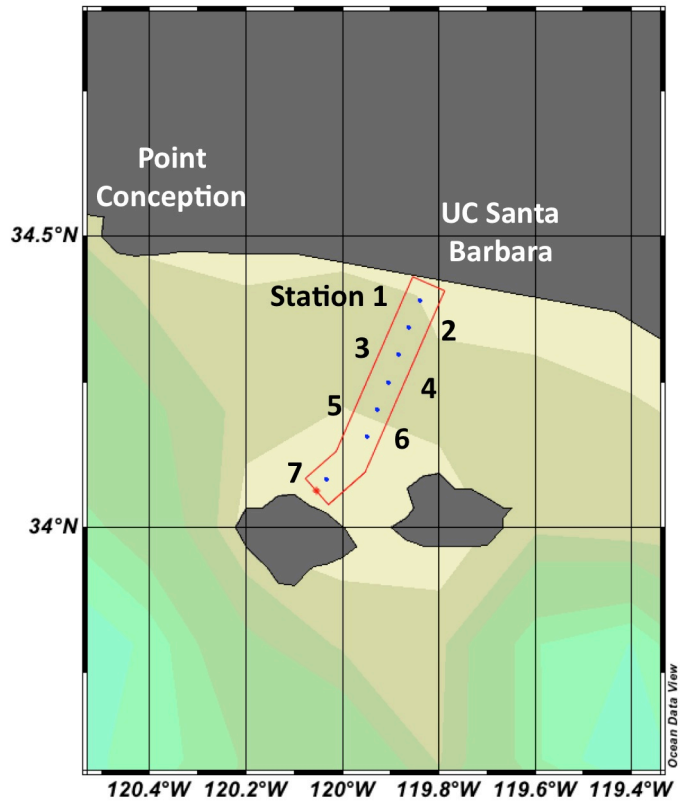
Fig. 2.1: Map of the PnB transect, from the northern Channel Islands in the south to the California mainland in the north.

A.

B.

C.

D.

59
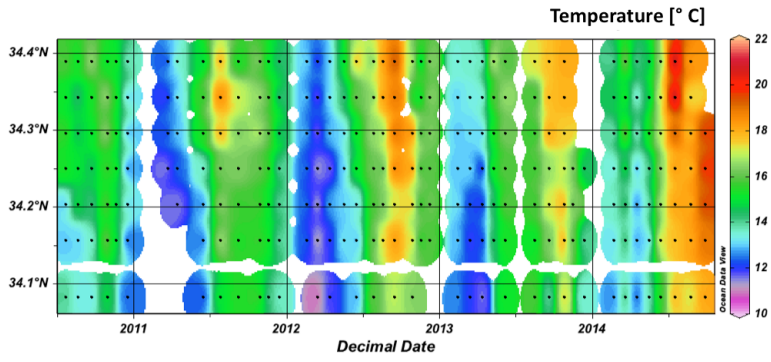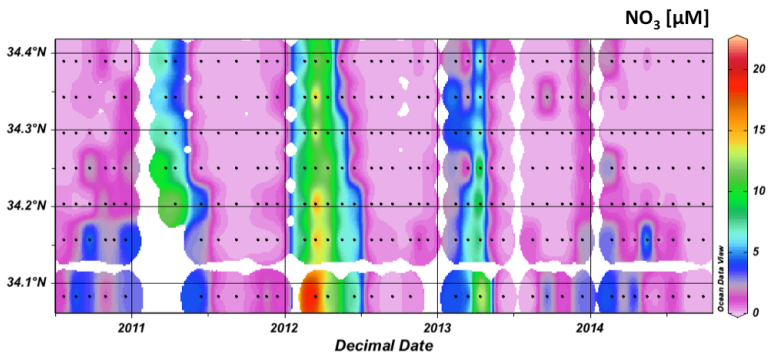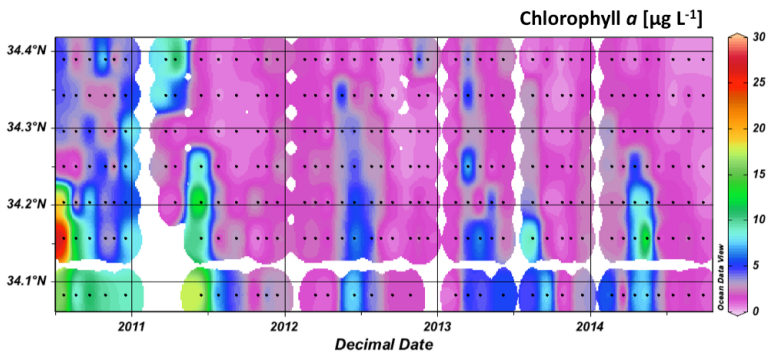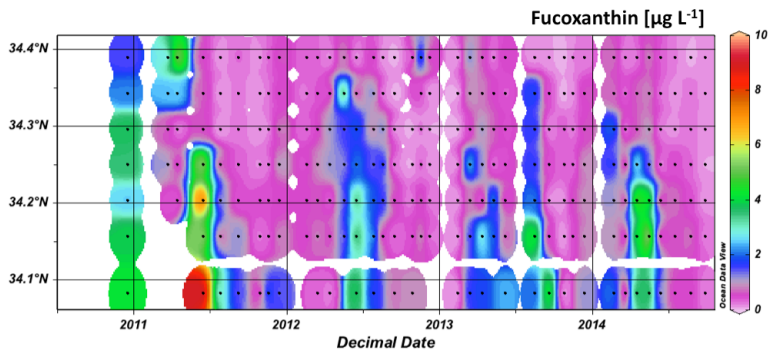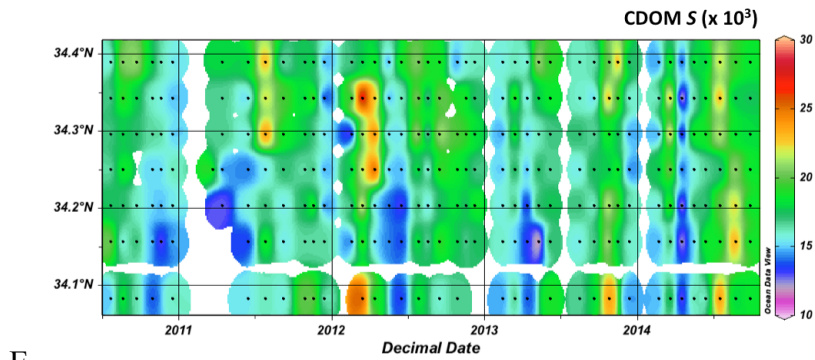
E.
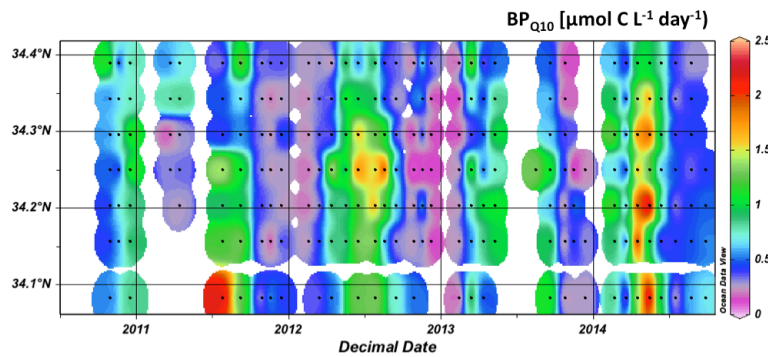
F.

Fig. 2.2: Maps of surface parameters. Surface maps are a birds-eye view of the PnB transect, as shown in Fig. 2.1, with latitude on the Y axis and time on the X axis. A: Temperature. B: Nitrate. C: Chlorophyll *a*. D: Fucoxanthin. E: CDOM spectral slope (*S*), multiplied by 10^3 for visual clarity. F: BP_{Q10}.

A.

B.

C.

D.

61
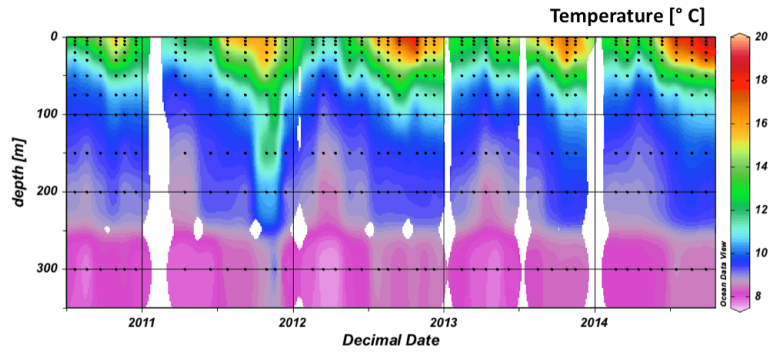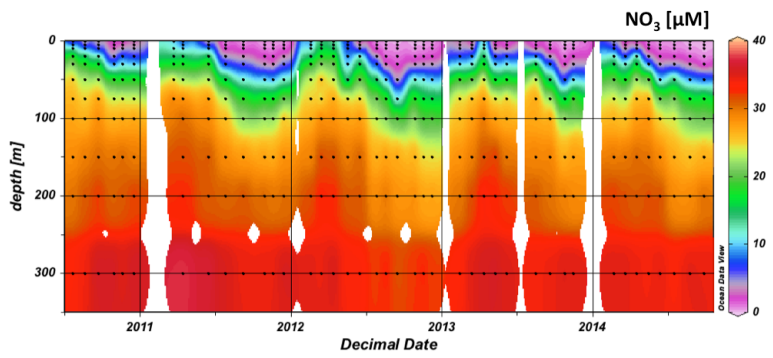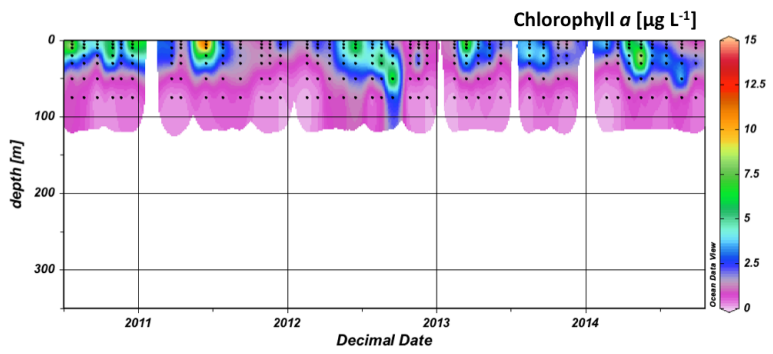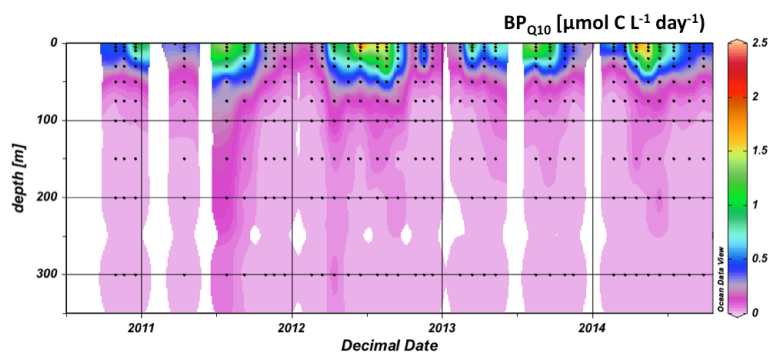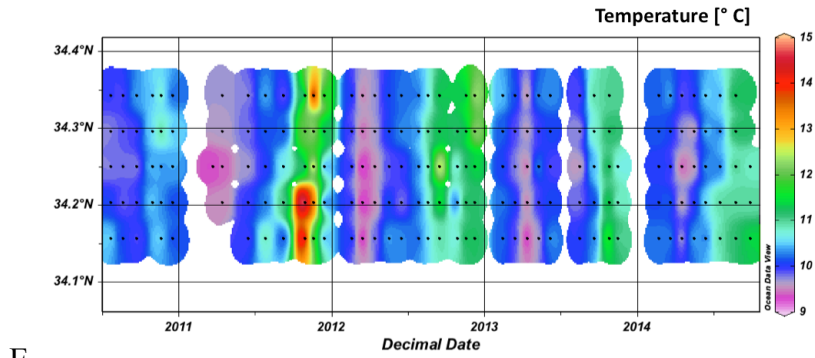
E.
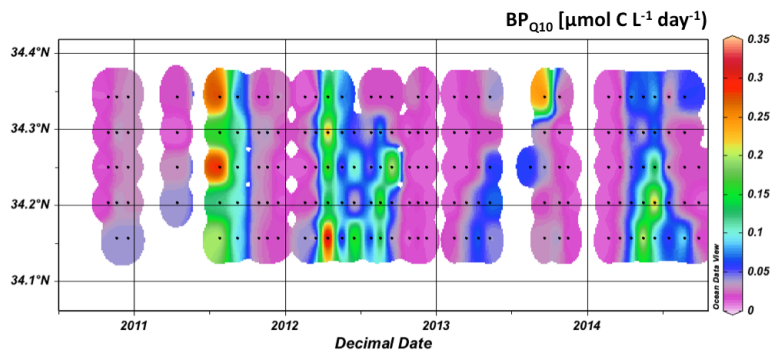
F.

Fig. 2.3: Depth profiles at Station 4 and 75 m surface maps of physicochemical parameters. Note that color bar scales vary across map types here and with Fig. 1. A: Temperature over depth, with time on the X axis. B: Nitrate over depth. C. Chlorophyll *a* over depth; chlorophyll is only measured to 75 m. D. BP$_{Q10}$ over depth. E. Temperature at 75 m, in a birds-eye view of the transect as in Fig. 2.2. Stations 1 and 7 are not sampled at 75 m, but surface maps were plotted on the same latitudinal scale as those in Fig. 2.2. F. BP$_{Q10}$ at 75 m.

A.

B.

C.
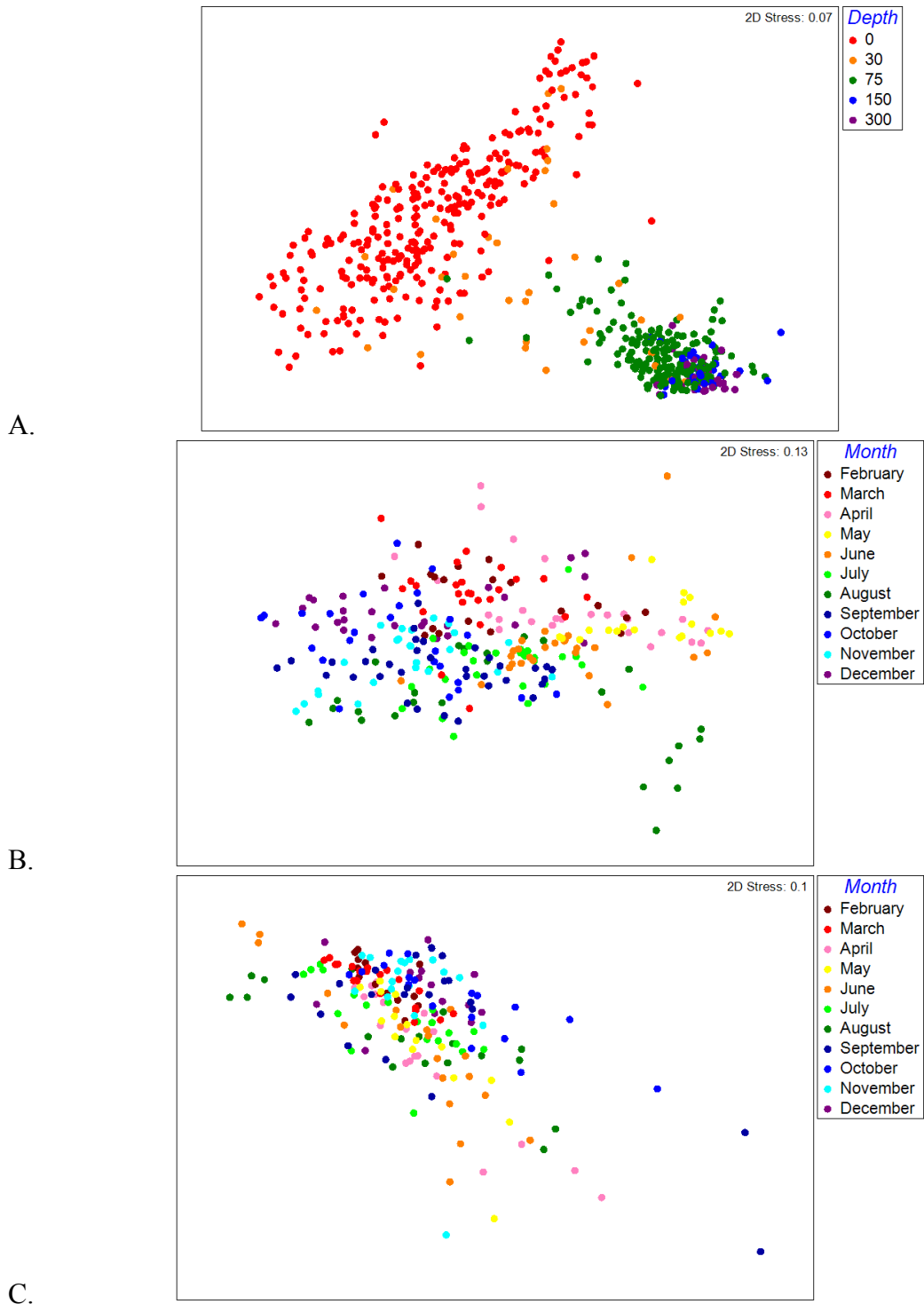
Fig. 2.4: NMS plots of samples using weighted UniFrac distance. A: All samples, colored by depth. B: Surface samples, colored by month, aligned so that the annual cycle is roughly clockwise from the top. Outliers on the bottom right are from August 2014. C: 75m samples, colored by month.

A.

B.

C.

64

D.
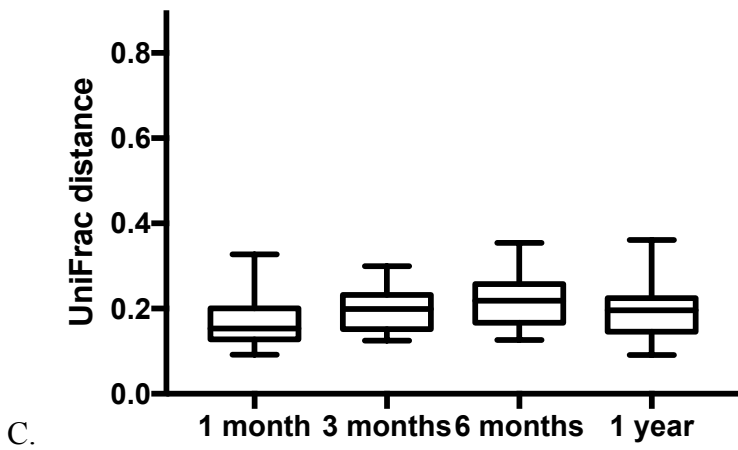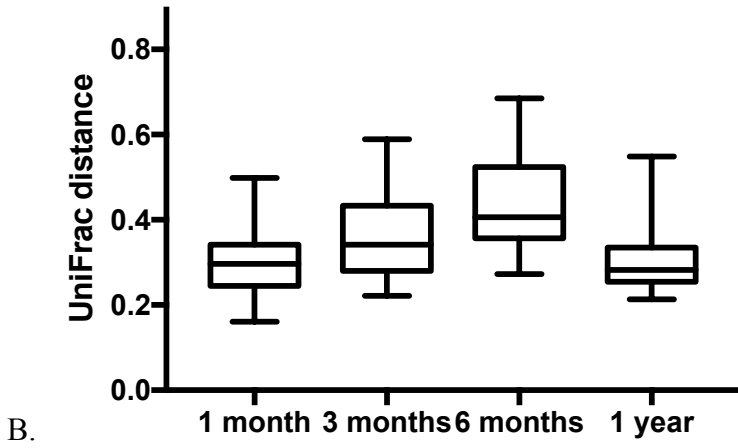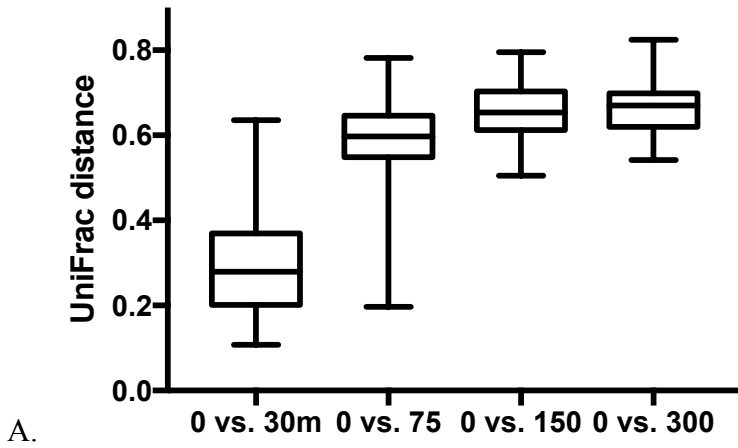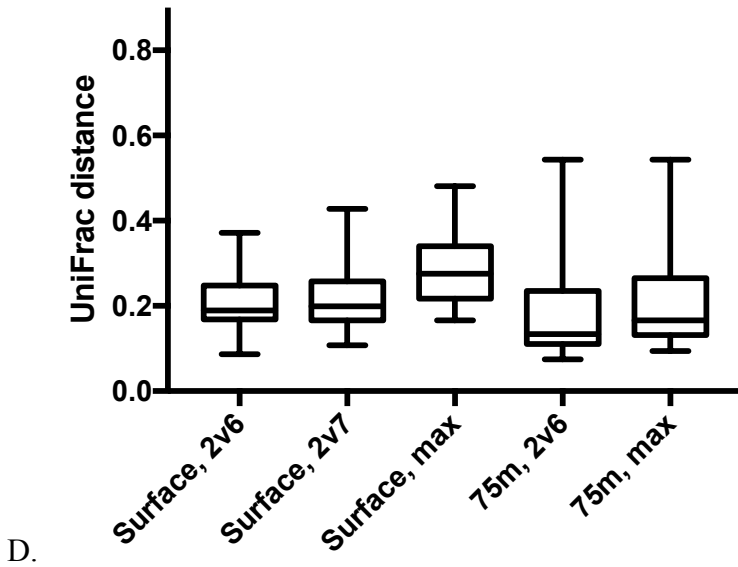
Fig. 2.5: UniFrac distance across scales of spatial and temporal variability. The center line is the median; the box delineates the 25-75th percentile; the whiskers show the maximum and minimum values observed for the specified comparison. All plots are on the same scale for comparative purposes. A: Over depth: surface vs. 30 m, 75 m, and 300 m samples from the same station. B. and C. Temporal variability at the surface and 75 m, respectively, using the average of all pairwise comparisons between the three center stations. Because the PnB cruises are not spaced at exactly one-month intervals, one month here is a nominal measure encompassing cruises taking place between 0.5 and 1.5 months apart, and so forth. D. Spatial: comparisons were made between points on opposite sides of the SBC, and the maximum UniFrac distance observed between points within a depth horizon in a single cruise was identified. For the surface, Stn. 1 was omitted because of strong ecological gradients (see text), and both 2v6 and 2v7 were considered because Stn. 7 is under-sampled within the time-series due to frequent high winds.
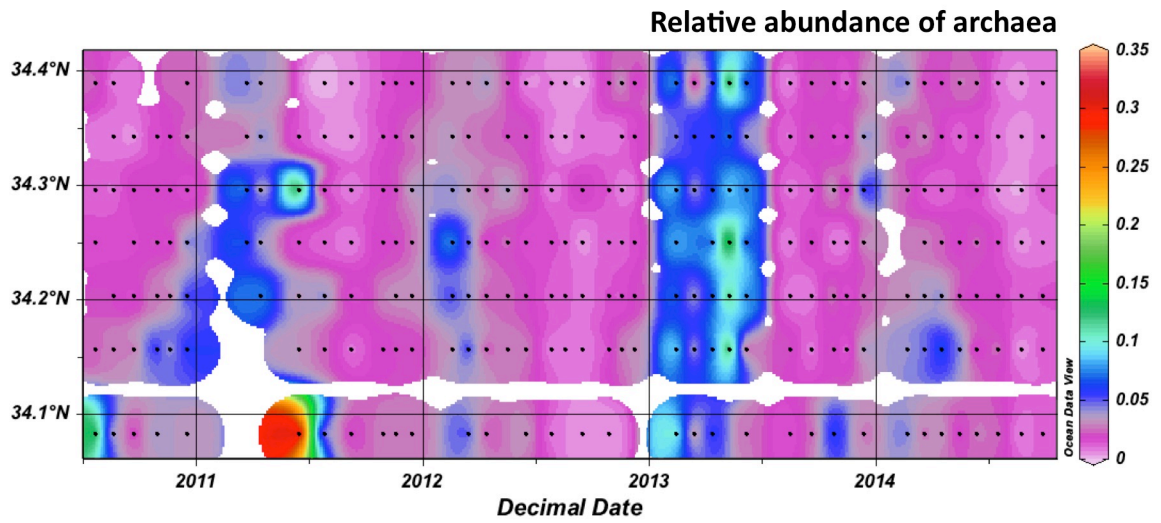
A.
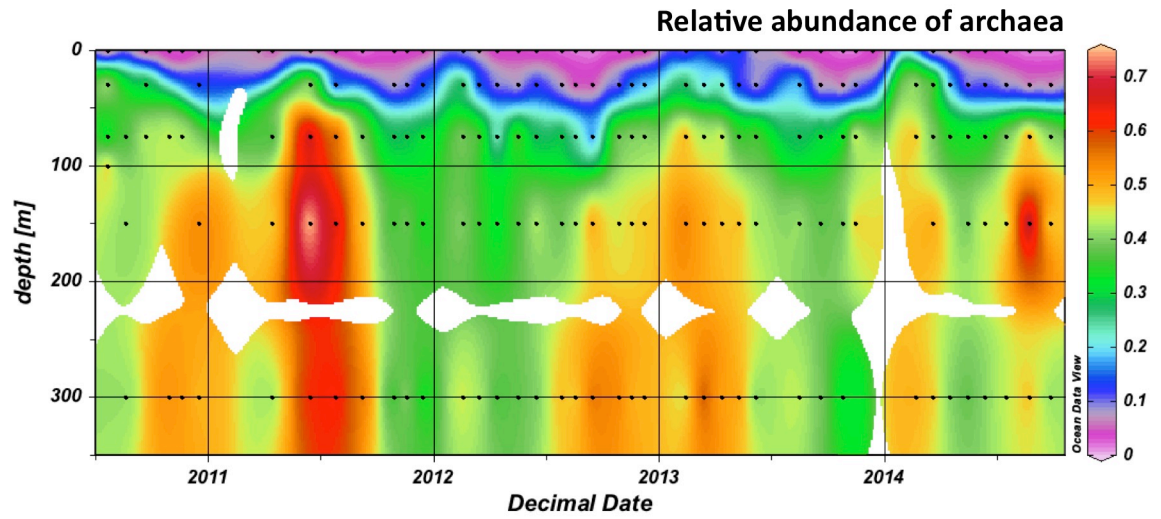
B.
Fig. 2.6: Total relative abundance of archaea in overall BCC. A: Surface map, with a birds-eye view of the time-series as in Fig. 1. B: Depth profile at Station 4. Note that color bar scales differ between the two plots.
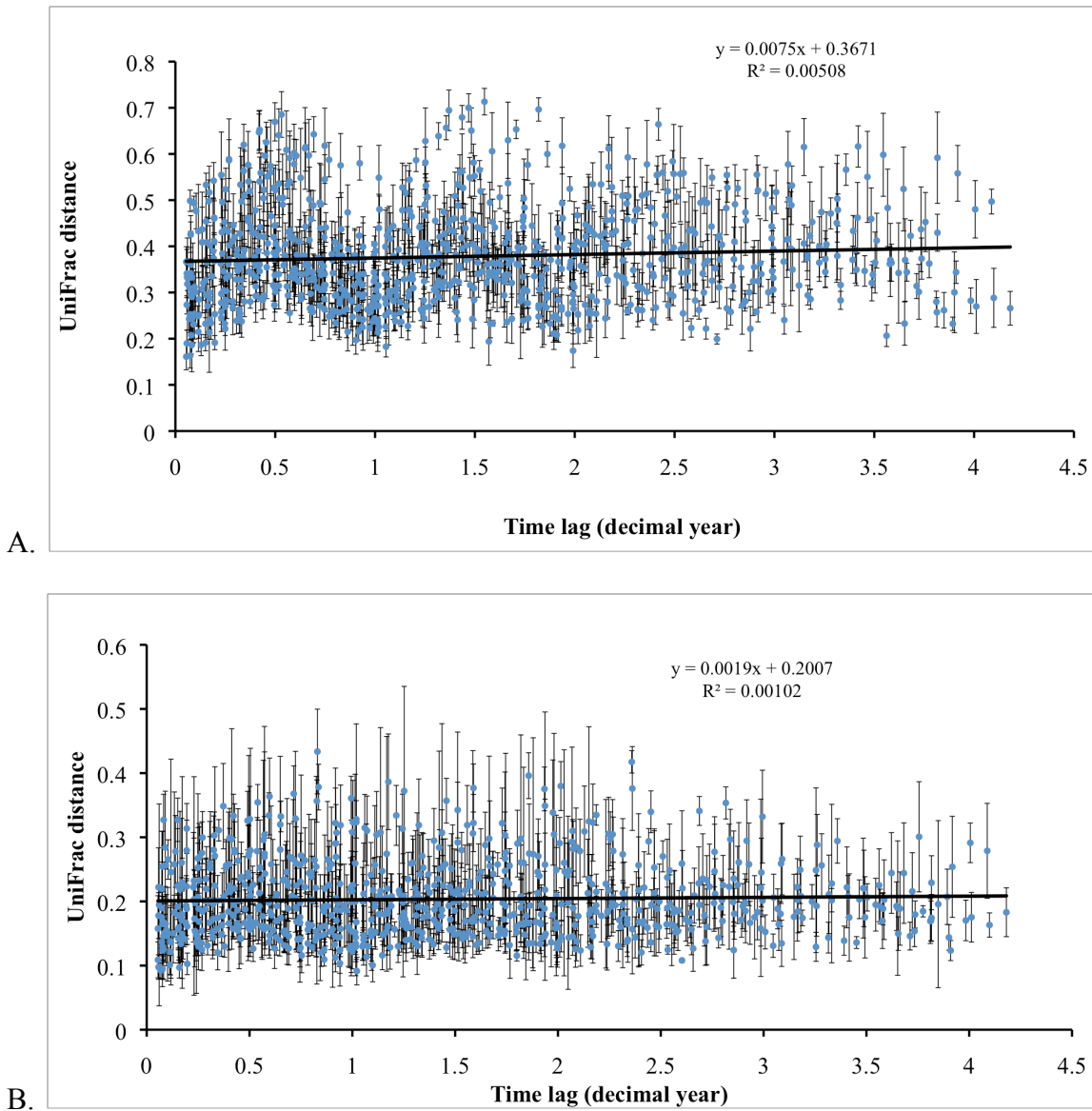
Fig. 2.7: Temporal patterns of UniFrac distance at surface (A) and 75 m (B). Plots show the mean UniFrac distance between all pairwise comparisons of the three center stations for each cruise, with error bars indicating the standard deviation within a cruise, at each depth horizon, against the respective time lag in decimal years. Note that the overall mean UniFrac distance and variability within a particular time lag are larger at the surface than at 75, as is the amplitude across the annual cycle. Linear trendlines show the lack of directional shifts in BCC over time, for comparison with the similar analysis in Chow et al. (2013).
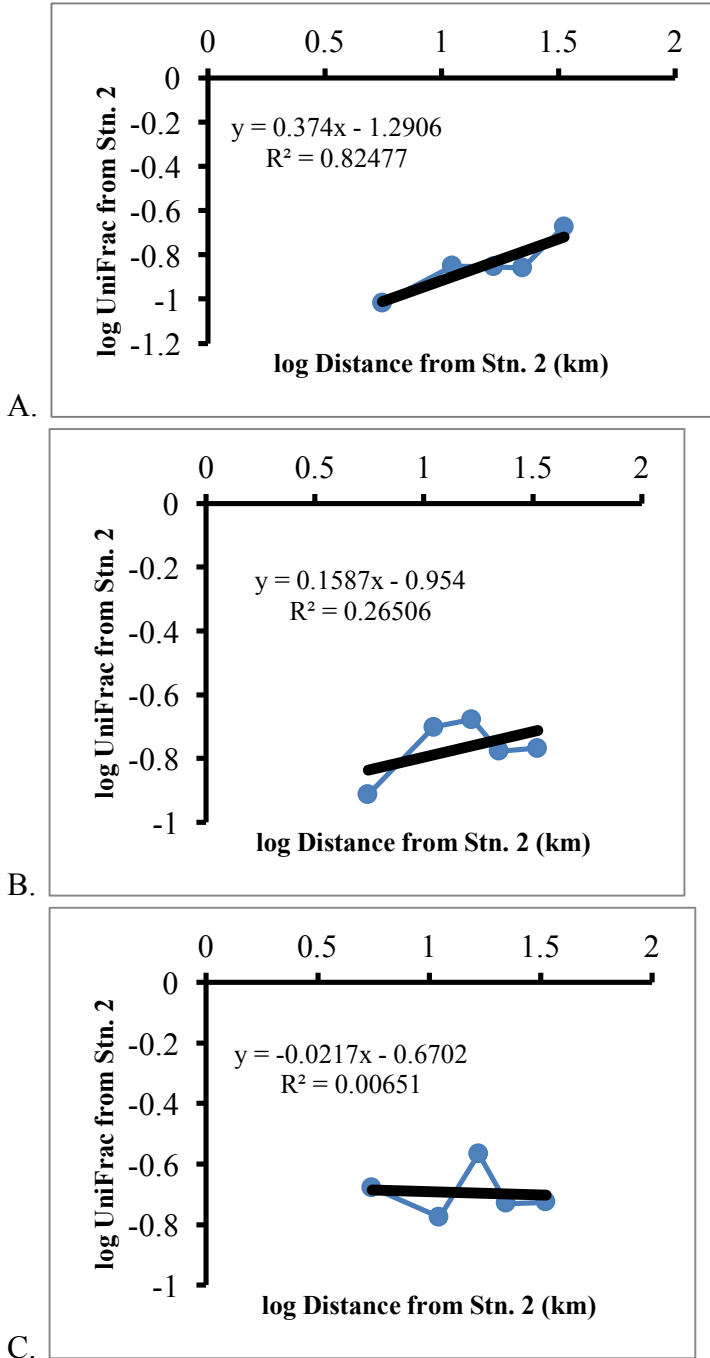
Fig. 2.8: Example distance decay patterns of surface BCC, relative to Stn. 2. Plots are log UniFrac distance, relative to Stn. 2, over log physical distance across the SBC in km. A. An example of distance decay, from November 2011. To be considered as distance decay, the plot needed to show a positive slope and have a linear curve fit R^2 of 0.5 or greater. Thirteen out of 42 cruises met these criteria. B and C. Examples of non-linear BCC patterns over spatial distance, from April 2013 and September 2013, respectively. Twenty-six of 42 cruises had concave, sawtooth, or variable spatial patterns, likely due to eddy and current dynamics. An additional 3 cruises showed an increase in BCC similarity with distance.
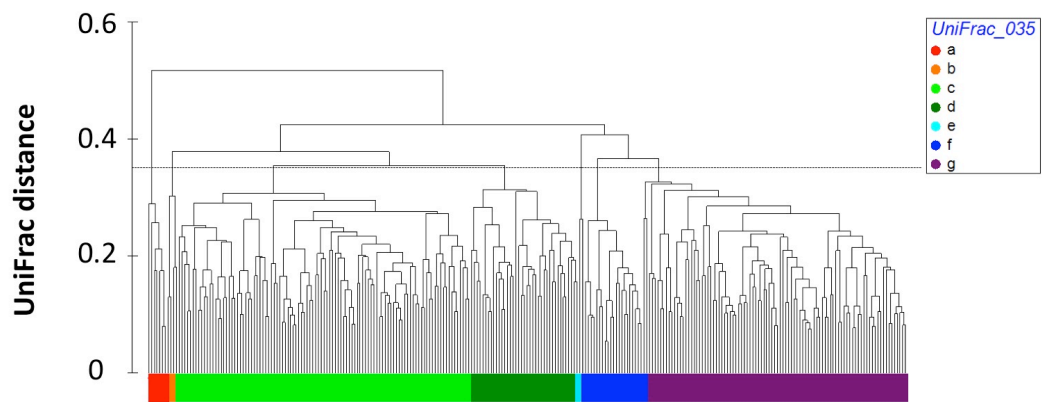
A.
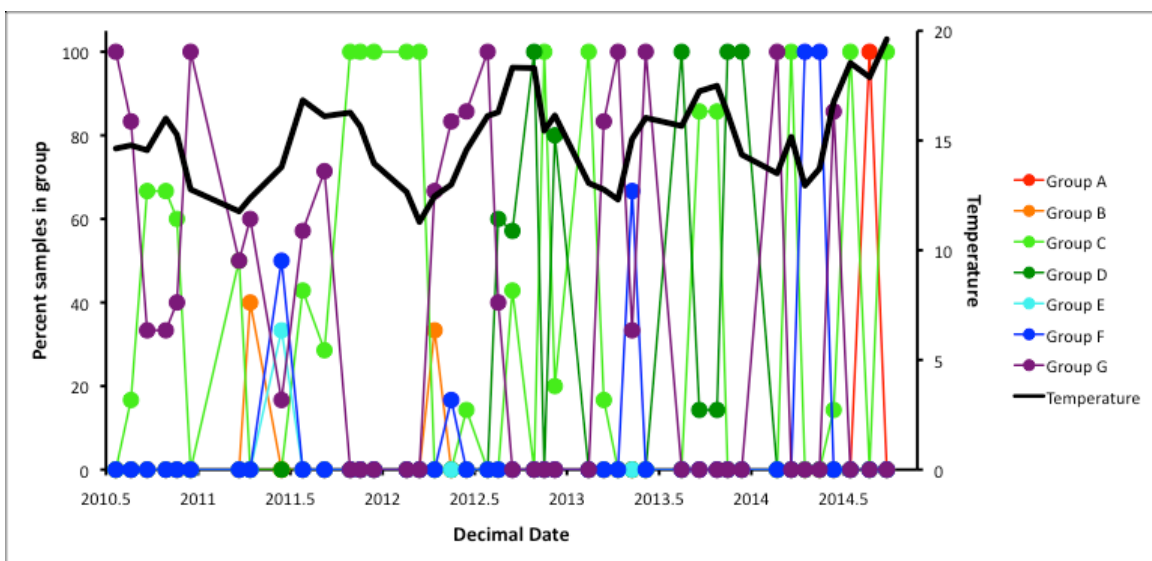
B.

C.
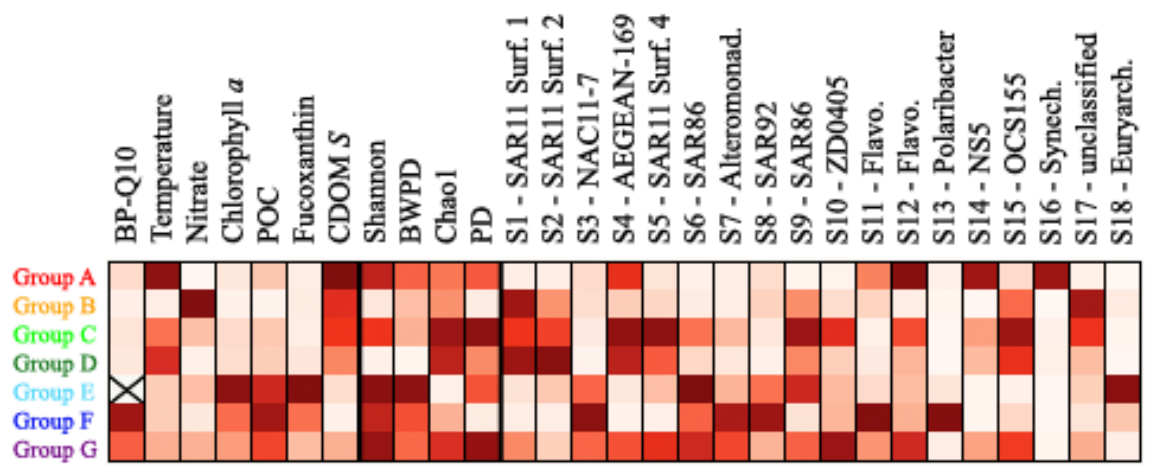
Fig. 2.9: UniFrac distance-based groupings of BCC samples. A. Cluster diagram of all samples, with a line demarcating the UniFrac distance of 0.35 that was used to define groups.

Groups are in alphabetical order from left to right. B. Temporal pattern of groups, as percent of total BCC samples within each cruise. C. Means of environmental parameters and most abundant OTUs from each of the seven groups. Darker colors indicate higher values. Each column is scaled independently, to highlight between-group differences rather than exact quantities; individual OTU means therefore do not represent actual relative abundance, and only trends, not magnitude, should be compared across OTUs. X = no data.
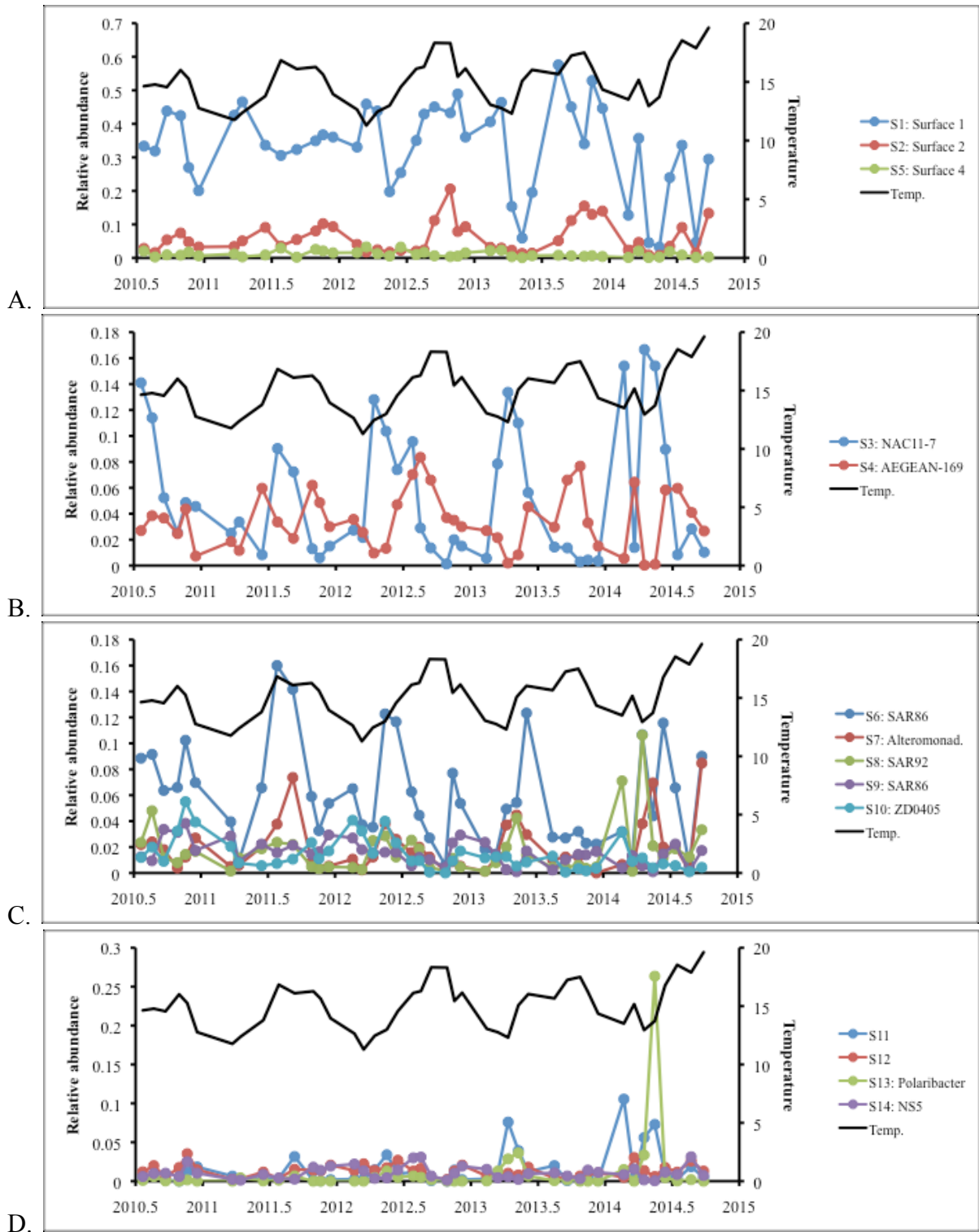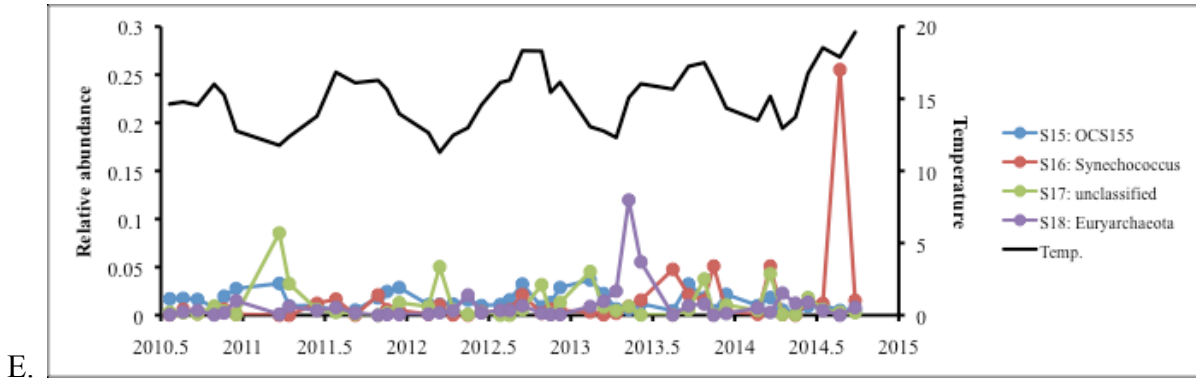
E.

Fig. 2.10: Temporal patterns of the most abundant surface OTUs, examined as the mean of the center three stations. OTU IDs are as defined in Table 2.2, with brief descriptors where useful. A: Temporal patterns of the SAR11 clade. Temperature is shown on all plots as an indicator of upwelling periods. B: Temporal patterns of all other Alphaproteobacteria. C. Temporal patterns of all Gammaproteobacteria. D. Temporal patterns of Flavobacteria. E. Temporal patterns of remaining OTUs.
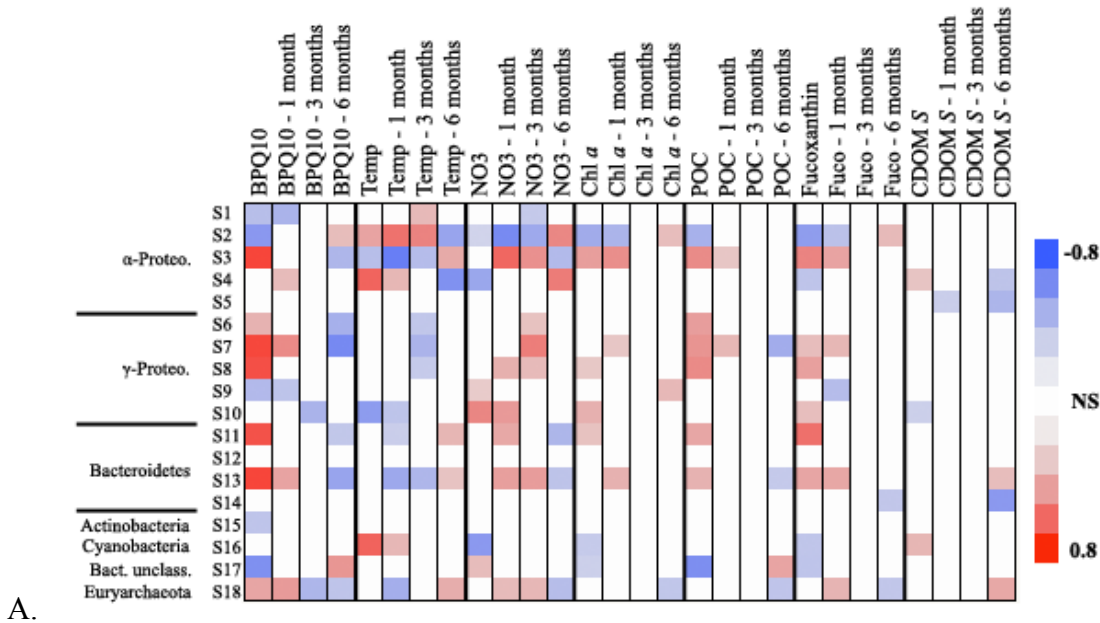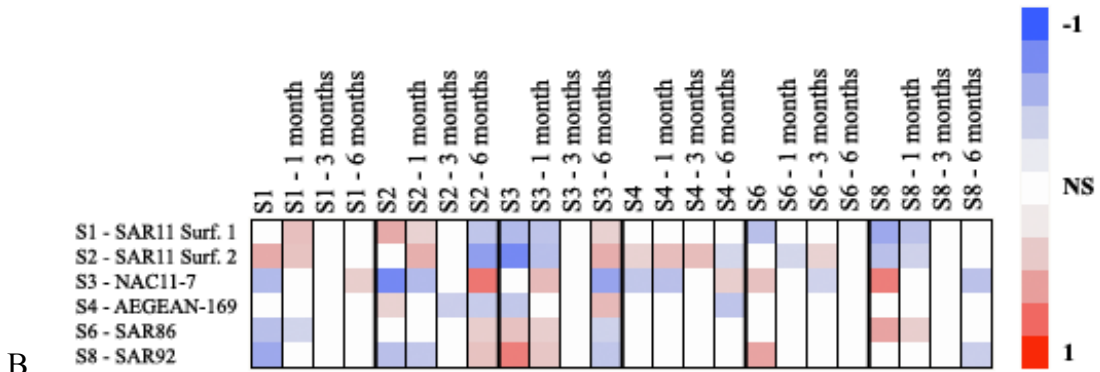
Fig. 2.11: Bottom-up correlates and cross-correlation analysis of the most abundant OTUs, examined as the mean of the center three stations. OTU IDs are as defined in Table 2. A: Bottom-up correlates (Spearman's *rho*) with environmental parameters, both simultaneous and at temporal lags of 1, 3, and 6 months (that is, the OTU relative abundance is correlated with the preceding environmental parameter). Nonsignificant correlations are shown as a zero value, i.e., a white square; all colored squares are thus significant correlations. B. Cross-correlations of a subset of the most abundant OTUs. No lag N = 43, 1 month N = 36, 3 months N = 34, 6 months N = 33.

A.

B.

C.

BWPD

D.

Chao1 estimated richness

E.

Chao1 estimated richness

F.

75
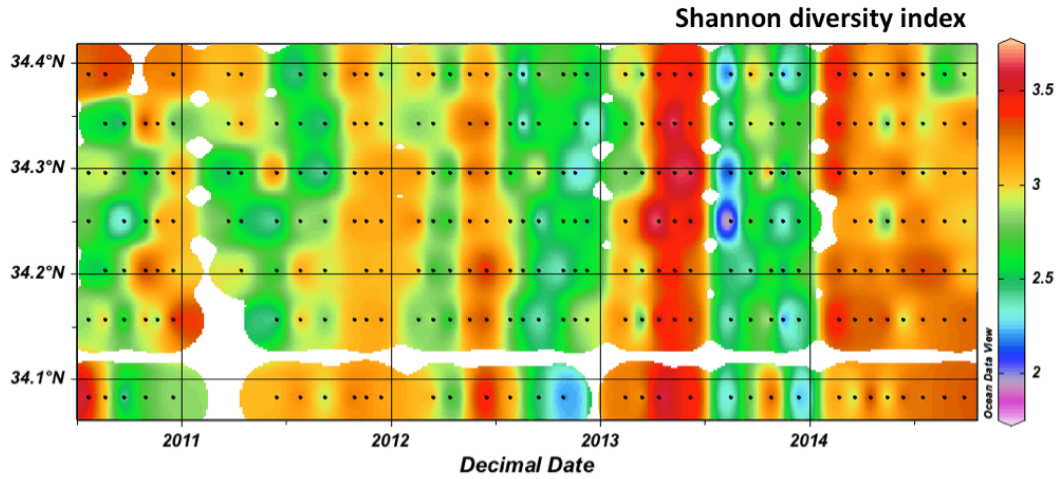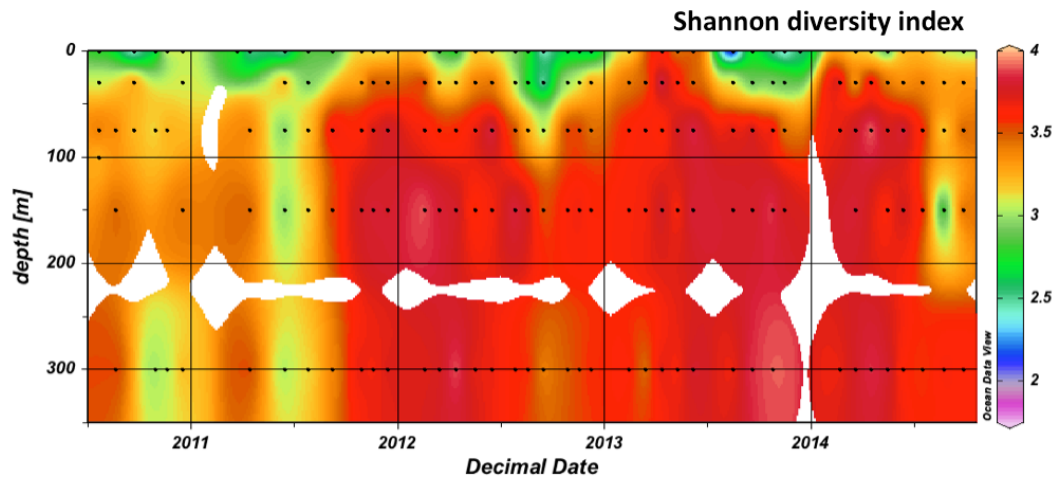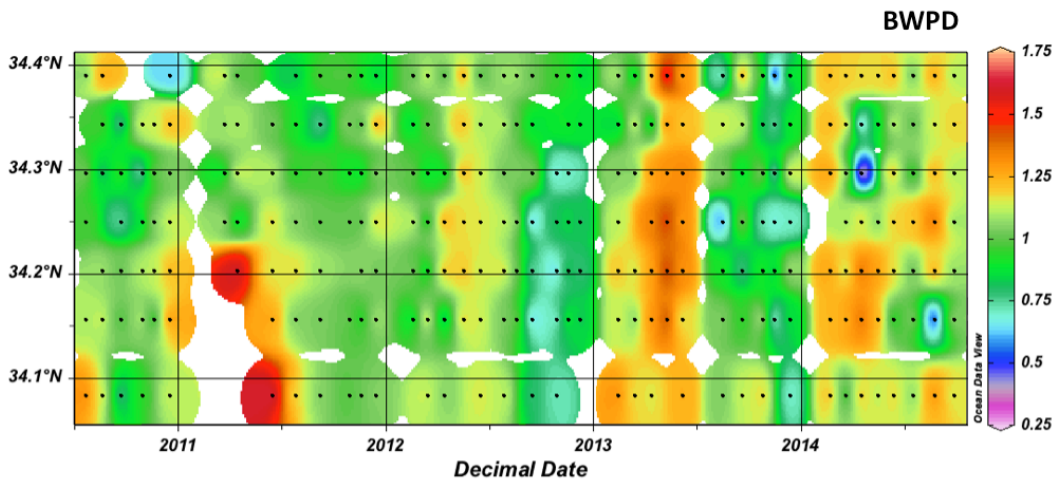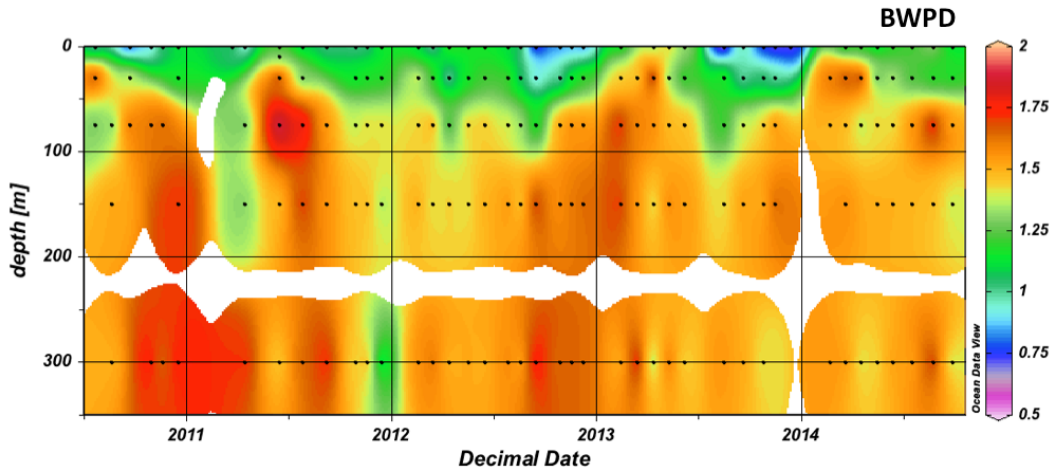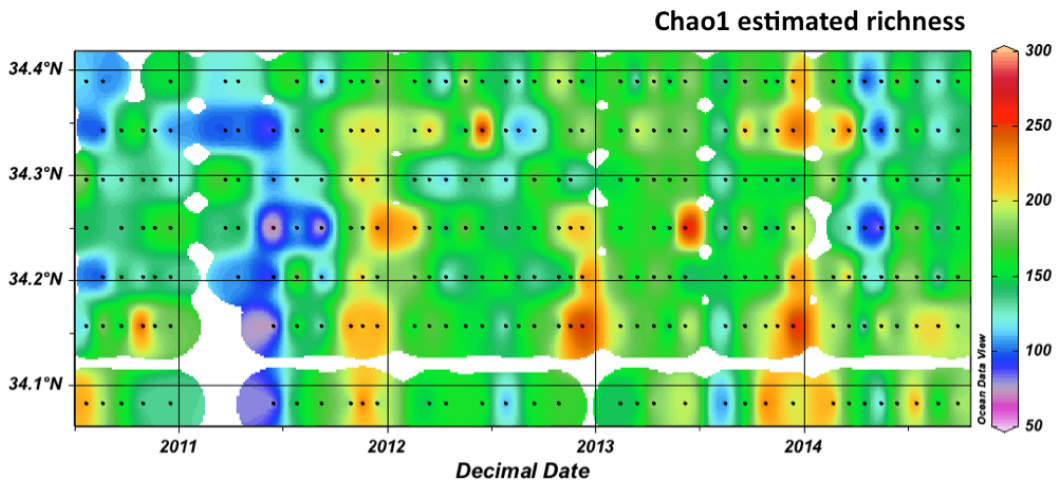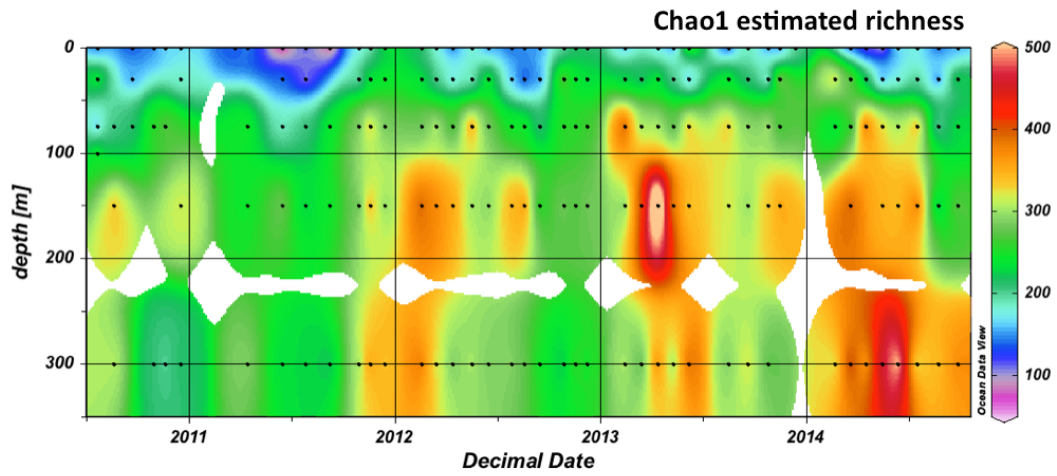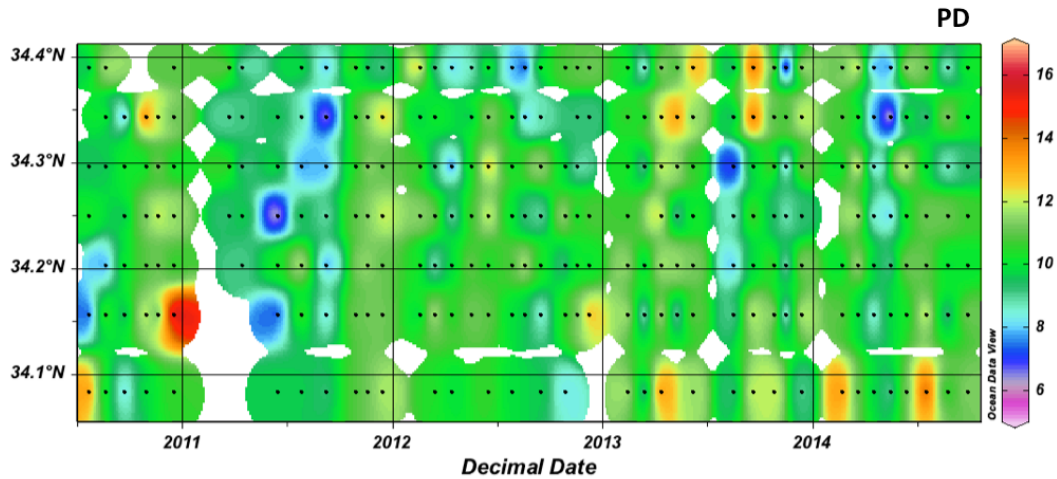
G.
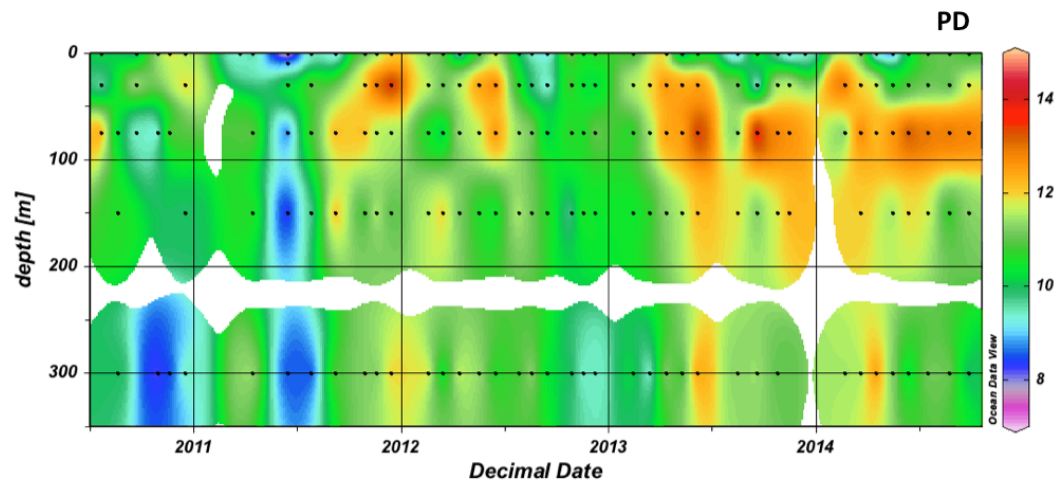
H.

Fig. 2.12: Distribution of Shannon diversity index and Chao1 estimated richness. A. Shannon index at the surface, as a birds-eye view of the time-series as in Fig. 1. B. Depth profile of Shannon index at Station 4. C. Balance-weighted phylogenetic diversity (BWPD) at the surface. D. Depth profile of BWPD. E. Chao1 at the surface. F. Depth profile of Chao1. G. Faith's phylogenetic diversity (PD) at the surface. H. Depth profile of PD. Note that color bar scales differ between surface maps and depth profiles.
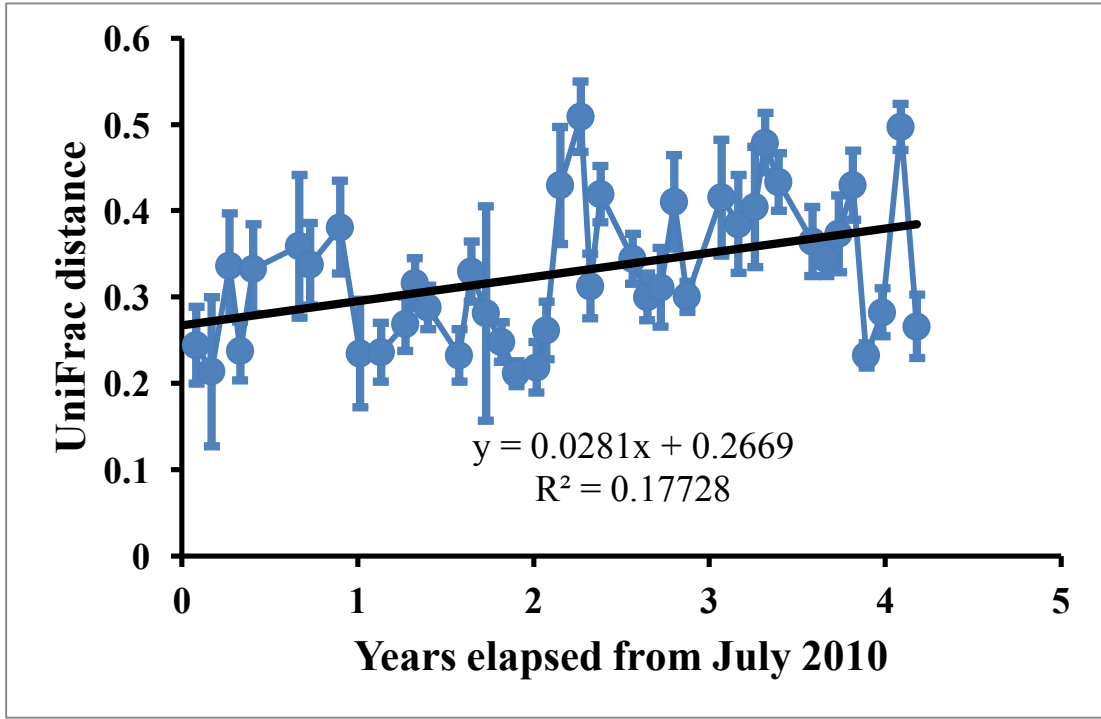
A.
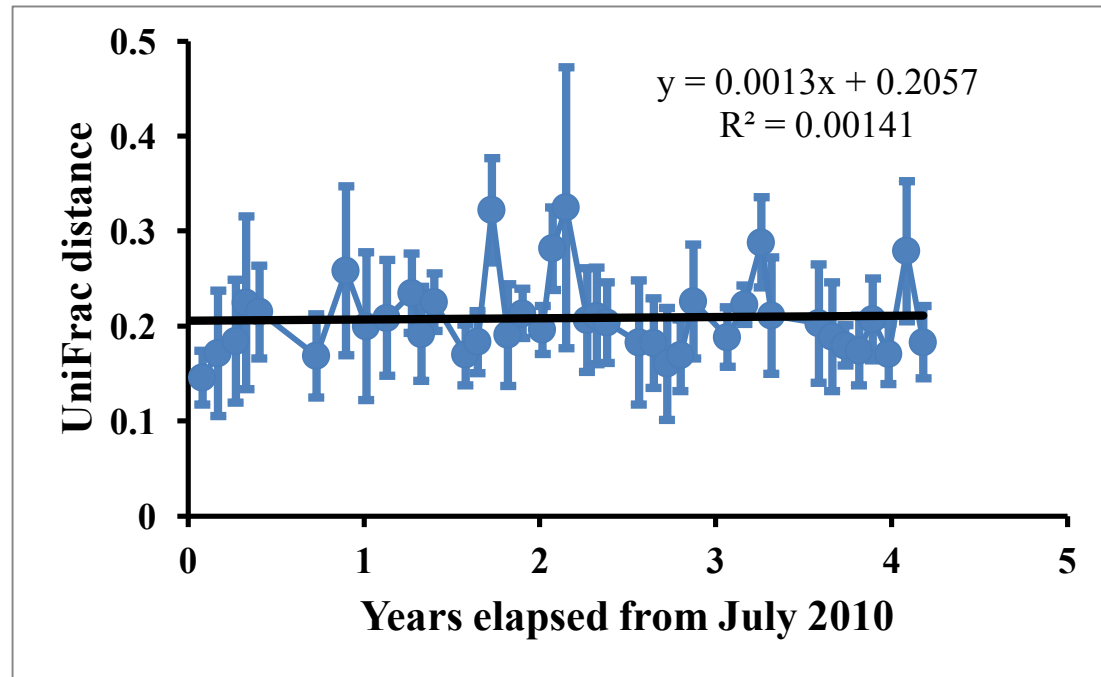
B.

Fig. 2.13: UniFrac distances between July 2010 and all subsequent samples, plotted over the time-lag between cruises (mean UniFrac distance of all pairwise comparisons between the three center stations from each cruise). A: Surface. B: 75 m.

III. Synchronous shifts in dissolved organic carbon bioavailability and bacterial community responses over the course of an upwelling-driven phytoplankton bloom

A. Abstract

Interactions between dissolved organic carbon (DOC) and bacterioplankton were examined during a diatom and *Phaeocystis* bloom in the Santa Barbara Channel (SBC) over 5 days following an upwelling event. The SBC was heterogeneous in physical state (recently upwelled vs. more stratified), nutrient concentration, and productivity, encompassing phytoplankton physiological states from a healthy bloom through the onset of silicon stress. DOC accumulated in the upper 10 m over the bloom, with compositional shifts indicated by chromophoric dissolved organic matter (CDOM) parameters. DOC bioavailability and bacterial growth and community composition responses were assessed with dilution batch-culture bioassays. In these experiments, bacterioplankton DOC usage increased over the bloom, with uptake of 1.5-5.3 µmol L^{-1} over 3 days, 1.5-5.7 µmol L^{-1} over 1 week, and 1.8-10.8 µmol L^{-1} over 10 weeks. DOC removal was poorly correlated with traditional proxies of bioavailability (chlorophyll *a* concentration, elemental ratios of dissolved organic matter, and

CDOM). However, bacterial growth efficiency (BGE) was strongly related to *in situ* conditions, with higher BGEs on fresher, late-bloom DOC. After 10 weeks, 1.6-15.7 µmol L$^-$^{1} of the DOC that accumulated during the bloom remained unutilized in the bioassays, with higher concentrations of persistent DOC in experiments from senescent bloom physiological states, supporting the putative relationship between phytoplankton blooms and seasonal DOC accumulation in the field. These experiments demonstrate that DOC released by the plankton community during a bloom fuels increased short-term and long-term bacterial activity, enhances presumed trophic transfer via increased BGEs, and leads to the accumulation of persistent, potentially exportable, DOC.

B. Introduction

Seasonal upwelling within the eastern boundary current is a characteristic biogeochemical driver of phytoplankton blooms along the coast of California. Upwelling-driven blooms are important sources of dissolved organic matter (DOM), a substrate that supports bacterioplankton growth and respiration and organic matter processing within the microbial loop, with increased proportions of primary production consumed by bacteria during various phases of such blooms (Montero et al. 2007; Halewood et al. 2012). These systems therefore provide an excellent opportunity to examine how shifts in the physiological state of a phytoplankton bloom affect the amount, bioavailability, and fate of DOM that is produced. Phytoplankton on average release 16-20% of their daily productivity as DOM (Baines and Pace 1991; Carlson and Hansell 2015), but the magnitude can vary greatly (2-80%), from low constitutive release to a response to stressors such as nutrient limitation and irradiance at the high end (Carlson and Hansell 2015). The partitioning of the most

bioavailable portion of this DOM between bacterial incorporation into biomass, with potential for subsequent trophic transfer, and respiration to inorganic constituents is of interest to the microbial ecologist, as is the relationship between DOM and bacterioplankton community composition (BCC). The portion of bloom-produced DOM that is produced as, or transformed to, recalcitrant compounds and that persists in dissolved form can have significant biogeochemical consequences, as the advection of dissolved organic carbon (DOC) to depth accounts for 20% of the global organic carbon export from the epipelagic zone (Carlson and Hansell 2015). Resolving the partitioning of net DOC production between bioavailable (labile) and persistent (semi-labile) pools can therefore inform our estimates across multiple scales of carbon cycling.

The canonical relationships between primary productivity, DOM, and heterotrophic bacterioplankton have been primarily inferred from cross-system studies, meta-analyses, and time-series work. Such studies have linked bacterial abundance with chlorophyll *a* (Chl *a*; Cole et al. 1988); bacterial production and bacterial growth efficiencies (BGEs) with net primary production (PP; Cole et al. 1988; del Giorgio and Cole 1998) and organic carbon to nitrogen ratios (del Giorgio and Cole 1998); and DOM bioavailability with compositional characteristics including molecular weight (Benner 2002), chromophoric DOM (CDOM) properties (Guillemette and del Giorgio 2011), elemental ratios (Sun et al. 1997), and diagenetic state (Benner 2002; Goldberg et al. 2009), as well as with Chl *a* (Guillemette and del Giorgio 2011). Time-series and cross-system studies have also demonstrated the contributions of phytoplankton blooms to DOC accumulation (Carlson et al. 1994; Williams 1995), variability in DOM quality (Goldberg et al. 2009), and DOC export (Carlson et al. 1994).

However, there is a paucity of field studies in which bacterial and DOM dynamics are assessed at high temporal and spatial resolution across a single phytoplankton bloom event, with most such studies focused on BCC (e.g., Teeling et al. 2012) or inferring shifts in DOM bioavailability from bacterial production (Barbosa et al. 2001) or enzymatic activity (Teeling et al. 2012). While the relationships measured in time-series and cross-system studies are often assumed to apply over ecologically relevant timeframes as well, this extrapolation likely misses subtleties inherent to the development and senescence of a discrete phytoplankton bloom, such as the shift from nutrient-replete to nutrient-stressed phytoplankton and the associated compositional changes in the DOM pool. Phytoplankton are thought to respond to incipient nutrient limitation by increasing the quantity and altering the chemical composition and stoichiometry of the DOM they produce (Williams 1995; Goldberg et al. 2009; Carlson and Hansell 2015), as Conan et al. (2007) saw in the elevated ratios of organic carbon to limiting nutrients and increased carbohydrate concentration in mesocosms experiencing various nutrient stresses. Although DOC released by phytoplankton is generally thought to be of high quality to bacterioplankton (del Giorgio and Cole 1998), the accumulation of C-rich DOM observed in the field after phytoplankton blooms (Carlson et al. 1994; Williams 1995) suggests that some DOM produced under nutrient stress is less bioavailable and can persist in the dissolved phase.

We repeatedly measured *in situ* biogeochemical parameters and experimentally assessed DOM bioavailability and bacterioplankton growth responses over 5 days across a heterogeneous, upwelling-driven phytoplankton bloom spanning conditions of recently upwelled water through the late-bloom onset of silicon stress (Si stress), in the Santa Barbara Channel (SBC), with the goal of assessing DOM-mediated effects of phytoplankton nutrient

stress on bacterioplankton activity. The SBC, an eastern boundary current system, features regular wind-driven upwelling of cold, nutrient-rich water in spring and early summer, prompting strong phytoplankton blooms (Otero and Siegel 2004). The fortuitous timing of an intensive process cruise immediately following such a wind event allowed us to sample the major physical driver of biogeochemistry in this system and its subsequent effects, and the high spatial heterogeneity of the SBC following the upwelling event enabled us to assess various physiological states of a phytoplankton bloom over a limited timeframe by sampling over a spatial grid.

C. Methods

1. Experimental design

Dilution batch-culture bioassay experiments were established 11-15 May 2011 (Table 3.1) on the SBDOM11 cruise aboard the R/V *Point Sur* in the western SBC, California, United States of America (Fig. 3.1). Water samples were collected within the upper 8 m of the water column (Table 3.1) using a conductivity temperature depth (CTD) profiling rosette equipped with 12 L Niskin bottles. Water was gravity-filtered directly from the Niskin bottle through two in-line mixed cellulose ester filters (1.2 μm (RAWP) and 0.2 μm (GSWP), Millipore, Billerica, MA) in polycarbonate cartridges that had been thoroughly flushed with Nanopure water or mesopelagic seawater (> 1 L) and sample seawater (0.5 L) to prevent organic contamination. Duplicate 500 mL polycarbonate bottles (previously washed in 5% hydrochloric acid) were rinsed then filled with 375 mL 0.2 μm filtrate (filter sterilized media) and 125 mL 1.2 μm filtrate (bacterial inoculum) collected from the same cast. Bottles were incubated in the dark in an upright incubator at 11°C (within 2.5°C of in situ temperatures;

Table 3.1) for 10 weeks. Samples for bacterial abundance, DOM, and DNA for BCC were collected by decanting from the bottles.

2. Sampling and analysis

a. Dissolved organic matter

In situ DOM samples were collected directly from the Niskin bottles through combusted GF/F filters (Whatman, Piscataway, NJ) in polycarbonate cartridges and into acid-washed high-density polyethylene bottles that were stored frozen at -20°C. Experimental seawater was initially filtered during bioassay set-up, as described above; to avoid contamination from handling, experimental DOM samples were collected without further filtration into combusted glass EPA vials with Teflon-lined silicone septa and frozen at -20° C. Experiments were sampled for DOC concentration at initiation, nominal 3 days, nominal 1 week, and 10 weeks. DOC values at the initial, 3-day, and 1-week time points were corrected by subtracting bacterial biomass (using a carbon conversion factor of 10 fg C cell^{-1}, consistent with the measured cellular carbon content of oceanic bacteria according to Fukuda et al. (1998)) before calculating DOC drawdown (to measure total bacterial carbon demand rather than just respiration). DOC and total dissolved nitrogen (TDN) were quantified by high-temperature combustion on a modified Shimadzu TOC-V calibrated as in Halewood et al. (2012). Dissolved organic nitrogen (DON) was calculated by subtracting dissolved inorganic nitrogen (measured as below) from TDN.

In situ CDOM samples were collected in amber glass bottles, filtered under low vacuum pressure through 0.2 μm polycarbonate filters (Nuclepore Track-Etch, Whatman), and stored in the dark at 4°C in combusted amber glass EPA vials with Teflon-lined silicone septa following Swan et al. (2009). UV-Visible absorption spectra were obtained from an

UltraPath single-beam instrument (World Precision Instruments, Sarasota, FL; as in Swan et al. 2009). Absorption values at 355 nm were normalized to in situ DOC concentrations (a355:DOC). Spectral slope coefficients (S) over 320-500 nm were calculated following Stedmon et al. (2000).

b. Bacterial abundance and production

Samples for bacterial abundance were collected in sterile cryovials daily for the first week, preserved with 0.2% final concentration paraformaldehyde (Electron Microscopy Sciences, Hatfield, PA), fixed at room temperature for >30 minutes, flash-frozen (liquid nitrogen or -40°C), and stored frozen until analysis. Bacterioplankton were stained with SYBR Green I (Molecular Probes) and enumerated with a BD LSRII flow cytometer (Becton Dickinson, San Jose, CA) with an autosampler attachment as in Halewood et al. (2012).

Bacterial production was measured by ^{3}H-leucine (^{3}H-Leu) incorporation (specific activity 54.1 Ci/mmol; Perkin Elmer, Boston, MA), using a modified microcentrifuge method (following Halewood et al. 2012). Samples were spiked to a final concentration of 15.7 nmol L^{-1} ^{3}H-Leu (preliminary experiments showed that uptake by SBC bacteria saturated at >10 nmol leucine L^{-1}) and incubated in the dark for 45-90 minutes at *in situ* temperature (±2°C). ^{3}H-Leu incorporation was converted to bacterial carbon production (BP) using the conversion factor of 1.5 kg C (mol leucine)$^{-1}$ (Simon and Azam 1989).

c. Physicochemical and phytoplankton data

Temperature, conductivity/salinity, depth, and photosynthetically active radiation (PAR) were obtained from a CTD sensor array (SBE9+; Sea-Bird Electronics, Inc., Bellevue, WA) equipped with, respectively: dual SBE 3Plus Temperature sensors, SBE 4C conductivity sensor, Tri-Tech altimeter, and Biospherical PAR sensor. Primary production

(PP) was measured by ^{14}C-bicarbonate tracer with 24-hour deck-board incubations as described in Anderson et al. (2006). Chl *a* was collected on 0.45 µm mixed cellulose ester filters (HAWP, Millipore), extracted in acetone, and quantified by fluorescence with acidification as in Anderson et al. (2006). Water for inorganic nutrient analysis was filtered through 0.6 µm polycarbonate filters (Nuclepore, Whatman), stored frozen, and analyzed using flow injection analysis on a QuikChem 8000 (Lachat Instruments, Loveland, CO; detection limits: nitrate+nitrite (N+N), 0.2 µmol L^{-1}; ammonium, 0.1 µmol L^{-1}; silicic acid, 1.0 µmol L^{-1}). Limitation of the rate of silicic acid uptake (Si stress) was assessed at the depth of the 50% light level in deckboard incubations using ^{32}Si(OH)$_4$ as a tracer. Si stress was quantified as the ratio of the rate of uptake of Si(OH)$_4$ at its ambient concentration to the rate obtained in the same water after a 20 µmol L^{-1} addition of sodium silicate (V_{amb}:V_{max}; Nelson et al. 2001); uptake was measured with additions of 280 Bq of high specific activity ^{32}Si (>40,000 Bq (µg Si)$^{-1}$) as sodium silicate (National Isotope Development Center, Oak Ridge National Laboratory). After 24-hour incubations to ensure a full photocycle, Si stress samples were filtered (0.6 µm polycarbonate) and processed as in Krause et al. (2011). Particulate organic carbon (POC) was collected on a GF/F filter (Whatman) and quantified by combustion elemental analysis on a CE440 Elemental Analyzer (Exeter Analytical Inc., North Chelmsford, MA). Wind data were obtained from National Data Buoy Center (http://www.ndbc.noaa.gov) stations 46053 (in the center of the SBC) and 46054 (at the western end of the SBC, south of Point Conception).

d. Bacterial community composition

In situ (i.e., starting community or T0) DNA from 1 L of water was prefiltered through 1.2 µm mixed cellulose ester filters (RAWP, Millipore) under low pressure using a

peristaltic pump and collected on 0.2 μm polyethersulfone filter cartridges (Sterivex-GP, Millipore), which were stored frozen (-20° at sea, -40° on shore). Experimental DNA was collected at day 3 (T3) from duplicate bottles combined (to conserve volume); 125 ml from each bottle was filtered through a 0.2 μm polyethersulfone filter (Supor-200, Pall, Port Washington, NY) under low vacuum pressure and filters were frozen in sterile cryovials. Samples were lysed in sucrose lysis buffer (40 mmol L^{-1} EDTA, 50 mmol L^{-1} Tris-HCl, 750 mmol L^{-1} sucrose, 400 mmol L^{-1} NaCl, pH adjusted to 8.0) with 1% w/v sodium dodecyl sulfate and 0.2 mg ml^{-1} proteinase-K at 55° C for 2 hours. Genomic DNA was extracted using a commercial silica centrifugation kit (DNEasy, Qiagen, Valencia, CA) and used to conduct multiplex amplicon pyrosequencing following Nelson et al. (2014). Briefly, 25 μL polymerase chain reactions were conducted with 4 μL genomic DNA template using primers targeting the V1 and V2 hypervariable regions of the 16S ribosomal ribonucleic acid (rRNA) gene (8F and 338R, with adaptors and oligonucleotide barcodes as in Nelson et al. 2014). Amplicons were pooled at equimolar quantities before pyrosequencing on a Roche/454 GS FLX using Titanium Chemistry (lab of Stephan Schuster, Pennsylvania State University). Results and barcodes were deposited in the NCBI Sequence Read Archive (http://trace.ncbi.nlm.nih.gov/Traces/sra) as run accession SRR1222603.

Sequence analysis was conducted in mothur (v1.28.0; Schloss et al. 2009) using a bioinformatic pipeline as described in Nelson and Carlson (2012) and Nelson et al. (2014). Quality-controlled sequences were aligned to a non-redundant subset of the SILVA SSU Ref 16S alignment database (v111) (Quast et al. 2013) curated as in Nelson et al. (2014). Sequences were assigned to operational taxonomic units (OTUs) by average-neighbor hierarchical clustering at the 95% identity level [over the highly variable V1-V2 region of the

16S gene examined here, a 5% difference is similar to a 3% difference over the full length of the 16S gene, and therefore this clustering is comparable with the 97% sequence identity commonly used for other amplified regions (Schloss 2010)] and OTUs were consensus classified at the 70% confidence level. Diversity metrics were calculated within mothur and weighted UniFrac (Lozupone and Knight 2005) was used to calculate phylogenetic distances between samples. Multivariate analyses (ordination and clustering algorithms) were conducted in PRIMER 6 (Clarke and Gorley 2006).

3. Calculations and statistics

To estimate net DOC and POC production during the bloom, it was necessary to determine the "background" DOC and POC values in upwelling source water at depth. We used salinity as a conservative tracer to identify the water masses from which recently upwelled surface water would have originated, assuming minimal isopycnal mixing, focusing on sub-euphotic zone water that should have experienced minimal biological activity resulting from the bloom; temperature was not used as a water mass tracer because upwelled water may have warmed at the surface. Salinities at 5 m nominal depth were between 33.76 and 33.84 under recently upwelled conditions (N+N >15 μmol L^{-1}); therefore, we identified potential upwelling source waters as those with salinity in this range and at less than 1% surface PAR. As this salinity range was found at two distinct depth ranges on 14 May 2011, suggesting the introduction of new water masses at depth, we excluded this and later sampling dates to focus on casts on 11-13 May 2011. The analysis was further restricted to casts at or north of 34.2° N latitude (approximately the northerly 2/3 of the basin; Fig. 3.1), as upwelling occurs primarily along the northward mainland coast in the western SBC, and to samples with >15 μmol L^{-1} N+N, where biological processing related to mixing with the

euphotic zone had presumably been minimal. Mean DOC and POC values within the samples

meeting all of these conditions were considered to represent background values (Table 3.2).

The proportion of freshly produced total organic carbon (TOC) that was partitioned into

DOC (TOC partitioning, or % DOC_{TOC}) (Carlson and Hansell 2003; Halewood et al. 2012),

was then calculated as:

Equation 1: % DOC_{TOC} = (in situ [DOC] – background mean [DOC]) x ((in situ [DOC] + in

situ [POC]) – (background mean [DOC] + background mean [POC]))$^{-1}$ x 100.

Persistent DOC, here defined as the freshly produced DOC that remained in the bioassays at

the final 10-week sampling, was calculated as:

Equation 2: persistent [DOC] = 10-week [DOC] – background mean [DOC].

Bacterial specific growth rate (μ) was calculated as the rate of change of the natural

log of cell abundance during exponential growth. Bacterial growth efficiency (BGE) was also

calculated over the exponential growth phase as the rate of change in bacterial cell biomass

divided by the slope of the DOC drawdown from experiment initiation to 1 week, with DOC

concentrations corrected for the bacterial biomass present at time of sampling. Exponential

growth phase for both μ and BGE was considered to extend from the end of lag phase to the

start of stationary phase or to the maximum biomass observed (with additional

abundance/biomass measures from lag and stationary phases averaged where available to

increase robustness of estimates). We assumed linear growth and DOC drawdown based on

observed linear bacterial growth curves and lag phases that did not exceed 24 hours.

Spearman's nonparametric correlation analyses were run (on means of parameters from replicate bottles where applicable) in PASW Statistics 18.0 (SPSS Inc.). CDOM slopes were calculated in JMP 9 (SAS Institute Inc.). Bootstrap analyses were run using Statistics101 2.8 (http://www.statistics101.net; 2013). Figures were generated in SigmaPlot 12.0 (Systat Software Inc.), Adobe Illustrator (Adobe Systems Incorporated), JMP, and PRIMER.

D. Results

1. In situ conditions

The SBC experienced a wind-driven upwelling event shortly before and during the early portion of the cruise. Winds south of Point Conception were elevated 7-14 May 2011, averaging 9.7 m s^{-1} out of the northwest, with gusts to 15.5 m s^{-1}; winds in the central SBC were elevated 9-10 May 2011, averaging 10.2 m s^{-1} out of the west-northwest, with gusts to 17.9 m s^{-1} (National Data Buoy Center). The upwelling from this physical forcing was reflected in the low temperatures, high inorganic nutrient concentrations, low phytoplankton biomass, and low DOC values measured in the early samples (11-12 May 2011) (Table 3.1). Over the course of the cruise, a strong phytoplankton bloom (mixed diatoms, dominated by *Guinardia striata*, and *Phaeocystis* sp.; L. Windecker, pers. comm.) developed in the SBC. Surface PP rates increased from a low of 1.2 to a high of 43.1 μmol C L^{-1} d^{-1}; Chl *a* from 0.2 to 14.1 μg L^{-1}; and POC from 6.2 to 70.7 μmol L^{-1} (Table 3.1). Because the phytoplankton bloom was spatially heterogeneous, we used *in situ* N+N concentration (which decreased from 24.7 to as low as 1.4 μmol L^{-1} over the sampling period) as an indicator of bloom

89

progression from upwelling through the onset of late-bloom nutrient stress. N+N

concentration was strongly negatively correlated with temperature and with *in situ* biological

parameters including POC and BP, supporting its use as an indicator of bloom state (Table

3.3, Fig. 3.2). N+N was also highly positively correlated with silicic acid such that N+N

concentration closely approximates the corresponding $Si(OH)_4$ concentrations (Table 3.1,

Table 3.3). Si stress (V_{amb}:V_{max} < 0.8, with lower values indicating higher stress; Nelson et

al. 2001) was observed in 15 of 24 samples with Si V_{amb}:V_{max} measurements (Table 3.1); Si

stress appeared related to the bloom progression, as Si V_{amb}:V_{max} was positively correlated

with N+N (i.e., Si stress was higher at lower N+N; Table 3.3; Fig. 3.3A) and negatively with

POC. However, Si stress did not increase linearly with inorganic nutrient drawdown, in that

limitation was first apparent at about 10 µmol L^{-1} $Si(OH)_4$ (Fig. 3.3A), consistent with the

known average half-saturation constant for Si uptake of about 2.5 µmol L^{-1} (Martin-Jézéquel

et al. 2000).

As the bloom developed, *in situ* DOC concentrations increased from 50.9 to 72.0

µmol L^{-1} (Table 3.1, Table 3.3, Fig. 3.2C). *In situ* bulk DOC:DON values were between 6.2

and 41.1, with a mean of 15.0, and with no discernable trends over the N+N gradient.

However, the strong increase in DOC (Fig. 3.2C) combined with the lack of significant trend

in DON over the N+N gradient (Fig. 3.2D) suggests that the accumulated DOM became

increasingly C-rich as nutrients were depleted. Shifts in DOM composition were also

indicated by an increase in CDOM specific absorbance (a355:DOC, from 2.974 to 4.438

a355 m^{-1} (mmol DOC L^{-1})$^{-1}$) (Table 3.1, Fig. 3.2E) and a decrease in CDOM spectral slope

coefficient values (*S*, 15.76 x10^3 to 13.32 x10^3) (Table 3.1, Fig. 3.2G) as N+N decreased,

suggesting an input of relatively fresh, high molecular weight, increasingly aromatic DOM

(Blough and Del Vecchio 2002). The phytoplankton bloom was accompanied by an increase in *in situ* BP, from 0.13 to 1.53 µmol C L^{-1} day^{-1} (Table 3.1).

Upwelling source waters were identified at depths between 13 and 72 m, with DOC and POC values each taken from 7 bottle samples between 30 and 50 m over 6 casts (Table 3.2). Samples that fit the background criteria showed little evidence of recent PP, with high mean N+N of 19.0 µmol L^{-1} and low mean Chl *a* of 1.3 µg L^{-1}. The mean DOC concentration in these samples was 49.3 µmol L^{-1} (45.7 to 51.8 µmol L^{-1}) and mean POC was 8.0 µmol L^{-1} (5.3 to 12.5 µmol L^{-1}); these mean values were taken to represent the background state of freshly upwelled waters. Elevated DOC and POC concentrations above these background values indicated that an average of 30% of newly produced TOC was partitioned to DOC (% DOC_{TOC} spanned 5 to 92% of new TOC), although % DOC_{TOC} did not vary systematically over the bloom (Table 3.1; Fig 3.2F).

2. DOC bioavailability and persistence

We analyzed 25 experiments that had at least one uncontaminated replicate bottle (exhibiting decreasing or stable DOC concentrations over time) (Table 3.4). After ~3 days (see Table 3.4 for exact durations), 9 experiments showed DOC drawdown greater than our detection limit (i.e., $\geq$1.5 µmol L^{-1}) with a range of 1.5 to 5.3 µmol L^{-1}, or between 2.3 and 7.6% remineralization of initial DOC concentrations (Table 3.4; Fig. 3.4A). This drawdown was positively correlated with µ (Table 3.3). Over the first week, 14 experiments showed significant drawdown between 1.5 and 5.7 µmol L^{-1}, or between 2.5 and 8.1% (Table 3.4; Fig. 3.4B); this drawdown was positively correlated with 10-week drawdown (Table 3.3). Over the total ten weeks, 22 of the 25 experiments had measureable drawdown of between 1.8 and 10.8 µmol L^{-1}, or 3.1 to 15.3% (Table 3.4; Fig. 3.3C). The 10-week DOC

91

remineralization was strongly related to conditions in the SBC at the time of sample collection, including indicators of bloom progression (N+N, negatively, Fig. 3.4C; and temperature, positively; Table 3.3) and biological parameters (POC and in situ DOC, both positively; Table 3.3). Persistent DOC was measureable in at least one replicate from all 25 experiments, at concentrations between 1.6 and 15.7 µmol L^{-1} (Table 3.4: Fig. 3.4D). The magnitude of persistent DOC was likewise negatively correlated with N+N (Fig. 3.4D; Table 3.3) and positively with temperature; positive correlations with parameters related to DOC composition and quality (in situ DOC, a355:DOC, % DOC_{TOC}, and 10-week DOC drawdown) and bacterial growth (maximum bacterial biomass and µ), and a negative correlation with Si V_{amb}:V_{max} (that is, a positive relationship with Si stress; Fig. 3.3D) (Table 3.3), collectively imply a relationship with bloom progression and the associated DOM alterations.

One caveat of our results is that we documented a variable, but measureable, difference in DOC concentrations between samples collected from the field and the initial samples from the corresponding bioassay experiments, presumably from handling contamination due to the multiple surfaces involved in filtration. We do not believe that this offset impacted our conclusions, as initial DOC concentrations in experiments were highly correlated to in situ DOC concentrations (Spearman's *rho*: $r = 0.835$, n = 23, $p < 0.0001$). This difference (mean increase of 3.7 µmol L^{-1} ± standard deviation of 3.4 in experiments, corresponding to a $6.6 \pm 5.9\%$ increase) showed no trends across the range of experiments and was not significantly correlated with any of the parameters discussed in Table 3.3 (Spearman's rho: all $p > 0.05$; not shown). Further, two-sample bootstrap analysis of the magnitude of this increase between samples with and without significant DOC drawdown

indicated that this increase was significantly larger in samples with measureable drawdown over the 1-week period (iterations = 1000000, p = 0.024) but was not different over the other two time periods over which DOC drawdown was assessed. Therefore, this concentration increase was not associated with a reduced ability to detect DOC consumption, as differences were only seen in samples where drawdown was measured, and the lack of correlation with any measured parameters suggests it is neither driving nor obscuring experimental responses.

3. Bacterial growth rates and efficiencies

Bacterial growth parameters within the experiments also showed strong relationships with in situ bloom state (Table 3.3; Fig. 3.4E and 3.4F). The maximum bacterial abundance measured in each bottle during the first week of the experiments (effectively the carrying capacity) increased from 0.63 to 2.06 x 10^9 cells L^{-1} across the bloom gradient, with higher abundances in experiments drawn from later bloom stages. This corresponded to maximum bacterial biomasses of 0.48 to 1.71 µmol C L^{-1} (Table 3.4), which were correlated with in situ and experimental parameters including N+N (Table 3.3, Fig. 3.4E). Specific growth rates increased from 0.20 to 1.10 day^{-1} across experiments as the bloom progressed (Table 3.4), as shown by a strong negative correlation with N+N, positive correlations with temperature, Chl a, POC, and DOC, and a negative correlation with Si V_{amb}:V_{max} (that is, a positive relationship with Si stress) (Table 3.3). Bacterial growth efficiency (BGE) was resolved in 13 experiments from the later portion of the bloom, with a mean of 40% and a range of 17 to 62% (Table 3.4). BGE was significantly correlated with several in situ factors indicating higher BGEs later in the bloom, including negative correlations with N+N (Fig. 3.4F) and CDOM slope and positive correlations with temperature, POC, BP, in situ DOC, and a355:DOC, as well as with a small number of experimental parameters (Table 3.3).

4. Bacterial community composition

The 16S rRNA gene amplicon pyrosequencing produced a total of 44,388 quality-filtered sequence reads over 45 samples, which clustered into 479 operational taxonomic units (OTUs). Across 21 initial (T0) samples that amplified well, we obtained between 347 and 1344 sequences per sample (median 1164) distributed among 54 to 122 OTUs (median 80). After discarding one sample with a highly contaminated replicate bottle, the 24 experimental day 3 (T3) samples had between 570 and 1444 sequences (median 924.5) among 35 to 96 OTUs (median 55.5).

BCC strongly clustered by time-point, with distinct community groupings at T0 and T3 (Fig. 3.5, Fig. 3.6). Within each time-point cluster, communities then sorted approximately along the N+N gradient (Fig. 3.5, Fig. 3.6), indicating that BCC first changed *in situ* in conjunction with the phytoplankton bloom and subsequently retained the signature of that change through the further compositional shifts in the experimental incubations. To quantify the magnitude of community differentiation response in the bioassays, we compared corresponding T0 and T3 samples. Weighted UniFrac distances are a phylogenetic community distance measure ranging from 0 to 1 that incorporate the relatedness of OTUs in two communities by constructing phylogenetic trees and comparing shared and unshared branch lengths, such that greater distances indicate lower community similarity (Lozupone and Knight 2005). UniFrac distances between corresponding T0 and T3 samples were between 0.27 and 0.49, with an average value of 0.40 (Table 3.5); these distances were not correlated with N+N or any experimental parameters (Table 3.3; Fig. 3.5B), though they were negatively correlated with Chl *a* and *in situ* BP. Shannon diversity index values were between 2.49 and 3.13 in the field and 1.74 and 3.32 in the experiments (Table 3.5). The

percent change in Shannon diversity between paired T0 and T3 samples was between -22.4%

and 16.8%, mean -6.7% (Table 3.5), with most paired samples showing a decrease in

diversity from T0 to T3; this percent change was not correlated with any short-term DOC

usage parameters or *in situ* bloom indicators (Table 3.3; Fig. 3.5C).

We observed a distinct shift in BCC within the experimental incubations, but the

divergence along the N+N gradient observed in T0 communities was maintained in the

experimental samples at T3 (Fig. 3.5A). While the specific details of the *in situ* BCC will be

discussed in a subsequent manuscript, this result is noteworthy here in that the bacterial

response to increased DOM bioavailability is not a wholesale, systematic shift to a reduced

number of copiotrophic phylotypes, as might be expected. Oligotrophic phylotypes such as

SAR11 and SAR116 decreased in relative abundance and known copiotrophs such as

Roseobacter and *Alteromonas* phylotypes increased from T0 to T3 samples, but these

changes were relatively subtle, and the magnitude of these shifts did not show directionality

along the N+N gradient (Fig. 3.6), in contrast with a typical copiotrophic response that would

correlate with the increased DOC bioavailability seen in the later bloom samples.

E. Discussion

This study demonstrates the pronounced bottom-up effects of an upwelling-driven

phytoplankton bloom, experiencing a gradient of Si stress, on both heterotrophic

bacterioplankton activity and DOM dynamics. We observed multiple lines of evidence for

the production and accumulation of new, compositionally distinct DOM, which influenced

bacterioplankton activity both in situ and in experimental bioassays, DOM bioavailability,

and the efficiency of DOC use. This study documents a novel relationship between *in situ*

conditions and subsequent remineralization responses in experiments derived from natural coastal waters spanning a range of physiological states within a phytoplankton bloom.

1. DOC accumulation, bioavailability, and persistence

Rather than using a Lagrangian approach to track an identified phytoplankton bloom, we substituted spatial heterogeneity across the SBC following an upwelling event for the temporal progression of a bloom. Because of the dynamic circulation in the SBC, which receives surface inflow from both the eastern and western ends of the Channel, we cannot say with certainty that the observed in situ gradients were produced by one discrete phytoplankton bloom. However, we were clearly sampling DOM derived from a recent bloom, whether it was centered in the SBC or continuously advected into it, rather than advected aged Southern California Bight water, which is low in nutrients and biomass. The increases in PP, POC, CDOM absorbance, and *in situ* BP, concurrent with a strong decrease in N+N, indicate that the increase in DOC concentrations over the course of the study was associated with fresh production; older, previously processed waters would also show elevated DOC and CDOM absorbance, but not the high biomass and production values that corresponded with low inorganic nutrients in our later samples.

As N+N concentrations decreased and phytoplankton biomass and Si stress increased, *in situ* DOC concentrations increased (Table 3.1, Fig. 3.2) and shifts in DOM optical properties (Table 3.1, Fig. 3.2E and 3.2G) suggest increases in molecular weight and aromaticity and therefore a fresher DOM pool (Blough and Del Vecchio 2002). Though we did not observe increases in bulk DOC:DON or in TOC partitioning towards the dissolved phase over the bloom, we did see evidence for a shift towards a C-rich pool of newly accumulated DOM as would be expected under the carbon overflow model (Williams 1995):

DOC concentrations increased by 20 µmol L^{-1} over the N+N gradient, while DON showed no trend and only a 6 µmol L^{-1} range (Table 3.1, Fig. 3.2C and 3.2D).

The majority of *in situ* parameters that are often interpreted as proxies of DOM bioavailability in long-term or cross-system work (Carlson and Hansell 2015) were not correlated with measured DOC drawdown in this study, including *in situ* BP, Chl *a* as a source indicator (Guillemette and del Giorgio 2011), and measures of DOM compositional quality such as DOC:DON (Sun et al. 1997) and CDOM parameters (Guillemette and del Giorgio 2011). The exception was *in situ* DOC concentration, which was positively correlated with long-term DOC drawdown, as in Guillemette and del Giorgio (2011). Some of these parameters were related to other aspects of DOC usage; for example, BGE was correlated with traditional quality indicators including *in situ* DOC concentration, *in situ* BP, and CDOM absorption and slope (Table 3.3).

The general lack of relationships between bloom development and short-term DOC bioavailability differs notably from the findings of both del Giorgio and Pace (2008) and Guillemette and del Giorgio (2011), which showed strong correlations between short-term DOC respiration in microcosms and in situ Chl *a* across multiple freshwater ecosystems. The contribution of allochthonous DOC in the freshwater systems may explain this discrepancy by setting up a contrast between terrestrial and phytoplankton-derived DOC bioavailability, compared to minimal terrestrial inputs in the SBC (Otero and Siegel 2004). In addition, tight coupling between *in situ* BP and DOM production may have led to minimal accumulation of the most labile DOM fraction during the SBC phytoplankton bloom, such that our experiments were measuring a portion of the semi-labile pool. This scenario was observed in the coastal Ross Sea, where a hyperproductive phytoplankton bloom was accompanied by a

commensurate increase in bacterial carbon demand, preventing DOM accumulation during the exponential growth phase of the bloom (Carlson and Hansell 2003). This disconnect between typical indicators of quality, source, and bulk composition and empirical measures of DOC drawdown indicates that, while these proxies may help in the assessment of chemical constituents and diagenetic state, they are nonetheless poor predictors of DOC turnover rates (Goldberg et al. 2009). Thus, direct measurements of DOC remineralization in bioassay experiments are required to assess true DOC bioavailability, rather than extrapolating from presumed quality based on properties of the bulk DOM stock, particularly over discrete events and in autochthonous-driven systems like the SBC.

In addition to supporting short-term remineralization and biomass production, a portion of the bloom-produced DOC was sufficiently recalcitrant to resist microbial degradation over weeks to months, at least while isolated under experimental conditions. The persistent pool, representing the carbon available for vertical and horizontal export from the system and potentially for long-term sequestration, was greater late in the bloom, as Si stress and senescence set in (Tables 3.1 and 3.4; Fig. 3.3D). A similar phenomenon has been observed over seasonal scales in the field, as recently-produced DOM accumulates over months in the surface ocean before dilution by convective overturn (Carlson et al. 1994; Williams 1995; Barbosa et al. 2001), and has also been observed in DOM-enriched microcosm experiments (Fry et al. 1996; Meon and Kirchman 2001) and mixed bacterial-phytoplankton mesocosms (Norrman et al. 1995).

Persistent DOC was positively related to bacterial growth and biomass in our experiments, suggesting that the food web processes responsible for the increased DOC concentration and bioavailability may have led to the secondary production of more

recalcitrant compounds. Heterotrophic processes can transform DOM by stripping away the most labile compounds and diagenetically altering the DOM (Benner 2002; Goldberg et al. 2009) or by producing recalcitrant byproducts through utilization of more labile compounds (Jiao et al. 2010). The observed increase in a355:DOC could indicate such *in situ* processing of DOM, as one hypothesized source of CDOM is a byproduct of phytoplankton-derived DOM processing by heterotrophic bacteria (Blough and Del Vecchio 2002). The phytoplankton bloom may have also directly contributed to the persistent DOC; Aluwihare and Repeta (1999) demonstrated the direct release of recalcitrant acyl-oligosaccharides by cultured phytoplankton. The persistent DOC in this study was approximately equivalent to or greater than the corresponding 10-week DOC removal (on average 2-fold and as much as 4-fold greater), making it a non-trivial component of carbon-cycling dynamics.

2. Bacterial community responses: BGE and BCC

The strong increase in BGE as the bloom progressed (Fig. 3.4F) indicated that the fresh DOM production, in combination with suitable inorganic nutrient availability and BCC, promoted greater potential trophic transfer of DOC by way of bacterial incorporation into biomass. A similar increase in BGE over the temporal progression of a phytoplankton bloom has been observed in other nutrient-rich coastal systems such as the Ross Sea (Carlson and Hansell 2003). The range of BGEs observed in this short-term study is comparable to that observed across many marine (particularly coastal) systems (del Giorgio and Cole 1998), although our results skew higher than the dominant range of 5-30% in that review, and generally higher than the open-ocean data reviewed by Carlson (2002); this supports our assessment that a portion of the DOM produced by this bloom was of high quality, at least to the resident bacterioplankton community over the short time period considered by BGE

calculations.

Our calculated BGE values were strongly negatively correlated with *in situ* inorganic nitrogen, in contrast with the positive correlation seen in an upwelling system by Lønborg et al. (2011), and strongly positively correlated with in situ temperature, in contrast with the negative correlations seen in a broad literature survey of the euphotic ocean (Rivkin and Legendre 2001) and the lack of relationship observed in a cross-system review (del Giorgio and Cole 1998). We believe these disagreements are due to the distinct progression of physical and chemical properties during an intensely sampled, upwelling-driven, short-term phytoplankton bloom, rather than the inorganic nitrogen and temperature per se: the upwelling-to-bloom progression that we sampled resulted in the production of highly bioavailable DOM in relatively warm, nutrient-poor water, setting up a contrast with the productive poles and oligotrophic tropics underlying cross-system comparisons in the global ocean. We do not expect that these temperature and nutrient relationships would have persisted if we had continued sampling after the bloom's termination. CDOM absorption and slope were highly correlated with BGE (positively and negatively, respectively), further suggesting that DOM composition impacted bacterial usage of the accumulated DOM. While we saw no correlation between BGE and bulk DOC:DON, we did find a positive correlation between *in situ* DOC concentrations and BGE. As we infer an increasingly C-rich DOM pool from the increase in DOC, there may be a relationship between BGE and DOM stoichiometry that is obscured by the bulk pool. However, in that case, our BGEs would show the opposite trend (an increase in BGE with increasing DOC:DON) of that seen by Lønborg et al. (2011), likely due to a combination of the freshly produced nature of the DOM and the continued availability of inorganic nitrogen (Table 3.1).

100

BGE was not correlated with the magnitude of short-term DOC removal (3 days or 1 week, the relevant timeframes to our BGE calculation) but was positively correlated with 10-week DOC drawdown in this study. A similar correlation was seen between BGE and 24-day DOC bioavailability by Apple and del Giorgio (2007), suggesting the systematic qualitative shifts across multiple sub-pools of the bioavailable DOM they posited might apply here as well. BGE was not significantly related to Chl *a* nor to PP, in contrast with cross-system analyses (del Giorgio and Cole 1998), further indicating that at high sampling resolution the significance of phytoplankton biomass and productivity is complicated by more subtle factors like the increase in DOM exudation from healthy log-phase phytoplankton growth to senescence (Carlson and Hansell 2003; Halewood et al. 2012) and the compositional shifts in that exudate upon phytoplankton nutrient stress (Williams 1995; Conan et al. 2007), versus the relatively simple presence of bloom conditions indicated by Chl *a* and PP in cross-system comparisons.

We want to emphasize two aspects of BCC in the context of increased bacterial growth across the bloom: First, community shifts between starting (T0) communities and experimental communities after 3 days (T3) were not merely a convergence on a limited number of copiotrophic OTUs (Fig. 3.5, Fig. 3.6), as has been noted in enrichment microcosms (McCarren et al. 2010; Nelson and Carlson 2012) and unenriched dilution culture experiments (Beardsley et al. 2003). Second, as bacterial growth within the experiments increased substantially as N+N values decreased, we expected to see a corresponding increase in community differentiation (an increased UniFrac distance) between paired T0 and T3 samples, a greater decline in diversity from T0 to T3 pairs (a more negative percent change of the Shannon diversity index), and higher relative abundances of

copiotrophic phylotypes in late-bloom T3 samples, yet none of these parameters showed trends across the N+N gradient (Table 3.5, Fig. 3.5). Rather, the BCC of the responding communities maintained a diverse assemblage with a resemblance to those found in the field, and therefore our rate parameters were not grossly skewed by shifts to "weed" species.

3. Effects of phytoplankton Si stress on DOC cycling

We observed the onset of, and an increase in, phytoplankton Si stress as the bloom progressed. The effects of this stress on DOM and bacterial parameters cannot be distinguished from the effects of the overall increase in phytoplankton biomass and productivity in this study, but the observed relationships are consistent with expectations from the literature (Williams 1995; Carlson and Hansell 2015). The accumulation of *in situ* DOC with increased Si stress (Fig. 3.3B) is consistent with the carbon overflow model in which C-rich DOM accumulates towards the nutrient-depleted phase of a phytoplankton bloom (Williams 1995). While the simultaneous increases in DOM bioavailability (although generally not significantly correlated with Si stress, Table 3.3) and μ (Table 3.3; Fig. 3.3C) would not be expected under the classic understanding of this mechanism, in situ inorganic nitrogen remained at measureable concentrations throughout the bloom (Table 3.1), possibly facilitating continued heterotrophic utilization of increasingly C-rich DOM. The complexity of the responses to nutrient stress may also relate to water mass history; the DOM pool in any given sample would integrate across previous bloom conditions, such that those samples with measured Si stress at the time of collection may have also previously experienced longer periods of nutrient-replete production and associated DOM accumulation. Nonetheless, this study supports the idea that persistent semi-labile DOC largely originates during the nutrient-stressed and senescent phases of phytoplankton blooms (Williams 1995), whether it is

produced in recalcitrant form (Aluwihare and Repeta 1999) or results from microbial processing of labile compounds (Jiao et al. 2010).

F. Conclusions

In this study, we have shown simultaneous shifts in DOM and bacterial composition and rates in association with a system-wide shift from recent upwelling to a mixed-composition phytoplankton bloom experiencing Si stress. *In situ* bloom conditions were related to parameters of DOC processing and shifts in bacterial activity and BCC within experimental bioassays, but traditional, cross-system proxy measurements of DOM bioavailability were more closely related to bacterial growth properties such as μ and BGE than to measured DOC drawdown. As Si stress increased, *in situ* DOC concentrations, bioavailable DOC, and persistent DOC all increased as well, supporting the putative relationship between phytoplankton blooms and observed seasonal DOC accumulation in the field. This series of remineralization experiments demonstrates that DOC "lost" by the plankton community during a bloom simultaneously fuels increases in short-term and long-term bacterial activity, enhances presumed trophic transfer by way of increased BGE, and leads to the accumulation of persistent, potentially exportable, DOC.

Table 3.1: In situ starting conditions, including DOM parameters, phytoplankton properties, and inorganic nutrient concentrations. Expt. ID: unique identifier used across tables. Stn: station number as indicated in Fig. 3.1. PP: primary production based on ^{14}C-bicarbonate incorporation. Si $V_{amb}:V_{max}$: phytoplankton Si stress expressed as the ratio of Si(OH)$_4$ uptake at its ambient concentration to the rate obtained in the same water after a 20 μmol L^{-1} addition of sodium silicate (see text for detailed methods). BP: bacterial production based on ^{3}H-leucine incorporation. S: CDOM spectral slope coefficient calculated following Stedmon et al. (2000). % DOC$_{TOC}$: percent of freshly produced organic matter partitioned into the dissolved phase (see text and Equation 1 for details on calculation). Blank spaces indicate no valid sample was obtained.

Expt. ID	Stn	Date sampled (2011)	Depth (m)	N+N (μmol L^{-1})	Si(OH)$_4$ (μmol L^{-1})	Temp. (°C)	Chl. a (μg L^{-1})	POC (μmol L^{-1})	PP (μmol C L^{-1} day^{-1})	Si V_{amb}:V_{max}	BP (μmol C L^{-1} day^{-1})	DOC (μmol L^{-1})	DON (μmol L^{-1})	CDOM abs. (α355 (m^{-1})	S (x10^3) (mmol C L^{-1})$^{-1}$)	% DOC$_{TOC}$
C10	16	11 May	4.2	24.7	26.3	10.0	0.2	6.2	1.2	1.3*	0.13				15.65	
C12	15	11 May	4.7	18.9	19.3	10.9	1.8	15.2	8.7	0.94	0.37	51.7	3.3	3.278	15.58	25.0
C14	14	11 May	2.7	13.5	13.8	11.7	3.3	26.1	24.7	1.1	0.43				15.21	
C16	13	11 May	3.5	10.5	10.8	12.3	3.7	19.6	23.8	0.93	0.32	53.1	6.5	3.806	13.92	24.6
C18	12	11 May	7.5	11.0	9.3	11.8	6.5	36.1	18.7	0.86	0.51	51.8	1.9	3.603	14.65	8.1
C19	7	12 May	4.7	21.5	22.3	10.6	1.9	13.3	8.3	0.90	0.20	53.1	3.3	2.974	15.14	41.4
C20	8	12 May	4.8	8.4	6.7	11.5	7.2	35.8	20.3	0.55	0.92	54.0	6.7	3.741	13.96	14.5
C21	9	12 May	5.0	11.9	7.4	11.6	14.1	45.0	15.8	0.67	0.91	57.6	1.4	4.069	14.22	18.3

*Value higher than reasonably expected with this technique; this value was qualitatively interpreted as replete but was not used in statistics or shown in Fig. 3.4.

Table continued on next page

Table 3.1, continued

Expt. ID	Stn	Date sampled (2011)	Depth	N+N	Si(OH)$_4$	Temp.	Chl. a	POC	PP	Si V_{amb}:V_{max}	BP	DOC	DON	CDOM abs.	S (x10^3)	% DOC$_{ROC}$
C22	10	12 May	4.5	11.1	10.2	11.6	5.9	36.8	22.9	0.67	0.48	50.9	8.2	3.238	15.16	5.1
C23	11	12 May	4.6	6.5	3.0	12.2	4.8	39.7	16.3	0.20	0.65	53.2	6.5	3.425	14.52	11.0
C24	12	12 May	4.8	10.3	10.1	12.3	5.6	51.2	43.1	0.62	0.47	55.1	5.2	3.683	15.06	11.8
C25	13	12 May	5.1	8.1	8.2	12.7	2.3	28.9	30.4	0.47	0.44	57.4	5.9	3.602	15.01	27.9
C26	14	12 May	4.6	5.0	5.4	13.0	1.6	17.9	9.0	0.55	0.31	60.5	7.7	3.958	14.98	52.9
C28	16	12 May	5.0	14.5	14.9	11.7	3.1	26.9	20.1	0.49	0.30	56.8	5.4	3.792	15.23	28.4
C29	17	13 May	6.9	10.4	12.0	12.0	8.0	33.7	20.9	1.0	0.91	60.4	2.8	3.756	14.34	30.1
C30	17.5	13 May	3.4	1.6	3.1	12.8	12.2	70.7			1.53	64.3	6.0			19.3
C31	18	13 May	3.5	1.4	1.8	13.4	6.8	46.9	21.6	0.33	0.93	64.9	4.9	4.104	13.32	28.6
C33	19	13 May	3.5	2.8	2.8	13.4	3.3	38.5	14.0	0.44	0.39	64.5	5.6	4.438	14.52	33.3
C35	20	13 May	5.2	5.1	5.5	13.5	2.0	24.6	17.0	1.1	0.33	63.4	5.0	4.160	15.46	45.8
C37	21	13 May	5.0	4.1	3.4	12.8	6.8	37.0	22.7	0.55	0.76	65.6	4.0	3.948	13.49	36.0
C38	22	14 May	4.9	8.2	8.2	12.6	1.0	8.6	2.9	0.80	0.52	56.8	2.7	4.242	14.24	92.1
C39	23	14 May	4.9	9.3	8.4	12.9	2.6	22.0	9.4	0.69	0.85	65.8	2.8	3.319	15.76	54.0
C40	24	14 May	5.1	3.2	4.0	13.3	3.7	53.5	20.7	0.39	0.63	72.0				33.3
C42	17	15 May	1.2	1.6	2.5	13.0	6.0	38.0	26.9	0.38	1.11	67.5	4.9			37.7
C46	19	15 May	1.9	2.5	1.8	13.3	9.2	65.0	34.9	0.17	0.55	57.3				12.4

Table 3.2: Characteristics of upwelled source water, which were used to estimate background DOC concentration at depth (see text for details on how these samples were identified). Date: date sampled. Lat: latitude (degrees north) sampled. Lon: longitude (degrees west) sampled. Depth of euphotic zone base: depth in cast where PAR < 1% of surface PAR. Depth of salinity range: depth range in cast, below the base of the euphotic zone, where target salinity range was observed. Depths of bottle samples: sampling depth of bottles fitting all specified qualifiers for background conditions. N+N, DOC, POC, and Chl *a*: all concentrations as measured at specified depths. Mean background values: mean of above measurements at depth, used for further calculations as applicable. Mean recently upwelled samples: mean of respective concentrations in surface samples that were identified as recently upwelled (N+N > 15 µmol L^{-1}) (see Table 3.1), shown here for comparison.

Date	Lat (°N)	Lon (°W)	Depth of euphotic zone base (m)	Depth of salinity range (m)	Depths of bottle samples (m)	N+N (µmol L^{-1})	DOC (µmol L^{-1})	POC (µmol L^{-1})	Chl *a* (µg L^{-1})
11 May 2011	34.39	120.31	23	23-41	30	20.1		12.5	3.1
11 May 2011	34.22	120.09	26	26-43	30	21.6	48.8	10.3	2.8
13 May 2011	34.38	120.11	13	27-67	30	23.4	51.5	5.4	0.6
13 May 2011	34.38	120.11	13	27-67	50	20.4	49.2	5.3	0.3
13 May 2011	34.31	120.00	14	20-64	30	15.3	51.8	11.0	1.8
13 May 2011	34.31	120.00	14	20-64	50	16.1	45.7	5.3	0.6
13 May 2011	34.27	119.95	22	22-40	40	17.7	50.3	5.8	0.7
13 May 2011	34.22	119.90	33	33-60	50	17.3	47.5		0.2
Mean background values						19.0	49.3	8.0	1.3
Mean recently upwelled surface sample values						20.9	52.9	13.1	1.6

Table 3.3: Correlation matrix (nonparametric Spearman's *rho*) of in situ parameters and experimental response variables. Significant correlations ($p < 0.05$) are indicated in bold.

	$Si(OH)_4$	Temp.	Chl. a	POC	PP	Si $V_{amb}{:}V_{max}$	BP	in situ DOC
N+N	**R = 0.939** **n = 25** ***p* < 0.0001**	**-0.874** **25** **<0.0001**	-0.362 25 0.076	**-0.608** **25** **0.001**	-0.339 24 0.105	**0.680** **20** **<0.0001**	**-0.564** **25** **0.003**	**-0.720** **23** **<0.0001**
$Si(OH)_4$		**-0.777** **25** **<0.0001**	**-0.458** **25** **0.021**	**-0.681** **25** **<0.0001**	-0.268 24 0.205	**0.746** **23** **<0.0001**	**-0.598** **25** **0.002**	**-0.618** **23** **0.002**
Temp.			0.105 25 0.617	**0.414** **25** **0.040**	0.277 24 0.190	**-0.430** **23** **0.041**	0.274 25 0.186	**0.765** **23** **<0.0001**
Chl. a				**0.793** **25** **<0.0001**	**0.577** **24** **0.003**	-0.307 23 0.154	**0.760** **25** **<0.0001**	0.143 23 0.515
POC					**0.591** **24** **0.002**	**-0.674** **23** **<0.0001**	**0.642** **25** **0.001**	0.350 23 0.102
PP						-0.267 23 0.218	0.326 24 0.120	0.089 22 0.695
Si $V_{amb}{:}V_{max}$							-0.368 23 0.084	-0.369 22 0.091
BP								**0.458** **23** **0.028**

(Table continues on next page)

Table 3.3 continued

in situ DON	DOC:DON	a355:DOC	CDOM spectral slope	% DOC$_{TOC}$	ΔDOC$_{3day}$	ΔDOC$_{1wk}$	**Variable**
-0.266 21 0.243	0.155 20 0.503	**-0.591** **19** **0.008**	**0.514** **21** **0.017**	-0.220 23 0.313	-0.269 9 0.484	-0.342 12 0.276	N+N
-0.211 21 0.359	0.097 21 0.676	**-0.590** **19** **0.008**	**0.570** **21** **0.007**	-0.056 23 0.798	-0.414 9 0.269	-0.169 12 0.599	Si(OH)$_4$
0.112 21 0.628	-0.029 21 0.902	**0.625** **19** **0.004**	-0.253 21 0.268	**0.427** **23** **0.042**	0.530 9 0.142	0.028 12 0.931	Temp.
-0.054 21 0.817	0.152 20 0.511	0.052 19 0.833	**-0.615** **21** **0.003**	**-0.557** **23** **0.006**	-0.013 9 0.974	0.384 12 0.217	Chl. a
0.138 21 0.549	-0.049 21 0.832	0.142 19 0.562	**-0.471** **21** **0.031**	**-0.497** **23** **0.016**	-0.017 9 0.966	0.366 12 0.242	POC
0.358 20 0.121	-0.335 20 0.148	-0.068 19 0.781	-0.282 21 0.216	**-0.465** **22** **0.029**	-0.156 8 0.713	-0.092 11 0.788	PP
-0.412 20 0.071	0.361 20 0.118	-0.147 19 0.549	0.359 20 0.120	0.166 22 0.460	-0.631 7 0.129	-0.202 11 0.552	Si V$_{amb}$:V$_{max}$
-0.188 21 0.415	0.288 21 0.206	0.118 19 0.629	-0.563 21 0.008	-0.133 23 0.544	0.017 9 0.966	0.338 12 0.283	BP
-0.156 21 0.499	0.271 21 0.235	**0.585** **19** **0.009**	-0.191 19 0.434	**0.584** **23** **0.003**	0.464 7 0.294	0.394 12 0.205	in situ DOC
	-0.977 **21** **<0.0001**	-0.092 19 0.707	0.010 19 0.967	-0.298 21 0.190	-0.543 6 0.266	-0.060 11 0.861	in situ DON
		0.112 19 0.647	-0.044 19 0.858	0.312 21 0.169	0.314 6 0.544	0.064 11 0.851	DOC:DON
			-0.509 **19** **0.026**	0.411 19 0.081	0.600 5 0.285	0.301 9 0.431	a355:DOC
				0.095 19 0.700	-0.523 7 0.229	-0.391 9 0.298	CDOM spectral slope
					0.643 7 0.119	0.211 12 0.510	% DOC$_{TOC}$
						0.551 6 0.257	ΔDOC$_{3day}$

(Table continues on next page)

Table 3.3 continued

ΔDOC$_{10wk}$	Persistent DOC	Max. bacterial biomass	μ	BGE	UniFrac distance	% Δ Shannon diversity index	**Variable**
-0.776 **20** **<0.0001**	**-0.792** **25** **<0.0001**	**-0.776** **25** **<0.0001**	**-0.649** **25** **<0.0001**	**-** **0.817** **13** **0.001**	-0.150 20 0.527	-0.150 20 0.527	N+N
-0.644 **20** **0.002**	**-0.700** **25** **<0.0001**	**-0.640** **25** **0.001**	**-0.738** **25** **<0.0001**	**-** **0.817** **13** **0.001**	-0.053 20 0.823	-0.114 20 0.613	Si(OH)$_4$
0.778 **20** **<0.0001**	**0.849** **25** **<0.0001**	**0.842** **25** **<0.0001**	**0.625** **25** **0.001**	**0.713** **13** **0.006**	0.349 20 0.131	0.331 20 0.154	Temp.
0.289 20 0.217	-0.026 25 0.902	0.225 25 0.280	**0.396** **25** **0.050**	0.531 13 0.062	**-0.500** **20** **0.025**	-0.386 20 0.093	Chl. a
0.540 **20** **0.014**	0.232 25 0.265	**0.414** **25** **0.040**	**0.636** **25** **0.001**	**0.670** **13** **0.012**	-0.362 20 0.116	-0.090 20 0.705	POC
0.325 19 0.175	0.189 24 0.377	0.334 24 0.111	0.338 24 0.106	0.189 12 0.557	0.030 19 0.904	0.051 19 0.836	PP
-0.464 18 0.053	**-0.423** **23** **0.045**	-0.313 23 0.146	**-0.644** **23** **0.001**	-0.490 12 0.106	0.054 19 0.825	-0.311 19 0.195	Si $V_{amb}{:}V_{max}$
0.316 20 0.175	0.282 25 0.173	0.201 25 0.336	0.394 25 0.051	**0.555** **13** **0.049**	**-0.522** **20** **0.018**	-0.357 20 0.122	BP
0.682 **18** **0.002**	**0.701** **23** **<0.0001**	**0.591** **23** **0.003**	**0.541** **23** **0.008**	**0.593** **13** **0.033**	0.018 19 0.943	0.112 19 0.647	in situ DOC
-0.001 16 0.996	0.014 21 0.951	0.254 21 0.266	0.095 21 0.684	-0.273 11 0.416	0.253 18 0.311	0.134 18 0.595	in situ DON
0.055 16 0.841	0.031 21 0.893	-0.152 21 0.511	-0.031 21 0.895	0.509 11 0.110	-0.243 18 0.332	-0.228 18 0.363	DOC:DON
0.511 14 0.062	**0.563** **19** **0.012**	**0.489** **19** **0.033**	0.382 19 0.106	**0.767** **9** **0.016**	0.105 17 0.687	0.169 17 0.516	a355:DOC
-0.240 16 0.370	-0.257 21 0.262	-0.333 21 0.141	-0.219 21 0.339	**-** **0.828** **9** **0.006**	0.230 18 0.358	0.193 18 0.443	CDOM spectral slope

(Table continues on next page)

Table 3.3 continued

ΔDOC$_{10wk}$	Persistent DOC	Max. bacterial biomass	μ	BGE	UniFrac distance	% Δ Shannon diversity index	**Variable**
0.380 18 0.120	**0.567 23 0.005**	0.242 23 0.267	0.018 23 0.937	0.432 13 0.141	0.262 19 0.279	0.193 19 0.428	% DOC$_{TOC}$
0.552 8 0.156	0.496 9 0.175	0.496 9 0.175	**0.689 9 0.040**	-0.429 6 0.397	0.559 7 0.192	0.018 7 0.969	ΔDOC$_{3day}$
0.653 12 0.021	-0.359 12 0.252	0.162 12 0.615	0.028 12 0.931	-0.009 11 0.979	-0.515 8 0.192	-0.515 8 0.192	ΔDOC$_{1wk}$
	0.522 20 0.018	**0.784 20 <0.0001**	**0.520 20 0.019**	**0.667 13 0.013**	0.150 15 0.593	-0.190 15 0.498	ΔDOC$_{10wk}$
		0.640 25 0.001	**0.597 25 0.002**	0.544 13 0.055	0.231 20 0.327	**0.583 20 0.007**	Persistent DOC
			0.454 25 0.023	**0.555 13 0.049**	0.382 20 0.097	0.192 20 0.416	Max. bacterial biomass
				0.513 13 0.073	-0.053 20 0.825	0.404 20 0.077	μ
					-0.050 9 0.898	-0.550 9 0.125	BGE
						0.071 20 0.767	UniFrac distance

Table 3.4: Experimental DOC and bacterial parameters. All values presented are median value of duplicates (range of duplicate values); a lack of a range indicates that only one sample had an acceptable value. Empty cells: no valid datapoint obtained; for DOC-associated values, generally because ΔDOC was below detection limits of 1.5 µmol L⁻¹. Expt. ID: unique identifier used across tables. Biomass: bacterial biomass converted from abundance values using a conversion factor of 10 fg C cell⁻¹. Days elapsed: duration of incubation time between experiment initiation and sampling for indicated parameter for nominal times. Max. biomass: maximum bacterial biomass observed over the first week of the experiment, at variable timepoints. Max. biomass: maximum bacterial biomass observed over the first week of the experiment, at variable timepoints, used to calculate BGE and µ (when a stationary phase was observed, the mean of those timepoints is reported; otherwise, this is the discrete maximum value observed in the first week of the remineralization experiments). BGE: bacterial growth efficiency (see text for details on calculation). µ: bacterial specific growth rate over the exponential phase. Persis. DOC: persistent DOC, i.e. the freshly produced DOC above background concentrations remaining in the experiments after 10 weeks (see text and Equation 2 for details on calculation).

| Expt. ID | Initial | | Day 3 | | | 1 week | | | 10 weeks | Max. biomass (µmol C L⁻¹) | BGE (%) | µ (day⁻¹) | Persis. DOC (µmol L⁻¹) |
	[DOC] (µmol L⁻¹)	Biomass (µmol C L⁻¹)	Days elapsed (DOC/ BB)	DOC (µmol L⁻¹)	Biomass (µmol C L⁻¹)	Days elapsed (DOC/ BB)	DOC (µmol L⁻¹)	Biomass (µmol C L⁻¹)	DOC (µmol L⁻¹)				
C10	51.7 (0.8)	0.26 (0.01)	3.3/3.2	50.2 (0.0)	0.31 (0.06)	7.3/7.4	50.8	0.55 (0.04)	50.9 (0.1)	0.54 (0.03)		0.20 (0.03)	1.6 (0.1)
C12	53.5 (0.8)	0.16	3.2/3.1	51.0	0.30 (0.02)	7.2/7.2	52.3 (1.3)	0.54 (0.01)	52.4 (0.1)	0.53 (0.01)		0.22 (0.01)	3.1 (0.1)
C14	56.2 (0.9)	0.18 (0.00)	3.0/3.0	53.5	0.44 (0.00)	7.1/7.1	56.6	0.73 (0.01)	55.3	0.71 (0.01)		0.30 (0.03)	6.0
C16	55.1	0.26 (0.03)	2.9/2.9	55.8	0.49 (0.02)	7.0/7.0	55.0	0.93 (0.01)	54.2	0.90 (0.00)		0.24 (0.01)	4.9
C18	60.0 (0.3)	0.11 (0.02)	2.8/2.8	60.0	0.44 (0.01)	6.9/6.9	58.4 (0.7)	0.56 (0.01)	56.4 (0.7)	0.76 (0.04)	38	0.37 (0.01)	7.1 (0.7)
C19	54.2 (0.1)	0.08 (0.01)	3.0/3.0	54.9 (0.3)	0.28 (0.02)	7.4/7.3	53.6 (0.3)	0.62 (0.02)	54.0 (0.0)	0.61 (0.02)		0.27 (0.00)	4.7 (0.0)
C20	58.1 (0.1)	0.09 (0.01)	2.9/2.9	57.4 (0.4)	0.43 (0.01)	7.3/7.2	58.5 (0.5)	0.29 (0.04)	55.6 (0.4)	0.57 (0.02)		0.42 (0.03)	6.3 (0.4)
C21	57.7 (0.5)	0.09 (0.01)	2.8/2.8	57.3	0.35 (0.00)	7.2/7.2	56.8 (0.1)	0.27 (0.02)	54.1 (0.4)	0.48 (0.02)	39	0.38 (0.03)	4.8 (0.4)
C22	57.2 (0.0)	0.18 (0.06)	2.8/2.8	56.2 (0.9)	0.38 (0.04)	7.1/7.1	54.1 (1.4)	0.64 (0.05)	53.4	0.70 (0.04)	30 (11)	0.33 (0.01)	4.1
C23	60.3 (0.4)	0.18 (0.01)	2.8/2.8	59.3 (0.7)	0.61 (0.10)	7.1/7.1	57.5 (0.4)	0.49 (0.10)	58.3 (0.3)	0.83 (0.01)	37 (12)	0.50 (0.19)	9.0 (0.3)

Table continued on next page

111

Table 3.4, continued

Expt. ID	[DOC] (μmol L⁻¹)	Biomass C (μmol L⁻¹)	Days elapsed (DOC/BB)	DOC (μmol L⁻¹)	Biomass C (μmol L⁻¹)	Days elapsed (DOC/BB)	DOC (μmol L⁻¹)	Biomass C (μmol L⁻¹)	DOC (μmol L⁻¹)	Max. biomass (μmol C L⁻¹)	BGE (%)	μ (day⁻¹)	Persis. DOC (μmol L⁻¹)
C23	60.3 (0.4)	0.18 (0.01)	2.8/2.8	59.3 (0.7)	0.61 (0.10)	7.1/7.1	57.5 (0.4)	0.49 (0.10)	58.3 (0.3)	0.83 (0.01)	37 (12)	0.50 (0.19)	9.0 (0.3)
C24	58.7 (0.3)	0.07 (0.00)	2.7/2.7	57.8 (1.1)	0.39 (0.03)	7.0/7.0	58.2 (0.4)	0.74 (0.04)	57.4 (1.0)	0.74 (0.03)		0.38 (0.05)	8.1 (1.0)
C25	64.2 (0.7)	0.09 (0.01)	2.6/2.6	63.9 (0.2)	0.33	7.0/7.0	62.7 (0.2)	0.87 (0.02)	60.4 (0.1)	0.87 (0.02)	36	0.33 (0.02)	11.1 (0.1)
C26	69.2 (1.4)	0.09[A]	2.6/2.6	67.0 (0.7)	0.40 (0.01)	6.9/6.9	66.0 (0.6)	1.08 (0.02)	63.1 (3.3)	1.08 (0.02)		0.33 (0.01)	13.8 (3.3)
C28	61.1 (0.8)	0.27 (0.02)	2.5/2.5	57.9 (0.0)	0.63 (0.05)	6.8/6.8	56.2 (0.4)	0.52 (0.03)	55.5 (0.1)	0.72 (0.01)	17 (2)	0.57 (0.02)	6.2 (0.1)
C29	62.4 (0.3)	0.15 (0.03)	3.0/3.0	62.1 (1.1)	0.48 (0.09)	7.4/7.4	61.3 (0.1)	0.74 (0.19)	58.1 (0.8)	1.00 (0.04)		0.28 (0.00)	8.8 (0.8)
C30	64.8	0.12	2.9/3.0	63.6 (0.2)	0.86 (0.06)	7.3/7.3	61.2	0.55 (0.03)	57.2 (0.6)	1.10 (0.01)	46	0.37 (0.02)	7.9 (0.6)
C31	70.2 (1.3)	0.15 (0.00)	2.9/2.9	64.8 (0.4)	1.29 (0.10)	7.3/7.3	64.5 (0.4)	0.70 (0.21)	59.4 (0.0)	1.71 (0.08)	42 (4)	0.39 (0.01)	10.1 (0.0)
C33	67.9 (0.0)	0.11 (0.00)	2.7/2.8	65.7 (0.4)	0.79 (0.04)	7.1/7.1	64.8 (1.0)	1.39 (0.01)	59.6 (1.0)	1.37 (0.01)	43	0.49 (0.02)	10.3 (1.0)
C35	67.2 (0.1)	0.07 (0.00)	2.6/2.7	66.6	0.56 (0.03)	7.0/7.0	65.5 (0.0)	1.16 (0.10)	62.1 (0.9)	1.47 (0.01)		0.77 (0.03)	12.8 (0.9)
C37	67.7 (0.4)	0.07	2.5/2.5	66.8	0.70	6.9/6.9	64.8	0.27	59.9	1.19	43	0.69	10.6
C38	64.2 (0.1)	0.07 (0.00)	3.3/3.3	64.9	0.22 (0.01)	7.3/7.3	63.1 (0.2)	0.62 (0.03)	60.5 (0.5)	0.62 (0.03)		0.31 (0.00)	11.2 (0.5)
C39	64.0	0.11 (0.03)	3.2/3.2	64.0	0.33 (0.01)	7.2/7.2	62.9 (0.0)	0.74 (0.04)	59.5 (0.9)	0.73 (0.04)		0.38 (0.03)	10.2 (0.4)
C40	67.5 (0.8)	0.06 (0.01)	3.2/3.2	67.7 (0.7)	0.43 (0.09)	7.2/7.2	66.2 (0.1)	0.98 (0.03)	60.5	0.98 (0.03)	40	0.74 (0.10)	11.2
C42	71.6 (0.5)	0.07 (0.02)	3.3/3.3	72.4	0.74 (0.01)	7.4/7.4	68.4 (0.0)	0.51 (0.09)	65.0 (0.1)	0.81 (0.05)	47 (10)	0.74 (0.02)	15.7 (0.1)
C46	66.2 (0.9)	0.07 (0.01)	3.1/3.1	64.2 (1.0)	0.79 (0.07)	7.2/7.2	63.9 (0.6)	0.18 (0.04)	60.1	0.92 (0.07)	62 (4)	1.10 (0.08)	10.8

A: Mean of adjacent initial samples C25 and C27 (0.08; sample not otherwise reported due to DOC contamination).

Table 3.5: Weighted UniFrac distances between paired T0 and T3 samples, Shannon diversity indices for each timepoint, and percent change in Shannon index between paired T0 and T3 samples. Blank cells indicate no valid sequencing results were obtained.

Expt. ID	UniFrac distance (T0-T3 pairs)	Shannon diversity index: T0	Shannon diversity index: T3	% change in Shannon index (T0-T3 pairs)
C10			1.74	
C12	0.45	2.84	2.21	-22.4
C14	0.40	2.85	2.59	-9.3
C16	0.42	2.79	2.51	-10.1
C18			2.37	
C19	0.41	2.96	2.59	-12.7
C20	0.38	2.81	2.40	-14.7
C21	0.27	2.58	2.26	-12.4
C22	0.39	2.87	2.45	-14.7
C23	0.38	2.54	2.97	16.8
C24	0.38	2.79	2.76	-1.2
C25	0.48	2.55	2.72	6.5
C26	0.47	2.56	2.55	-0.4
C28	0.36	2.91	3.32	14.3
C29	0.35	3.02	2.69	-10.8
C30	0.28	2.98	2.45	-17.6
C31	0.45	2.69	2.15	-20.1
C33	0.48	2.49	2.28	-8.2
C35	0.49	2.49	2.46	-1.4
C37		2.62		
C38	0.32	3.13	3.03	-3.2
C39	0.40	2.83	2.65	-6.3
C40	0.35	2.67	2.53	-5.3
C42			2.58	
C46			2.44	

Figure 3.1: Map of the study site in the Santa Barbara Channel, California, USA, with locator map in inset. Numbers indicate stations sampled on the SBDOM11 cruise and correspond to those listed in Table 3.1. Triangles indicate the location of buoys from which wind data was obtained. Bathymetry depth is in meters.
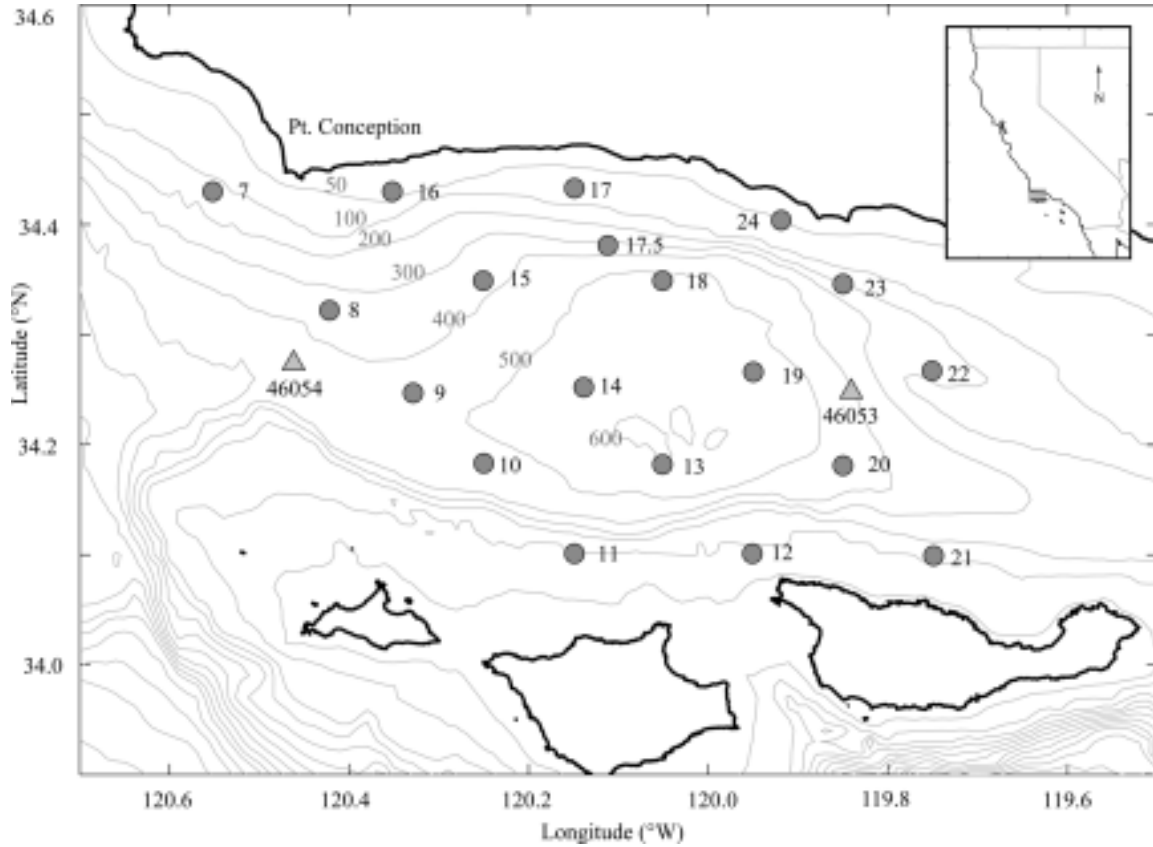
Figure 3.2: *In situ* physical and biological conditions and DOM concentration and composition followed shifts in N+N concentration. Symbols indicate corresponding Si stress: gray triangle, Si replete (V_{amb}:V_{max} ≥ 0.8); black square, low Si stress (V_{amb}:V_{max} 0.4-0.8); gray circle, high Si stress (V_{amb}:V_{max} 0-0.4); open triangle, missing Si stress data. High vs. low Si stress here is somewhat arbitrarily defined at the halfway point of the V_{amb}:V_{max} range and is intended only as a visual guide. A. Chl *a*. B. POC. C. *In situ* DOC concentration. D. *In situ* DON concentration. E: *In situ* CDOM absorbance at 355 nm normalized to *in situ* DOC concentrations (a355:DOC). F. The percent of freshly produced total organic carbon partitioned as DOC (% DOC$_{TOC}$); see text for description of calculation. G. *In situ* CDOM spectral slope coefficient, calculated following Stedmon et al. (2000).
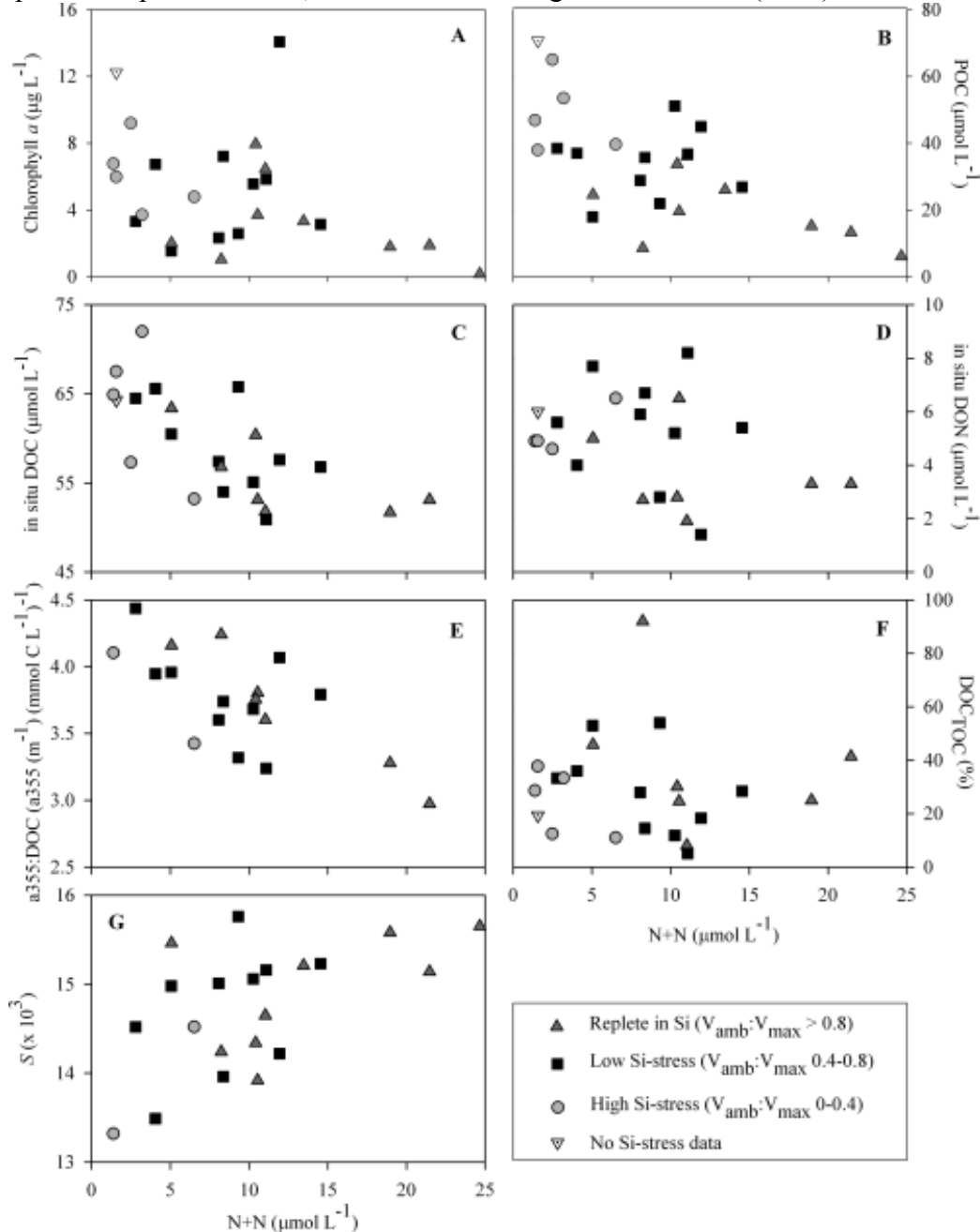
Figure 3.3: Relationship between Si stress and DOM accumulation and persistence, where Si stress increases as Si V_{amb}:V_{max} decreases (see text for methodological details). Symbols as in Fig. 3.2; for C and D, values are medians with error bars ± range where two good values, one from each experimental replicate, were obtained; points without error bars indicate only one good value was obtained. A. Si stress over the bloom, indicated by N+N. B. Si stress and *in situ* DOC. C. Si stress and μ. D. Si stress and persistent DOC.
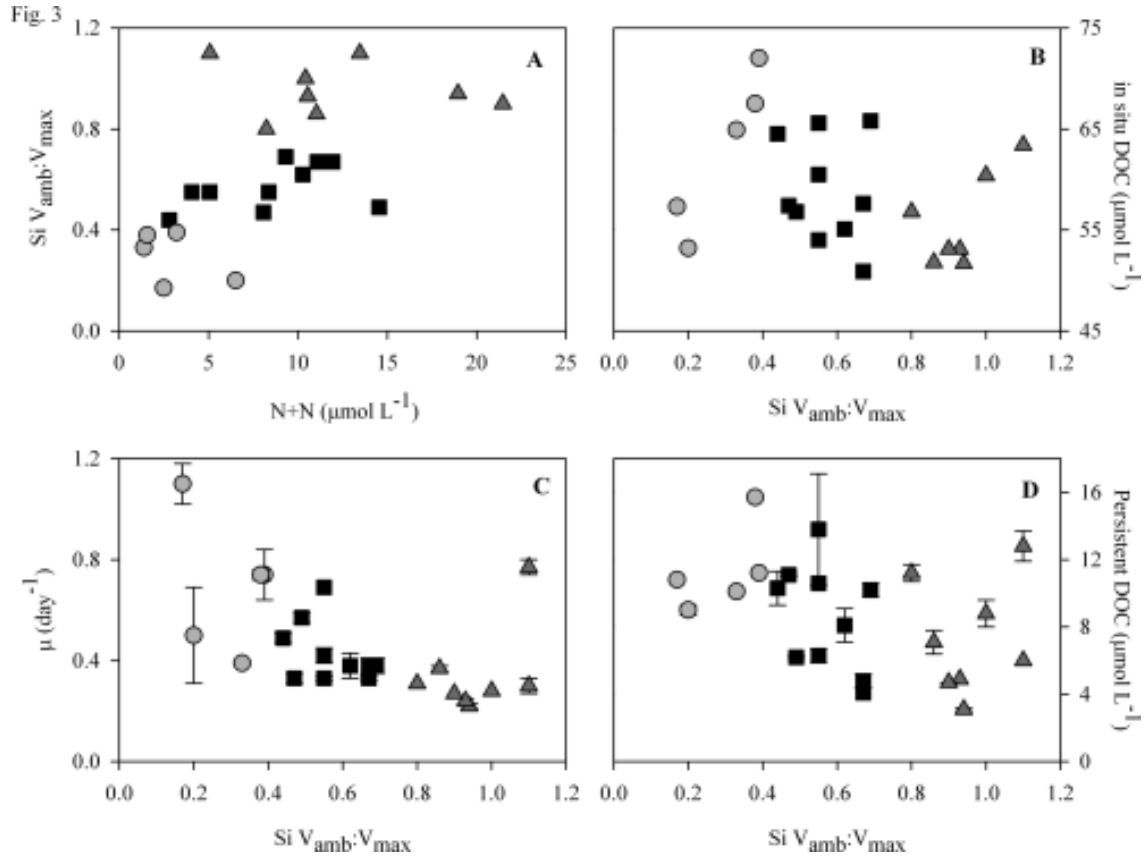
Figure 3.4: Experimental DOC dynamics and bacterial growth responses changed in conjunction with N+N concentrations. Symbols as in Fig. 3.2; values are medians with error bars ± range where two good values, one from each experimental replicate, were obtained; points without error bars indicate only one good value was obtained. For A-C, gray hatched section indicates values less than 1.5 µmol L^{-1}, which are below the analytical detection limit and which were not used in calculation of correlation values or any further analysis. A. DOC drawdown between experiment initiation and day 3. B. DOC drawdown between experiment initiation and one week. C. DOC drawdown between experiment initiation and ten weeks. D. Persistent DOC remaining above background concentrations after 10 weeks' remineralization (see text for details on calculation). E. Maximum bacterial biomass obtained in experiments (mean of stationary phase when applicable). F. BGE over the exponential growth phase.
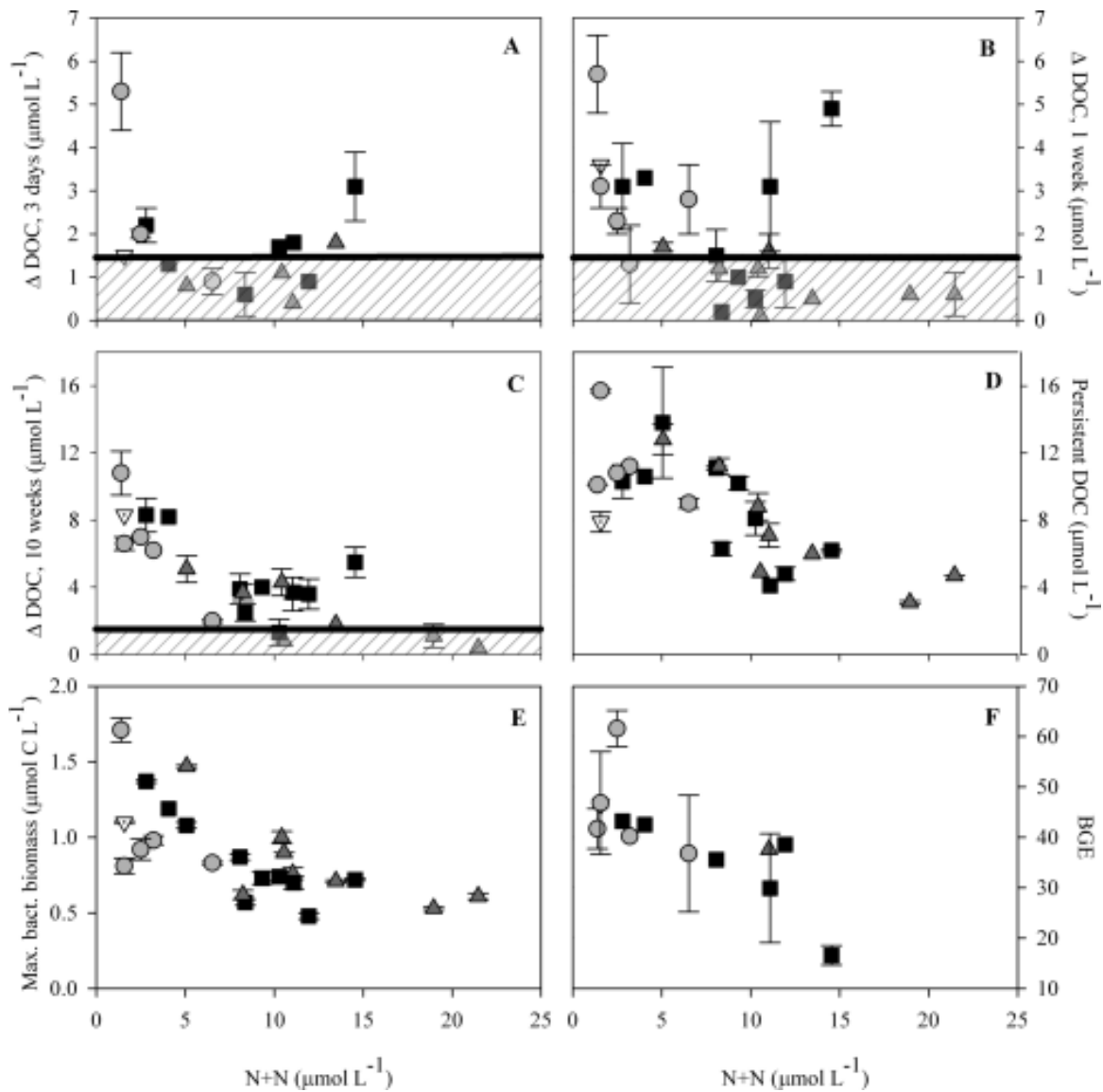
Figure 3.5: Shifts in bacterial community composition from starting (T0) to day 3 (T3). B and C, symbols as in Fig. 3.2. A. Non-metric multidimensional scaling ordination plot of in situ and experimental BCC, with symbols indicating timepoint (circles, T0; triangles, T3) and N+N concentration (μmol L^{-1}) divided into four ranges for clarity. B. UniFrac distances between T0 and T3 pairs of bacterial community composition. C. Percent change in Shannon diversity index from paired T0 to T3 samples.
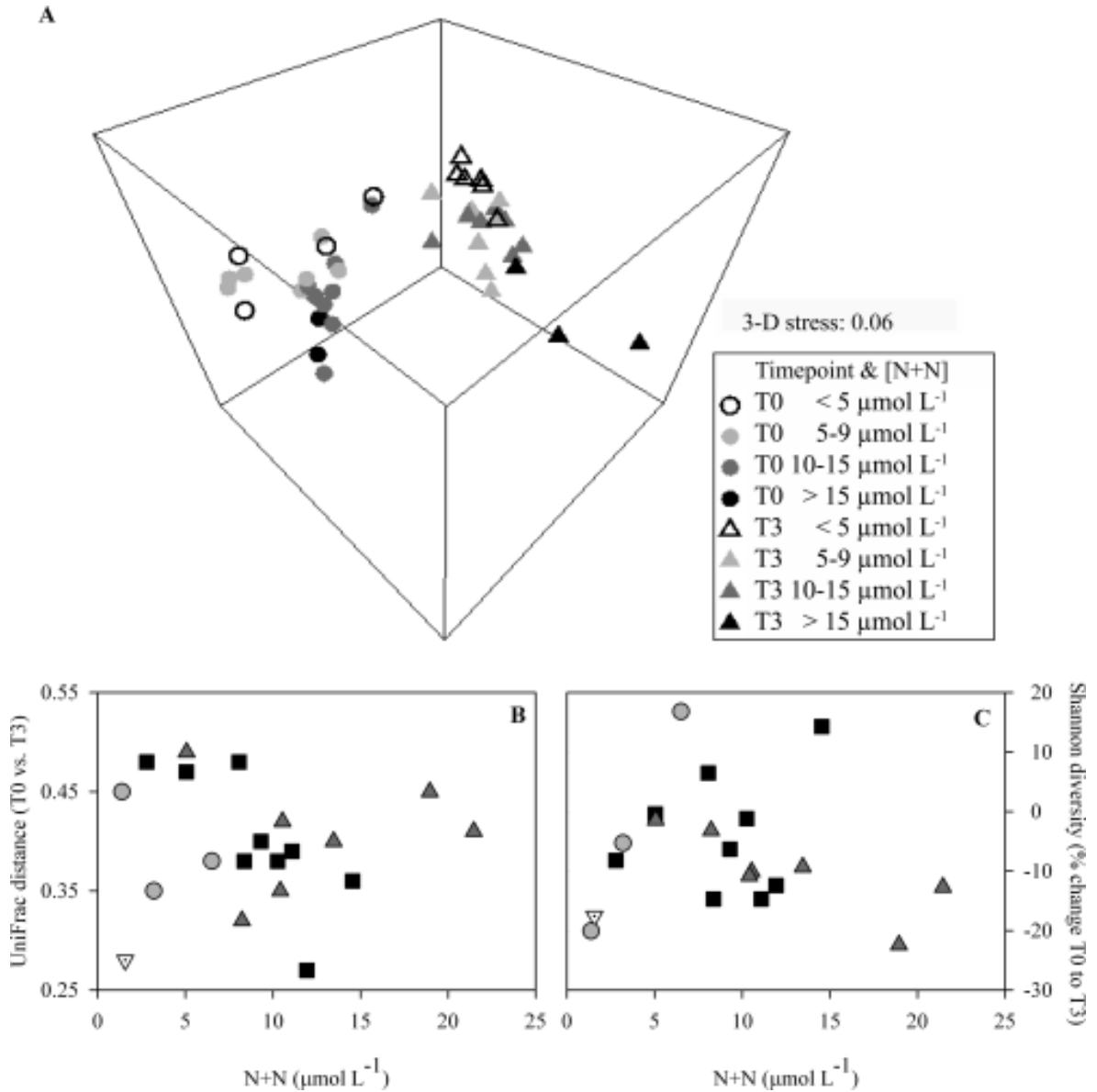
Figure 3.6: Phylotypes (approximately genus level) comprising greater than 0.1% mean T0 or T3 communities. Communities were clustered based on UniFrac distance (right axis) and arranged to maximally follow the N+N gradient. Phylotypes (in columns) were standardized [(phylotype value – mean of phylotype) (standard deviation of phylotype)$^{-1}$] such that each phylotype is plotted on the same scale, with darker colors representing an enriched relative abundance of that particular phylotype in one sample relative to another sample, although not necessarily an increased abundance relative to other phylotypes within the same sample.
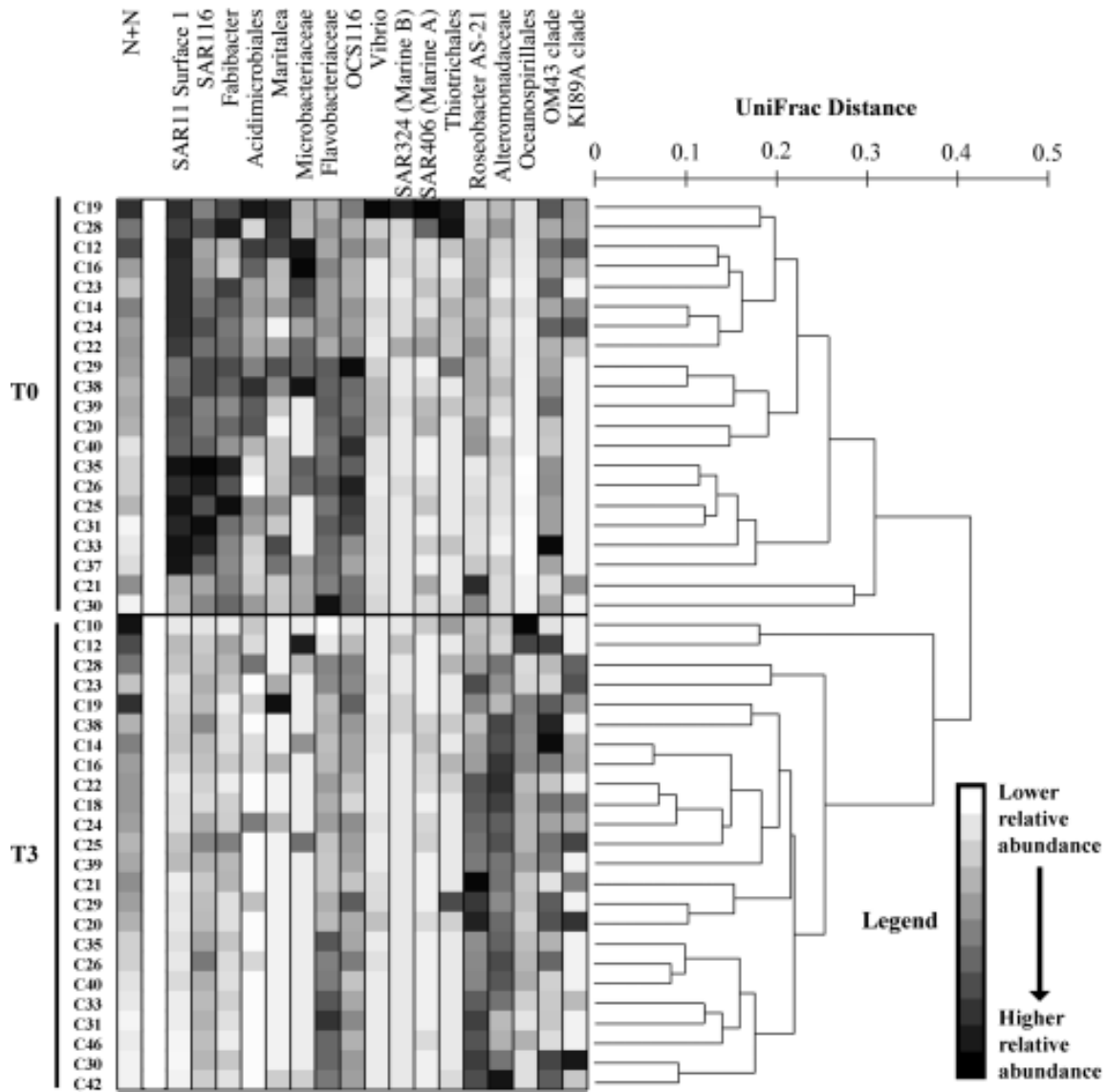
IV. Roles of diatom nutrient stress and species identity in determining the short- and long-term bioavailability of diatom exudates to bacterioplankton

A. Abstract

Phytoplankton exude carbon-rich dissolved organic matter (DOM) upon nutrient stress, yet the ecological role of this exudate in stimulating bacterial growth is not well understood. We harvested DOM produced by four coastal diatoms (*Skeletonema marinoi*, *Chaetoceros socialis*, *Thalassiosira weissflogii*, and *Odontella aurita*) subjected to depletion of nitrogen (N), silicon (Si), or N + Si simultaneously in batch culture and assessed its bioavailability to natural bacterioplankton communities using dilution batch-culture remineralization bioassays. Short-term, ecologically-relevant responses were affected both by diatom source species and by the nutrient stress under which the DOM was produced. Si-stress DOM was generally more bioavailable over the first week than that produced under N or N + Si stress, and led to higher bacterial growth efficiencies. In contrast, the amount of diatom-derived total organic carbon (TOC) that persisted over months in the same experiments differed among source diatom species, with no evidence of a nutrient stress effect. These results nuance the carbon overflow hypothesis of DOM release, which has been suggested to be maladaptive due to the possibility of DOC release allowing bacterioplankton

to better compete for the same nutrient that is limiting the phytoplankton. Our results suggest that bacterial activity is most promoted when diatoms are limited by Si, a nutrient that is not subject to competition with bacteria. They imply that the identity of the nutrient that terminates a diatom bloom impacts heterotrophic activity in the short term; however, source diatom species has the greater influence on DOC persistence in surface waters and its potential export from the system.

B. Introduction

Extracellular release of organic matter is a substantial component of marine productivity, with on average 10–20%, and at times up to 80%, of marine primary productivity released by living phytoplankton as dissolved organic matter (DOM) (Carlson 2002; Nagata 2000). Two non-exclusive hypotheses address DOM release by living phytoplankton (Carlson and Hansell 2015): constant, passive diffusion or "leakage" of low-molecular-weight compounds across the semi-permeable cell membrane and active release as a stress-response carbon "overflow" mechanism. Under the carbon overflow hypothesis, excess energy taken up under high irradiance, and in the sudden absence of nutrients needed to build biomass, is shunted into the synthesis of carbon-rich compounds that are then exuded, preventing the build-up of free radicals until the cell can deactivate photosystems (Fogg 1983; Wood and van Valen 1990). While both hypotheses are generally accepted in the literature as mechanisms of DOM release (Carlson and Hansell 2015), the ecological consequences of the latter remain less well understood. The major outstanding objection to the carbon overflow hypothesis posits that releasing DOM, which would spark heterotrophic bacterial activity and thus increase competition for inorganic nutrients, would be

121

counterproductive for nutrient-limited phytoplankton (Bjørnsen 1988; Bratbak and Thingstad 1985).

Nonetheless, increased DOM release when phytoplankton become nutrient stressed has been observed directly in culture studies (Goldman et al. 1992; Obernosterer and Herndl 1995), in microcosms and in mesocosms (Børsheim et al. 2005; Meon and Kirchman 2001; Smith et al. 1998; Wetz and Wheeler 2004), and, indirectly, by DOM accumulation in the field as phytoplankton blooms senesce (Carlson et al. 1994; Wear et al. 2015; Williams 1995). This DOM is enriched in carbon (Conan et al. 2007; Carlson and Hansell 2015; Wetz and Wheeler 2004) and in carbohydrates (Børsheim et al. 2005; Conan et al. 2007; Carlson and Ducklow 1996; Meador and Aluwihare 2014; Myklestad 1995). The bioavailability of this DOM can affect ecological interactions, as bacteria incorporate C into biomass and bacterial community composition (BCC) possibly shifts. DOM bioavailability can also have biogeochemical implications, as C that resists or escapes microbial remineralization and persists as dissolved organic carbon (DOC) for long enough to be entrained in physical mixing can contribute to the ~ 20% of global export production attributed to DOC (Carlson and Hansell 2015).

Diatoms are estimated to be responsible for ~ 40% of total marine primary production and up to 75% in areas such as coastal upwelling zones that experience strong seasonal blooms (Nelson, Tréguer, Brzezinski, Leynaert, and Quéguiner 1995). Nitrogen limitation controls diatom growth in about half of the global ocean during the summer (Moore, Doney, Glover, and Fung 2002); silicon limitation is the primary diatom stressor in ~ 10% of the ocean, including portions of productive regions such as the northern North Atlantic Ocean (Martin-Jézéquel et al. 2000; Moore et al. 2002; and Sieracki et al. 1993). While exuded

DOM differs in composition from phytoplankton cellular components (Benner 2002; Myklestad 1974; Repeta 2015), the physiological changes induced in diatoms by nitrogen versus silicon stress (N and Si stress, respectively) are substantially different and may lead to the release of distinct qualities and quantities of exudate. Intracellular C:N ratios increase under N stress, as phytoplankton temporarily continue to build biomass (Gilpin et al. 2004; Shifrin and Chisholm 1981); C:N ratios are equivocal under Si stress, with some studies showing moderately increased intracellular C:N (Harrison, Conway, Holmes, and Davis 1977) and others no change (Gilpin et al. 2004). Diatoms can rapidly increase their carbohydrate content and decrease their protein content under N stress, while maintaining a composition similar to replete cells under Si stress over scales of hours (Harrison, Thompson, and Calderwood 1990). Differential responses to N and Si stress extend to concentrations of cell C (Harrison et al. 1977), lipids (Shifrin and Chisholm 1981), pigments (Harrison et al. 1977), and storage compounds (Gilpin et al. 2004; Granum et al. 2002; and Myklestad 1995). Overall, Si-stressed diatoms are capable of a rapid return to normal growth upon reintroduction of Si, while N-stressed diatoms recover more slowly, presumably having undergone more unfavorable physiological shifts (De La Rocha and Passow 2004).

Studies investigating bacterial utilization of DOM produced by nutrient-stressed phytoplankton have yielded conflicting results. Pete, Davidson, Hart, Gutierrez, and Miller (2010) found enhanced bacterial production and abundance, and a community shift to copiotrophic *Gammaproteobacteria*, with DOM derived from diatoms under Si stress, but not from those under N stress. In a field study, Wear et al. (2015) measured increases in bioavailable DOC, bacterial growth rates, and bacterial growth efficiencies (BGEs) as an upwelling-induced phytoplankton bloom transitioned from nutrient-replete to a Si-stressed

state. Wetz and Wheeler (2004) observed elevated growth rates of bacterioplankton with high nucleic acid content in microcosms following increased DOM production under N stress. In contrast, Conan et al. (2007) measured similar total microbial respiration in mesocosms exposed to inorganic amendments covering a range of N:P and with or without added Si, despite great variability in the resulting DOM composition. Because these studies used a variety of methods and manipulated numerous phytoplankton species with different nutrients, it is difficult to generalize about how the bioavailability of phytoplankton-produced DOM varies with nutrient stress.

Here, we examined the bacterioplankton response to exudate produced by multiple diatom species under multiple nutrient stresses to test the hypothesis that DOM produced under Si stress would be a better substrate for bacterioplankton growth than DOM produced under N stress. That is, we expected that Si-stress DOM would: be more bioavailable (more DOC consumed); yield higher BGEs, due to anticipated lower DOC:DON; and lead to distinct bacterial communities compared to N-stress DOM. Conducting dilution batch-culture bioassays to assess DOC bioavailability independent of continuous primary production allowed us to measure DOC utilization more accurately. By measuring both remineralization and bacterial growth, we tracked the fate of the DOC over short-term timeframes relevant to ecological questions and long-term timeframes more relevant to the biogeochemical potential of exudates to contribute to horizontal or vertical carbon export. Using this experimental design, we were able to examine whether Si- and N-stress affect the bioavailability of diatom-derived DOM in ways that can be generalized across limiting nutrient or diatom source species.

C. Methods

1. Diatom exudate production

DOM exudate was harvested from batch cultures of four coastal, centric diatoms obtained from the National Center for Marine Algae and Microbiota (NCMA; http://ncma.bigelow.org): *Skeletonema marinoi* (strain CCMP1332), *Chaetoceros socialis* (CCMP172), *Thalassiosira weissflogii* (CCMP1051), and *Odontella aurita* (CCMP595). Batch cultures were designed to stress diatoms by depletion of nitrogen as nitrate (N stress), silicon as silicic acid (Si stress), and nitrate and silicic acid simultaneously (N + Si stress). The *S. marinoi* N-stress treatment will not be discussed, as it also depleted Si. Experiments on each species were conducted sequentially, rather than simultaneously, for logistical reasons (Table 4.1). Diatom growth dynamics will be discussed in detail elsewhere (Windecker et al. in prep); only relevant parameters and time-points are presented in this paper. As several parameters were measured in both the diatom cultures and the subsequent remineralization-focused dilution batch-culture bioassays, the experimental component will be indicated by subscript (e.g., *S. marinoi*$_{diatom}$ and *S. marinoi*$_{remin}$ for parameters measured in the diatom cultures and the remineralization bioassays, respectively) and when neither is specified (e.g., *S. marinoi*) the diatom itself is referenced.

Media consisted of seawater from the Santa Barbara Channel (SBC), California, USA, that was aged in the dark for up to two weeks to remineralize the most labile ambient DOC. The aged seawater was then gravity filtered through a 0.2 µm filter (polyethersulfone filter cartridge, Pall, Port Washington, NY, or mixed cellulose ester, GSWP, EMD Millipore, Billerica, MA, in a polycarbonate (PC) holder) to remove particulate organic matter (POM), including the extant microbial community. Media seawater was collected and aged

independently in advance of each experiment. Duplicate acid-washed 20 L PC carboys with spigots (Nalgene Labware) were filled with 0.2 μm filtrate, enriched with nutrients (NO_3 and $Si(OH)_4$ at concentrations estimated to produce the same nutrient-replete diatom biomass in each treatment [roughly normalized to the biomass produced with 40 μM NO_3], Table 4.1; PO_4 and standard vitamins and metals sufficient to remain replete), and inoculated with diatom cells in exponential growth. Batch cultures were grown at 14 °C, on a 14:10 light:dark cycle at ~ 200 μmol photons s^{-1} m^{-2}, with daily sampling to monitor [NO_3] and [$Si(OH)_4$] timed to the end of the light period.

The DOM generated from the diatom cultures was harvested 48 h after the target nutrient concentration was too low to sustain the next day's doubling (< ca. 3 μM, Appendix I) and used as media for the dilution batch-culture bioassays. Replicate diatom cultures were combined, thereby eliminating any variance in the exudate pool in terms of concentration and composition of diatom production, allowing us to focus on the bacterial response. Pooled exudates were gravity-filtered through a 3 μm mixed cellulose ester filter (SSWP, EMD Millipore) followed by sequential gravity filtration through two 0.2 μm mixed cellulose ester filters (GSWP). The filtered diatom exudate was therefore operationally defined as dissolved and contained a continuum from truly dissolved compounds to colloids (e.g., transparent exopolymers) (Carlson and Hansell 2015). Filters were rinsed copiously with deionized water before use and changed frequently over the course of the filtration, which took several hours. The exudate was collected in duplicate acid-washed and sample-rinsed 8 L PC spigoted carboys and stored overnight at 4 °C.

2. Dilution batch-culture bioassay design

To assess the bioavailability of the ambient DOM that remained in the aged seawater

126

filtrate used to construct the diatom culture media, a portion of the aged seawater filtrate for each experiment was set aside to serve as an unmanipulated control during the corresponding dilution batch-culture bioassays. Control filtrates were stored at 4 °C for the duration of each diatom culture and were re-filtered with a 0.2 μm filter (GSWP) before use. Natural surface bacterial communities for inocula were collected from the near-shore SBC (~ 200–400 yards offshore) for *S. marinoi*remin, *C. socialis*remin, and *T. weissflogii*remin, and from the central SBC for *O. aurita*remin. Each inoculum was gravity-filtered through a 1.2 μm mixed cellulose ester filter (RAWP, EMD Millipore) to largely remove POM and flagellate grazers, and the filtrate was sampled for DOM, nutrients, and DNA. Exudates and unamended controls were combined with 25% inoculum to a total of 8 L; bioassay volumes varied slightly in the *S. marinoi*remin experiment based on the volume of diatom exudate obtained (between 5.3 and 8 L total volume; Appendix I). Bioassays were incubated in the dark at 14°C for 16 weeks.

To verify that bacterial responses were the result of DOM variability rather than of non-limiting nutrients remaining in the exudate, we conducted parallel experiments to examine the effects of inorganic nutrients alone alongside the *O. aurita*remin exudate bioassays. Two 8 L duplicated treatments consisted of the same aged seawater as the *O. aurita*remin control treatment, but with PO_4 and either NO_3 (Aged SW + N&P) or $Si(OH)_4$ (Aged SW + Si&P) added at the approximate concentrations remaining in the carboys not stressed by NO_3 or $Si(OH)_4$, respectively (Appendix II). To control for bacterial responses induced by DOM or nutrients that were added when inoculating the diatom culture, two 2 L duplicated treatments were amended with F/2 media (Aged SW + F/2) or 0.2-μm filtered media from a primary *O. aurita* culture in exponential growth (Aged SW + Culture; resembling the diatom inoculum media) at concentrations approximating their initial

presence in the diatom cultures (18:1000 dilution). These experiments were sampled less frequently and for fewer variables than the larger-volume experiments (Appendix I).

3. Organic matter and inorganic nutrients

Samples for DOM analysis were collected daily during the growth of the diatom culture. During the bioassays, samples were collected daily for one week followed by weekly then monthly sampling. Samples were stored frozen at − 20 °C in acid-washed high-density polyethylene bottles or combusted glass EPA vials with Teflon-lined septa. DOM samples collected from the diatom cultures were gravity-filtered through an inline combusted glass fiber filter (GF/F, Whatman, Pittsburgh, PA) in a PC holder. To avoid contamination from handling, DOM samples from the bioassays were collected without further filtration, as biomass concentrations in the bioassays were several orders of magnitude lower than in the diatom cultures. Bioassay DOM concentrations are therefore most accurately interpreted as total organic carbon (TOC) and nitrogen (TON), as they do contain bacterial biomass. DOC, TOC, and total dissolved nitrogen (TDN) were quantified via high-temperature combustion as in Halewood, Carlson, Brzezinski, Reed, and Goodman (2012). DON and TON were calculated by subtracting dissolved inorganic nitrogen from TDN. In the diatom cultures only, particulate organic carbon (POC) was collected on a combusted GF/F and measured by elemental analysis as in Wear et al. (2015). Samples for inorganic nutrients were filtered if collected from the diatom experiments or unfiltered if from the bioassays and were analyzed using flow injection analysis as in Wear et al. (2015). Silicic acid was measured using the manual colorimetric method of Brzezinski and Nelson (1995; detection limit 0.3 μM, 2 times the standard deviation of the blank).

To examine TOC remineralization in the bioassays independently of variable starting

concentrations, the percent of newly added TOC that was remineralized from the start of the experiment (T_0) to a subset of later time-points (T_X), or $\%_{new}$ TOC, was calculated as:

Equation 1: $\%_{new}$ TOC = ([T_0 TOC] – [T_X TOC]) * ([T_0 TOC] – mean of [16-week TOC] in corresponding control bioassays)$^{-1}$ *100.

The final (16-week) TOC concentration in each experiment's respective control was taken to represent the recalcitrant, bulk background concentration, while any initial TOC in excess of the 16-week concentration in the exudate treatments would have originated from either the diatom exudate or bioavailable TOC introduced with the media and inoculum (assumed to be similar across treatments within an experiment). Conversely, persistent TOC in the diatom-derived bioassays that remained in excess of the respective control bioassays after 16 weeks was calculated as:

Equation 2: [persistent TOC] = [16-week TOC] – mean of [16-week TOC] in corresponding control bioassays.

To better estimate total DOC usage by accounting for incorporation of DOC into bacterial biomass, bacterial carbon demand (BCD) was calculated at 4 days:

Equation 3: BCD = ([T_0 TOC] – [T_0 bacterial biomass]) – ([$T_{4\ day}$ TOC] - [$T_{4\ day}$ bacterial biomass]).

4. Bacterial growth rates, production, and growth efficiencies

Samples for bacterial abundance were collected twice daily for the first week of the dilution batch-culture bioassays and preserved as in Wear et al. (2015). Bacteria were enumerated on a BD LSRII flow cytometer (Becton Dickinson, San Jose, CA) equipped with an autosampler as in Halewood et al. (2012). Bacterial abundance at time-points where biomass was calculated (for BGE and BCD calculations) was determined from epifluorescence microscopy of 4′6-diamidino-2-phenylindole (DAPI) stained slides (Porter and Feig 1980), as preliminary comparisons showed that the flow cytometer accurately captured growth rates but had offset absolute cell abundance relative to DAPI slides. Bacterial abundance was converted to biomass (BB) using 30 fg C cell^{-1} [the mean C cell^{-1} measured in similar bioassays using phytoplankton exudate additions and SBC bacterioplankton (A. Cano, unpublished)]. Preliminary measurements of cell cross-sectional areas indicated that bacteria did not vary significantly in size between experiments or treatments at time-points used in BGE calculations (not shown) and therefore a consistent conversion factor was reasonable. Bacterial production (BP) was measured daily on whole water and filtered (3 μm) samples from the diatom experiments (Appendix III) and daily on whole water for the first 6 days of the bioassays via ^{3}H-leucine (^{3}H-Leu) incorporation (14–19 nmol L^{-1} ^{3}H-Leu; specific activity 54.1 Ci/mmol; PerkinElmer, Boston, MA), using a modified microcentrifuge method (Halewood et al. 2012; Wear et al. 2015).

Bacterial specific growth rate (μ) was calculated as the rate of change of the natural log of cell abundances during exponential growth (the timeframes of which varied and are specified in Appendix IV). BGE was calculated as the increase in bacterial biomass over the exponential phase (with all biomass measures from the lag or stationary phase averaged to

increase measurement robustness) divided by the change in true [DOC] (the change in [TOC] corrected for [BB]) over the same time period:

Equation 4: BGE = ((mean [$T_{stationary}$ BB] – mean [T_{lag} BB]) * ((mean [T_{lag} TOC] – mean [T_{lag} BB]) – (mean [$T_{stationary}$ TOC] – mean [$T_{stationary}$ BB]))$^{-1}$) * 100.

5. Bacterial community composition (BCC)

DNA samples for BCC analysis were collected from the bioassays at T_0 and at 1, 2 and 4 days. BCC was assessed via terminal restriction fragment length polymorphism (T-RFLP) to compare frequency distributions of 16S ribosomal RNA gene amplicons, following a modified protocol of Morris et al. (2005) (see Appendix V for detailed methods). Genomic DNA was amplified with the universal bacterial primers 8f-FAM and 519r; amplicons were digested with *Hae*III restriction endonuclease and analyzed by capillary gel electrophoresis. T-RFLP peaks were manually assigned using integer-length fragment groups (Nelson, 2009). Bacterial groups associated with the observed terminal restriction fragments (T-RFs) were putatively identified from *in silico* digests of 16S rRNA gene amplicon sequences from the SBC (Wear et al. 2015; Appendix V).

6. Statistical analyses

Statistical analyses were performed using SPSS Statistics 22.0 (IBM). Figures were made in Sigma Plot 12.0 (Systat Software Inc.), JMP 9 (SAS Institute Inc.), and Microsoft Office. Full results are available through the Biological and Chemical Oceanography Data Management Office (http://www.bco-dmo.org; project name "SBDOM").

D. Results

The major findings of these experiments are summarized in Fig. 4.1. While there are exceptions to the patterns shown in this conceptual diagram, it is intended to highlight the overall trends in the following results.

Because each experiment (that is, the examination of DOM from each diatom species) was conducted separately, the aged seawater media used for the various diatom cultures and the bacterial inoculum in the dilution batch-culture bioassays were necessarily different for each experiment. Results should therefore be compared primarily within experiments (e.g., whether the bioavailability of Si-stress DOM and N-stress DOM from one given diatom differ), as the media and inoculum are internally consistent.

1. Diatom culture DOM yield

All diatom batch cultures produced substantial biomass, as evidenced by ca. 10- to 100-fold increases in POC over the experiments through the time-point preceding harvest (T_H; Table 4.1), indicating normal growth occurred prior to the onset of their respective nutrient stresses. Net DOC production was observed in all batch cultures by T_H, between 4.8 and 21.6 μM DOC (Table 4.1). In some bioassays, the initial observed [DOC] differed from that calculated via mass balance of the inoculum and the pre-harvest (T_H) [DOC] in the diatom cultures (Table 4.1 and Table 4.2), which we attribute to continued exudation or remineralization during the several hours needed to filter the diatom cultures and to general effects of handling, possibly including diatom cell breakage. We observed no accumulation of DON above our detection limit of 1.5 μM during the diatom growth experiments (Appendix VI). At T_H, DOC:DON ratios of the bulk DOM fell between 11.6 and 17.9, with no clear trends between nutrient stresses (Table 4.1). Growth and exudation dynamics will be

132

discussed in greater detail in a subsequent manuscript (Windecker et al. in prep).

The diatom cultures were not axenic, as we measured ^{3}H-Leu incorporation in both whole water and filtered (i.e., diatom-free) samples (Appendix III). The highest incorporation was observed in the *C. socialis*$_{diatom}$ attached bacteria fraction, suggesting the most active bacteria were part of the phycosphere. We made a substantial effort to reduce bacteria by filtering media seawater, rinsing diatom primary cultures (prior to inoculation) with sterile seawater, and treating some diatom primary cultures with a standard antibiotic cocktail (*S. marinoi*, *C. socialis*, and *T. weissflogii*: penicillin G, gentamicin, and dihydrostreptomycin HCl following Guillard (2005)). Autoclaving diatom growth media to further inhibit bacteria would have undermined our goal of low background DOC concentrations, as preliminary work has shown that autoclaving seawater results in measureable increases in DOC (C. Carlson, unpublished). Despite these efforts, bacterioplankton grew in diatom cultures (Appendix III); thus, we acknowledge that we measured net rather than gross DOM production. Microbial processing of DOM during the diatom experiments would make the harvested exudate most realistically resemble a mix of the labile and semi-labile pools (Carlson and Hansell 2015), comparable to the DOM that accumulates in the field as a bloom senesces (Wear et al. 2015; Williams 1995).

2. Short-term DOM bioavailability

TOC remineralization (that is, respiration) was calculated as the change in TOC between T_0 and subsequent time-points throughout the dilution batch-culture bioassays (Table 4.2; Fig. 4.2). Four days after T_0, which corresponded to peak bacterial growth in many treatments and the final BCC time-point, TOC remineralization ranged between no resolvable change (i.e., < 1.5 μM C) and 24.8 μM (Table 4.2; Fig. 4.2), with no clear patterns

by nutrient stress or source diatom species. Because our duplicate bioassays represent the pooled exudate from duplicate diatom cultures rather than an evaluation of each diatom culture independently, we have insufficient replication to analyze the statistical significance of species or nutrient effects when a two-way crossed ANOVA would be the appropriate test. As the range of starting [TOC] spanned 30 μM, we calculated the percent bioavailability of "new" TOC (the combined bioavailability of the diatom exudate, bioavailable TOC introduced with the bacterial inoculum, and bioavailable TOC from the aged seawater media, i.e., TOC above the 16-week mean [TOC] in each experiment's respective control bioassays (Eq. 1). At day 4, %$_{new}$ TOC remineralization ranged from below detection limits to 52%$_{new}$. BCD over 4 days ranged between 1.9 and 34.2 μM C (in experiments where it could be resolved) and likewise showed no clear patterns between nutrient-stress treatments and source diatom species (Table 4.2; Appendix IV).

After 1 week, TOC remineralization showed clearer patterns between nutrient-stress treatments. Both absolute and %$_{new}$ TOC remineralization were consistently highest within the Si-stress DOM treatments in each source diatom group (or one of two approximately equally high in the case of *O. aurita*$_{remin}$) (Table 4.2; Fig. 4.3A and C). While TOC remineralization in the Si-stress treatments varied by a factor of 10 between source diatom species, the remineralization in all other treatments was similar in magnitude across all diatom species (between ~ 2 and 5 μM C), suggesting any potential diatom species effects on short-term TOC bioavailability were overshadowed by the effects of diatom nutrient stress. The crash of bacterioplankton cell abundance at 1 week, associated with prevalent nanoflagellate grazers in several bioassays (as is common for this type of dilution culture experiment), made accurate estimates of BCD impossible.

Initial TOC:TON in the bioassays was between 11.7 and 20.4, with no systematic variability by diatom species or by nutrient stress treatment (Table 4.2). We observed no resolvable TON remineralization over 8 weeks within the bioassays (Appendix VII).

3. Long-term DOM bioavailability and persistent TOC

At 16 weeks, absolute and $\%_{new}$ TOC remineralization resembled one another, with the clear Si-stress pattern seen at 1 week no longer apparent (Table 4.2; Fig. 4.3B and D). The highest remineralization was seen in the Si-stress DOM treatments in *S. marinoi*$_{remin}$ and *C. socialis*$_{remin}$, the N-stress DOM treatment in *T. weissflogii*$_{remin}$, and the N + Si-stress DOM treatment in *O. aurita*$_{remin}$, albeit with dampened variability in the $\%_{new}$ remineralization relative to the absolute drawdown (Table 4.2). Therefore, while remineralization of Si-stress TOC appeared universally elevated relative to that produced under N stress over a week, nutrient stress effects were no longer clear over timescales of months. The magnitude of long-term absolute TOC remineralization was strongly correlated with initial TOC concentrations (Table 4.2; Fig. 4.2; Table 4.3); however, the persistence of the patterns between treatments after remineralization was normalized to a percentage suggests that there were differences in the inherent bioavailability of the exudate produced under the different nutrient stresses by the various diatoms and that remineralization patterns were not solely driven by bulk carbon availability.

Notably in Fig. 4.2, [TOC] in each of the diatom exudate bioassays remained in excess of the [TOC] in their respective control bioassays at 16 weeks, that is, every exudate bioassay had measureable persistent TOC at the end of the experiment. Persistent TOC was between 4.8 and 15.4 μM, or 16–69% of the "new" TOC (Table 4.2; Fig. 4.3E). Persistent TOC varied between diatom source species (*S. marinoi*$_{remin}$: mean 7.2 μM; *C. socialis*$_{remin}$:

10.5 μM; *T. weissflogii*remin: 5.3 μM; *O. aurita*remin: 13.6 μM), but the nutrient stress imposed on the diatoms did not have an obvious effect within experiments from a given species. A one-way ANOVA for species effects with Ryan-Einot-Gabriel-Welsch Range post-hoc showed that persistent TOC was lower in *T. weissflogii*remin than in *C. socialis*remin and higher in *O. aurita*remin than in all other experiments at $p < 0.05$ ($F_{3,7} = 26.540$, $p < 0.0001$; Fig. 4.3E).

4. Bacterial growth parameters and BGEs

The bacterioplankton specific growth rate, μ, was between 0.09 and 1.85 doublings day^{-1}, with the highest rate in the *S. marinoi*remin Si-stress DOM treatment by more than 2-fold (Table 4.4, Fig. 4.3F). In general, the N-stress DOM treatments had the lowest μ and the Si-stress DOM treatments had the highest μ within experiments. ^{3}H-Leu incorporation was more variable, with 2- to 3-fold higher 1-week integrated ^{3}H-Leu incorporation in the *S. marinoi*remin and *C. socialis*remin Si-stress DOM treatments (127.7 and 109.5 nmol ^{3}H-Leu L^{-1} week^{-1}, respectively) than in any other treatments (between 7.7 and 41.6 nmol ^{3}H-Leu L^{-1} week^{-1}) (Table 4.4; Fig. 4.3G). Maximum bacterial biomass (the mean biomass during stationary phase) was between 1.4 and 9.7 μM C (Table 4.4; Appendix IV), with the highest values again in the *S. marinoi*remin and *C. socialis*remin Si-stress DOM treatments and an overall pattern resembling that of the ^{3}H-Leu incorporation rates.

BGEs were between 27 and 61% (Table 4.4; Fig. 4.3H). Surprisingly, despite the extremely high biomass production in the *S. marinoi*remin Si-stress DOM bioassay, this experiment had one of the lowest resolvable BGEs. In general, however, BGEs were higher in Si-stress DOM bioassays than in the corresponding N-stress DOM bioassays, with the N + Si-stress DOM bioassays varying in relation to the other treatments within diatom source

species. Based on the moderately elevated BGEs observed in two of the N + Si-stress treatments that lacked residual DIN (Table 4.4; Fig. 4.3H), it is unlikely that the elevated BGEs seen in the Si-stress DOM treatments were solely attributable to inorganic nitrogen carried over from the diatom cultures.

5. Carbon parameter relationships

We examined the relationships between numerous parameters of TOC usage and bacterial growth using Spearman's *rho* non-parametric correlation analysis (Table 4.3). Overall, few parameters correlated, suggesting additional aspects of substrate quantity and composition were likely impacting the various processes. Notably, the majority of short-term and long-term TOC remineralization measures were not significantly correlated with one another. Measures of TOC remineralization (particularly $\%_{new}$ remineralization) and persistent TOC were generally not related to initial concentrations or stoichiometry (T_0 [TOC], [TON], and TOC:TON), with the exception of the positive correlation between 16-week TOC remineralization and T_0 [TOC]. Maximum BB and integrated BP were more closely related to starting [TOC], suggesting that initial DOM availability may have influenced bacterial anabolism. μ was correlated with 4-day BCD and with absolute and $\%_{new}$ TOC remineralization over 1 week. Unexpectedly, BGE was not correlated with any of the other carbon-processing or bacterial growth parameters measured (Table 4.3).

6. Inorganic nutrient amendments

The inorganic nutrient amendment treatments were designed to elucidate any effects of remnant inorganic nutrients from the diatom media (in particular, NO_3 remaining in the Si-stress DOM treatments, which would be consistent with an Si-stress scenario in the field but which could also disproportionately increase bacterial metabolism). We did not see enhanced

overall TOC remineralization in the nutrient amended treatments relative to the unamended control, nor significantly enhanced BCD (Table 4.2; Fig. 4.2E). These experiments had μ between 0.11 and 0.28 doublings day^{-1} (Table 4.4), with the greatest μ by a factor of 2–3 observed in the Aged SW + N&P amendment (analogous to the inorganic nutrients remaining in the Si-stress DOM treatments). This suggests the elevated μ seen in the Si-stress DOM treatments might be associated with the presence of readily available inorganic nitrogen, allowing for rapid cell replication despite carbon-rich DOC; supporting this, μ was positively correlated with T_0 N + N concentrations in the exudate and control bioassays (Spearman's *rho* = 0.601, N = 15, *p* = 0.018). BP over 1 week was indistinguishable between the *O. aurita*$_{remin}$ unamended control and the Aged SW + N&P and Aged SW + Si&P treatments (Table 4.4), as was the maximum BB (Table 4.4). BCC in the inorganic nutrient amended treatments was likewise indistinguishable from that of the unamended *O. aurita*$_{remin}$ controls (Appendix V); therefore, the observed shifts in BCC in the exudate bioassays were presumably driven by the DOM, not by non-limiting inorganic nutrients remaining in the experiments.

7. Bacterial community composition

T-RFLP profiles were obtained for 146 samples, with 5 samples discarded for poor amplification. Individual samples contained 12 to 27 T-RFs, from a total of 72 distinct peaks between 31 and 568 base pairs in length across all samples. BCC in all treatments deviated from the respective inoculum over 4 days (Fig. 4.4; Appendix V). We interpret changes in the control treatment communities as resulting from growth on DOM present in the inoculum and in the background aged seawater from the diatom media; further changes from the control treatment would then represent the bottom-up effects of the additional DOM in the

138

exudate bioassays. Within an experiment, BCC in all exudate bioassays changed similarly, with minor differences between nutrient stress treatments (Fig. 4.4; Appendix V). The BCC response was dominated by strong increases in the relative abundance of putative copiotrophs (the 33 base pair peak, which constituted 33–72% of the DOM treatment communities at day 4) and decreases in putative oligotrophs such as SAR11 Surface 1 (the 114 base pair peak; Fig. 4.4; Appendix V).

4. Discussion

Our hypothesis that Si-stress DOM would be more bioavailable than N-stress DOM was supported over the first week of the experiment (Table 4.2; Fig. 4.3A and C), although nutrient stress effects on TOC bioavailability were not evident over timescales of months (Table 4.2; Fig. 4.3B and D). Rather, after 16 weeks, we observed consistent concentrations of persistent TOC within experiments from a given source diatom, regardless of nutrient stress treatment (Table 4.2; Fig. 4.3E). Our prediction that Si-stress DOM would yield higher BGEs was supported in most experiments; however, the mechanism we expected to underlie this response, lower TOC:TON ratios in Si-stress DOM treatments, was not substantiated (Table 4.2). Finally, our hypothesis of variable BCC between nutrient stress treatments was not supported at the resolution attainable by T-RFLP (Fig. 4.4; Appendix V), with all treatments overwhelmingly shifting to copiotrophic phylotypes.

1. DOC bioavailability

We observed very rapid DOC remineralization over the first week in several treatments, most notably in the Si-stress DOM treatments of the *S. marinoi*$_{remin}$ (28.7 μM) and *C. socialis*$_{remin}$ (12.1 μM) that had correspondingly high initial DOC concentrations (Fig.

4.2A-D; Fig. 4.3A). This DOC remineralization was several-fold higher than the < 7 μM 1-week remineralization of DOM from a diatom-dominated phytoplankton bloom in the SBC (Wear et al. 2015) but comparable with the 15 μM DOC drawdown observed within 1 week on water from an SBC kelp forest (Halewood et al. 2012), indicating that such high DOC remineralization is plausible for the SBC, albeit not common. This high DOC remineralization is consistent with that seen in seawater amended with labile DOM (~ 10 to 35 μM over 1 week, Carlson and Ducklow 1996; ~ 10 to 40 μM over 3 days, Cherrier et al. 1996), while the lower remineralization in the other experiments more closely resembles the range of magnitudes seen in dilution-culture bioassays of unamended seawater (unresolvable to ~ 7 μM over 1 week, Carlson and Ducklow 1996 and Wear et al. 2015).

DOC remineralization followed a pattern of very high drawdown over the first week, slowing and approaching an asymptote over several months (Fig. 4.2), that is congruent with the average marine DOC drawdown as calculated by del Giogrio and Davis (2003). The high initial DOC remineralization in some treatments and the general lack of correlation between short-term and long-term DOC bioavailability (Table 4.3) suggest the presence of distinct pools of DOM with independent reactivity. The initial rapid, and variable, remineralization may therefore most reflect the C-rich compounds produced in response to nutrient stress (e.g., as with the bacterial response to phytoplankton-produced glycolate, which is primarily respired rather than incorporated into biomass; Fogg 1983).

2. Bacterial growth efficiency response

The measured BGEs (Table 4.4; Fig. 4.3H) were high for pelagic systems (where values ca. 10–20% are more common; Carlson 2002). However, they closely resemble those observed during a phytoplankton bloom in the SBC, when BGEs increased from 17 to 62%

as the bloom progressed (Wear et al. 2015). The high BGE values are in part attributable to the high cellular carbon conversion factor we used to estimate bacterial biomass (30 fg C cell^{-1}); however, the pattern between experiments and treatments is consistent regardless of the conversion factor chosen. We interpret the higher BGEs in the Si-stress DOM treatments relative to the N-stress DOM treatments as an indication of a higher-quality substrate for the bacterioplankton produced by diatoms under Si-stress, allowing the bacteria to incorporate relatively more DOC into biomass. While inorganic nitrogen carried over from the diatom cultures in the Si-stress DOM treatments could also lead to elevated BGEs, we saw high BGEs in two N + Si-stress DOM treatments that did not contain significant inorganic nitrogen (Appendix VII). Given this apparent difference in DOM quality as a growth substrate (in the sense of del Giorgio and Cole 1998), it was surprising that BGEs were not correlated with initial TOC and TON concentrations or stoichiometry, TOC remineralization over any timeframe, or bacterial growth (i.e., any of the other parameters in Table 4.3). This decoupling between TOC bioavailability and BGEs suggests that other factors are limiting biomass production at the expense of bulk DOC uptake; thus, further investigation of the composition of DOM produced by nutrient-stressed phytoplankton and resolution of the role of micronutrient dynamics in these types of experiments is warranted.

3. Persistent TOC

Persistent TOC was present at concentrations between 5 and 15 μM above the control treatments in every DOM bioassay at 16 weeks, analogous to the accumulated DOC observed in the field after phytoplankton blooms (Carlson et al. 1994; Williams 1995) and similar to that observed persisting in prior experiments assessing diatom-produced DOC (Fry et al. 1996; Meon and Kirchman 2001; Wear et al. 2015). Given the high variability in initial

[TOC] and TOC remineralization within bioassays from a given diatom source (Table 4.2; Fig. 4.2), the consistency of the corresponding persistent TOC is surprising (Fig. 4.3E). Dilution batch-culture bioassay experiments are by design removed from *in situ* conditions and therefore we cannot say that persistent TOC was solely an effect of the diatom species, or whether there might have been an additional influence from the seawater media or bacterioplankton inoculum. Persistent TOC should consist primarily of true DOC and only minimally of bacterial biomass; BB at 1 week, the final time-point where it was measured, was between 0.7 and 2.5 μM C within the cultures that had clearly begun to decline in abundance (Appendix IV). Previous unpublished work in the SBC and elsewhere has shown that bacterial biomass subsequent to the death phase remains close to its T_0 concentration, presumably due to tight coupling between bacterial production and mortality due to nanoflagellate grazing and viral lysis. Thus, while we cannot rule it out, it is highly unlikely that BB would contribute significantly to total TOC in the later stages of these experiments. Because persistent TOC was calculated relative to the corresponding control treatment (Eq. 2), we feel confident that this carbon was a remnant of the diatom exudate, whether it was produced by the diatoms in a recalcitrant form (e.g., as in Aluwihare and Repeta 1999) or transformed to a recalcitrant composition by bacterial processing of more labile precursors (i.e., the microbial carbon pump; Jiao et al. 2010).

The consistent amounts of persistent TOC suggest that, from a biogeochemical perspective, knowing the nutrient stress that terminated a diatom bloom will not inform expectations of potentially exportable TOC production, but rather that improved estimates of the fate of post-phytoplankton bloom TOC may rely on knowledge of source species identity. In this case, treating multiple diatom species as a single functional group could obscure a

potential 2-fold difference in the quantity of phytoplankton-produced TOC that persists following a diatom bloom (Fig. 4.3E). This finding differs from the results of Wear et al. (2015), wherein concentrations of persistent DOC (remaining after 10 weeks in dilution batch-culture bioassays derived from field samples during a diatom and *Phaeocystis* sp. bloom) covered a similar range of magnitudes but increased with increasing *in situ* Si stress. Therefore, while we saw no effect of stressor nutrient identity on persistent TOC concentrations in the experiments described here, this conclusion would need to be verified for situations of varying levels of nutrient stress prior to extrapolating these results.

4. Effects of nutrient stress on DOM utilization

We observed greater variability in bacterioplankton responses to DOM produced under different nutrient stresses than has been seen in previous studies. Conan et al. (2007) saw variable partitioning of phytoplankton production into DOC, but similar microbial respiration, in mesocosms experiencing a range of N or P stresses. Pete et al. (2010), who used N and Si additions similar to those we employed to elicit diatom nutrient stress, measured elevated BP and bacterial abundance on Si-stress DOM from *Skeletonema costatum*, similar to our observations of elevated BP and μ on *S. marinoi*$_{remin}$ Si-stress DOM. However, their N-stress DOM did not elicit bacterial responses that were different from the controls, despite an approximately 70 μM DOC addition, while we observed that N-stress DOM consistently produced higher BP (Table 4.4) and a shift in BCC (Fig. 4.4; Appendix V) relative to our unamended controls. It is difficult to compare the two studies, as Pete et al. (2010) do not specify when after the onset of nutrient stress they harvested their DOM, only that they grew the cultures for 14 days (ca. twice as long as in this study; Appendix III), and therefore their DOM pools might have been more enriched in recalcitrant compounds.

We hypothesize that the higher bioavailability of DOM produced under Si stress may be an adaptive strategy for diatoms, allowing them to use the activity of bacterioplankton for their benefit, rather than sparking competition. Bacteria have been shown to degrade organic matrices associated with dead diatom frustules, enhancing frustule dissolution to dissolved Si (Bidle and Azam 2001), and therefore priming this degradation process with bioavailable DOM could be advantageous during the onset of Si stress. This hypothesis counters the objections of Bjørnsen (1988) and Bratbak and Thingstad (1985) to the carbon overflow mechanism, which suggested that releasing bioavailable DOM would harm phytoplankton by stimulating further competition with bacterioplankton, and expands on the hypothesis of Wood and van Valen (1990) that Si stress could be an exception to the diatom and bacterioplankton competition scenario. We did not test Si recycling with this experiment, as diatom frustules were removed with the overall diatom biomass prior to bioassay inoculation, and therefore this scenario is strictly hypothetical. This idea of selective bacterial stimulation likely would not translate to other phytoplankton groups, as diatoms are relatively unique in their requirement for a major nutrient that is not used by heterotrophic bacteria, nor would it explain the smaller releases of bioavailable DOC under N and N + Si stress.

5. Bacterial community composition

Bacterial communities in all of our experiments shifted towards a greater relative abundance of presumed copiotrophs, those phylotypes that grow rapidly upon introduction of labile DOM (predominantly the 33 base pair T-RF; Fig. 4.4 and Appendix V). This contrasts with Pete et al. (2010), who observed an increase in copiotrophic *Gammaproteobacteria* in bacterial communities growing on exudate produced by diatoms under Si stress and a decrease on exudate produced under N stress. The similarities in BCC within our

experiments were surprising given the variability in μ and BGEs. We would have expected variable community composition to accompany these differences in growth rates, which imply differing substrate quality and thus phylogenetic selective pressure (e.g., Cottrell and Kirchman 2000; Nelson et al. 2013). Instead, while diatom nutrient stress had a strong impact on DOC bioavailability, effects of nutrient stress on DOM composition appeared minimally influential in shaping subsequent BCC, at least at the taxonomic resolution obtained via T-RFLP and over scales of days.

While BCC dominated by copiotrophs might indicate a growth of rare "weed" species in bioassays established from the oligotrophic ocean, the responding phylotypes in these experiments are ecologically relevant to an upwelling system and to a phytoplankton bloom scenario. An *in silico* digest of 16S rRNA gene amplicon sequences from the SBC allowed us to putatively identify our 33 base pair T-RF peak as a mix of *Roseobacter*s, *Flavobacteria*, and *Gammaproteobacteria* including *Vibrio* sp., *Pseudoalteromonas* sp., and SAR92 (Fig. 4.4B-D and Appendix V). These phylotypes are common to the coastal ocean and include presumed generalists known to respond to phytoplankton-derived compounds (Mou, Sun, Edwards, Hodson, and Moran 2008). These clades can be strongly associated with diatom blooms in the field (Amin et al. 2012; Buchan et al., 2014), and previous work in the SBC has demonstrated a strong response by *Roseobacter*s in DOM remineralization experiments conducted during a diatom bloom (Wear et al. 2015). Some *Gammaproteobacteria* are further known to facilitate Si regeneration through hydrolysis of detrital diatom organic matrices (Bidle and Azam 2001).

6. Conclusions

The results point to a transition in the relative importance of diatom nutrient stress

and species identity on the bioavailability of exudates to bacterioplankton between timescales of days and timescales of months (Fig. 4.1). The effects of nutrient stress on the bioavailability and suitability of DOM exuded by diatoms as a bacterial growth substrate varied over ecologically relevant timescales of days, with the exception of generally higher BGEs yielded on Si-stress DOM. And over 1 week, DOM produced by diatoms under Si stress was generally more bioavailable. We hypothesize that this exudation could be advantageous for Si-stressed diatoms, as in that scenario promoting bacterial activity could regenerate dissolved Si rather than stimulating competition for nutrients. Bacterial community composition did not reflect this enhanced growth on Si-stress DOM, as all treatments shifted towards copiotrophs commonly found in association with coastal phytoplankton blooms. On a timescale relevant for seasonal export, the concentrations of diatom-produced TOC persisting in the experiments after 16 weeks were not dependent on nutrient stress treatment, but rather varied by diatom species that produced the exudate. These experiments suggest that the identity of the nutrient that terminates a phytoplankton bloom may impact subsequent heterotrophic activity in the short term, but it is unlikely to have a strong influence on TOC persistence and potential export from the system, where instead phytoplankton species identity appears more influential.

Table 4.1. Diatom growth culture dynamics and dilution batch-culture bioassay inocula parameters. All values are: mean of duplicate carboys (range of duplicate carboys). Expt. & treatment: Diatom species that was source of exudate and nutrient stress under which exudate was produced. Days to T_H: duration of culture prior to DOM harvest. T_0: values at initiation of growth culture. T_H: values at last time-point sampled before exuded DOM was harvested for use in dilution-culture bioassays, usually a few hours before harvest filtration began. Diatom data adapted from Windecker et al. (in prep).

Expt. & treatment	Days to T_H	[NO3] (µM) T_0	[NO3] (µM) T_H	[Si(OH)4] (µM) T_0	[Si(OH)4] (µM) T_H	[POC] (µM) T_0	[POC] (µM) T_H	[DOC] (µM) T_0	[DOC] (µM) T_H	DOC:DON[A] T_0	DOC:DON[A] T_H
*S. marinoi*phyto Si stress	9	133.6 (10.4)	16.1 (0.6)	10.1 (0.9)	no data[C]	7.2 (2.9)	258.7 (17.0)	68.8 (1.0)	89.0 (10.1)	3.1 (1.4)	11.6 (1.8)
*S. marinoi*phyto N+Si stress	9	37.1 (0.0)	BDL[B]	9.1 (0.2)	no data[C]	2.5 (0.3)	242.0 (20.2)	70.8 (1.3)	75.7 (0.2)	7.4 (0.7)	13.6 (0.2)
*C. socialis*phyto N stress	6	41.6 (0.2)	BDL	113.5 (3.2)	75.8 (1.5)	18.4 (0.5)	571.9 (10.2)	80.5 (1.7)	86.8 (1.4)	9.3 (0.2)	14.0 (0.5)
*C. socialis*phyto Si stress	6	86.1 (1.1)	20.7 (3.2)	16.4 (0.5)	BDL	29.2 (13.7)	532.6 (1.4)	75.8 (2.4)	96.0 (7.3)	9.7	16.6 (3.5)
*C. socialis*phyto N+Si stress	6	42.5 (0.4)	BDL	16.4 (0.3)	BDL	18.1 (0.3)	547.1 (8.6)	79.9 (1.6)	94.8 (0.3)	14.4 (0.4)	13.9 (0.5)
*T. weissflogii*phyto N stress	5	35.6 (0.3)	BDL	103.0 (3.1)	56.3 (0.7)	45.7 (1.0)	728.5 (4.1)	77.2 (1.7)	93.2 (2.3)	9.9 (1.9)	13.0 (0.0)
*T. weissflogii*phyto Si stress	5	84.9 (0.8)	20.3 (1.3)	16.6 (0.0)	BDL	42.6 (0.5)	599.5 (18.7)	77.1 (0.1)	86.3 (2.8)	7.8 (3.3)	17.9 (6.0)
*T. weissflogii*phyto N+Si stress	5	36.9 (0.1)	BDL	16.5 (0.2)	BDL	44.8 (1.5)	567.8 (16.7)	76.3 (1.8)	83.9 (1.4)	7.5 (1.0)	14.9 (0.8)
*O. aurita*phyto N stress	6	36.0 (0.2)	BDL	89.2 (0.4)	21.4 (2.6)	18.1 (0.6)	702.6 (31.2)	79.3 (0.0)	100.9 (0.3)	11.0 (0.1)	14.6 (0.2)
*O. aurita*phyto Si stress	6	89.5 (0.6)	14.6 (2.1)	28.0 (0.1)	BDL	17.3 (0.3)	621.7 (19.6)	79.4 (1.2)	95.5 (0.5)	6.3 (1.1)	12.3 (0.6)
*O. aurita*phyto N+Si stress	6	36.5 (0.4)	BDL	28.5 (0.1)	BDL	16.5 (0.1)	670.1 (43.6)	77.1 (1.4)	88.4 (3.5)	11.6 (0.7)	13.4 (0.3)

Dilution batch-culture bioassay inocula

	[DOC] (µM)	DOC:DON	Date bioassays inoculated	[DIN] (µM)
*S. marinoi*remin	63.8	5.6	8 April 2011	12.6
*C. socialis*remin	68.6	N/A[D]	4 August 2011	N/A[D]
*T. weissflogii*remin	72.9	13.5	4 December 2011	4.3
*O. aurita*remin	74.0	15.7	17 August 2012	0.6[E]

A: For DON concentrations, see Appendix VI. B: BDL = below detection limit (0.2 µM for N+N and therefore for NO3; 0.3 µM for Si(OH)4). C: data not available, but both were BDL at preceding timepoint. D: DIN data not available, but total dissolved nitrogen (TDN) was 5.0 µM, indicating both DON and DIN must be below that value. E: N+N BDL, therefore set to the detection limit of 0.2 µM for this sample only.

Table 4.2. Select organic matter composition and remineralization parameters from the dilution batch-culture bioassay experiments. All values are: mean of duplicate carboys (range of duplicate carboys); where only one value is presented, only one valid result was obtained, often because duplicate was below detection limit. Expt. & treatment: diatom species that was source of exudate and nutrient stress under which exudate was produced. $\%_{new}$ TOC: the percentage of the "added" DOC remineralized (Eq. 1); when $\%_{new}$ TOC is labeled BDL, that is based on absolute drawdown. BCD: bacterial carbon demand, the sum of TOC remineralization and bacterial biomass produced (Eq. 3). Pers. TOC: persistent TOC, the concentration of diatom-sourced TOC remaining in excess of the unamended control at week 16 (Eq. 2).

149

Expt. & Treatment	Initial conditions		TOC remineralization: Δ µM			TOC remineralization: %new			Total BCD at 4 days		Persistent TOC (µM)
	[TOC] (µM)	TOC:TON	4 days	1 week	16 weeks	4 days	1 week	16 weeks	µM	%new	
*S. marinoi*remin Si stress	109.4* (0.3)	20.4 (2.5)	24.8 (3.2)	28.7 (2.3)	40.4 (1.7)	52 (6)	60 (5)	84 (3)	34.2 (3.1)	72 (17)	7.6 (1.5)
*S. marinoi*remin N+Si stress	78.0 (0.2)	11.9 (0.1)	4.8 (1.4)	5.3 (2.4)	9.9 (2.3)	29 (8)	31 (14)	66 (6)	6.1 (1.3)	61 (21)	6.7 (2.2)
*S. marinoi*remin Control	66.1 (0.4)	12.2 (0.5)	BDL[A]	BDL	4.7 (1.8)	N/A	N/A	N/A	BDL	N/A	N/A[B]
*C. socialis*remin N stress	82.2 (0.0)	13.2 (0.3)	2.3	4.2 (0.6)	7.6	13	24 (3)	44	2.9 (1.4)	57 (33)	9.9
*C. socialis*remin Si stress	96.4* (0.4)	16.1 (0.7)	3.7 (0.8)	12.1 (1.0)	19.7 (2.0)	11 (2)	38 (3)	62 (7)	9.1 (1.3)	35 (0)	12.0 (2.4)
*C. socialis*remin N+Si stress	84.3 (2.8)	14.2 (0.8)	BDL	4.7 (1.7)	10.1 (2.1)	BDL	23 (5)	51 (4)	3.6	37	9.5 (0.6)
*C. socialis*remin Control	68.4 (0.9)	15.8 (1.1)	1.8	3.0 (0.1)	2.8	N/A	N/A	N/A	4.3	N/A	N/A
*T. weissflogii*remin N stress	88.9 (3.0)	13.1 (0.8)	6.1	3.7 (0.9)	17.5 (1.7)	24	16 (2)	79 (3)	8.9	69	4.8 (1.3)
*T. weissflogii*remin Si stress	83.8 (0.2)	15.0 (1.0)	4.9	6.0 (0.2)	11.9 (0.2)	28	35 (2)	69 (0)	5.3 (1.8)	57 (12)	5.3 (0.0)
*T. weissflogii*remin N+Si stress	82.7 (0.9)	11.7 (0.1)	4.7 (1.8)	3.3 (1.4)	10.2 (3.0)	29 (10)	20 (8)	62 (15)	7.2 (2.1)	83 (13)	5.9 (2.1)
*T. weissflogii*remin Control	70.8 (0.5)	13.3 (0.8)	4.5 (0.3)	3.0 (0.1)	4.2 (0.4)	N/A	N/A	N/A	6.1 (0.3)	N/A	N/A
*O. aurita*remin N stress	86.7* (0.2)	14.0 (0.4)	2.2	2.2 (0.7)	11.3 (1.1)	9	9 (3)	48 (5)	2.3	20	12.1 (1.4)
*O. aurita*remin Si stress	85.7 (1.3)	13.2 (0.8)	BDL	3.1	6.9 (1.2)	BDL	13	31 (4)	BDL	BDL	15.4 (0.0)
*O. aurita*remin N+Si stress	92.3* (0.3)	15.3 (0.8)	BDL	3.8 (0.3)	15.7 (0.3)	BDL	13 (1)	54 (0)	2.8	13	13.3 (0.1)
*O. aurita*remin Control	69.7 (0.0)	14.4 (0.2)	BDL	2.9	6.5 (1.6)	N/A	N/A	N/A	1.9	N/A	N/A

*Bulk [TOC] in dilution culture bioassays coming from diatom cultures (calculated by mass balance with inoculum [DOC]) is ≥10% different from the [DOC] in the diatom cultures at the time point prior to harvest (T_H, Table 1), which we attribute to a combination of continued exudation or remineralization during filtration and general handling. A: BDL = below detection limit (1.5 µM for TOC and BCD). B: N/A = parameter not measured for this experiment.

Table continues on next page

Table 4.2, continued

Inorganic nutrient amendments to aged seawater used for *O. aurita*remin Control

Expt. & Treatment	Initial conditions		TOC remineralization: Δ µM			TOC remineralization: %new			Total BCD at 4 days		Persistent TOC (µM)
	[TOC] (µM)	TOC:TON	4 days	1 week	16 weeks	4 days	1 week	16 weeks	µM	%new	
Aged SW +N&P	67.9 (1.4)	12.1 (0.0)	1.9	1.9	4.0	N/A	N/A	N/A	3.3	N/A	N/A
Aged SW +Si&P	69.4 (1.4)	14.9 (1.3)	1.6	BDL	3.4 (1.4)	N/A	N/A	N/A	2.5 (0.4)	N/A	N/A
Aged SW +Culture	72.5 (0.4)	13.1 (0.9)	BDL	3.0	2.6 (0.3)	N/A	N/A	N/A	N/A	N/A	N/A
Aged SW +F/2	71.6 (0.0)	12.8 (0.5)	BDL	1.7	N/A	N/A	N/A	N/A	N/A	N/A	N/A

*Bulk [TOC] in dilution culture bioassays coming from diatom cultures (calculated by mass balance with inoculum [DOC]) is $\geq 10\%$ different from the [DOC] in the diatom cultures at the time point prior to harvest (T_H, Table 1), which we attribute to a combination of continued exudation or remineralization during filtration and general handling. A: BDL = below detection limit (1.5 µM for TOC and BCD). B: N/A = parameter not measured for this experiment.

Table 4.3. Correlations between various TOC processing and bacterial growth parameters and multiple timeframes. Spearman's *rho* non-parametric correlations; significant correlations ($p < 0.05$) are in bold. Control seawater and inorganic nutrient amendment samples were omitted, as their starting conditions and overall growth were substantially different. Correlations were run on the mean of duplicate carboy values where applicable. TOC remineralization values that were below detection limits were omitted from the analysis.

	[TON] T_0	TOC:TON T_0	BCD 4 days	%$_{new}$ BCD 4 days	Δ TOC 1 week	%$_{new}$ TOC 1 week	Δ TOC 16 weeks
[TOC] T_0	$R = -0.487$ $N = 11$ $p = 0.128$	**0.729** **11** **0.011**	0.358 10 0.310	-0.237 10 0.510	0.191 11 0.574	0.041 11 0.905	**0.791** **11** **0.004**
[TON] T_0		**-0.932** **11** **< 0.0001**	-0.122 10 0.738	0.311 10 0.382	**-0.670** **11** **0.024**	-0.516 11 0.104	-0.474 11 0.141
TOC:TON T_0			0.164 10 0.651	-0.426 10 0.220	0.583 11 0.060	0.395 11 0.229	**0.624** **11** **0.040**
BCD 4 days				**0.663** **10** **0.037**	0.564 10 0.090	**0.673** **10** **0.033**	0.564 10 0.090
%$_{new}$ BCD 4 days					0.109 10 0.763	0.347 10 0.327	0.000 10 1.0000
Δ TOC 1 week						**0.943** **11** **<0.0001**	0.464 11 0.151
%$_{new}$ TOC 1 week							0.360 11 0.277
Δ TOC 16 weeks							
Δ TOC (16-1) weeks*							
%$_{new}$ TOC 16 weeks							
Pers. TOC							
μ							
Max. BB							
Integ. BP							

(Table continues on next page.)

Table 4.3 continued.

	Δ TOC (16-1) weeks*	%$_{new}$ TOC 16 weeks	Pers. TOC	μ	Max. BB	Integ. BP	BGE
[TOC] T$_0$	**0.745** **11** **0.008**	0.269 11 0.424	0.282 11 0.401	-0.064 11 0.852	**0.802** **11** **0.003**	**0.709** **11** **0.015**	0.041 11 0.905
[TON] T$_0$	-0.132 11 0.699	-0.199 11 0.558	-0.164 11 0.630	-0.365 11 0.269	-0.221 11 0.513	**-0.633** **11** **0.036**	-0.144 11 0.672
TOC:TON T$_0$	0.342 11 0.304	0.174 11 0.610	0.328 11 0.325	0.208 11 0.540	0.461 11 0.153	**0.729** **11** **0.011**	0.188 11 0.581
BCD 4 days	0.224 10 0.533	**0.784** **10** **0.007**	-0.527 10 0.117	**0.709** **10** **0.022**	0.584 10 0.077	0.382 10 0.276	0.134 10 0.712
%$_{new}$ BCD 4 days	-0.073 10 0.841	0.604 10 0.065	**-0.802** **10** **0.005**	0.608 10 0.062	0.104 10 0.776	-0.188 10 0.602	-0.073 10 0.840
Δ TOC 1 week	0.000 11 1.000	0.588 11 0.057	-0.300 11 0.370	**0.747** **11** **0.008**	0.164 11 0.630	0.573 11 0.066	0.110 11 0.748
%$_{new}$ TOC 1 week	-0.137 11 0.689	0.580 11 0.061	-0.415 11 0.205	**0.874** **11** **<0.0001**	0.132 11 0.698	0.415 11 0.205	0.151 11 0.658
Δ TOC 16 weeks	**0.855** **11** **0.001**	**0.715** **11** **0.013**	-0.255 11 0.450	0.292 11 0.384	0.497 11 0.120	**0.682** **11** **0.021**	0.027 11 0.936
Δ TOC (16-1) weeks*		0.551 11 0.079	-0.173 11 0.612	-0.123 11 0.719	0.410 11 0.210	0.473 11 0.142	-0.164 11 0.629
%$_{new}$ TOC 16 weeks			**-0.761** **11** **0.007**	**0.612** **11** **0.045**	0.135 11 0.693	0.333 11 0.318	-0.105 11 0.758
Pers. TOC				-0.547 11 0.082	0.260 11 0.441	0.027 11 0.937	0.064 11 0.852
μ					0.100 11 0.769	0.118 11 0.729	0.268 11 0.426
Max. BB						0.556 11 0.076	0.217 11 0.521
Integ. BP							-0.178 11 0.600

*Δ TOC at 1 week was subtracted from Δ TOC at 16 weeks to give an independent measure of long-term TOC remineralization; otherwise, the 16-week remineralization was in some cases up to 75% determined by remineralization in the first week.

Table 4.4. Bacterial growth parameters from the dilution batch-culture bioassay experiments. All values are mean of duplicate carboys (range of duplicate carboys). Expt. & treatment: diatom species that was source of exudate and nutrient stress under which exudate was produced. μ: specific growth rate over exponential phase (times vary; see Appendix IV). Integrated BP: total ^{3}H-Leucine incorporation over the first week of the experiment. Max. BB: maximum bacterial biomass observed over the first week of the experiment. BGE: bacterial growth efficiency over exponential phase. BDL: below detection limits. N/A: not calculated for this sample.

Expt. & Treatment	μ (day^{-1})	Integrated BP (nmol ^{3}H-Leu L^{-1} week^{-1})	Max BB (μM C)	BGE (%)
S. marinoi$_{remin}$ Si stress	1.85 (0.09)	127.7 (15.0)	9.7 (0.0)	29 (3)
S. marinoi$_{remin}$ N+Si stress	0.47 (0.00)	26.2 (2.5)	1.7 (0.1)	27 (7)
S. marinoi$_{remin}$ Control	0.31 (0.03)	9.6 (1.1)	1.4 (0.0)	BDL
C. socialis$_{remin}$ N stress	0.19 (0.01)	33.7 (1.8)	2.7 (0.4)	44 (3)
C. socialis$_{remin}$ Si stress	0.50 (0.03)	109.5 (9.0)	6.4 (0.6)	58 (3)
C. socialis$_{remin}$ N+Si stress	0.26 (0.02)	41.6 (1.1)	3.4 (0.1)	34
C. socialis$_{remin}$ Control	0.36 (0.06)	17.1 (0.8)	3.5 (0.3)	57
T. weissflogii$_{remin}$ N stress	0.18 (0.03)	39.6 (0.5)	3.6 (0.0)	34
T. weissflogii$_{remin}$ Si stress	0.73 (0.03)	26.7 (0.1)	2.5 (0.1)	61
T. weissflogii$_{remin}$ N+Si stress	0.55 (0.05)	24.7 (0.4)	3.4 (0.1)	52 (19)
T. weissflogii$_{remin}$ Control	0.62 (0.03)	21.4 (1.0)	2.4 (0.0)	28 (3)
O. aurita$_{remin}$ N stress	0.09 (0.03)	31.5 (1.8)	2.6 (0.0)	27 (5)
O. aurita$_{remin}$ Si stress	0.18 (0.00)	24.9 (0.5)	4.1 (0.3)	57 (4)
O. aurita$_{remin}$ N+Si stress	0.14 (0.04)	38.0 (1.4)	3.5 (0.1)	46 (11)
O. aurita$_{remin}$ Control	0.19 (0.08)	7.7 (1.0)	3.2 (0.1)	35
Aged SW +N&P	0.28 (0.02)	7.7 (0.4)	2.9 (0.3)	64
Aged SW +Si&P	0.11 (0.01)	8.0 (0.5)	3.1 (0.0)	BDL
Aged SW +Culture	0.11 (0.00)	N/A	N/A	N/A
Aged SW +F/2	0.13 (0.01)	N/A	N/A	N/A

Fig. 4.1. Conceptual diagram of the major conclusions of the paper, contrasting short-term and long-term effects of the nutrient stress under which DOM was produced. Arrows indicate carbon flow from the diatom cultures, through the mixed bacterial community inoculum, to select outcomes of the dilution batch-culture bioassays. Arrow color indicates nutrient stress treatment (as labeled in Panel A) and arrow size indicates relative carbon flow through that pathway. A: Short-term effects: over timescales of days to 1 week, nutrient stress effects were apparent in the differential remineralization and incorporation of diatom exudate into bacterioplankton biomass. Si-stress exudate was generally most bioavailable (although biomass production varied, as indicated by the two Si-stress arrows), while source diatom species effects were relatively muted. B: Long-term effects: after 16 weeks, nutrient stress effects were no longer obvious, and the amount of diatom-produced persistent TOC (see Eq. 2) remaining in the experiments varied between diatom source species.
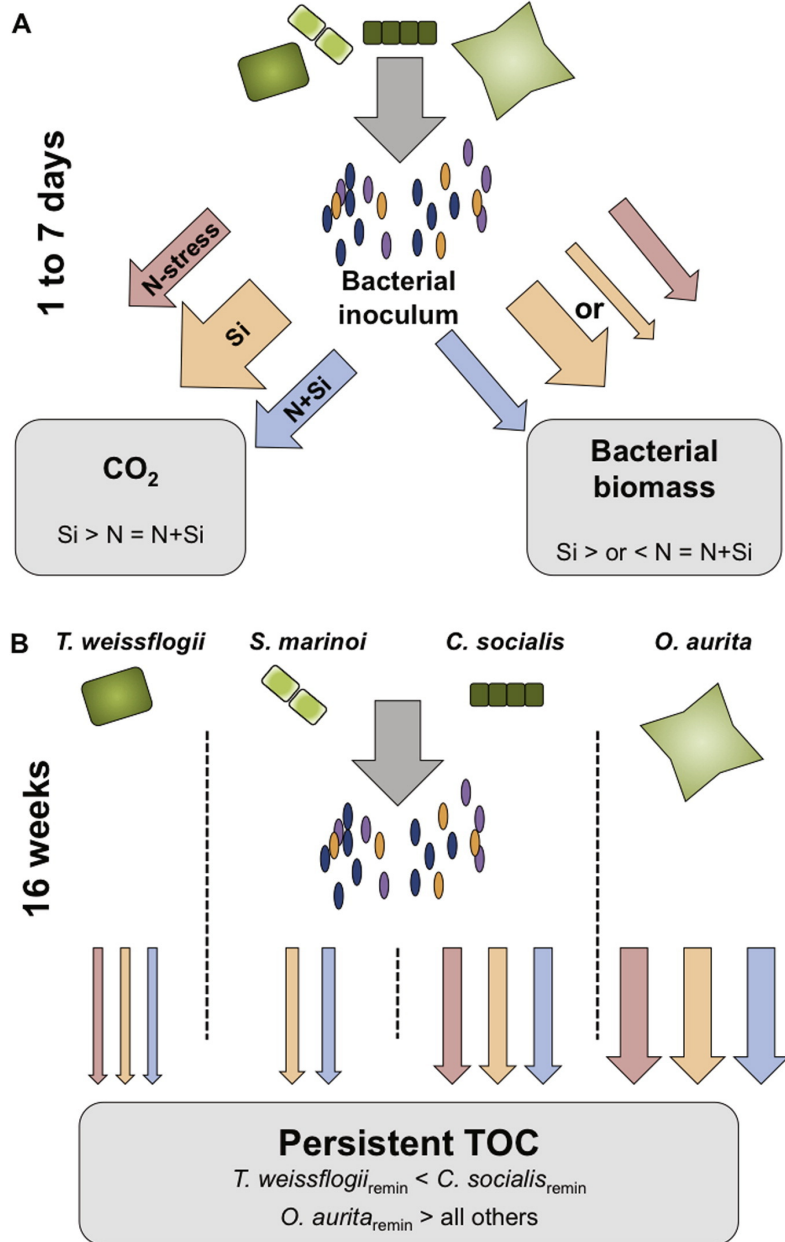
Fig. 4.2. TOC concentrations over time. A–D, legend as in B; E, separate legend. Points are means of duplicate bioassays; error bars indicate range of duplicates. No error bars indicate only one valid sample at that time-point. Please note different X-axis scales on each side of axis break. A: *S. marinoi*remin. B: *C. socialis*remin. C: *T. weissflogii*remin. D: *O. aurita*remin, with persistent TOC indicated (Eq. (2)). E: *O. aurita*remin inorganic nutrient amendments.
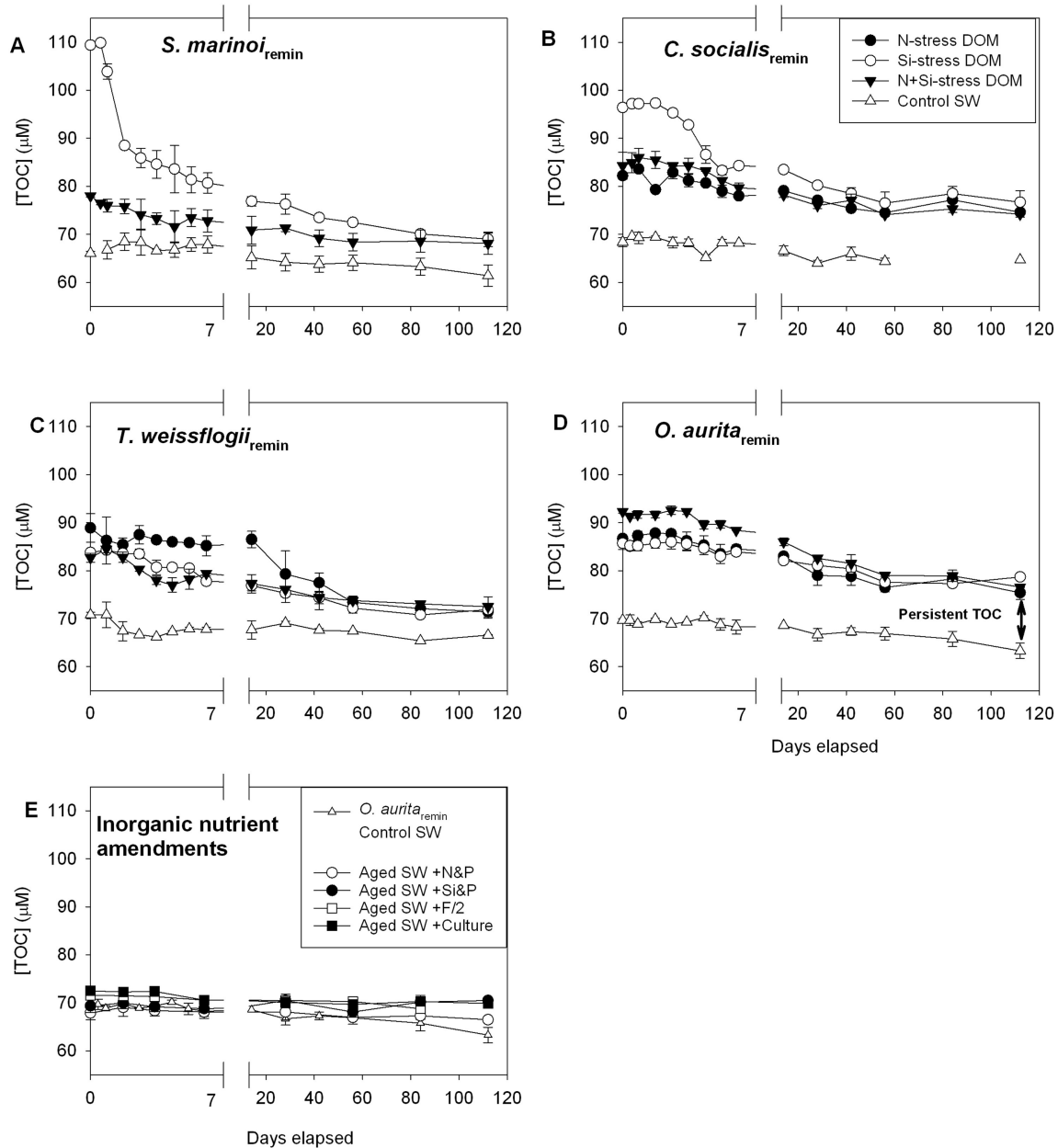
Fig. 4.3. TOC remineralization, persistent TOC, and bacterial growth parameters. All plots are medians of duplicate samples, with error bars indicating range of duplicates. No error bars indicate only one valid sample. Plots C, D, and E intentionally do not contain Control SW data, due to the calculation of the data presented. A: [TOC] remineralized after 1 week. B: [TOC] remineralized after 16 weeks. C: %$_{bioav}$ TOC after 1 week. D: %$_{bioav}$ TOC after 16 weeks. E: Persistent TOC at 16 weeks; letters indicate significantly different source diatom groups based on an ANOVA. F: μ. G: integrated BP over the first week of the experiment. H: BGE.

Fig. 4.4. A: Cell plot of relative abundance of common T-RFs. BCC at T_0 (mean of all samples) and day 4 (mean of duplicate samples, with "Si" here indicating "Si-stress DOM treatment," and so forth), with common T-RFs included here operationally identified as those constituting a mean of 1% or more of either the T_0 or day 4 communities, and "Rare" T-RFs as the sum of the remainder. Putative T-RF identifications are based on *in silico* digests of pyrosequenced 16S rRNA gene amplicons from the SBC (Wear et al. 2015; see Appendix V for methodological details). B: The number of operational taxonomic units (OTUs) within each clade contained in the 33 base pair peak, according to the aforementioned *in silico* digest. C: Proportion of these OTUs represented by each clade in the surface SBC during a diatom-dominated phytoplankton bloom (Wear et al. 2015). D: Proportion of these OTUs represented by each clade in dilution-culture bioassays initiated with SBC water from the same phytoplankton bloom after 3 days.

Chapter IV Appendices

Appendix I. Diagrams of experimental set-up, bioassay starting volumes, and sampling schedule

Appendix I, Figure 1: Diagram of experimental set-up, as detailed in Methods. Inset: An example N-stress phytoplankton culture incubation, showing how NO_3 drawdown (squares) and DOC production (circles) were used to determine the timing of the DOM harvest.
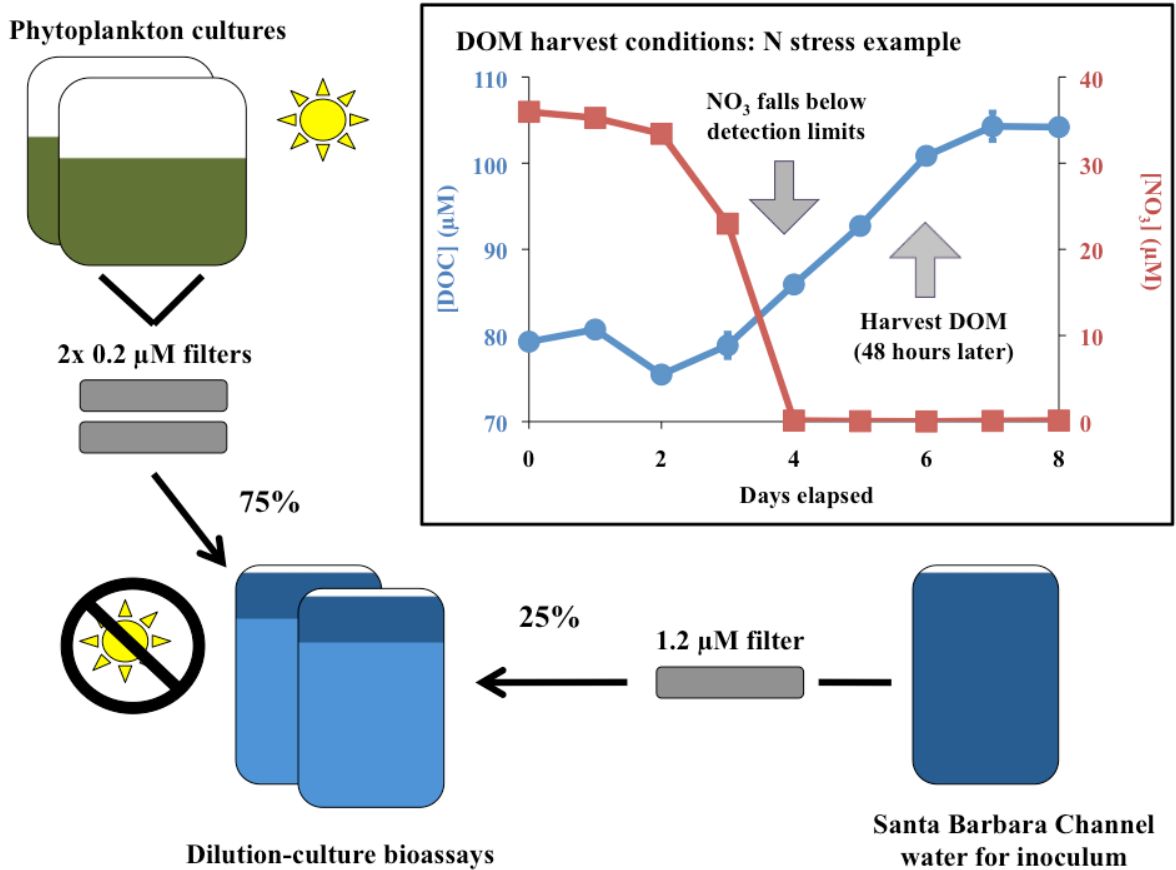
Appendix I, Table 1: Dilution batch-culture bioassay initial volumes (total volume, encompassing 75% exudate and 25% bacterial inoculum)

Expt. & Treatment	Volume (L)	Expt. & Treatment	Volume (L)	Inorganic nutrient amendments	Volume (L)
*S. marinoi*_{remin} Si	5.3	*T. weissflogii*_{remin} N	8	Aged SW +N&P	8
*S. marinoi*_{remin} N+Si	7.7	*T. weissflogii*_{remin} Si	8	Aged SW +Si&P	8
*S. marinoi*_{remin} Control	8	*T. weissflogii*_{remin} N+Si	8	Aged SW +F/2	2
		*T. weissflogii*_{remin} Control	8	Aged SW +Culture	2
*C. socialis*_{remin} N	8	*O. aurita*_{remin} N	8		
*C. socialis*_{remin} Si	8	*O. aurita*_{remin} Si	8		
*C. socialis*_{remin} N+Si	8	*O. aurita*_{remin} N+Si	8		
*C. socialis*_{remin} Control	8	*O. aurita*_{remin} Control	8		

Appendix I, Table 2: Parameters sampled during diatom cultures and dilution batch-culture bioassays. Blank cell indicates parameter was not sampled (or results are not discussed here, for some diatom culture parameters).

	Diatom cultures	Dilution batch-culture bioassays and Aged SW +N&P and +Si&P	Aged SW +F/2 and +Culture (2L experiments)
DOC/TOC and TDN	Daily	Daily for 1 week, then weekly to monthly to 16 weeks	T_0, days 2 and 4, 1 week, then monthly to 16 weeks
Inorganic nitrogen	Daily	T_0, 1 week, 8 weeks	T_0, 1 week, 8 weeks
Silicic acid	Daily	T_0, 1 week, 8 weeks (*O. aurita*_{remin} and inorg. nutrient amendments only)	T_0, 1 week, 8 weeks
POC	Daily		
BA (flow cytometry)		Twice a day for 1 week	Twice a day for 1 week
BA (microscopy)		Daily for 1 week	
BP (^{3}H-leucine)	Daily (all but *S. marinoi*_{diatom})	Daily for 6 days	
DNA		T_0 and days 1, 2, and 4	T_0 and days 2 and 4

Appendix I Figure 2: Timeframes over which parameters discussed in the text were calculated, using one replicate of an *S. marinoi*remin Si-stress DOM experiment as an example. Timeframes marked in red varied between samples due to variable growth curves; parameters marked in blue were measured at a consistent time across all samples. A: Bacterial abundance from flow cytometry (measured every ~12 hours) and DAPI slide counts (collected every ~24 hours and counted only at relevant time-points) over time, with growth phases, and the parameters they were used to calculate, identified. Flow cytometry counts were used to identify growth phases and to calculate μ. DAPI counts were used to estimate bacterial biomass for BGE (Equation 4) and BCD (Equation 3) calculations. B: [TOC] over time. Changes in [TOC] to the left of the blue line (7 days or shorter) are discussed as short-term drawdown in the text; changes in [TOC] to the right of the line (14 days or longer) are considered long-term TOC drawdown.

161
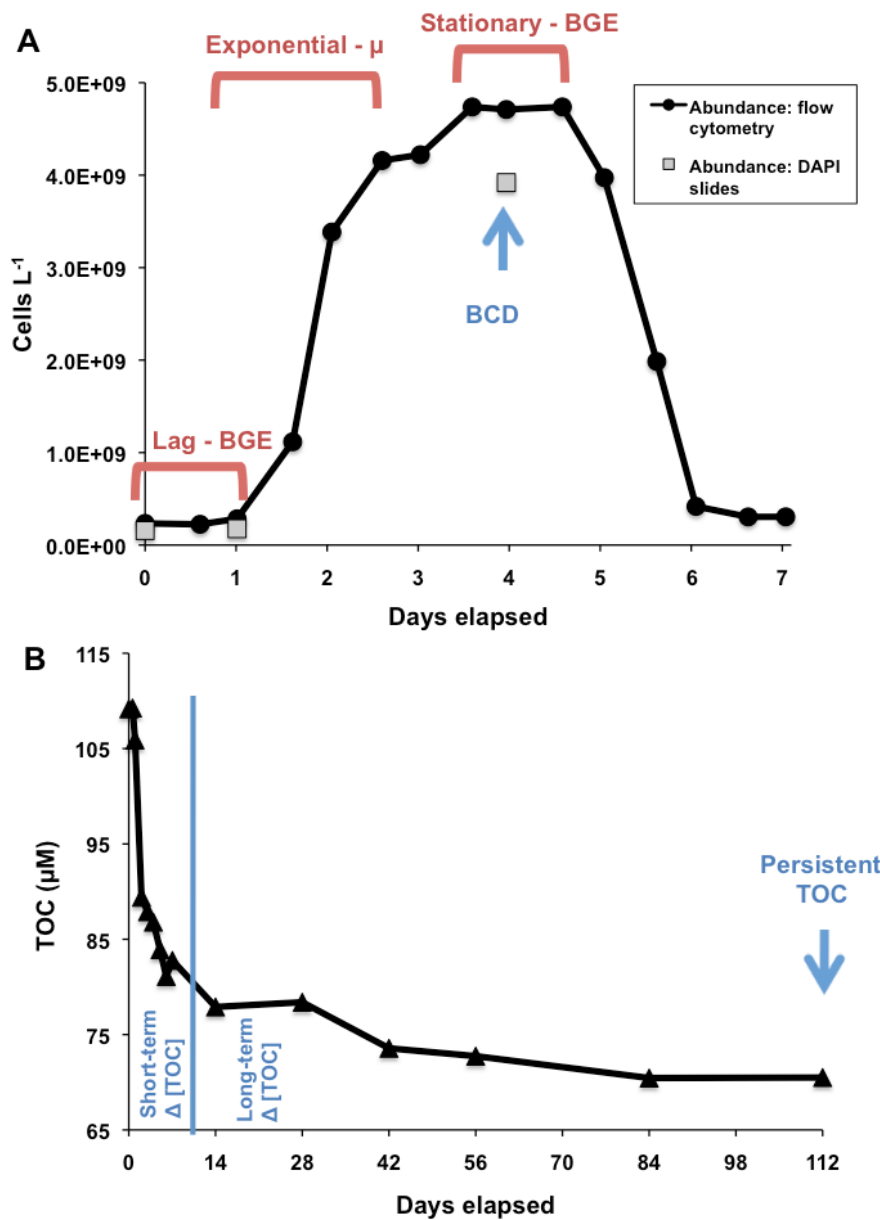
Appendix II. Inorganic nutrient amendments to aged seawater used for *O. aurita*remin Control and *O. aurita*remin samples (i.e. target concentrations for comparison)

	NO_3+NO_2 (µM)			$Si(OH)_4$ (µM)			PO_4 (µM)		
	T_0	1 week	8 weeks	T_0	1 week	8 weeks	T_0	1 week	8 weeks
*O. aurita*remin N stress	BDL	BDL	0.2 (0.0)	14.8 (0.3)	14.4 (0.6)	15.2 (0.4)	4.8 (0.0)	4.7 (0.1)	4.9 (0.0)
*O. aurita*remin Si stress	8.9 (0.0)	8.9 (0.1)	8.9 (0.1)	BDL	BDL	BDL	2.9 (0.0)	2.9 (0.1)	3.1 (0.0)
*O. aurita*remin N+Si stress	0.2 (0.0)	BDL	BDL	BDL	BDL	BDL	5.6 (0.1)	5.4 (0.0)	5.9 (0.1)
*O. aurita*remin Control	BDL	BDL	0.7 (0.4)	0.4 (0.0)	0.4 (0.0)	0.4 (0.0)	0.3 (0.0)	0.3 (0.0)	0.3 (0.0)
Aged SW +N&P	7.5 (0.0)	7.5 (0.1)	7.8 (0.3)	0.4 (0.0)	0.4 (0.0)	0.4 (0.0)	3.4 (0.1)	3.1 (0.1)	3.7 (0.0)
Aged SW +Si&P	BDL	BDL	0.7 (0.6)	16.7 (0.3)	17.3 (0.1)	16.9 (0.2)	3.5 (0.2)	3.3 (0.2)	3.7 (0.1)
Aged SW +Culture	1.7 (0.0)	1.7 (0.0)	3.7 (0.0)	2.7 (0.1)	3.1 (0.3)	2.7 (0.0)	0.4 (0.0)	0.4 (0.0)	0.5 (0.0)
Aged SW +F/2	2.6 (0.1)	2.6 (0.1)	4.4 (0.3)	3.6 (0.1)	3.6 (0.1)	3.7 (0.1)	0.5 (0.0)	0.5 (0.0)	0.6 (0.0)

Mean of duplicate samples (range). Detection limits: NO_3+NO_2: 0.2 µM; PO_4: 0.1 µM; $Si(OH)_4$: 0.3 µM. BDL = below detection limit.

Appendix III. Bacterial production in diatom experiments

Supplemental methods: ^{3}H-Leucine incorporation was measured as described for the dilution batch-culture bioassays (as in Halewood et al. 2012). To assess the distribution between free-living bacteria and those attached to phytoplankton and other particles (e.g., transparent exopolymer particles, or TEP), samples were filtered through a 3 μm polycarbonate filter (Millipore TSTP) under gentle pressure from a rubber-free syringe. Both filtrate and whole water samples were assessed simultaneously.

BP was not measured during the *S. marinoi*$_{phyto}$ phytoplankton growth experiment. However, we note that one of the *S. marinoi*$_{phyto}$ Si-stress treatments appeared cloudy prior to DOM harvest, suggesting bacterial and/or viral activity was likely in this experiment as well.

Appendix III Table 1: Bacterial production in diatom experiments.

| | | Integrated BP (T_0 to T_H) – nmol Leu L^{-1} | | |
	Days to $T_H{}^A$	Whole water	Filtered water (< 3 μm)	Attached bacteria[B] (> 3 μm)
*C. socialis*phyto N stress	6	537.9 (1.8)	112.1 (56.3)	425.8 (58.1)
*C. socialis*phyto Si stress	6	563.5 (17.9)	76.2 (18.2)	487.3 (0.3)
*C. socialis*phyto N+Si stress	6	545.2 (33.4)	72.4 (23.9)	472.8 (9.5)
*T. weissflogii*phyto N stress	5	32.5 (0.3)	17.7 (1.0)	14.7 (1.3)
*T. weissflogii*phyto Si stress	5	42.9 (4.4)	25.0 (2.2)	17.9 (2.2)
*T. weissflogii*phyto N+Si stress	5	32.7 (2.4)	20.6 (0.8)	12.1 (1.6)
*O. aurita*phyto N stress	6	24.7 (2.6)	20.0 (1.9)	4.7 (0.7)
*O. aurita*phyto Si stress	6	37.0 (0.8)	32.6 (0.0)	4.4 (0.7)
*O. aurita*phyto N+Si stress	6	25.0 (1.9)	21.2 (1.1)	3.8 (0.7)

Mean of duplicate samples (range). A: T_H: last sampling point before DOM was harvested for dilution-culture remineralization bioassays. Therefore, "Days to T_H" represents the number of days over which the total Integrated BP was calculated. B: Attached bacteria BP was calculated as the difference between whole water BP and filtered BP.

Appendix IV. Bacterial abundance and biomass in bioassays

Appendix IV, Figure 1: Bacterial abundance over the first week of the bioassays. Legends as specified at bottom right; note variable Y-axis scales. Points are means and error bars are ranges of duplicate bioassays. The bacterial abundance in Fig. 1 is derived from flow cytometry data, while the bacterial biomass data presented in Table 1 below were converted from epifluorescence microscopy counts, as we have observed an offset in absolute abundance between the two methods. The abundance data here were used to calculate μ and to identify the correct time-points for our BGE calculations; for exact time-points selected, see Appendix IV, Table 1. A: *S. marinoi*remin. B: *C. socialis*remin. C: *T. weissflogii*remin. D: *O. aurita*remin. E: *O. aurita*remin inorganic nutrient amendments.
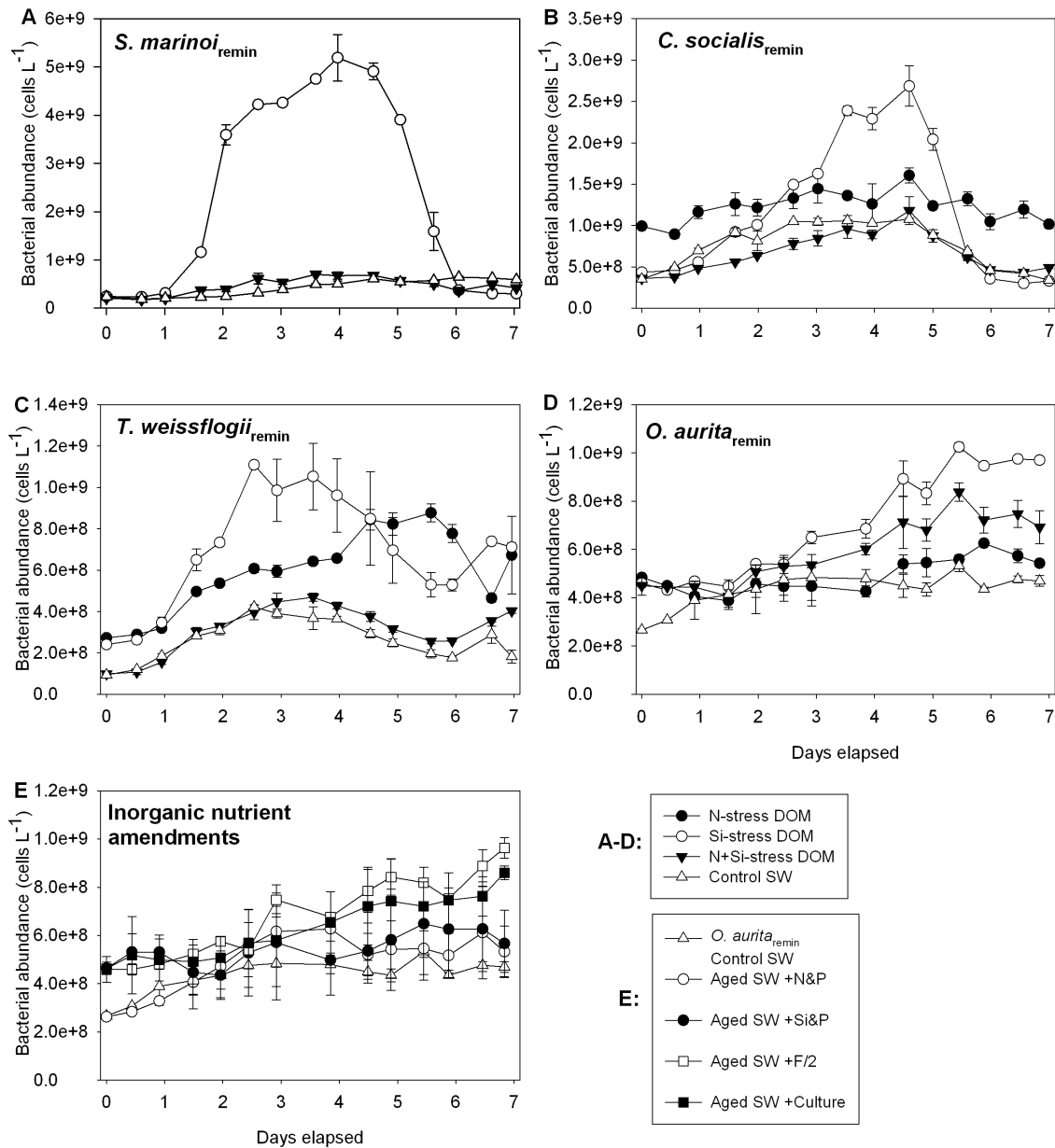
Appendix IV, Table 1: Bacterial biomass (BB) used in BCD and BGE calculations, and the timeframes over which BGEs were calculated. Biomass was converted from bacterial abundance as measured by epifluorescence microscopy of 4'6-diamidino-2-phenylindole (DAPI) stained slides (Porter and Feig 1980), using a factor of 30 fg C cell^{-1} (A. Cano, unpublished).

Expt. & Treatment	Bacterial biomass mean (range)			BGE timepoints and bacterial biomass (two replicate carboys are on two lines)			
	T_0 µM	4 days µM	1 week µM	Lag timepoints (days)	Mean BB µM	Stationary timepoints (days)	Mean BB µM
*S. marinoi*remin Si	0.4 (0.0)	9.7 (0.0)	1.0 (0.0)*	0-1	0.4	3.5-4.5	9.8
				0-1	0.4	3.5-4.5	9.7
*S. marinoi*remin N+Si	0.4 (0.0)	1.7 (0.1)	1.3*	0-1	0.5	3.5-4.5	1.8
				0-1	0.5	3.5-4.5	1.6
*S. marinoi*remin Control	0.5 (0.1)	1.9 (0.1)	2.3 (0.1)	0-1.5	0.5	6	1.3
				0-2	0.4	4.5-6.5	1.4
*C. socialis*remin N	1.1 (0.0)	3.0 (0.1)	0.8 (0.2)*	0-0.5	1.1	1.5-3.5	2.3
				0-0.5	1.1	3-4.5	3.1
*C. socialis*remin Si	0.9 (0.1)	6.4 (0.6)	0.7 (0.2)*	0-1	1.1	4	6.9
				0-0.5	0.9	3.5-4.5	5.8
*C. socialis*remin N+Si	1.1 (0.1)	3.6 (0.1)	1.2 (0.4)*	0-0.5	1.2	5	3.2
				0-0.5	1.0	4	3.5
*C. socialis*remin Control	1.1 (0.1)	3.3 (0.4)	1.0 (0.0)*	0	1.2	2.5-4.5	3.8
				0	1.0	2.5-4.5	3.2
*T. weissflogii*remin N	0.9 (0.1)	3.6 (0.0)	1.6 (0.1)*	0	1.0	4.5-5.5	3.6
				0	0.9	5-5.5	3.7
*T. weissflogii*remin Si	0.7 (0.1)	2.9 (0.0)	2.5 (0.5)*	0-0.5	0.6	3	2.4
				0-0.5	0.8	3	2.6
*T. weissflogii*remin N+Si	0.8 (0.1)	3.3 (0.2)	2.9 (0.1)	0-0.5	0.8	3-4	3.2
				0-0.5	0.9	3	3.5
*T. weissflogii*remin Control	0.8 (0.1)	2.3 (0.0)	1.5 (0.1)*	0-0.5	0.7	2.5-4	2.5
				0-0.5	0.8	2.5-3	2.4
*O. aurita*remin N	1.7 (0.4)	2.3 (0.0)	2.7	1	1.3	6	2.7
				0-2	1.7	6-7	2.6
*O. aurita*remin Si	1.6 (0.1)	2.7 (0.4)	3.5 (0.5)	0-1	1.5	6	4.4
				0-1	1.7	6-7	3.9
*O. aurita*remin N+Si	1.7 (0.1)	3.0 (0.6)	3.1 (0.4)	0-2	1.9	5-7	3.6
				0-2	1.7	6	3.4
*O. aurita*remin Control	1.7 (0.0)	2.9 (0.2)	3.1 (0.2)	0	1.7	5-7	3.3
				0	1.7	6-7	3.1
Aged SW +N&P	1.5 (0.0)	2.8 (0.1)	3.2 (0.6)	0	1.5	3-5	3.1
				0	1.5	2-4	2.6
Aged SW +Si&P	1.8 (0.2)	2.9 (0.3)	2.8 (0.1)	2	2.1	6	3.1
				2	2.5	5-6	3.1

*Cultures that had clearly entered death phase by 1 week are noted (see Discussion on persistent TOC for context of long-term biomass after death phase).

Appendix IV, Figure 2: Maximum bacterial biomass and BCD. Columns are means and error bars are ranges of duplicate samples. A: Maximum bacterial biomass observed over the first week (the biomass at stationary phase, as identified from cell abundance as counted by flow cytometer, and converted from abundance data derived by epifluorescence microscopy). B: Absolute BCD at 4 days (see Methods for details on calculation). C: %$_{new}$ BCD at 4 days (Control SW is intentionally omitted).
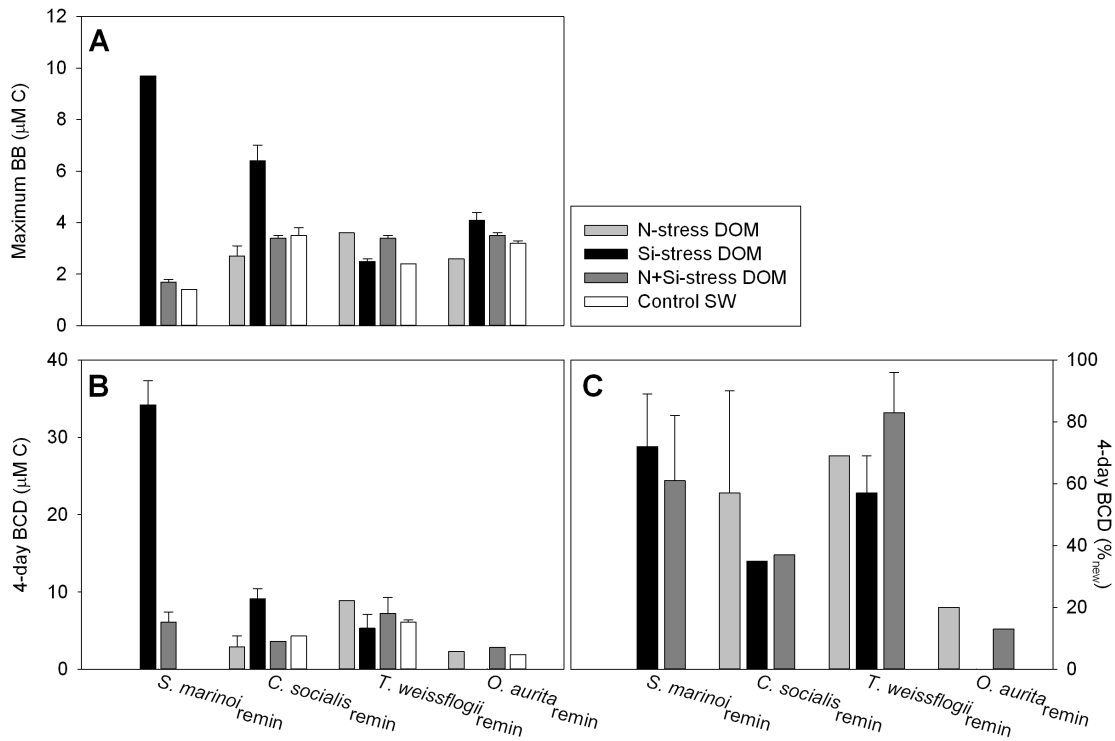
Appendix V. Bacterial community composition: Methods, NMS plots, and results for *in silico* digest for putative T-RF identifications

Supplemental complete methods for T-RFLP analysis:

Samples for bacterial community composition (BCC) analysis were collected at the initial sampling and at 1, 2 and 4 days. Sample water (300 mL) was filtered through a 0.2 μm polyethersulfone filter (Supor-200, Pall) in an acid-washed plastic housing under low vacuum pressure. Filters were placed in sterile cryovials and stored frozen at -40° C. Samples were lysed in sucrose lysis buffer (40 mmol L^{-1} EDTA, 50 mmol L^{-1} Tris-HCl, 750 mmol L^{-1} sucrose, 400 mmol L^{-1} NaCl, pH adjusted to 8.0) with 1% w/v sodium dodecyl sulfate and 0.2 mg ml^{-1} proteinase-K at 55° C for 2 hours. Genomic DNA was immediately extracted using a commercial silica centrifugation kit (DNEasy, Qiagen, Valencia, CA).

After DNA was extracted, BCC was assessed via the DNA fingerprinting technique terminal restriction fragment length polymorphism (T-RFLP) to compare frequency distributions of 16S ribosomal RNA gene amplicons. Polymerase chain reactions (PCR: 4 μL genomic DNA template in 25 μL reaction mixture containing 1 U *Taq* (5PRIME Inc., Gaithersburg, MD) in 1x 5Prime buffer amended to 4 mM $MgCl_2$, 400 μM dNTPs, 5% acetamide, and 200 nM each of universal bacterial primers 8f-FAM (5′-AGRGTTYGATYMTGGCTCAG-3′) and 519r (5′-GWATTACCGCGGCKGCTG-3′; Morris et al, 2005)) were thermally cycled for an initial 3 minutes at 94° C; 30 cycles of 30 seconds at 94° C, 30 seconds at 57° C, and 1 minute at 72° C; and a final extension of 10 minutes at 72° C.

Amplicons were digested with *Hae*III restriction endonuclease (New England

Biolabs, Ipswich, MA, USA) for 4 hours at 37° C, denatured with formamide, and analyzed

by capillary gel electrophoresis at the University of California, Berkeley DNA Sequencing

Facility. T-RFLP peaks were aligned to a custom fragment size standard (30 to 600 basepair

range; BioVentures Inc., Murfreesboro, TN, USA) using PeakScanner v1.0 (Applied

Biosystems, Foster City, CA, USA) with sample peak identification minimum cutoff of 50

relative fluorescence units (RFU) and standard peak cutoff of 20 RFU. Peaks were manually

assigned using integer-length fragment groups (Nelson 2009), with minima of ≥1% total

sample area for peak definition and ≥ 0.5% for inclusion in the sample matrix. Samples that

had amplified poorly were discarded, and the Sørensen similarity index (Sørensen 1948) was

used as the basis for nonmetric multidimensional scaling (NMS) ordination analysis

conducted in Primer 6 (Clarke and Gorley 2006).

Supplemental methods for *in silico digest*:

       Putative T-RF identifications were derived from *in silico* digests of pyrosequencing

results from the Santa Barbara Channel and dilution batch-culture bioassays of ambient

DOM during a phytoplankton bloom (Wear et al. 2015). Briefly, 16S rRNA gene amplicons

were: generated using 8F and 338R primers; pyrosequenced on a Roche/454 GS FLX using

Titanium Chemistry; aligned to a non-redundant subset of the SILVA SSU Ref 16S

alignment database; and assigned to operational taxonomic units (OTUs) by average-

neighbor hierarchical clustering at the 95% identity level (for this highly variable region of

the 16S gene, the equivalent of a 97% identity level over the entire 16S gene; Schloss 2010).

The consensus sequences for the 40 most abundant OTUs were put through a simulated *in silico Hae*III digest. Because the amplicons were sequenced from the reverse primer, the consensus sequences generally did not extent far enough in the 5' direction to encompass the forward primer and thus could not give us an accurate T-RF length on their own, as our T-RFLP FAM label is on the forward primer. Therefore, ca. 150 basepairs of the consensus sequences were run through the Basic Local Alignment Search Tool nucleotide database (BLASTn; http:// http://blast.be-md.ncbi.nlm.nih.gov/Blast.cgi) to find amplicons that extended far enough in the 5' direction to partially cover the 8F primer. Results generally were 99-100% identical with the search sequence (results down to 97% similarity were tolerated in a few cases when they were the best available), and most matches came from aquatic environmental samples. BLAST result sequences were then subjected to the same *in silico Hae*III digest.

These results were compared to those of Morris et al. (2005), who used *in silico* digests and clone libraries to derive similar putative T-RF identifications in the Sargasso Sea.

T-RFs were only assigned a putative phylogenetic identification when there were unambiguous peaks in the region of interest, as there was generally an offset between the *in silico* results and measured T-RF length in well-known OTUs. For example, SAR11 Surface 1 had an *in silico* expected T-RF length of 117 basepairs and a measured length of 114; because this was the most prominent peak for at least 30 basepairs in either direction, the putative identity could be assigned with high confidence. In contrast, a SAR11 Surface 2 sequence had an expected length of 293; because there were measured T-RF peaks at 292, 293, 294, and 295 basepairs, with those at 293 and 295 both fairly abundant, we could not assign this phylotype to any single one of those peaks with high confidence.

Appendix V, Figure 1: NMS ordination of all T-RFLP samples (inocula, nutrient stress and control experiments, and inorganic nutrient amendments, from all sampled time-points) together. Each experiment was inoculated with a distinct bacterioplankton community collected from the SBC at different times of the year, yet the resulting experimental communities overlap substantially rather than developing distinct groupings.
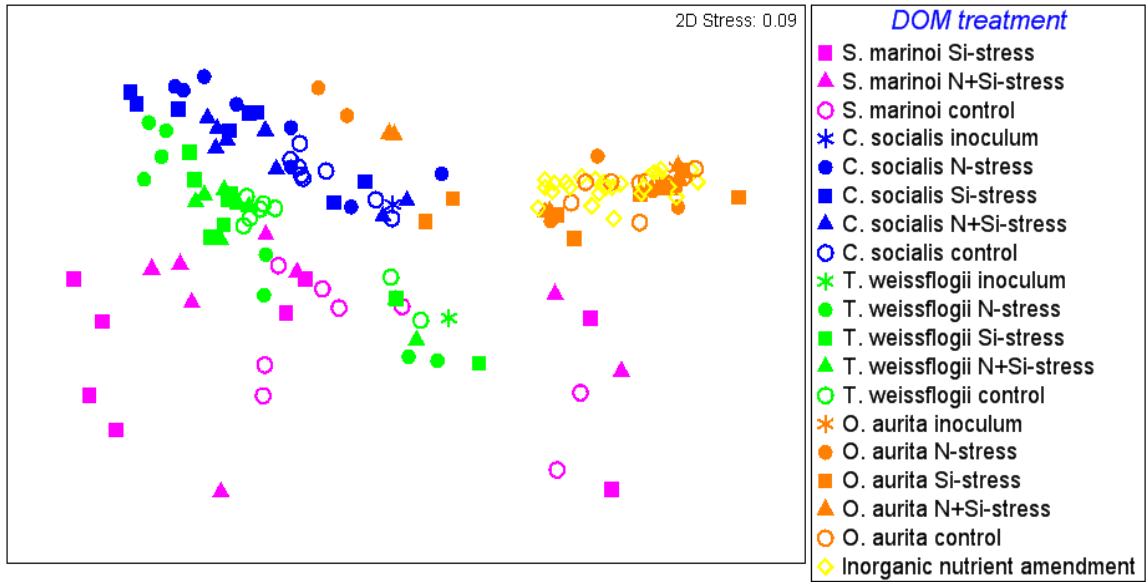
Appendix V, Figure 2: NMS ordination plots of individual experiments. All NMS plots are oriented with T_0 samples in the upper left corner and day 4 at the terminal end of the lines, generally towards the bottom right corner. Black and gray symbols of the same shape are duplicate carboys. All inorganic nutrient controls were given the same symbol for clarity, as none of the communities are distinct from the unamended control seawater communities; note that inorganic nutrient controls are only shown in panel D. A: *S. marinoi*remin NMS. B: *C. socialis*remin NMS. C: *T. weissflogii*remin NMS. D: *O. aurita*remin NMS, including inorganic nutrient amendments.

172
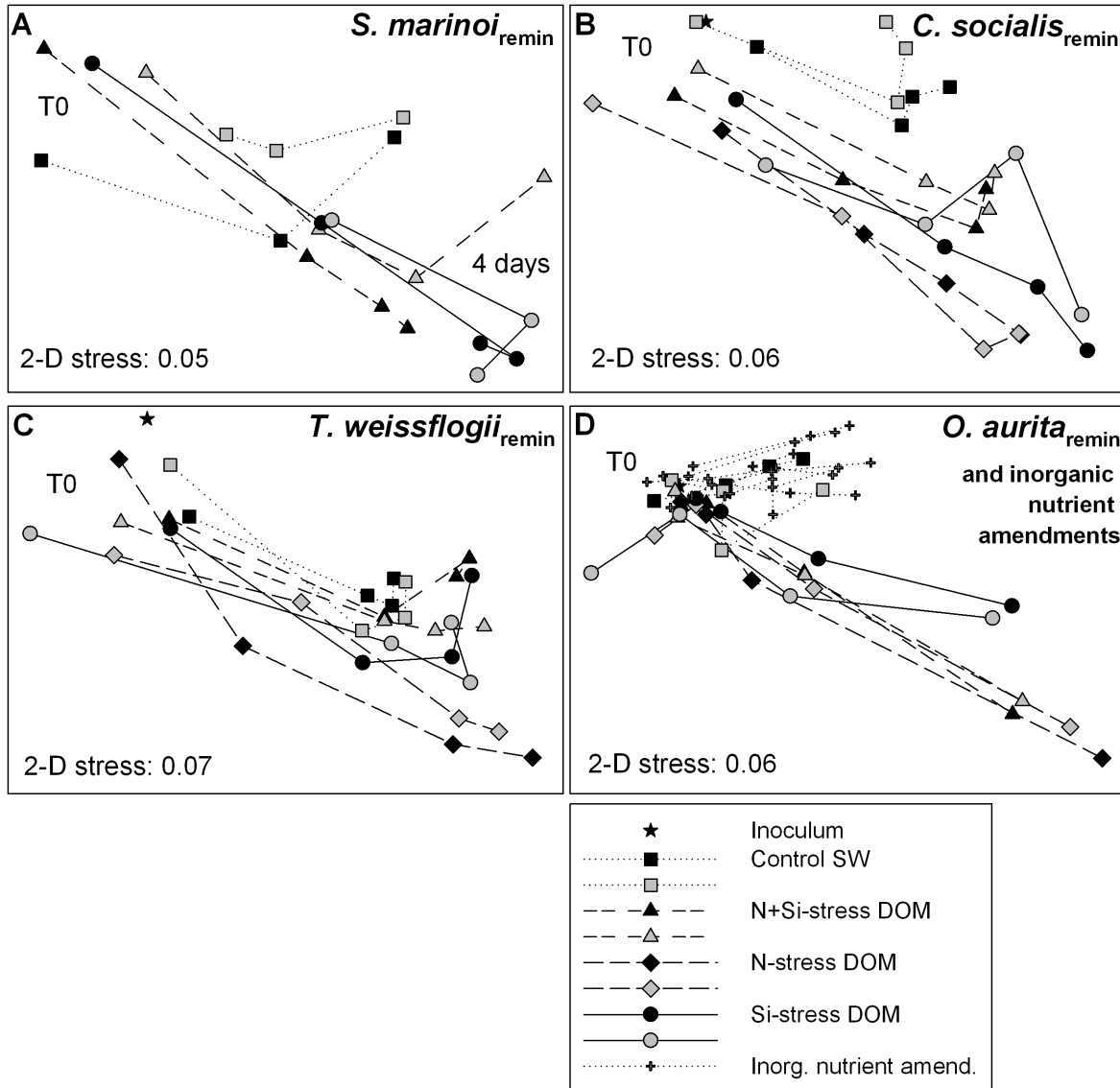
Appendix V, Table 1: Putative identities of T-RF peaks based on *in silico* digest of 16S rRNA gene amplicon pyrosequencing of samples collected in the Santa Barbara Channel (Wear et al. 2015). Phylotype identities are grouped by approximate expected base pair length of corresponding T-RF.

Phylotype, to lowest clade identified in sequence processing pipeline	Base pairs, *in silico* digest of consensus sequence	Base pairs, *in silico* digest of BLAST result sequence	Base pairs, Morris et al. (2005) (*in silico*/ assigned)	Base pairs, putative assigned peak
Actinobacteria: Acidimicrobiia: Acidimicrobiales: Sva0996 marine group		39		33
α-proteobacteria: OCS116 clade		39		33
α-proteobacteria: Rhodobacterales: Rhodobacteraceae: Pacificibacter		39		33
α-proteobacteria: Rhodobacterales: Rhodobacteraceae: Roseobacter clade AS-21 lineage		39		33
α-proteobacteria: Rhodobacterales: Rhodobacteraceae: Roseobacter clade DC5-80-3 lineage		39		33
α-proteobacteria: Rhodobacterales: Rhodobacteraceae: Roseobacter clade OCT lineage	39	39		33
α-proteobacteria: Rhodobacterales: Rhodobacteraceae		39		33
Bacteroidetes: Cytophagia: Cytophagales: Flammeovirgaceae: Fabibacter		39		33
Bacteroidetes: Flavobacteria: Flavobacteriales: Cryomorphaceae: Fluviicola		39		33
Bacteroidetes: Flavobacteria: Flavobacteriales: Flavobacteriaceae: NS4 marine group		39		33
Bacteroidetes: Flavobacteria: Flavobacteriales: Flavobacteriaceae: NS5 marine group		39		33
γ-proteobacteria: Alteromonadales: Alteromonadaceae: SAR92 clade (2 OTUs)		39	39/ ND	33
γ-proteobacteria: Alteromonadales: Pseudoalteromonadaceae: Pseudoalteromonas		39	39/ ND	33
γ-proteobacteria: Oceanospirillales: Oceanospirillaceae: Balneatrix		39	39/ ND	33
γ-proteobacteria: Vibrionales: Vibrionaceae: Vibrio		39	39/ ND	33
α-proteobacteria: SAR11: Surface 1		117	117/ 113	114
γ-proteobacteria: Oceanospirillales: SAR86 clade		188	188/187 and 189/188	
α-proteobacteria: Rickettsiales: SAR116 clade: *Candidatus Puniceispirillum*		189		
γ-proteobacteria: Oceanospirillales: Oceanospirillaceae: Pseudospirillum		190		
α-proteobacteria: Rickettsiales: SAR116 clade		193	193/ 192	
γ-proteobacteria: Alteromonadales: Ferrimonadaceae: Paraferrimonas		204		

γ-proteobacteria: Oceanospirillales: Oceanospirillaceae: Spongiispira		223		
β-proteobacteria: Methylophilales: Methylophilaceae: OM43 clade		223		
α-proteobacteria: Rickettsiales: SAR116 clade		224		
α-proteobacteria: Rickettsiales: SAR116 clade		226		
α-proteobacteria: SAR11: Surface 1		228	228/ 227 and 230/ 228	
Bacteroidetes: Flavobacteria: Flavobacteriales: Flavobacteriaceae: Polaribacter		284		284
α-proteobacteria: SAR11: Surface 2		293	293/ 291	
α-proteobacteria: SAR11: Deep 1		293		
α-proteobacteria: SAR11: Deep 1		293		
α-proteobacteria: Rhodospirillales: Rhodospirillaceae: AEGEAN-169 marine group		294		
γ-proteobacteria: Oceanospirillales: ZD0405		323	326/ 325	324
γ-proteobacteria: Oceanospirillales: Oceanospirillaceae: Marinomonas		323	326/ 325	324
δ-proteobacteria: SAR324 clade (Marine group B)		405	405/ 405	
Bacteroidetes: Flavobacteria: Flavobacteriales: Flavobacteriaceae: Polaribacter		409		
Bacteroidetes: Flavobacteria: Flavobacteriales: Flavobacteriaceae: NS5 marine group		411		
γ-proteobacteria: Oceanospirillales: Oceanospirillaceae: Balneatrix		412		
Bacteroidetes: Flavobacteria: Flavobacteriales: Flavobacteriaceae: NS5 marine group (2 OTUs)		> 600*		

*: > 600: no digest site found in sequence, nor 519r primer – would be edited out based on our T-RFLP QC guidelines.

Appendix VI: DON dynamics in diatom batch cultures and bacterial inocula

Appendix VI, Table 1: DON dynamics in diatom batch cultures and bacterial inocula. [NO_3] is presented for comparison. All values are: mean of duplicate carboys (range of duplicate carboys). Expt. & treatment: Diatom species that was source of exudate and nutrient stress under which exudate was produced. T_0: values at initiation of growth culture. T_H: values at last timepoint sampled before exuded DOM was harvested for use in dilution-culture bioassays, usually a few hours before harvest filtration began. Diatom data adapted from Windecker et al. (in prep).

Expt. & treatment	NO_3 (μM)		DON (μM)	
	T_0	T_H	T_0	T_H
S. marinoi$_{phyto}$ Si stress	133.6 (10.4)	16.1 (0.6)	26.8 (11.3)[A]	7.7 (0.3)
S. marinoi$_{phyto}$ N+Si stress	37.1 (0.0)	BDL[A]	9.7 (0.8)	5.6 (0.0)
C. socialis$_{phyto}$ N stress	41.6 (0.2)	BDL	8.7 (0.0)	6.2 (0.3)
C. socialis$_{phyto}$ Si stress	86.1 (1.1)	20.7 (3.2)	7.6	6.0 (0.8)
C. socialis$_{phyto}$ N+Si stress	42.5 (0.4)	BDL	5.5 (0.0)	6.9 (0.2)
T. weissflogii$_{phyto}$ N stress	35.6 (0.3)	BDL	8.0 (1.3)	7.2 (0.2)
T. weissflogii$_{phyto}$ Si stress	84.9 (0.8)	20.3 (1.3)	12.0 (5.1)	5.5 (2.0)
T. weissflogii$_{phyto}$ N+Si stress	36.9 (0.1)	BDL	10.3 (1.5)	5.6 (0.4)
O. aurita$_{phyto}$ N stress	36.0 (0.2)	BDL	7.2 (0.1)	6.9 (0.1)
O. aurita$_{phyto}$ Si stress	89.5 (0.6)	14.6 (2.1)	13.1 (2.5)	7.8 (0.4)
O. aurita$_{phyto}$ N+Si stress	36.5 (0.4)	BDL	6.7 (0.5)	6.6 (0.4)
Dilution batch-culture bioassay inocula				
	DIN (μM)		DON (μM)	
S. marinoi$_{remin}$	12.6		11.3	
C. socialis$_{remin}$	N/A		N/A (TDN 5.0)[B]	
T. weissflogii$_{remin}$	4.3		5.4	
O. aurita$_{remin}$	0.6[C]		4.7	

A: This experiment had tightly replicated TDN between duplicate carboys, but a 20 μM difference in NO_3 at T_0. As this discrepancy was no longer apparent by the subsequent time-point (~24 hours later), it was likely due to point-source contamination in the sampling/filtering process. As we cannot identify which sample is incorrect, we are reporting both. B: DIN data not available, but total dissolved nitrogen (TDN) was 5.0 μM, indicating both DON and DIN must be below that value. C: N+N BDL, therefore set to the detection limit of 0.2 μM for this sample only.

Appendix VII. DIN, DON, and DOC:DON at all time-points where measured in dilution batch-culture bioassays

	NO₃+NO₂ (µM)			NH₄ (µM)		
	T_0	1 week	8 weeks	T_0	1 week	8 weeks
*S. marinoi*remin Si	13.9 (0.1)	11.7 (0.0)	12.0 (0.0)	1.1 (0.3)	1.7 (0.0)	2.6 (0.2)
*S. marinoi*remin N+Si	3.2 (0.0)	3.2 (0.1)	4.5 (0.0)	0.9 (0.1)	0.8 (0.0)	BDL
*S. marinoi*remin Control	4.0 (0.8)	5.3 (0.1)	6.7 (0.0)	2.1 (0.2)	0.8 (0.0)	0.2/BDL
*C. socialis*remin N	0.3/BDL	0.2/BDL	BDL	0.2 (0.0)	0.2 (0.1)	0.9 (0.0)
*C. socialis*remin Si	15.4 (0.0)	14.6 (0.3)	14.6 (0.0)	0.2 (0.0)	1.1 (0.1)	2.1 (0.1)
*C. socialis*remin N+Si	0.3 (0.1)	BDL	BDL	BDL	BDL	0.8 (0.1)
*C. socialis*remin Control	0.2/BDL	0.2/BDL	1.5 (0.1)	1.3 (0.0)	1.3 (0.0)	0.1/BDL
*T. weissflogii*remin N	0.5 (0.0)	0.5 (0.0)	0.5 (0.0)	0.6 (0.0)	0.5 (0.0)	0.8 (0.1)
*T. weissflogii*remin Si	15.0 (0.2)	15.1 (0.0)	15.2 (0.0)	0.6 (0.0)	0.6 (0.0)	0.9 (0.1)
*T. weissflogii*remin N+Si	0.4 (0.0)	0.4 (0.0)	0.7 (0.1)	0.6 (0.1)	0.6 (0.0)	0.8 (0.1)
*T. weissflogii*remin Control	0.5 (0.0)	0.4 (0.0)	1.9 (0.0)	1.0 (0.0)	1.0 (0.0)	0.1/BDL
*O. aurita*remin N	BDL	BDL	0.2 (0.0)	0.3 (0.1)	0.3 (0.1)	0.7 (0.0)
*O. aurita*remin Si	8.9 (0.0)	8.9 (0.1)	8.9 (0.1)	0.4 (0.1)	0.3 (0.0)	0.7 (0.1)
*O. aurita*remin N+Si	0.2 (0.0)	BDL	BDL	0.3 (0.0)	0.3 (0.0)	0.7 (0.1)
*O. aurita*remin Control	BDL	BDL	0.7 (0.4)	2.2 (0.1)	2.6 (0.3)	1.8 (0.5)
Inorganic nutrient amendments to aged seawater used for *O. aurita*remin Control						
Aged SW +N&P	7.5 (0.0)	7.5 (0.1)	7.8 (0.3)	2.3 (0.1)	2.2 (0.0)	2.3 (0.3)
Aged SW +Si&P	BDL	BDL	1.3/BDL	2.3 (0.0)	2.3 (0.1)	1.9 (0.6)
Aged SW +Culture	1.7 (0.0)	1.7 (0.0)	3.7 (0.0)	2.3 (0.0)	2.2 (0.0)	0.5 (0.1)
Aged SW +F/2	2.6 (0.1)	2.6 (0.1)	4.4 (0.3)	2.4 (0.0)	2.6 (0.3)	0.6 (0.0)

Mean of duplicate samples (range). Detection limits: NO₃+NO₂: 0.2 µM; NH4: 0.1 µM. BDL = below detection limits; value/BDL = only one of two replicate samples was BDL.

	DON (µM)			DOC:DON		
	T_0	1 week	8 weeks	T_0	1 week	8 weeks
*S. marinoi*remin Si	5.5 (0.6)	6.0 (0.2)	5.2 (0.1)	20.4 (2.5)	13.5 (0.1)	14.1 (0.1)
*S. marinoi*remin N+Si	6.6 (0.0)	6.1 (0.1)	6.0 (0.5)	11.9 (0.1)	11.9 (0.6)	11.6 (1.2)
*S. marinoi*remin Control	5.5 (0.2)	5.2 (0.6)	4.6 (0.2)	12.2 (0.5)	11.6	14.0 (1.0)
*C. socialis*remin N	6.3 (0.2)	5.9 (0.0)	6.0 (0.5)	13.2 (0.3)	13.2 (0.1)	11.6
*C. socialis*remin Si	6.0 (0.3)	6.1 (0.1)	5.6 (0.7)	16.1 (0.7)	13.9 (0.0)	14.1 (2.3)
*C. socialis*remin N+Si	6.0 (0.2)	6.5 (0.1)	6.4 (0.2)	14.2 (0.8)	12.3 (0.3)	11.7 (0.2)
*C. socialis*remin Control	4.4 (0.3)	4.8 (0.2)*	5.1 (0.5)*	15.8 (1.1)	14.4 (0.4)	12.7 (1.1)
*T. weissflogii*remin N	6.9 (0.7)	6.9 (0.6)	6.2	13.1 (0.8)	12.4 (0.8)	11.6
*T. weissflogii*remin Si	5.6 (0.4)	5.4 (0.7)	5.9 (0.5)	15.0 (1.0)	14.8 (1.9)	12.4 (1.0)
*T. weissflogii*remin N+Si	7.1 (0.1)	6.7 (0.5)	8.0 (0.7)	11.7 (0.1)	11.9 (1.0)	9.3 (0.9)
*T. weissflogii*remin Control	5.4 (0.4)	5.2 (0.0)	6.4 (0.2)	13.3 (0.8)	13.2 (0.1)	10.6 (0.2)
*O. aurita*remin N	6.2 (0.2)	6.8 (0.3)	6.2 (0.2)	14.0 (0.4)	12.5 (0.6)	12.4 (0.5)
*O. aurita*remin Si	6.5 (0.3)	6.6 (0.1)	6.2 (0.1)	13.2 (0.8)	12.7 (0.2)	12.5 (0.4)
*O. aurita*remin N+Si	6.1 (0.4)	6.2 (0.2)	5.7 (0.3)	15.3 (0.8)	14.3 (0.5)	14.0 (0.6)
*O. aurita*remin Control	4.9 (0.0)	4.4 (0.6)	5.0 (0.3)	14.4 (0.2)	15.9 (1.7)	13.5 (0.4)
Inorganic nutrient amendments to aged seawater used for *O. aurita*remin Control						
Aged SW +N&P	5.6 (0.1)	6.1 (0.1)	5.1 (0.2)	12.1 (0.0)	11.2 (0.1)	12.5 (0.4)
Aged SW +Si&P	4.7 (0.5)	4.4 (0.4)	4.2 (0.2)	14.9 (1.3)	15.9 (0.9)	15.9 (0.8)
Aged SW +Culture	5.6 (0.4)	5.9 (0.3)	5.3 (0.2)	13.1 (0.9)	12.1 (0.4)	13.3 (0.3)
Aged SW +F/2	5.6 (0.2)	5.7 (0.1)	5.5 (0.4)	12.8 (0.5)	12.4 (0.1)	12.8 (0.8)

Mean of duplicate samples (range); no range value indicates only one valid replicate. *Because DIN was below detection limits in both NO₃+NO₂ and NH₄ for these samples, we used an assumed DIN value of 0.1 µM.

REFERENCES CITED

Alderkamp A-C, E Sintes, and GJ Herndl. 2006. Abundance and activity of major groups of prokaryotic plankton in the coastal North Sea during spring and summer. Aquatic Microbial Ecology 45: 237-246. doi:10.3354/ame045237

Aluwihare, LI, and DJ Repeta. 1999. A comparison of the chemical characteristics of oceanic DOM and extracellular DOM produced by marine algae. Marine Ecology Progress Series 186: 105-117. doi:10.3354/meps186105

Amin, SA, MS Parker, and EV Armbrust. 2012. Interactions between diatoms and bacteria. Microbiology and Molecular Biology Reviews 76: 667-684. doi:10.1128/MMBR.00007-12

Amon, RMW, and R Benner. 1994. Rapid cycling of high-molecular-weight dissolved organic matter in the ocean. Nature 369: 549-552. doi:10.1038/369549a0

Amon, RMW, and R Benner. 1996. Bacterial utilization of different size classes of dissolved organic matter. Limnology and Oceanography 41: 41-51. doi:10.4319/lo.1996.41.1.0041

Anderson, CR, MA Brzezinski, L Washburn, and R Kudela. 2006. Circulation and environmental conditions during a toxigenic *Pseudo-nitzschia australis* bloom in the Santa Barbara Channel, California. Marine Ecology Progress Series 327: 119-133. doi:10.3354/meps327119

Antoine, D, DA Siegel, T Kostadinov, S Maritorena, NB Nelson, B Gentili, V Vellucci, and N Guillocheau. 2011. Variability in optical particle backscattering in contrasting bio-optical oceanic regimes. Limnology and Oceanography 56: 955-973. doi:10.4319/lo.2011.56.3.0955

Apple, JK, and PA del Giorgio. 2007. Organic substrate quality as the link between bacterioplankton carbon demand and growth efficiency in a temperate salt-marsh estuary. The ISME Journal 1: 729-742. doi:10.1038/ismej.2007.86

Apprill A, S McNally, R Parsons, and L Weber. 2015. Minor revision to V4 region SSU rRNA 806R gene primer greatly increases detection of SAR11 bacterioplankton. Aquatic Microbial Ecology 75: 129-137. doi:10.3354/ame01753

Arrieta, JM, E Mayol, RL Hansman, GJ Herndl, T Dittmar, and CM Duarte. 2015. Dilution limits dissolved organic carbon utilization in the deep ocean. Science 348:331-333. doi:10.1126/science.1258955

Arrieta, JM, MG Weinbauer, and GJ Herndl. 2000. Interspecific variability in sensitivity to UV radiation and subsequent recovery in selected isolates of marine bacteria. Applied and Environmental Microbiology 66: 1468-1473. doi:10.1128/AEM.66.4.1468-1473.2000

Azam, F, T Fenchel, JG Field, JS Gray, LA Meyer-Reil, and F Thingstad. 1983. The ecological role of water-column microbes in the sea. Marine Ecology Progress Series 10: 257-263. doi:10.3354/meps010257

Baines, SB, and ML Pace. 1991. The production of dissolved organic matter by phytoplankton and its importance to bacteria: patterns across marine and freshwater systems. Limnology and Oceanography 36: 1078-1090. doi:10.4319/lo.1991.36.6.1078

Barbosa, AB, HM Galvão, PA Mendes, XA Álvarez-Salgado, FG Figueiras, and I Joint. 2001. Short-term variability of heterotrophic bacterioplankton during upwelling off

the NW Iberian margin. Progress in Oceanography 51: 339-359.
doi:10.1016/S0079-6611(01)00074-X

Barrón RK. 2014. Constraining the variability of optical properties in the Santa Barbara Channel, CA: A phytoplankton story. PhD dissertation, University of California, Santa Barbara. ProQuest (number 3682870).

Barrón RK, DA Siegel, and N Guillocheau. 2014. Evaluating the importance of phytoplankton community structure to the optical properties of the Santa Barbara Channel, California. Limnology and Oceanography 59: 927-946. doi: 10.4319/lo.2014.59.3.0927

Bauer, JE. 2002. Carbon isotopic composition of DOM. In Biogeochemistry of Dissolved Organic Matter. DA Hansell and CA Carlson, eds. Academic Press, New York: 774 pp.

Beardsley, C, J Pernthaler, W Wosniok, and R Amann. 2003. Are readily culturable bacteria in coastal North Sea waters suppressed by selective grazing mortality? Applied and Environmental Microbiology 69: 2624-2630. doi: 10.1128/AEM.69.5.2624-2630.2003

Béjà, O, L Aravind, EV Koonin, MT Suzuki, A Hadd, NP Nguyen, SB Jovanovich, CM Gates, RA Feldman, JL Spudich, EN Spudich, and EF DeLong. 2000. Bacterial rhodopsin: evidence for a new type of phototrophy in the sea. Science 289: 1902-1906. doi:10.1126/science.289.5486.1902

Benner, RH. 2002. Composition and reactivity. In Biogeochemistry of Dissolved Organic Matter. DA Hansell and CA Carlson, eds. Academic Press, New York: 774 pp.

Benner, R, B Biddanda, B Black, and M McCarthy. 1997. Abundance, size distribution, and stable carbon and nitrogen isotopic compositions of marine organic matter isolated by tangential-flow ultrafiltration. Marine Chemistry 57: 243-263. doi:10.1016/S0304-4203(97)00013-3

Bidle, KD, and F Azam. 2001. Bacterial control of silicon regeneration from diatom detritus: Significance of bacterial ectohydrolases and species identity. Limnology and Oceanography 46: 1606-1623. doi:10.4319/lo.2001.46.7.1606

Bjørnsen, PK. 1988. Phytoplankton exudation of organic matter: why do healthy cells do it? Limnology and Oceanography 33: 151-154. doi:10.4319/lo.1988.33.1.0151

Blough, NV, and R Del Vecchio. 2002. Chromophoric DOM in the coastal environment. In Biogeochemistry of Dissolved Organic Matter. DA Hansell and CA Carlson, eds. Academic Press, New York: 774 pp.

Borch, NH, and DL Kirchman. 1997. Concentration and composition of dissolved combined neutral sugars (polysaccharides) in seawater determined by HPLC-PAD. Marine Chemistry 57: 85-95. doi:10.1016/S0304-4203(97)00002-9

Børsheim, KY, O Vadstein, SM Myklestad, H Reinertsen, S Kirkvold, and Y Olsen. 2005. Photosynthetic algal production, accumulation and release of phytoplankton storage carbohydrates and bacterial production in a gradient in daily nutrient supply. Journal of Plankton Research 27: 743-755. doi:10.1093/plankt/fbi047

Bouvier, TC, and PA del Giorgio. 2002. Compositional changes in free-living bacterial communities along a salinity gradient in two temperate estuaries. Limnology and Oceanography 47: 453-470. doi:10.4319/lo.2002.47.2.0453

Bratbak, G, and TF Thingstad. 1985. Phytoplankton-bacteria interactions: an apparent paradox? Analysis of a model system with both competition and commensalism.

Marine Ecology Progress Series 25: 23-30.

Breitbart, M. 2012. Marine viruses: truth or dare. Annual Reviews of Marine Science 4: 425-448. doi:10.1146/annurev-marine-120709-142805

Brown, MV, FM Lauro, MZ DeMaere, L Muir, D Wilkins, T Thomas, MJ Riddle, JA Fuhrman, C Andrews-Pfannkoch, JM Hoffman, JB McQuaid, A Allen, SR Rintoul, and R Cavicchioli. 2012. Global biogeography of SAR11 marine bacteria. Molecular Systems Biology 8: 595. doi:10.1038/msb.2012.28

Brown, MV, GK Philip, JA Bunge, MC Smith, A Bissett, FM Lauro, JA Fuhrman, and SP Donachie. 2009. Microbial community structure in the North Pacific ocean. The ISME Journal 3: 1374-1386. doi:10.1038/ismej.2009.86

Bryant, JA, FO Aylward, JM Eppley, DM Karl, MJ Church, and EF DeLong. 2016. Wind and sunlight shape microbial diversity in surface waters of the North Pacific Subtropical Gyre. The ISME Journal 10: 1308-1322. doi:10.1038/ismej.2015.221

Bryson, S, Z Li, J Pett-Ridge, RL Hettich X Mayali, C Pan, and RS Mueller. 2016. Proteomic stable isotope probing reveals taxonomically distinct patterns in amino acid assimilation by coastal marine bacterioplankton. mSystems 1: e00027-15. doi:10.1128/mSystems.00027-15

Brzezinski, MA, and DM Nelson. 1995. The annual silica cycle in the Sargasso Sea near Bermuda. Deep-Sea Research I 42: 1215-1237. doi:10.1016/0967-0637(95)93592-3

Brzezinski, MA, and L Washburn. 2011. Phytoplankton primary productivity in the Santa Barbara Channel: Effects of wind-driven upwelling and mesoscale eddies. Journal of Geophysical Research 116: C12013. doi:10.1029/2011JC007397

Buchan A, JM González JM, and MA Moran. 2005. Overview of the marine *Roseobacter* lineage. Applied and Environmental Microbiology 71: 5665-5677. doi:10.1128/AEM.71.10.5665-5677.2005

Buchan, A, GR LeCleir, CA Gulvik, and JM González. 2014. Master recyclers: features and functions of bacteria associated with phytoplankton blooms. Nature Reviews Microbiology 12: 686-698. doi:10.1038/nrmicro3326

Bunse C, and J Pinhassi. 2017 (in press). Marine bacterioplankton seasonal succession dynamics. Trends in Microbiology. doi:10.1016/j.tim.2016.12.013

Campbell, BJ, L Yu, JF Heidelberg, and DL Kirchman. 2011. Activity of abundant and rare bacteria in a coastal ocean. PNAS 108: 12776-12781. doi:10.1073/pnas.1101405108

Canfield, DE, FJ Stewart, B Thamdrup, L De Brabandere, T Dalsgaard, EF DeLong, NP Revsbech, and O Ulloa. 2010. A cryptic sulfur cycle in oxygen-minimum-zone waters off the Chilean coast. Science 330: 1375-1378. doi:10.1126/science.1196889

Caporaso, JG, CL Lauber, WA Walters, D Berg-Lyons, CA Lozupone, PJ Turnbaugh, N Fierer, and R Knight. 2011. Global patterns of 16S rRNA diversity at a depth of millions of sequences per sample. Proceedings of the National Academy of Sciences USA 108: 4516-4522. doi:10.1073/pnas.1000080107

Carlson, CA. 2002. Production and removal processes. In Biogeochemistry of Dissolved Organic Matter. DA Hansell and CA Carlson, eds. Academic Press, New York: 774 pp.

Carlson, CA, PA del Giorgio, and GJ Herndl. 2007. Microbes and the dissipation of energy and respiration: from cells to ecosystems. Oceanography 20: 89-100.

Carlson, CA, HW Ducklow, and AF Michaels. 1994. Annual flux of dissolved organic carbon from the euphotic zone in the northwestern Sargasso Sea. Nature 371: 405-

408. doi:10.1038/371405a0

Carlson, CA, and HW Ducklow. 1996. Growth of bacterioplankton and consumption of dissolved organic carbon in the Sargasso Sea. Aquatic Microbial Ecology 10: 69-85. doi:10.3354/ame010069

Carlson, CA, SJ Giovannoni, DA Hansell, SJ Goldberg, R Parsons, and K Vergin. 2004. Interactions among dissolved organic matter, microbial processes, and community structure in the mesopelagic zone of the northwestern Sargasso Sea. Limnology and Oceanography 49: 1073-1083. doi:10.4319/lo.2004.49.4.1073

Carlson, CA, and DA Hansell. 2003. The contribution of dissolved organic carbon and nitrogen to the biogeochemistry of the Ross Sea. In Biogeochemistry of the Ross Sea. GR Ditullio and RB Dunbar, eds. American Geophysical Union, Washington, D.C., doi:10.1029/078ARS08

Carlson, CA, and DA Hansell. 2015. DOM sources, sinks, reactivity, and budgets. In Biogeochemistry of Dissolved Organic Matter, 2nd e. DA Hansell and CA Carlson, eds. Academic Press, New York: 693 pp.

Carlson, CA, R Morris, R Parsons, AH Treusch, SJ Giovannoni, and K Vergin. 2009. Seasonal dynamics of SAR11 populations in the euphotic and mesopelagic zones of the northwestern Sargasso Sea. The ISME Journal 3: 283-295. doi:10.1038/ismej.2008.117

Cauwet, G. 2002. DOM in the coastal zone. In Biogeochemistry of Dissolved Organic Matter. DA Hansell and CA Carlson, eds. Academic Press, New York: 774 pp.

Chandler, JW, Y Lin, PJ Gainer, AF Post, ZI Johnson, and ER Zinser. 2016. Variable but persistent coexistence of *Prochlorococcus* ecotypes along temperature gradients in the ocean's surface mixed layer. Environmental Microbiology Reports 8: 272-284. doi:10.1111/1758-2229.12378

Chao A. Nonparametric estimation of the number of classes in a population. Scandinavian Journal of Statistics 11: 265-270.

Cherrier, J, JE Bauer, and ERM Druffel. 1996. Utilization and turnover of labile dissolved organic matter by bacterial heterotrophs in eastern North Pacific surface waters. Marine Ecology Progress Series 139: 267-279. doi:10.3354/meps139267

Cho, BC, and F Azam. 1988. Major roles of bacteria in biogeochemical fluxes in the ocean's interior. Nature 332: 441-443. doi:10.1038/332441a0

Chow, C-ET, R Sachdeva, JA Cram, JA Steele, DM Needham, A Patel, AE Parada, and JA Fuhrman. 2013. Temporal variability and coherence of euphotic zone bacterial communities over a decade in the Southern California Bight. The ISME Journal 7: 2259-2273. doi:10.1038/ismej.2013.122

Clark, LL, ED Ingall, and R Benner. 1998. Marine phosphorus is selectively remineralized. Nature 393: 426. doi:10.1038/30881

Clarke, KR, and RN Gorley. 2006. PRIMER v6: User manual/tutorial. PRIMER-E.

Coble, PG. 1996. Characterization of marine and terrestrial DOM in seawater using excitation-emission matrix spectroscopy. Marine Chemistry 51: 325-346. doi:10.1016/0304-4203(95)00062-3

Cole, JJ, S Findlay, and ML Pace. 1988. Bacterial production in fresh and saltwater ecosystems: a cross-system overview. Marine Ecology Progress Series 43: 1-10.

Conan, P, M Søndergaard, T Kragh, F Thingstad, M Pujo-Pay, PJ leB Williams, S Markager, G Cauwet, N Henrik Borch, D Evans, and B Riemann. 2007. Partitioning

of organic production in marine plankton communities: The effects of inorganic nutrient ratios and community composition on new dissolved organic matter. Limnology and Oceanography 52: 753-765. doi:10.4319/lo.2007.52.2.0753

Cottrell, MT, and DL Kirchman. 2000. Natural assemblages of marine Proteobacteria and members of the *Cytophaga-Flavobacter* cluster consuming low- and high-molecular weight dissolved organic matter. Applied and Environmental Microbiology 66: 1692-1697. doi:10.1128/AEM.66.4.1692-1697.2000

Cram JA, C-ET Chow, R Sachdeva, DM Needham, AE Parada, JA Steele, and JA Fuhrman. 2015. Seasonal and interannual variability of the marine bacterioplankton community throughout the water column over ten years. The ISME Journal 9: 53-580. doi:10.1038/ismej.2014.153

Crump, BC, CS Hopkinson, ML Sogin, and JE Hobbie. 2004. Microbial biogeography along an estuarine salinity gradient: combined influences of bacterial growth and residence time. Applied and Environmental Microbiology 70: 1494-1505. doi:10.1128/AEM.70.3.1494-1505.2004

De La Rocha, CL, and U Passow. 2004. Recovery of *Thalassiosira weissflogii* from nitrogen and silicon starvation. Limnology and Oceanography 49: 245-255. doi:10.4319/lo.2004.49.1.0245

del Giorgio, PA, and JJ Cole. 1998. Bacterial growth efficiency in natural aquatic systems. Annual Review of Ecology and Systematics 29: 503-541. doi:10.1146/annurev.ecolsys.29.1.503

del Giorgio, PA, and JJ Cole. 2000. Bacterial energetics and growth efficiency. In Microbial Ecology of the Oceans, First Edition. DL Kirchman, ed. Wiley-Liss, New York: 542 pp.

del Giorgio, PA, and J Davis. 2003. Patterns in dissolved organic matter lability and consumption across aquatic ecosystems. In Aquatic Ecosystems: Interactivity of Dissolved Organic Matter. SEG Findlay and RL Sinsabaugh, eds. Academic Press, San Diego, CA: 512 pp.

del Giorgio, PA, and ML Pace. 2008. Relative importance of dissolved organic carbon transport and processing in a large temperate river: The Hudson River as both pipe and reactor. Limnology and Oceanography 53: 185-197. doi:10.4319/lo.2008.53.1.0185

DeLong, EF, CM Preston, T Mincer, V Rich, SJ Hallam, N-U Frigaard, A Martinez, MB Sullivan, R Edwards, BR Brito, SW Chisholm, and DM Karl. 2006. Community genomics among stratified microbial assemblages in the ocean's interior. Science 311: 496-503. doi:10.1126/science.1120250

DeLong, EF. 2009. The microbial ocean from genomes to biomes. Nature 459: 200-206. doi: 10.1038/nature08059

Dittmar, T. 2015. Reasons behind the long-term stability of dissolved organic matter. In Biogeochemistry of Dissolved Organic Matter, 2nd e. DA Hansell and CA Carlson, eds. Academic Press, New York: 693 pp.

Ducklow, HW. 2000. Bacterial production and biomass in the oceans. In Microbial Ecology of the Oceans, First Edition. DL Kirchman, ed. Wiley-Liss, New York: 542 pp.

Ducklow, HW, DA Purdie, PJ LeB Williams, and JM Davies. 1986. Bacterioplankton: a sink for carbon in a coastal marine plankton community. Science 232: 865-867. doi:10.1126/science.232.4752.865

Dyhrman, ST, CR Benitez-Nelson, ED Orchard, ST Haley, and PJ Pellechia. 2009. A microbial source of phosphonates in oligotrophic marine systems. Nature Geosciences 2: 696-699. doi:10.1038/ngeo639

Eiler A, DH Hayakawa, and MS Rappé. 2011. Non-random assembly of bacterioplankton communities in the subtropical North Pacific Ocean. Frontiers in Microbiology 2: 140. doi:10.3389/fmicb.2011.00140

Faith DP. 1992. Conservation evaluation and phylogenetic diversity. Biological Conservation 61: 1-10. doi:10.1016/0006-3207(92)91201-3

Fiore, CL, K Longnecker, MC Kido Soule, and EB Kujawinski. 2015. Release of ecologically relevant metabolites by the cyanobacterium *Synechococcus elongates* CCMP 1631. Environmental Microbiology 17: 3949-3963. doi:10.1111/1462-2920.12899

Flerus, R, OJ Lechtenfeld, BP Koch, SL McCallister, P Schmitt-Kopplin, R Benner, K Kaiser, and G Kattner. 2012. A molecular perspective on the ageing of marine dissolved organic matter. Biogeosciences 9: 1935-1955. doi:10.5194/bg-9-1935-2012

Fogg, GE. 1983. The ecological significance of extracellular products of phytoplankton photosynthesis. Botanica Marina 26: 3-14. doi:10.1515/botm.1983.26.1.3

Fry, B, CS Hopkinson, Jr., A Nolin, B Norrman, and UL Zweifel. 1996. Long-term decomposition of DOC from experimental diatom blooms. Limnology and Oceanography 41: 1344-1347. doi:10.4319/lo.1996.41.6.1344

Fuhrman, J. 2000. Impact of viruses on bacterial processes. In Microbial Ecology of the Oceans, First Edition. DL Kirchman, ed. Wiley-Liss, New York: 542 pp.

Fuhrman, JA. 2008. Marine viruses and their biogeochemical and ecological effects. Nature 399: 541-548. doi:10.1038/21119

Fuhrman, JA. 2009. Microbial community structure and its functional implications. Nature 459: 193-199. doi:10.1038/nature08058

Fuhrman, JA, and F Azam. 1982. Thymidine incorporation as a measure of heterotrophic bacterioplankton production in marine surface waters: evaluation and field results. Marine Biology 66: 109-120. doi:10.1007/BF00397184

Fuhrman, JA, JA Cram, and DM Needham. 2015. Marine microbial community dynamics and their ecological interpretation. Nature Reviews Microbiology 13: 133-146. doi:10.1038/nrmicro3417

Fuhrman, JA, and Ä Hagström. 2008. Bacterial and archaeal community structure and its patterns. In Microbial Ecology of the Oceans, Second Edition. DL Kirchman, ed. Wiley-Blackwell, New York. 593 pp.

Fuhrman, JA, I Hewson, MS Schwalbach, JA Steele, MV Brown, and S Naeem. 2006. Annually reoccurring bacterial communities are predictable from ocean conditions. PNAS 103: 13104-13109.

Fuhrman, JA, and JA Steele. 2008. Community structure of marine bacterioplankton: patterns, networks, and relationships to function. Aquatic Microbial Ecology 53: 69-81. doi:10.3354/ame01222

Fukuda, R, H Ogawa, T Nagata, and I Koike. 1998. Direct determination of carbon and nitrogen contents of natural bacterial assemblages in marine environments. Applied and Environmental Microbiology 64: 3352-3358.

Gentemann CL, MR Fewings, and M García-Reyes. 2017. Satellite seas surface temperatures along the West Coast of the United States during the 2014-2016 northeast Pacific marine heat wave. Geophysical Research Letters 44: 312-319. doi:10.1002/2016GL071039

Gifford, SM, S Sharma, M Booth, and MA Moran. 2013. Expression patterns reveal niche diversification in a marine microbial assemblage. The ISME Journal 7: 281-298. doi:10.1038/ismej.2012.96

Gilbert, JA, JA Steele, JG Caporaso, L Steinbrück, J Reeder, B Temperton, S Huse, AC McHardy, R Knight, I Joint, P Somerfield, JA Fuhrman, and D Field. 2012. Defining seasonal marine microbial community dynamics. The ISME Journal 6: 298-308. doi:10.1038/ismej.2011.107

Gilpin, LC, K Davidson, and E Roberts. 2004. The influences of changes in nitrogen: silicon ratios on diatom growth dynamics. Journal of Sea Research 51: 21-35. doi:10.1016/j.seares.2003.05.005

Giovannoni SJ. 2017. SAR11 bacteria: the most abundant plankton in the oceans. Annual Reviews in Marine Science 9: 231-255. doi:10.1124/annurev-marine-010814-015934

Giovannoni, S, and M Rappé. 2000. Evolution, diversity, and molecular ecology of marine prokaryotes. In Microbial Ecology of the Oceans, First Edition. DL Kirchman, ed. Wiley-Liss, New York: 542 pp.

Giovannoni, S, and U Stingl. 2007. The importance of culturing bacterioplankton in the 'omics' age. Nature Reviews Microbiology 5: 820-826. doi:10.1038/nrmicro1752

Goldberg, SJ, CA Carlson, DA Hansell, NB Nelson, and DA Siegel. 2009. Temporal dynamics of dissolved combined neutral sugars and the quality of dissolved organic matter in the Northwestern Sargasso Sea. Deep-Sea Research I 56: 672-685. doi:10.1016/j.dsr.2008.12.013

Goldberg, SJ, CA Carlson, B Bock, NB Nelson, and DA Siegel. 2010. Meridional variability in dissolved organic matter stocks and diagenetic state within the euphotic and mesopelagic zone of the North Atlantic subtropical gyre. Marine Chemistry 119: 9-21. doi:10.1016/j.marchem.2009.12.002

Goldberg, SJ, CA Carlson, M Brzezinski, NB Nelson, and DA Siegel. 2011. Systematic removal of neutral sugars within dissolved organic matter across ocean basins. Geophysical Research Letters 38: L17606. doi:10.1029/2011GL048620

Goldman, JC, DA Hansell, and MR Dennett. 1992. Chemical characterization of three large oceanic diatoms: potential impact on water column chemistry. Marine Ecology Progress Series 88: 257-270.

Gómez-Consarnau, L, MV Lindh, JM Gasol, and J Pinhassi. 2012. Structuring of bacterioplankton communities by specific dissolved organic carbon compounds. Environmental Microbiology 14: 2361-2378. doi:10.1111/j.1462-2920.2012.02804.x

Granéli, E, and JT Turner. 2006. An introduction to harmful algae. In Ecology of Harmful Algae. E Granéli and JT Turner, eds. Springer, New York: 413 pp.

Granum, E, S Kirkvold, and SM Myklestad. 2002. Cellular and extracellular production of carbohydrates and amino acids by the marine diatom *Skeletonema costatum*: diel variations and effects of N depletion. Marine Ecology Progress Series 242: 83-94. doi:10.3354/meps242083

Guidi, L, S Chaffron, L Bittner, D Eveillard, A Larhlimi, S Roux, Y Darzi, S Audic, L Berline, JR Brum, LP Coelho, JCI Espinoza, S Malviya, S Sunagawa, C Dimier, S

Kandels-Lewis, M Picheral, J Poulain, S Searson, *Tara* Oceans Coordinators, L Stemmann, F Not, P Hingamp, S Speich, M Follows, L Karp-Boss, E Boss, H Ogata, S Pesant, J Weissenbach, P Wincker, SG Acinas, P Bork, C de Vargas, D Iudicone, MB Sullivan, J Raes, E Karsenti, C Bowler, and G Gorsky. 2016. Plankton networks driving carbon export in the oligotrophic ocean. Nature 532: 465-470. doi:10.1038/nature16942

Guillard, RRL. 2005. Purification methods for microalgae. In Algae Culturing Techniques. RA Anderson, ed. Elsevier, San Diego, CA, pp. 117-132.

Guillemette, F, and PA del Giorgio. 2011. Reconstructing the various facets of dissolved organic carbon bioavailability in freshwater ecosystems. Limnology and Oceanography 56: 743-748. doi:10.4319/lo.2011.56.2.0734

Guillemette, F, SL McCallister, and PA del Giorgio. 2016. Selective consumption and metabolic allocation of terrestrial and algal carbon determine allochthony in lake bacteria. The ISME Journal 10: 1373-1382. doi:10.1038/ismej.2015.215

Guo, L, N Tanaka, DM Schell, and PH Santschi. 2003. Nitrogen and carbon isotopic composition of high-molecular-weight dissolved organic matter in marine environments. Marine Ecology Progress Series 252: 51-60. doi:10.3354/meps252051

Halewood, ER, CA Carlson, MA Brzezinski, DC Reed, and J Goodman. 2012. Annual cycle of organic matter partitioning and its availability to bacteria across the Santa Barbara Channel continental shelf. Aquatic Microbial Ecology 67: 189-209. doi:10.3354/ame01586

Hansell, DA. 2002. DOC in the global ocean carbon cycle. In Biogeochemistry of Dissolved Organic Matter. DA Hansell and CA Carlson, eds. Academic Press, New York: 774 pp.

Hansell, DA. 2013. Recalcitrant dissolved organic carbon fractions. Annual Reviews of Marine Science 5: 421-45. doi:10.1146/annurev-marine-120710-100757

Hansell, DA, CA Carlson, DJ Repeta, and R Schlitzer. 2009. Dissolved organic matter in the ocean: a controversy stimulates new insights. Oceanography 22: 202-211. doi:10.5670/oceanog.2009.109

Harms, S, and CD Winant. 1998. Characteristic patterns of the circulation in the Santa Barbara Channel. Journal of Geophysical Research 103: 3041-3065. doi:10.1029/97JC02393

Harrison, PJ, HL Conway, RW Holmes, and CO Davis. 1977. Marine diatoms grown in chemostats under silicate or ammonium limitation. III. Cellular composition and morphology of *Chaetoceros debilis*, *Skeletonema costatum*, and *Thalassiosira gravida*. Marine Biology 43: 19-31. doi:10.1007/BF00392568

Harrison, PJ, PA Thompson, and GS Calderwood. 1990. Effects of nutrient and light limitation on the biochemical composition of phytoplankton. Journal of Applied Phycology 2: 45-56. doi:10.1007/BF02179768

Hedges, JI. 2002. Why dissolved organics matter. In Biogeochemistry of Dissolved Organic Matter. DA Hansell and CA Carlson, eds. Academic Press, New York: 774 pp.

Hedges, JI, JA Baldock, Y Gélinas, C Lee, ML Peterson, and SG Wakeham. 2002. The biochemical and elemental compositions of marine plankton: a NMR perspective. Marine Chemistry 78: 47-63. doi:10.1016/S0304-4203(02)00009-9

Hewson, I, JA Steele, DG Capone, and JA Fuhrman. 2006. Temporal and spatial scales of variation in bacterioplankton assemblages of oligotrophic surface waters. Marine Ecology Progress Series 311: 67-77. doi:10.3354/meps311067

Hughes, JB, JJ Hellmann, TH Ricketts, and BJM Bohannan. Counting the uncountable: statistical approaches to estimating microbial diversity. Applied and Environmental Microbiology 67: 4399-4406. doi:10.1128/AEM.67.10.4399-4406.2001

Jansson, JK, JD Neufeld, MA Moran, and JA Gilbert. 2012. Omics for understanding microbial functional dynamics. Environmental Microbiology 14: 1-3. doi:10.1111/j.1462-2920.2011.02518.x

Jiao, N, GJ Herndl, DA Hansell, R Benner, G Kattner, SW Wilhelm, DL Kirchman, MG Weinbauer, T Luo, F Chen, and F Azam. 2010. Microbial production of recalcitrant dissolved organic matter: long-term carbon storage in the global ocean. Nature Reviews Microbiology 8: 593-599. doi:10.1038/nrmicro2386

Jiao, N, C Robinson, F Azam, H Thomas, F Baltar, H Dang, NJ Hardman-Mountford, M Johnson, DL Kirchman, BP Koch, L Legendre, C Li, J Liu, T Luo, Y-W Luo, A Mitra, A Romanou, K Tang, X Wang, C Zhang, and R Zhang. 2014. Mechanisms of microbial carbon sequestration in the ocean – future research directions. Biogeosciences 11: 5285-5306. doi:10.5194/bg-11-5285-2014

Johnson, ZI, ER Zinser, A Coe, NP McNulty, EMS Woodward, and SW Chisholm. 2006. Niche partitioning among *Prochlorococcus* ecotypes along ocean-scale environmental gradients. Science 311: 1737-1740. doi:10.1126/science.1118052

Jones, SE, and JT Lennon. 2010. Dormancy contributes to the maintenance of microbial diversity. Proceedings of the National Academy of Sciences USA 107: 5881-5886. doi:10.1073/pnas.0912765107

Jørgensen, L, CA Stedmon, T Kragh, S Markager, M Middelboe, and M Søndergaard. 2011. Global trends in the fluorescence characteristics and distribution of marine dissolved organic matter. Marine Chemistry 126: 139-148. doi:10.1016/j.marchem.2011.05.002

Jürgens, K, and R Massana. 2008. Protistan grazing on marine bacterioplankton. In Microbial Ecology of the Oceans, Second Edition. DL Kirchman, ed. Wiley-Blackwell, New York. 593 pp.

Kaiser, K, and R Benner. 2008. Major bacterial contribution to the ocean reservoir of detrital organic carbon and nitrogen. Limnology and Oceanography 53: 99-112. doi:10.4319/lo.2008.53.1.0099

Karner, MB, EF DeLong, and DM Karl. 2001. Archaeal dominance in the mesopelagic zone of the Pacific Ocean. Nature 409: 507-510. doi:10.1038/35054051

Kashtan, N, SE Roggensack, S Rodrigue, JW Thompson, SJ Biller, A Coe, H Ding, P Marttinen, RR Malmstrom, R Stocker, MJ Follows, R Stepanauskas, and SW Chisholm. 2014. Single-cell genomics reveals hundreds of coexisting subpopulations in wild *Prochlorococcus*. Science 344: 416-420. doi:10.1126/science.1248575

Keil, RG, and DL Kirchman. 1993. Dissolved combined amino acids: chemical form and utilization by marine bacteria. Limnology and Oceanography 38: 1256-1270. doi:10.4319/lo.1993.38.6.1256

Kirchman, DL. 1990. Limitation of bacterial growth by dissolved organic matter in the subarctic Pacific. Marine Ecology Progress Series 62: 47-54.

Kirchman, DL. 2016. Growth rates of microbes in the oceans. Annual Reviews of Marine

Science 8: 285-309. doi:10.1146/annurev-marine-122414-033938

Kirchman, DL, AI Dittel, RR Malmstrom, and MT Cottrell. 2005. Biogeography of major bacterial groups in the Delaware Estuary. Limnology and Oceanography 50:1697-1706. doi:10.4319/lo.2005.50.5.1697

Kirchman, DL, E K'nees, and R Hodson. 1985. Leucine incorporation and its potential as a measure of protein synthesis by bacteria in natural aquatic systems. Applied and Environmental Microbiology 49: 599-607.

Kleindienst, S, S Grim, M Sogin, A Bracco, M Crespo-Medina, and SB Joye. Diverse, rare microbial taxa responded to the *Deepwater Horizon* deep-sea hydrocarbon plume. The ISME Journal 10: 400-415. doi:10.1038/ismej.2015.121

Kolowith, LC, ED Ingall, and R Benner. 2001. Composition and cycling of marine phosphorus. Limnology and Oceanography 46: 309-320. doi:10.4319/lo.2001.46.2.0309

Kostadinov, TS, DA Siegel, S Maritorena, and N Guillocheau. 2007. Ocean color observations and modeling for an optically complex site: Santa Barbara Channel, California, USA. Journal of Geophysical Research 112: C07011. doi:10.1029/2006JC003526

Kozich, JJ, SL Westcott, NT Baxter, SK Highlander, and PD Schloss. 2013. Development of a dual-index strategy and curation pipeline for analyzing amplicon sequence data on the MiSeq Illumina sequencing platform. Appl. Environ. Microbiol. 79: 5112-5120.

Krause, JW, MA Brzezinski, and JL Jones. 2011. Application of low-level beta counting of ^{32}Si for the measurement of silica production rates in aquatic environments. Marine Chemistry 127: 40-47. doi:10.1016/j.marchem.2011.07.001

Krause, JW, MA Brzezinski, DA Siegel, and RC Thunell. 2013. Biogenic silica standing stock and export in the Santa Barbara Channel ecosystem. Journal of Geophysical Research. 118: 736-749. doi:10.1029/2012JC008070

Kujawinski, EB, K Longnecker, NV Blough, R Del Vecchio, L Finlay, JB Kitner, and SJ Giovannoni. 2009. Identification of possible source markers in marine dissolved organic matter using ultrahigh resolution mass spectroscopy. Geochimica et Cosmochimica Acta 73: 4384-4399. doi:10.1016/j.gca.2009.04.033

Kujawinski, EB. 2011. The impact of microbial metabolism on marine dissolved organic matter. Annual Review of Marine Science 3: 567-599. doi:10.1146/annurev-marine-120308-081003

Kuczynski, J, Z Liu, C Lozupone, D McDonald, N Fierer, and R Knight. 2010. Microbial community resemblance methods differ in their ability to detect biologically relevant patterns. Nature Methods 7: 813-819. doi:10.1038/nmeth.1499

Lamy, D, I Obernosterer, M Laghdass, LF Artigas, E Breton, JD Grattepanche, E Lecuyer, N Degros, P Lebaron, and U Christaki. 2009. Temporal changes of major bacterial groups and bacterial heterotrophic activity during a *Phaeocystis globosa* bloom in the eastern English Channel. Aquatic Microbial Ecology 58: 95-107. doi:10.3354/ame01359

Lauro, FM, D McDougald, T Thomas, TJ Williams, S Egan, S Rice, MZ DeMaere, L Ting, H Ertan, J Johnson, S Ferriera, A Lapidus, I Anderson, N Kyrpides, AC Munk, C Defter, CS Hans, MV Brown, FT Robb, S Kjelleberg, R Cavicchioli, and RR Colwell. 2009. The genomic basis of throphic strategy in marine bacteria. Proceedings of the National Academy of Sciences USA 106: 15527-15533.

doi:10.1073/pnas.0903507106

Lechtenfeld, OJ, N Hertkorn, Y Shen, M Witt, and R Benner. 2015. Marine sequestration of carbon in bacterial metabolites. Nature Communications 6: 6711. doi:10.1038/ncomms7711

Lima-Mendez, G, K Faust, N Henry, J Decelle, S Colin, F Carcillo, S Chaffron, JC Ignacio-Espinosa, S Roux, F Vincent, L Bittner, Y Darzi, J Wang, S Audic, L Berline, G Bontempi, AM Cabello, L Coppola, FM Cornejo-Castillo, F d'Ovidio, L De Meester, I Ferrera, M-J Garet-Delmas, L Guidi, E Lara, S Pesant, M Royo-Llonch, G Salazar, P Sánchez, M Sebastian, C Souffreau, C Dimier, M Picheral, S Searson, S Kandels-Lewis, *Tara* Oceans Coordinators, G Gorsky, F Not, H Ogata, S Speich, L Stemmann, J Weissenbach, P Wincker, SG Acinas, S Sunagawa, P Bork, MB Sullivan, E Karsenti, C Bowler, C de Vargas, and J Raes. 2015. Determinants of community structure in the global plankton interactome. Science 348:1262073-1-9. doi:10.1126/science.1262073

Lindh, MV, J Sjöstedt, AF Andersson, F Baltar, LW Hugerth, D Lundin, S Muthusamy, C Legrand , and J Pinhassi. 2015. Disentangling seasonal bacterioplankton population dynamics by high-frequency sampling. Environmental Microbiology 17: 2459-2476. doi:10.1111/1462-2920.12720

Logue, JB, CA Stedmon, AM Kellerman, NJ Nielson, AF Andersson, H Laudon, ES Lindström, and ES Kritzberg. 2016. Experimental insights into the importance of aquatic bacterial community composition to the degradation of organic matter. The ISME Journal 10: 533-545. doi:10.1038/ismej.2015.131

Lønborg, C, S Martínez-García, E Teira, and XA Álvarez-Salgado. 2011. Bacterial carbon demand and growth efficiency in a coastal upwelling system. Aquatic Microbial Ecology 63: 183-191. doi:10.3354/ame01495

Lønborg, C, M Nieto-Cid, V Hernando-Morales, M Hernández-Ruiz, E Teira, and XA Álvarez-Salgado. 2016. Photochemical alteration of dissolved organic matter and the subsequent effects on bacterial carbon cycling and diversity. FEMS Microbiology Ecology 92. doi:10.1093/femsec/fiw048

Longnecker, K, MC Kido Soule, and EB Kujawinski. 2015. Dissolved organic matter produced by *Thalassiosira pseudonana*. Marine Chemistry 168: 114-123. doi:10.1016/j.marchem.2014.11.003

Lozupone, C, and R Knight. 2005. UniFrac: a new phylogenetic method for comparing microbial communities. Applied and Environmental Microbiology 71: 8228-8235. doi: 10.1128/AEM.71.12.8228–8235.2005

Luo, H, and MA Moran. 2015. How do divergent ecological strategies emerge among marine bacterioplankton lineages? Trends in Microbiology 23: 577-584. doi:10.1016/j.tim.2015.05.004

Luo, H, BB Tolar, BK Swan, CL Zhang, R Stepanauskas, MA Moran, and JT Hollibaugh. 2014. Single-cell genomics shedding light on marine Thaumarchaeota diversification. The ISME Journal 8: 732-736. doi:10.1038/ismej.2013.202

Lynch, MDJ, and JD Neufeld. 2015. Ecology and exploration of the rare biosphere. 2015. Nature Reviews Microbiology 13: 217-229. doi:10.1038/nrmicro3400

Martin-Jézéquel, V, M Hildebrand, and MA Brzezinski. 2000. Silicon metabolism in diatoms: Implications for growth. Journal of Phycology 36: 821-840. doi:10.1046/j.1529-8817.2000.00019.x

Martinez, J, DC Smith, GF Steward, and F Azam. 1996. Variability in ectohydrolytic enzyme activities of pelagic marine bacteria and its significance for substrate processing in the sea. Aquatic Microbial Ecology 10: 223-230. doi:10.3354/ame010223

Martiny, AC, A Talarmin, C Mouginot, JA Lee, JS Huang, AG Gellene, and DA Caron. 2016. Biogeochemical interactions control a temporal succession in the elemental composition of marine communities. Limnology and Oceanography 61: 531-542. doi:10.1002/lno.10233

Matsen, FA, RB Kodner, and EV Armbrust. 2010. pplacer: linear time maximum-likelihood and Bayesian phylogenetic placement of sequences onto a fixed reference tree. BMC Bioinformatics 11: 538. doi: 10.1186/1471-2105-11-538

McCarren, J, JW Becker, DJ Repeta, Y Shi, CR Young, RR Malmstrom, SW Chisholm, and EF DeLong. 2010. Microbial community transcriptomes reveal microbes and metabolic pathways associated with dissolved organic matter turnover in the sea. Proceedings of the National Academy of Sciences USA 107: 16420-16427. doi:10.1073/pnas.1010732107

McCarthy, M, JI Hedges, and R Benner. 1998. Major bacterial contribution to marine dissolved organic nitrogen. Science 281: 231-234. doi:10.1126/science.281.5374.231

McCoy, CO, and FA Matsen. 2013. Abundance-weighted phylogenetic diversity measures distinguish microbial community states and are robust to sampling depth. PeerJ1:e157. doi:10.7717/peerj.157

Meador, TB, and LI Aluwihare. 2014. Production of dissolved organic carbon enriched in deoxy sugars representing an additional sink for biological C drawdown in the Amazon River plume. Global Biogeochemical Cycles 28: 1149-1161. doi:10.1002/2013GB004778

Meon, B, and DL Kirchman. 2001. Dynamics and molecular composition of dissolved organic material during experimental phytoplankton blooms. Marine Chemistry 75: 185-199. doi:10.1016/S0304-4203(01)00036-6

Methé, BA, and JP Zehr. 1999. Diversity of bacterial communities in Adirondack lakes: do species assemblages reflect lake water chemistry? Hydrobiologia 401: 77-96.

Meyers-Schulte, KJ, and JI Hedges. 1986. Molecular evidence for a terrestrial component of organic matter dissolved in ocean water. Nature 321: 61-63. doi:10.1038/321061a0

Milici, M, J Tomasch, ML Wos-Oxley, J Decelle, R Jáuregui, H Wang, Z-L Deng, I Plumeier , H-A Giebel, TH Badewien, M Wurst, DH Pieper, M Simon, and I Wagner-Döbler. 2016. Bacterioplankton biogeography of the Atlantic Ocean: a case study of the distance-decay relationship. Frontiers in Microbiology 7: 590. doi:10.3389/fmicb.2016.00590

Montero, P, G Daneri, LA Cuevas, HE González, B Jacob, L Lizárraga, and E Menschel. 2007. Productivity cycles in the coastal upwelling area off Concepción: The importance of diatoms and bacterioplankton in the organic carbon flux. Progress in Oceanography 75: 518-530. doi:10.1016/j.pocean.2007.08.013

Moore, JK, SC Doney, DM Glover, and IY Fung. 2002. Iron cycling and nutrient-limitation patterns in surface waters of the World Ocean. Deep-Sea Research II 49: 463-507. doi:10.1016/S0967-0645(01)00109-6

Mopper, K, and DJ Kieber. 2002. Photochemistry and the cycling of carbon, sulfur, nitrogen and phosphorus. In Biogeochemistry of Marine Dissolved Organic Matter. DA

Hansell and CA Carlson, eds. Academic Press, San Diego: 774 p.

Mopper, K. DJ Kieber, and A Stubbins. 2015. Marine photochemistry of organic matter: processes and impacts. In Biogeochemistry of Dissolved Organic Matter, 2nd e. DA Hansell and CA Carlson, eds. Academic Press, New York: 693 pp.

Mopper, K, A Stubbins, JD Ritchie, HM Bialk, and PG Hatcher. 2007. Advanced instrumental approaches for characterization of marine dissolved organic matter: extraction techniques, mass spectrometry, and nuclear magnetic resonance spectroscopy. Chemical Reviews 107: 419-442. doi:10.1021/cr050359b

Moran, MA, and RE Hodson. 1990. Bacterial production on humic and nonhumic components of dissolved organic carbon. Limnology and Oceanography 35: 1744-1756. doi:10.4319/lo.1990.35.8.1744

Moran, MA, EB Kujawinski, A Stubbins, R Fatland, LI Aluwihare, A Buchan, BC Crump, PC Dorrestein, ST Dyhrman, NJ Hess, B Howe, K Longnecker, PM Medeiros, J Niggemann, I Obernosterer, DJ Repeta, and JR Waldbauer. 2016. Deciphering ocean carbon in a changing world. PNAS 113: 3143-3151.

Moran, MA, LR Pomeroy, ES Sheppard, LP Atkinson, and RE Hodson. 1991. Distribution of terrestrially derived dissolved organic matter on the southeastern U.S. continental shelf. Limnology and Oceanography 36: 1134-1149. doi:10.4319/lo.1991.36.6.1134

Morris RM, CD Frazar, and CA Carlson. 2012. Basin-scale patterns in the abundance of SAR11 subclades, marine *Actinobacteria* (OM11), members of the *Roseobacter* clade and OCS116 in the South Atlantic. Environmental Microbiology 14: 1133-1144. doi:10.1111/j.1462-2920.2011.02694.x

Morris, RM, KL Vergin, J-C Cho, M Rappé, CA Carlson, and SJ Giovannoni. 2005. Temporal and spatial response of bacterioplankton lineages to annual convective overturn at the Bermuda Atlantic Time-series Study site. Limnology and Oceanography 50: 1687-1696. doi:10.4319/lo.2005.50.5.1687

Mou X, RE Hodson, and MA Moran. 2007. Bacterioplankton assemblages transforming dissolved organic compounds in coastal seawater. Environmental Microbiology 9: 2025-2037. doi:10.1111/j.1462-2920.2007.01318.x

Mou, X, S Sun, RA Edwards, RE Hodson, and MA Moran. 2008. Bacterial carbon processing by generalist species in the coastal ocean. Nature 451: 708-711. doi:10.1038/nature06513

Murray, AE, A Blakis, R Massana, S Strawzewski, U Passow, A Alldredge, and EF DeLong. 1999. A time series assessment of planktonic archaeal variability in the Santa Barbara Channel. Aquatic Microbial Ecology 20: 129-145.

Myklestad, SM. 1974. Production of carbohydrates by marine planktonic diatom, I. Comparison of nine different species in culture. Journal of Experimental Marine Biology and Ecology 15: 261-274. doi:10.1016/0022-0981(74)90049-5

Myklestad, SM. 1995. Release of extracellular products by phytoplankton with special emphasis on polysaccharides. Science of the Total Environment 165: 155-164. doi:10.1016/0048-9697(95)04549-G

Myklestad, SM. 2000. Dissolved organic carbon from phytoplankton. In The Handbook of Environmental Chemistry Vol. 5 Part D: Marine Chemistry. P Wangersky, ed. Springer-Verlag, Berlin.

Nagata, T. 2000. Production mechanisms of dissolved organic matter. In Microbial Ecology of the Oceans, First Edition. DL Kirchman, ed. Wiley-Liss, New York: 542 pp.

Needham, DM, and JA Fuhrman. 2016. Pronounced daily succession of phytoplankton, archaea and bacteria following a spring bloom. Nature Microbiology 1: 16005. doi:10.1038/nmicrobiol.2016.5

Nelson, CE. 2009. Phenology of high-elevation pelagic bacteria: the roles of meteorological variability, catchment inputs and thermal stratification in structuring communities. The ISME Journal 3: 13-30. doi:10.1038/ismej.2008.81

Nelson, CE, and CA Carlson. 2012. Tracking differential incorporation of dissolved organic carbon types among diverse lineages of Sargasso Sea bacterioplankton. Environmental Microbiology 14: 1500-1516. doi:10.1111/j.1462-2920.2012.02738.x

Nelson, CE, CA Carlson, CS Ewart, and ER Halewood. 2014. Community differentiation and population enrichment of Sargasso Sea bacterioplankton in the euphotic zone of a mesoscale mode-water eddy. Environmental Microbiology 16: 871-887. doi:10.1111/1462-2920.12241

Nelson, CE, SJ Goldberg, LW Kelly, AF Haas, JE Smith, F Rohwer, and CA Carlson. 2013. Coral and macroalgal exudates vary in neutral sugar composition and differentially enrich reef bacterioplankton lineages. The ISME Journal 7: 962-979. doi:10.1038/ismej.2012.161

Nelson, DM, MA Brzezinski, DE Sigmon, and VM Frank. 2001. A seasonal progression of Si limitation in the Pacific sector of the Southern Ocean. Deep-Sea Research Part II 48: 3973-3995. doi:10.1016/S0967-0645(01)00076-5

Nelson, DM, P Tréguer, M Brzezinski, A Leynaert, and B Quéguiner. 1995. Production and dissolution of biogenic silica in the ocean: Revised global estimates, comparison with regional data and relationship to biogenic sedimentation. Global Biogeochemical Cycles 9: 359-372. doi:10.1029/95GB01070

Nelson, NB, and DA Siegel. 2002. Chromophoric DOM in the open ocean. In Biogeochemistry of Dissolved Organic Matter. DA Hansell and CA Carlson, eds. Academic Press, New York: 774 pp.

Newton, RJ, LE Griffin, KM Bowles, C Meile, S Gifford, CE Givens, EC Howard, E King, CA Oakley, CR Reisch, JM Rinta-Kanto, S Sharma, S Sun, V Varaljay, M Villa-Costa, JR Westrich, and MA Moran. 2010. Genome characteristics of a generalist marine bacterial lineage. The ISME Journal 4: 784-798. doi:10.1038/ismej.2009.150

Nikrad, MP, MT Cottrell, and DA Kirchman. 2014. Uptake of dissolved organic carbon by gammaproteobacterial subgroups in coastal waters of the West Antarctic Peninsula. Applied and Environmental Microbiology 80: 3362-3368. doi:10.1128/AEM.00121-14

Norrman, B, UL Zweifel, CS Hopkinson, Jr., and B Fry. 1995. Production and utilization of dissolved organic carbon during an experimental diatom bloom. Limnology and Oceanography 40: 898-907. doi:10.4319/lo.1995.40.5.0898

Obernosterer, I, and GJ Herndl. 1995. Phytoplankton extracellular release and bacterial growth: dependence on the inorganic N:P ratio. Marine Ecology Progress Series 116: 247-257.

Opsahl, S, and R Benner. 1997. Distribution and cycling of terrigenous dissolved organic matter in the ocean. Nature 386: 480-482. doi:10.1038/386480a0

Orsi WD, JM Smith, HM Wilcox, JE Swalwell, P Carini, AZ Worden, and AE Santoro. 2015. Ecophysiology of uncultivated marine euryarchaea is linked to particulate organic matter. The ISME Journal 9: 1747-1763. doi:10.1038/ismej.2014.260

Otero, MP, and DA Siegel. 2004. Spatial and temporal characteristics of sediment plumes and phytoplankton blooms in the Santa Barbara Channel. Deep-Sea Research Part II 51: 1129-1149. doi:10.1016/j.dsr2.2004.04.004

Parada, AE, DM Needham, and JA Fuhrman. 2016. Every base matters: assessing small subunit rRNA primers for marine microbiomes with mock communities, time series and global field samples. Environmental Microbiology 18: 1403-1414. doi:10.1111/1462-2920.13023

Passow, U. 2002. Transparent exoploymer particles (TEP) in aquatic environments. Progress in Oceanography 55: 287-333. doi:10.1016/S0079-6611(02)00138-6

Pedler, BE, LI Aluwihare, and F Azam. 2014. Single bacterial strain capable of significant contribution to carbon cycling in the surface ocean. PNAS 111: 7202-7207. doi:10.1073/pnas.1401887111

Pete, R, K Davidson, MC Hart, T Gutierrez, and AEJ Miller. 2010. Diatom derived dissolved organic matter as a driver of bacterial productivity: The role of nutrient limitation. Journal of Experimental Marine Biology and Ecology 391: 20-26. doi:10.1016/j.jembe.2010.06.002

Pittera, J, F Humily, M Thorel, D Grulois, L Garczarek, and C Six. 2014. Connecting thermal physiology and latitudinal niche partitioning in marine *Synechococcus*. The ISME Journal 8: 1221-1236. doi: 10.1038/ismej.2013.228

Pomeroy, LR. 1974. The ocean's food web, a changing paradigm. Bioscience 24: 499-504. doi:10.2307/1296885

Porter, KG, and YS Feig. 1980. The use of DAPI for identifying and counting aquatic microflora. Limnology and Oceanography 25: 943-948.

Quast, C, E Pruesse, P Yilmaz, J Gerken, T Schweer, P Yarza, J Peplies, and FO Glöckner. 2013. The SILVA ribosomal RNA gene database project: improved data processing and web-based tools. Nucleic Acids Research 41: D590-D596. doi:10.1093/nar/gks1219

Reed D, L Washburn, A Rassweiler, R Miller, T Bell, and S Harrer. 2016. Extreme warning challenges sentinel status of kelp forests as indicators of climate change. Nature Communications 7: 13757. doi:10.1038/ncomms/13757

Repeta, DJ. 2015. Chemical characterization and cycling of dissolved organic matter. In Biogeochemistry of Marine Dissolved Organic Matter. DA Hansell and CA Carlson, eds. Academic Press, San Diego: 774 p.

Repeta, DJ, and LI Aluwihare. 2006. Radiocarbon analysis of neutral sugars in high molecular-weight dissolved organic carbon: implications for organic carbon cycling. Limnology and Oceanography 51: 1045-1053. doi:10.4319/lo.2006.51.2.1045

Rivkin, RB, MR Anderson, and C Lajzerowicz. 1996. Microbial processes in cold oceans. I. Relationship between temperature and bacterial growth rate. Aquatic Microbial Ecology 10: 243-254. doi:10.3354/ame010243

Rivkin, RB, and L Legendre. 2001. Biogenic carbon cycling in the upper ocean: effects of microbial respiration. Science 291: 2398-2400. doi:10.1126/science.291.5512.2398

Rocap, G, DL Distel, JB Waterbury, and SW Chisholm. 2002. Resolution of *Prochlorococcus* and *Synechococcus* ecotypes by using 16S-23S ribosomal DNA internal transcribed spacer sequences. Applied and Environmental Microbiology 68: 1180-1191. doi:10.1128/AEM.68.3.1180-1191.2002

Rognes, T, T Flouri, B Nichols, C Quince, and F Mahé. 2016. VSEARCH: a versatile open source tool for metagenomics. PeerJ 4:e2584.

Rusch, DB, AL Halpern, G Sutton, KB Heidelberg, S Williamson, S Yooseph, D Wu, JA Eisen, JM Hoffman, K Remington, K Beeson, B Tran, H Smith, H Baden-Tillson, C Stewart, J Thorpe, J Freeman, C Andrews-Pfannkoch, JE Venter, K Li, S Kravitz, JF Heidelberg, T Utterback, Y-H Rogers, LI Falcón, V Souza, G Bonilla-Rosso, LE Eguiarte, DM Karl, S Sathyendranath, T Platt, E Bermingham, V Gallardo, G Tamayo-Castillo, MR Ferrari, RL Strausberg, K Nealson, R Friedman, M Frazier, and JC Venter. 2007. The *Sorcerer II* Global Ocean Sampling Expedition: northwest Atlantic through eastern tropical Pacific. PLoS Biology 5: e77. doi:10.1371/journal.pbio.0050077

Salter, I, PE Galand, SK Fagervold, P Lebaron, I Obernosterer, MJ Oliver, MT Suzuki, and C Tricoire. 2015. Seasonal dynamics of active SAR11 ecotypes in the oligotrophic Northwest Mediterranean Sea. The ISME Journal 9: 347-360. doi:10.1038/ismej.2014.129

Santschi, PH, L Guo, M Baskaran, S Trumbore, J Southon, TS Bianchi, B Honeyman, and L Cifuentes. 1995. Isotopic evidence for the contemporary origin of high-molecular weight organic matter in oceanic environments. Geochimica et Cosmochimica Acta 59: 625-631. doi:10.1016/0016-7037(94)00378-Y

Sarmento, H, and JM Gasol. 2012. Use of phytoplankton-derived dissolved organic carbon by different types of bacterioplankton. Environmental Microbiology 14: 2348-2360. doi:10.1111/j.1462.2920.02787.x

Sarmento, H, C Morana, and JM Gasol. 2016. Bacterioplankton niche partitioning in the use of phytoplankton-derived dissolved organic carbon: quantity is more important than quality. The ISME Journal 10: 2582-2592. doi:10.1038/ismej.2016.66

Schloss, PD. 2010. The effects of alignment quality, distance calculation method, sequence filtering, and region on the analysis of 16S rRNA gene-based studies. PLOS Computational Biology 6: e1000844. doi:10.1371/journal.pcbi.1000844

Schloss, PD, SL Westcott, T Ryabin, JR Hall, M Hartmann, EB Hollister, RA Lesniewski, BB Oakley, DH Parks, CJ Robinson, JW Sahl, B Stres, GG Thallinger, DJ Van Horn, and CF Weber. 2009. Introducing mothur: open-source, platform-independent, community-supported software for describing and comparing microbial communities. Applied and Environmental Microbiology 75: 7537-7541. doi:10.1128/AEM.01541-09

Shade, A, SE Jones, JG Caporaso, J Handelsman, R Knight, N Fierer, and JA Gilbert. 2014. Conditionally rare taxa disproportionately contribute to temporal changes in microbial diversity. mBio 5: e01371-14. doi:10.1128/mBio.01371-14.

Sharp, JH. 2002. Analytical methods for total DOM pools. In Biogeochemistry of Dissolved Organic Matter. DA Hansell and CA Carlson, eds. Academic Press, New York: 774 pp.

Shifrin, NS, and SW Chisholm. 1981. Phytoplankton lipids: interspecific differences and effects of nitrate, silicate and light-dark cycles. Journal of Phycology 17: 374-384. doi:10.1111/j.1529-8817.1981.tb00865.x

Sieracki, ME, PG Verity, and DK Stoecker. 1993. Plankton community response to sequential silicate and nitrate depletion during the 1989 North Atlantic spring bloom. Deep-Sea Research II 40: 213-225. doi:10.1016/0967-0645(93)90014-E

Simon, M, and F Azam. 1989. Protein content and protein synthesis rates of planktonic marine bacteria. Marine Ecology Progress Series 51: 201-213. doi:10.3354/meps051201

Skoog, A, and R Benner. 1997. Aldoses in various size fractions of marine organic matter: implications for carbon cycling. Limnology and Oceanography 42: 1803-1813. doi:10.4319/lo.1997.42.8.1803

Smith, EM, and R Benner. 2005. Photochemical transformations of riverine dissolved organic matter: effects on estuarine bacterial metabolism and nutrient demand. Aquatic Microbial Ecology 40: 37-50. doi:10.3354/ame040037

Smith, Jr., WO, CA Carlson, HW Ducklow, and DA Hansell. 1998. Growth dynamics of *Phaeocystis antarctica*-dominated plankton assemblages from the Ross Sea. Marine Ecology Progress Series 168: 229-244. doi:10.3354/meps168229

Sogin, ML, HG Morrison, JA Huber, DM Welch, SM Huse, PR Neal, JM Arrieta, and GJ Herndl. 2006. Microbial diversity in the deep sea and the underexplored "rare biosphere." Proceedings of the National Academy of Sciences of the USA 103: 12115-12120. doi:10.1073/pnas.0605127103

Sohm, JA, NA Ahlgren, ZJ Thomson, C Williams, JW Moffett, MA Saito, EA Webb, and G Rocap. 2016. Co-occurring *Synechococcus* ecotypes occupy four major oceanic regimes defined by temperature, macronutrients and iron. The ISME Journal 10: 333-345. doi:10.1038/ismej.2015.115

Sørensen, TA. 1948. A method of establishing groups of equal amplitude in plant sociology based on similarity of species content, and its applications to analyses of the vegetation on Danish commons. Biologiske Skrifter Kongelige Danske Videnskabernes Selskab 5: 1-34.

Stedmon, CA, S Markager, and H Kaas. 2000. Optical properties and signatures of chromophoric dissolved organic matter (CDOM) in Danish coastal waters. Estuarine Coastal and Shelf Science 51: 267-278. doi:10.1006/ecss.2000.0645.

Stocker, R. 2012. Marine microbes see a sea of gradients. Science 338: 628-633. doi:10.1126/science.1208929

Stocker R, JR Seymour, A Samadani, DE Hunt, and MF Polz. 2008. Rapid chemotactic response enables marine bacteria to exploit ephemeral microscale nutrient patches. PNAS 105: 4209-4214. doi: 10.1073 pnas.0709765105

Straza, TRA, and DL Kirchman. 2011. Single-cell response of bacterial groups to light and other environmental factors in the Delaware Bay, USA. Aquatic Microbial Ecology 62: 267-277. doi:10.3354/ame01469

Strom, SL. 2000. Bacterivory: interactions between bacteria and their grazers. In Microbial Ecology of the Oceans, First Edition. DL Kirchman, ed. Wiley-Liss, New York: 542 pp.

Sun, L, EM Purdue, JL Meyer, and J Weis. 1997. Use of elemental composition to predict bioavailability of dissolved organic matter in a Georgia river. Limnology and Oceanography 42: 714-721. doi:10.4319/lo.1997.42.4.0714

Sunagawa, S, LP Coelho, S Chaffron, JR Kultima, K Labadie, G Salazar, B Djahanschiri, G Zeller, DR Mende, A Alberti, FM Cornejo-Castillo, PI Costea, C Cruaud, F d'Ovidio, S Engelen, I Ferrera, JM Gasol, L Guidi, F Hildebrand, F Kokoszka, C Lepoivre, G Lima-Mendez, J Poulain, BT Poulos, M Royo-Llonch, H Sarmento, S Vieira-Silva, C Dimier, M Picheral, S Searson, S Kandels-Lewis, *Tara* Oceans

coordinators, C Bowler, C de Vargas, G Gorsky, N Grimsley, P Hingamp, D Iudicone, O Jaillon, F Not, H Ogata, S Pesant, S Speich, L Stemmann, MB Sullivan, J Weissenbach, P Wincker, E Karsenti, J Raes, SG Acinas, and P Bork. 2015. Strtucture and function of the global ocean microbiome. Science 348: 1261359-1-9. doi:10.1126/science.1261359.

Swan, BK, B Tupper, A Sczyrba, FM Lauro, M Martinez-Garcia, JM González, H Luo, JJ Wright, ZC Landry, NW Hanson, BP Thompson, NJ Poulton, P Schwientek, SG Acinas, SJ giovannoni, MA Moran, SJ Hallam, R Cavicchioli, T Woyke, and R Stepanauskas. 2013. Prevalent genome streamlining and latitudinal divergence of planktonic bacteria in the surface ocean. Proceedings of the National Academy of Sciences USA 110: 11463-11468. doi:10.1073/pnas.1304246110

Swan, CM, DA Siegel, NB Nelson, CA Carlson, and E Nasir. 2009. Biogeochemical and hydrographic controls on chromophoric dissolved organic matter distribution in the Pacific Ocean. Deep-Sea Research Part I 56: 2175-2192. doi:10.1016/j.dsr.2009.09.002

Teeling, H, BM Fuchs, D Becher, C Klockow, A Gardebrecht, CM Bennke, M Kassagby, S Huang, AJ Mann, J Waldmann, M Weber, A Klindworth, A Otto, J Lange, J Bernhardt, C Reinsch, M Hecker, J Peplies, FD Bockelmann, U Callies, G Gerdts, A Wichels, KH Wiltshire, FO Glöckner, T Schweder, and R Amann. 2012. Substrate-controlled succession of marine bacterioplankton populations induced by a phytoplankton bloom. Science 336: 608-611. doi:10.1126/science.1218344

Traving, SJ, UH Thygesen, L Riemann, and CA Stedmon. 2015. A model of extracellular enzymes in free-living microbes: which strategy pays off? Applied and Environmental Microbiology 81: 7385-7393. doi:10.1128/AEM.02070-15

Treusch, AH, KL Vergin, LA Finlay, MG Donatz, RM Burton, CA Carlson, and SJ Giovannoni. 2009. Seasonality and vertical structure of microbial communities in an ocean gyre. The ISME Journal 3: 1148-1163. doi:10.1038/ismej.2009.60

Venter, JC, K Remington, JF Heidelberg, AL Halpern, D Rusch, JA Eisen, D Wu, I Paulsen, KE Nelson, W Nelson, DE Fouts, S Levy, AH Knap, MW Lomas, K Nealson, O White, J Peterson, J Hoffman, R Parsons, H Baden-Tillson, C Pfannkoch, Y-H Rogers, and HO Smith. 2004. Environmental genome shotgun sequencing of the Sargasso Sea. Science 304:66-74. doi:10.1126/science.1093857

Vergin, KL, B Done, CA Carlson, and SJ Giovannoni. 2013. Spatiotemporal distributions of rare bacterioplankton populations indicate adaptive strategies in the oligotrophic ocean. Aquatic Microbial Ecology 71: 1-13. doi:10.3354/ame01661

Villar, E, GK Farrant, M Follows, L Garczarek, S Speich, S Audic, L Bittner, B Blanke, JR Brum, C Brunet, R Casotti, A Chase, JR Dolan, F d'Ortenzio, J-P Gattuso, N Grima, L Guidi, CN Hill, O Jahn, J-L Jamet, H Le Goff, C Lepoivre, S Malviya, E Pelletier, J-B Romagnan, S Roux, S Santini, E Scalco, SM Schwenck, A Tanaka, P Testor, T Vannier, F Vincent, A Zingone, C Dimier, M Picheral, S Searson, S Kandels-Lewis, *Tara* Oceans Coordinators, SG Acinas, P Bork, E Boss, C de Vargas, G Gorsky, H Ogata, S Pesant, MB Sullivan, S Sunagawa, P Wincker, E Karsenti, C Bowler, F Not, P Hingamp, and D Iudicone. 2015. Environmental characteristics of Agulhas rings affect interocean plankton transport. Science 348: 1261447-1-11. doi:10.1126/science.1261447

Vraspir, JM, and A Butler. 2009. Chemistry of marine ligands and siderophores. Annual

Review of Marine Science 1: 43-63. doi:10.1146/annurev.marine.010908.163712

Walsh, EA, JB Kirkpatrick, SD Rutherford, DC Smith, M Sogin, and S D'Hondt. 2016. Bacterial diversity and community composition from seasurface to subseafloor. The ISME Journal 10: 979-989. doi:10.1038/ismej.2015.175

Wear, EK, CA Carlson, AK James, MA Brzezinski, LA Windecker, and CE Nelson. 2015. Synchronous shifts in dissolved organic carbon bioavailability and bacterial community responses over the course of an upwelling-driven phytoplankton bloom. Limnology and Oceanography 60: 657-677. doi:10.1002/lno.10042

Wear, EK, CA Carlson, LA Windecker, and MA Brzezinski. 2015. Roles of diatom nutrient stress and species identity in determining the short- and long-term bioavailability of diatom exudates to bacterioplankton. Marine Chemistry 177: 335-348. doi:10.1016/j.marchem.2015.09.001

Wetz, MS, and PA Wheeler. 2004. Response of bacteria to simulated upwelling phytoplankton blooms. Marine Ecology Progress Series 272: 49-57. doi:10.3354/meps272049

Williams, PJ leB. 1995. Evidence for the seasonal accumulation of carbon-rich dissolved organic matter, its scale in comparison with changes in particulate material and the consequential effects on net C/N assimilation ratios. Marine Chemistry 51: 17-29. doi:10.1016/0304-4203(95)00046-T

Williams, PJ le B. 2000. Heterotrophic bacteria and the dynamics of dissolved organic matter. In Microbial Ecology of the Oceans, First Edition. DL Kirchman, ed. Wiley-Liss, New York: 542 pp.

Williams, PM, and ERM Druffel. 1987. Radiocarbon in dissolved organic matter in the central North Pacific Ocean. Nature 330: 246-248. doi:10.1038/330246a0

Winant, CD, EP Dever, and MC Hendershott. 2003. Characteristic patterns of shelf circulation at the boundary between central and southern California. Journal of Geophysical Research 108: 3021. doi:10.1029/2001JC001302

Windecker, LA. 2016. Extracellular release in marine phytoplankton. PhD dissertation, University of California, Santa Barbara. ProQuest (number 10159653).

Winter, C, MM Moeseneder, and GJ Herndl. 2001. Impact of UV radiation on bacterioplankton community composition. Applied and Environmental Microbiology 67: 665-672. doi:10.1128/AEM.67.2.665-672.2001

Wood, AM, and LM van Valen. 1990. Paradox lost? On the release of energy-rich compounds by phytoplankton. Marine Microbial Food Webs 4: 103-116.

Yamashita, Y, and E Tanoue. 2008. Production of bio-refractory fluorescent dissolved organic matter in the ocean interior. Nature Geoscience 1: 579-582. doi:10.1038/ngeo279

Yannarell, AC, and EW Triplett. 2005. Geographic and environmental sources of variation in lake bacterial community composition. Applied and Environmental Microbiology 71: 227-239. doi:10.1128/AEM.71.1.227-239.2005

Yokokawa, T, and T Nagata. 2010. Linking bacterial community structure to carbon fluxes in marine environments. Journal of Oceanography 66: 1-12. doi:10.1007/s10872-010-0001-4

Yooseph, S, KH Nealson, DB Rusch, JP McCrow, CL Dupont, M Kim, J Johnson, R Montgomery, S Ferriera, K Beeson, SJ Williamson, A Tovchigrechko, AE Allen, LA Zeigler, G Sutton, E Einstadt, Y-H Rogers, R Friedman, M Frazier, and JC Venter.

2010. Genomic and functional adaptation in surface ocean planktonic prokaryotes. Nature 468: 60-67. doi:10.1038/nature09530

Zinger, L, LA Amaral-Zettler, JA Fuhrman, MC Horner-Devine, SM Huse, DM Mark Welch, JBH Martiny, M Sogin, A Boetius, and A Ramette. 2011. Global patterns of bacterial beta-diversity in seafloor and seawater ecosystems. PLoS ONE 6: e24570. doi:10.1371/journal.pone.0024570